CARBON MONOXIDE IN THE ATMOSPHERES OF THE TERRESTRIAL PLANETS

Thesis by

ROBERT TODD CLANCY

In Partial Fulfillment of the Requirements

for the Degree of

Doctor of Philosophy

California Institute of Technology

Pasadena, California

1983

(Submitted 14 February 1983)

my family

ACKNOWLEDGMENTS

If I were to compose a list of those to whom I am thankful, there would not be room for a thesis to follow and still, I could not express the gratitude that I feel. I must acknowledge Caltech for the education and confidence that it has given me. Foremost is the guidance, concern, and friendship that my thesis advisor, Professor Duane Muhleman, has always found time to give me.

I am also thankful to Dr. Glenn Berge for friendship and for the selfless help he has provided me in my work. To Professors Yuk Yung and Andrew Ingersoll and to Dr. Mark Allen and Ed Danielson, I have enjoyed very much working with them and benefitting from their experience. I am also indebted to the staff of the Owens Valley Radio Observatory, particularly Drs. Ed Sutton, Colin Masson, Dave Woody and Professor Peter Wanier, and to the staff of the NRAO at Kitt Peak, particularly Dr. Richard Howard. Furthermore, I am grateful for considerable cooperation in work by Professor Pete Schloerb and Dr. Bill Wilson.

For unfaltering secretarial and administrative assistance in the face of emminent childbirth, flu, etc., I must commend and thank Donna Lathrop and Kay Campbell. I am also grateful for timely assistance from Shirley Taylor, Dorothy Coy and Barbara Niles.

I am forever indebted to my fellow students who have made graduate school more than bearable and who have made me fortunate to be a student in planetary science. To Steve, Jay, Bruce, Dan, Tony, Judy, Peter, Jim(s), Lucien, Carolyn, Randy, Jack, Jon, Mike, Don, Dave(s), John, Quinn, JoBea, Rich, and Bill.

This work was supported by NASA grants NGR 05-002-114 and NGL 05-002-003.

I am most grateful to and for the family that I have and will yet have. To Maria, whom I love.

ABSTRACT

Microwave spectra of carbon monoxide (^{12}CO) in the mesosphere of Venus were measured in December of 1978; May and December of 1980; and January, September, and November of 1982. These spectra are analyzed to provide mixing profiles of CO in the Venus mesosphere and best constrain the mixing profile of CO between ~ 100 and 80 kilometers altitude. From the January 1982 measurement (which, of all our spectra, best constrains the abundance of CO below 80 km altitude) we find an upper limit for the CO mixing ratio below 80 kilometers altitude that is 2-3 times smaller than the stratospheric (~ 65 km) value of $4.5 \pm 1.0 \times 10^{-6}$ determined by Connes et al. (1968) in 1967, indicating a possible long-term change in the lower atmospheric concentration of CO.

Intercomparison among the individual CO profiles derived from our spectra indicates considerable short-term temporal and/or spatial variation in the profile of CO mixing in the Venus mesosphere above 80 kilometers. A more complete comparison with previously published CO microwave spectra from a number of authors (Kakar et al., 1976; Gulkis et al., 1977; Schloerb et al., 1980; Wilson and Klein, 1981; Schloerb et al., 1981) specifies the basic diurnal nature of mesospheric CO variability. CO abundance above ~ 95 kilometers in the Venus atmosphere shows approximately a factor of 2-4 enhancement on the nightside relative to the dayside of Venus. The magnitude of this nightside CO bulge is in good agreement with the dynamical modeling results of Dickinson and Ridley (1977), indicating that subsolar to antisolar circulation proposed for the thermosphere of Venus by Dickinson and Ridley extends to below 100 km altitude in the Venus mesosphere. Furthermore, peak nightside CO abundance above ~ 95 kilometers occurs very near to the antisolar point on Venus (local time of peak CO abundance above ~ 95 kilometers occurs at $0.6^{+0.7}_{-0.6}$ hours after midnight on

Venus), strongly suggesting that retrograde zonal flow is substantially reduced at an altitude of 100 kilometers in the Venus mesosphere.

By contrast, CO abundances between 80 and 90 kilometers altitude show a maximum that is shifted from the antisolar point towards the morning side of Venus (local time of peak CO abundance between 80 and 90 kilometers occurs at 8.5 ± 1.0 hours past midnight on Venus). The magnitude of the diurnal variation of CO abundance between 80 and 90 kilometers is again, approximately a factor of 2-4. Given the recombination of CO strongly peaks in this altitude region (Yung and DeMore, 1982), we investigated the possible effects of diurnal photochemistry as a driving force for diurnal CO variations between 70 and 90 kilometers from model calculations. We find that the likely magnitude of diurnal CO variability due to photochemistry and vertical eddy diffusion is smaller than that indicated by the microwave data, and that such variations cannot predict the observed phase behavior of the diurnal variations. Photochemical models invariably predict peak CO abundances in the afternoon rather than morning hours on Venus. However, a simple model for the circulation of the Venus mesosphere is presented to explain the observed diurnal variations of CO both above 90 kilometers altitude and between 80 and 90 kilometers altitude. We propose that the subsolar to antisolar circulation of the Venus thermosphere (and the resulting nightside enhancement of CO) persists down to altitudes of ~ 80 kilometers. Above ~ 90 kilometers zonal flow is small and the nightside CO bulge remains centered near the antisolar point on Venus. Below ~ 90 kilometers altitude retrograde zonal wind velocities increase abruptly to several tens of meters/sec displacing the nightside enhancement of CO towards the morningside of Venus.

We also present a $J = 1 \rightarrow 2$ spectrum of ^{13}CO absorption in the mesosphere of Venus. This ^{13}CO spectrum was measured at the same time as our high quality, January 1982 ^{12}CO spectrum. Radiative transfer models employing a single pressure-temperature model of the Venus mesosphere are fit to both the ^{13}CO and ^{12}CO spectra. The ^{12}CO spectrum is used to specify the altitude distribution of CO. Subsequently, we solve for the ratio $^{12}CO/^{13}CO = 185$ in order to best fit the ^{13}CO spectrum. Based on an extensive error analysis we believe that the standard deviation of this value is $\pm$ 69. This result applies only to the mesosphere of Venus, i.e. from 80 to 110 km. Values of the $^{12}CO/^{13}CO$ ratio measured deeper in the Venus atmosphere are closer to the terrestrial value of 89. We suggest several fractionation mechanisms in order to account for the difference between our result and the terrestrial value. However, as yet, none of these mechanisms is known to produce significant fractionation of CO isotopes in the upper atmosphere of Venus.

In January of 1982 we measured a microwave spectrum of CO in the Martian atmosphere utilizing the rotational $J = 1 \rightarrow 2$ transition of CO. We have analyzed our data and reanalyzed the microwave spectra of Kakar et al. (1967, measured in 1975) and Good and Schloerb (1981, measured in 1980) in order to constrain estimates of the temporal variability of CO abundance in the Martian atmosphere. Long-term ($\gtrsim 1$ year) variations in CO abundance have been predicted on the basis of possible variations in eddy diffusion (McElroy and Donahue, 1972) and/or condensible H_xO_y compounds (Hunten, 1974) in the Martian atmosphere. Our values of CO column density from the data of Kakar et al., Good and Schloerb, and our own are $1.7 \pm 0.9 \times 10^{20}$ cm^{-2}, $3.0 \pm 1.0 \times 10^{20}$ cm^{-2}, and $4.6 \pm 2.0 \times 10^{20}$ cm^{-2}, respectively. The most recent estimate of CO column density from the 1967 infrared spectra of Connes et al. (1969) is

$2.0 \pm 0.8 \times 10^{20}$ cm^{-2} (Young and Young, 1977). The large uncertainties given for the microwave measurements are due primarily to uncertainty in the difference between the continuum brightness temperature and atmospheric temperatures of Mars. We have accurately calculated the variation among the observations of the continuum (surface) brightness temperature of Mars, which is primarily a function of the observed aspect of Mars. A more difficult problem to consider is variability of global atmospheric temperatures among the observations, particularly the effects of global dust storms and the ellipticity of the orbit of Mars. The large error bars accompanying our estimates of CO column density from the three sets of microwave measurements are primarily caused by an assumed uncertainty of ± 10 K in our atmospheric temperature model due to possible dust in the atmosphere. A qualitative consideration of seasonal variability of global atmospheric temperatures among the measurements suggests that there is not strong evidence for variability of the column abundance of CO on Mars, although variability of 0-100% over a time scale of several years is allowed by the data set. The implication for the variability of Mars O_2 (which is directly tied to photodissociation of CO_2) is, crudely, a factor of two less. We find that the altitude distribution of CO in the atmosphere of Mars is not well constrained by any of the spectra, although our spectrum is marginally better fit by an altitude increasing profile of CO mixing ratios.

Finally, we consider variations in the CO content of the terrestrial mesosphere. The Earth's mesospheric carbon monoxide was observed in absorption against the Moon in early December of 1979 and late January of 1982 at a wavelength of 1.3 mm, and in early December of 1980 at a wavelength of 2.6 mm. The January 1982 spectrum was also measured in emission with very high signal-to-noise ratios. The observed wavelengths correspond to the respective

rotational transitions of CO, $J = 1 \rightarrow 2$ and $J = 0 \rightarrow 1$. No significant change in the column density of CO above ~65 km is found between the 1979 and 1980 observations, but the January 1982 measurement indicates an ~30% reduction in column density relative to the December observations. Inversion of the spectra did not provide unique CO mixing ratio profiles for a direct quantitative comparison of December 1979 and 1980 and January 1982 profiles, due to limited signal-to-noise ratios for the 1979, 1980 observations. One of the best constrained mixing profiles published to date is presented for the very high signal-to-noise January 1982 emission spectrum. Comparison with other published spectra of mesospheric CO suggests a large seasonal variation (~ a factor of 2-4) in the column density of CO above 65 km, with a maximum in winter and a minimum in summer. The phase of this seasonal variation in CO abundance is opposite to the phase of seasonal variation in insolation suggesting that a hemispheric pattern of circulation is responsible for seasonal variations in the Earth's mesosphere.

We summarize by noting the very different time scales for variations of CO in the upper atmospheres of Venus, the Earth, and Mars. The long diurnal period of Venus produces a very strong diurnal variation in mesospheric CO which is driven primarily by subsolar to antisolar circulation. CO in the terrestrial mesosphere shows strong seasonal variation which is apparently produced by seasonally driven meridional circulation. By contrast, if atmospheric CO does vary on Mars, it is most likely controlled by long-term changes in the chemistry and/or vertical mixing in the Martian atmosphere.

TABLE OF CONTENTS

PART I

Diurnal Variations of Carbon Monoxide in the Mesosphere of Venus

1. INTRODUCTION

A significant feature of microwave spectra of CO in the mesosphere of Venus is the striking variation of the CO spectra with the phase of Venus. Concerning published spectra, both Wilson et al. (1981) and Schloerb et al., (1980) noted that the nightside of Venus (towards inferior conjunction) is characterized by very deep and narrow CO absorption lines whereas the dayside (towards superior conjunction) is characterized by shallow, broad spectra (e.g., see Figure 15). Implications for the variable distribution of CO in the mesosphere of Venus are very important particularly given our lack of knowledge of the Venus atmosphere between 70 and 120 kilometers altitude. Questions such as the extension of the 100 m/s zonal flow into the mesosphere of Venus are not well addressed by other data sets. On the basis of all available CO microwave spectra of Venus including our own measured spectra, we intend to show the constraints that such microwave data place on the dynamics and chemistry of the mesosphere of Venus. We proceed first with a summary of what is known about the mesosphere of Venus particularly with regard to what is known about the more completely measured lower (cloud tops and below) and upper (above ~ 120 kilometers) atmosphere of Venus. We follow with description and analysis of the CO microwave data in order to determine the variability and the altitude distribution of CO in the mesosphere of Venus. Finally we present the results of time dependent photochemical modeling and a qualitative circulation model for the mesosphere of Venus. We use the diagnostic behavior of CO to place constraints and boundary conditions on our mesospheric models of Venus.

2. THE MESOSPHERE OF VENUS

2.1 Dynamics

Apart from the sheer mass of the Venus atmosphere, one of its most interesting and least understood aspects is a truly global pattern of circulation. The atmosphere of Venus may be crudely separated into two regimes: the massive lower atmosphere (below ~60 km), in which the radiative time constant is much greater than the solar day on Venus (117 days); and the upper atmosphere, for which the radiative time constant is much smaller than the solar day (e.g., Chamberlain, 1978). For such conditions one would expect the lower atmosphere to exhibit primarily equator to pole temperature gradients and a rather straightforward Hadley cell circulation between equator and poles, given the small inclination of the Venus rotational axis and the very slow rotation of Venus (Schubert et al., 1977). On the other hand, the upper atmosphere should develop large day-night temperature gradients. Circulation in this region should be dominated by axially symmetric subsolar to antisolar flow (e.g., Dickinson, 1971). The transitional region of the atmosphere between these very distinct regimes of circulation is, roughly, the mesosphere of Venus.

Before discussing the circulation of the mesosphere it is important to note that the circulation of the lower Venus atmosphere is far from what simple inferences had suggested. Measurements of the global circulation of Venus provide the following conclusions to be drawn about the dynamics of the upper and lower atmosphere of Venus.

2.1.1 Below 70 km

Both spacecraft and ground observations indicate that the lower atmosphere of Venus (below ~70 km) is characterized by retrograde zonal rather

than meridional flow with peak velocities of approximately 100 m/s in the cloud layers of Venus. The Doppler tracking of Venera and Pioneer Venus probes show that these zonal winds decrease in a roughly linear fashion to velocities of a few meters per second near the surface of Venus (Venera 7-10, —Marov et al., 1973; Ainsworth and Herman, 1975; Keldysh, 1977; Pioneer Venus —Counselman et al., 1980). Comparison of the individual wind profiles measured by these probes also indicates substantial variations in zonal flow with time and position on Venus (Schubert et al., 1980). The global extent of zonal flow on Venus is best studied by visual and spectroscopic observations of the roughly 4 day (~ 100 m/s) circulation of the Venus cloud system and associated UV markings. The 4 day periodicity of the dark UV markings was first observed by Boyer and Carmichel (1961), with subsequent observations by Smith (1967), Boyer and Guerin (1969), Scott and Reese (1972), and Boyer (1973). By tracing the progress of these markings across the observed hemisphere of Venus, Scott and Reese (1972) and Boyer (1973) obtained respective velocity ranges of 66-127 m/s and 50-133 m/s (in the retrograde sense). The measured variability is a function of both time and position on Venus. Spacecraft observations of the dark UV markings indicate a latitudinal distribution of zonal velocities characteristic of constant angular velocity accompanied by midlatitude jets (Rossow et al., 1980; Limaye and Suomi, 1980; Rossow and Kinsella, 1982). These jets are much more pronounced in the Mariner 10 profiles relative to the Pioneer Venus data (Rossow et al., 1980), again indicating temporal variability of zonal flow. Finally, Traub and Carlton (1975) measured wind velocities in the cloud regions of Venus directly, using Doppler shifts of a CO_2 absorption line of scattered sunlight at 8710 Å. They found average zonal velocities of 83 ± 10 m/s with variability between 2 and 125 m/s on a "timescale greater than one week." They also

determined an afternoon-morning asymmetry in zonal velocities with higher average velocities in the afternoon (111 m/s) relative to the morning (73 m/s) on Venus. Boyer (1973) noted a similar asymmetry (morning, 83 m/s versus afternoon, 122 m/s) on the basis of his observations of the UV dark markings.

Meridional flow in the lower Venus atmosphere is substantially weaker and more poorly determined than the observed zonal circulation and correspondingly poorer determined. Meridional velocities are generally a few meters per second below 40 km (Counselman et al., 1980) and increase to values on the order of 10 m/s near the cloud regions (Counselman et al., 1980; Rossow et al., 1980). The general circulation of the lower atmosphere of Venus is primarily retrograde zonal flow with considerable temporal and spatial variation.

2.1.2 Above 120 km

Information on the circulation of the Venus atmosphere above 70 km is much more limited both because of the reduced mass of the atmosphere at these altitudes and the lack of any traceable markers comparable to the dark UV markings. At present, it appears that the assumption of subsolar to antisolar flow as the dominant circulation of the upper atmosphere is correct. The dynamical modeling of Dickinson and Ridley (1975, 1977) is by far the most complete theoretical treatment of circulation in the thermosphere of Venus and very roughly corresponds to what is known about the Venus thermosphere ($\gtrsim$ 120 km). Dickinson and Ridley constructed a nonlinear time-dependent hydrodynamic model in which mechanisms of heating, cooling, photodissociation of CO_2 and dynamical flow lead to very strong asymmetry in day-night temperatures and composition. The prognostic features of their model are: (1) horizontal velocities on the order of 50-300 m/s from the subsolar to the antisolar point; (2) vertical velocities of 10-300 cm/s rising near the subsolar point and

descending near the antisolar point; (3) very strong concentration of maximum vertical and horizontal velocities near the terminators; (4) thermospheric temperatures (above ~ 150 km) of 150-250 K on the nightside versus 300-600 K on the dayside; (5) roughly equal number densities (to within ~ 20%) at all altitudes between the day and nightside; (6) at identical altitudes (and pressures), larger mixing ratios of O and CO on the nightside relative to the dayside. This last effect is primarily due to the vertical motions in their models. Both O and CO mixing ratios increase with altitude in the thermosphere and, because the atmosphere is rising on the dayside and descending on the nightside, altitude levels for particular mixing ratios of CO and O are lower on the nightside relative to the dayside by ~ 15-20 km. The models of Dickinson and Ridley did not include vertical eddy diffusion which is found to be significant in the thermosphere of Venus (von Zahn et al., 1980). Hence, their models predicted a nightside atmosphere of predominantly O above ~ 150 km, due to molecular diffusion.

Many of the above predictions were considerably altered by Pioneer Venus measurements of the thermosphere of Venus. One of the more surprising discoveries is that day-night contrast in the thermosphere is much more extreme than suggested by the models of Dickinson and Ridley. Exospheric temperatures drop much more sharply across the terminators, from 300 K on the dayside to 100 K on the nightside (Keating et al., 1980). In addition atmospheric number densities fall sharply by two orders of magnitude across the terminators at an altitude of 160 km (Niemann et al., 1980). This divergence in pressure and number density between day and night begins at ~ 100 km altitude (Seiff and Kirk, 1981). Concentrations of O and CO are enhanced on the nightside at altitudes of 160 km but the predicted bulge in O number density on the nightside is not observed, possibly due to rapid downward transport of O by eddy

diffusion (e.g., Niemann et al., 1980).

The extreme gradients in number density and pressure across the terminators suggest that the subsolar to antisolar circulation of Dickinson and Ridley does occur in the thermosphere of Venus. Horizontal flow velocities are likely to reach sound speeds ($\sim$200 m/s) across the terminators from day to night (Niemann et al., 1980). However, as yet there is no direct measurement of wind velocities in the thermosphere of Venus. Betz et al. (1976, 1977) measured line of sight wind velocities near the lower boundary of the thermosphere (100-120 km) using Doppler shifts of 10 μ CO_2 emission spectra observed across the disk of Venus. They conclude that the $\sim$ 115 km region of the Venus atmosphere is roughly characterized by symmetric subsolar to antisolar flow with 25-130 m/s wind velocities and considerable temporal variability. Betz et al. found no evidence of zonal circulation ($\lesssim$ 10 m/s) at 115 km altitude. In contrast, Mayr et al. (1980) suggest that offsets of He, O and H maximum number densities from the antisolar point (Niemann et al., 1980; Brinton et al., 1979) indicate extension of 50 m/s zonal flow to altitudes in excess of 160 km.

2.1.3 70-120 km

The circulation of the mesosphere of Venus (for our purposes defined as 70-120 km) is more poorly constrained, by both theory and measurements, than either the lower or upper atmosphere of Venus. Hence there is much contradiction among proposed models of circulation for this region. The mesosphere is likely characterized by transitional circulation between the predominantly zonal flow of the lower atmosphere ($\lesssim$ 70 km) and the subsolar to antisolar circulation of the thermosphere ($\gtrsim$ 120 km). It remains unclear whether significant zonal circulation extends through the mesosphere into the thermosphere of Venus. The highest altitude for which zonal circulation has been measured is in

the region of 70-80 km (Betz et al., 1977) from Doppler shifts of 10 μ ^{13}CO spectra. Betz et al. find average retrograde zonal circulation of 90 ± 7 m/s and significant temporal variation between 50 and 150 m/s. However, Betz et al. also report average vertical velocities of 45 m/s in the same altitude region. Such high vertical velocities in the 20 mbar level of a planetary atmosphere are surely unphysical. In addition Betz et al. find polar to equatorial flow on the order of 0-120 m/s with striking asymmetry between the north and south poles.

Present theoretical modeling of circulation in the mesosphere is based upon measurements of mesospheric temperature and pressure profiles as determined by Pioneer Venus probe entry data (Seiff et al., 1980) and Pioneer Venus Orbiting Infrared Radiometry (OIR) observations (Taylor et al., 1980). The probe data are limited by poor global coverage, as only 4 regions over the globe of Venus were sampled. Comparing the north (latitude = 59.3°N) and day (latitude = 31.2°S) entry pressure profiles, Seiff et al. found higher relative atmospheric pressures at all altitudes between 65 km and 120 km for the lower latitude day profile (i.e. constant pressure surfaces slope downwards from the equator to the poles). On the basis of this comparison Seiff et al. proposed that the global latitudinal gradient of atmospheric pressure above 65 km is in the sense of cyclostrophic balance with strong zonal circulation. Assuming cyclostrophic balance and a lower boundary zonal velocity of 150 m/s at 70 km altitude, they derive zonal wind velocities which remain above 100 m/s up to an altitude of 100 km. More recently, Seiff and Kirk (1982) analyzed the nightside entry pressure profile and find that zonal flow decreases to zero near 100 km altitude. Seiff (1982) also indicates that subsolar to antisolar flow should predominate above 100 km altitude.

The OIR data are far more global in coverage although the altitude resolution is considerably reduced from the probe data. Taylor et al. (1980) determine that the global latitudinal geopotential gradient reverses sign from the behavior measured by Seiff et al. for the day and north probes so that at altitudes above ~ 70-80 km isobars are actually inclined downwards from the poles to the equator. For such a case the pressure gradient cannot be balanced by cyclostrophic flow. Elson (1979) constructed circulation models on the basis of the IOR determined pressure surfaces and concludes that the strong zonal flow of the lower atmosphere must be replaced by equally strong meridional flow (from the poles to the equator) in the mesosphere of Venus. The altitude at which this transition occurs ($\gtrsim$ 75 km) is a function of a number of model parameters, of which the most important are the lower boundary (70 km) zonal velocity and latitude. The transition is also quite abrupt, occurring over an ~ 5 km altitude interval.

At present it would appear that both modeling and measurements of the circulation of the Venus mesosphere are incomplete and somewhat contradictory. The mesosphere may be characterized by zonal flow, meridional flow, subsolar to antisolar flow, or variable contributions from each of these circulation patterns.

2.2 Chemistry

2.2.1 Observations

The bulk of the Venus atmosphere is composed of CO_2 (~ 96%) with N_2 (~ 4%) as the next most abundant species (e.g. Hoffman et al., 1980). The third most abundant species in the mesosphere of Venus is CO (~ 0.01%), which is the best measured trace component of the mesosphere due to extensive microwave

measurements (Waters et al., 1975; Gulkis et al., 1977; Muhleman et al., 1978; Schloerb et al., 1980; Wilson et al., 1981). Observations of the chemistry of the mesosphere are in fact essentially limited to microwave spectra of CO. However, a number of important ground based and spacecraft measurements bear upon the abundances of H_2O, HCl, HF, CO, O_2 and SO_2 at altitudes between 60 and 70 km in the Venus atmosphere.

On the basis of infrared absorption lines, Fink et al. (1972) reported disk average water vapor mixing ratios of $0.6-1.0 \times 10^{-6}$ at an altitude of ~ 60 km. Barker (1975) measured 8798 Å absorption lines to determine the H_2O column abundance at ~ 60 km altitude as a function of time, Venus phase, and position of the Venus disk and found water vapor mixing ratios in the range 0.5×10^{-6} to 4×10^{-5}. He attributed much of the variation to patchiness in the cloud layers which may affect absolute water vapor abundances, and certainly affects the path lengths sampled by each spectrum. HCl, HF, and CO were measured by Connes et al. (1967, 1968) observing infrared absorption of solar radiation reflected from the cloud layers of Venus. Connes et al. (1967) found mixing ratios of $6 \pm 1.2 \times 10^{-7}$ and 5×10^{-9} for HCl and HF, respectively. The accuracy of the HF measurement was reported to be "within a factor of two." Connes et al. (1968) also determined a CO mixing ratio of $4.5 \pm 1 \times 10^{-5}$ in approximately the same region of the Venus atmosphere (~ 60 km).

Only upper limits have been reported for O_2 which appears to be significantly depleted relative to CO (see page 11) between 60 and 70 km in the Venus atmosphere. Traub and Carlton searched for O_2 absorption lines of scattered solar radiation at 7635 Å. Their failure to detect O_2 places an upper limit of 10^{-6} for the mixing ratio of O_2 in the region of 60-70 km (Traub and Carlton, 1974). From recent observations Trauger and Lunine (J. Trauger, personal

communication, 1982) have determined an even more severe limit of 5×10^{-7} for the mixing ratio of O_2 in this region.

The chemistry of the Venus atmosphere between 60 and 140 km was not well sampled by the Pioneer Venus experiments. The Pioneer Venus orbiter UV spectrometer confirmed the presence of SO_2 in the cloud region of Venus (Stewart et al., 1979; Esposito et al., 1979), which was previously detected from Earth base measurements (Barker, 1979; Conway et al., 1979). From detailed study of Pioneer Venus UVS images of Venus, Esposito and Gates (1981) find significant spatial and temporal variation of SO_2 abundance at the ~40 mbar level ranging from "less than 5 ppb to more than 100 ppb." They find a weighted average abundance of 2×10^{-8} with SO_2 scale heights between 1 and 3 km at the 40 mbar pressure level. The UV spectral reflectances measured by the Pioneer Venus UVS instrument have also been used to infer the existence of a second UV absorber in the upper cloud region of Venus (~60 km). Pollack et al. (1980) suggest that a Cl_2 abundance of 10^{-6} would match the spectral reflectance of Venus above 0.32 μm, but the presence of Cl_2 is yet to be definitively proven.

2.2.2 Modeling

Photochemical modeling of the mesosphere of Venus was initially motivated by the relatively low abundance of CO measured by Connes et al. (1968). On the basis of the very slow rate of CO recombination by

$$CO + O + M \rightarrow CO_2 + M$$

one would expect CO abundance to be substantially greater than 4×10^{-5} in the mesosphere of Venus (e.g. Prinn, 1971). McElroy and Donahue (1972) proposed the catalytic scheme

$$CO + OH \rightarrow CO_2 + H \qquad (A)$$

to explain a similar depletion of CO in the Mars atmosphere. For Mars, the OH is ultimately supplied by photodissociation of H_2O. For the case of Venus the ultimate source of the catalytic odd hydrogens is most likely photodissociation of HCl (Prinn, 1971). Furthermore, catalytic cycles involving Cl rather than the odd hydrogen may control the recombination of CO in the Venus mesosphere (Krasnopolsky and Parshev, 1981; Yung and DeMore, 1982).

$$COCl + O_2 \rightarrow CO_2 + ClO \qquad (B)$$

The particular catalytic scheme that dominates in the mesosphere of Venus appears to depend on the H_2 abundance in the Venus mesosphere. Large amounts of H_2 lead to recombination of free chlorine into HCl and diminished importance for (B); very low levels of H_2 allow substantial buildup of free Cl (perhaps providing the Cl_2 of Pollack et al., 1980), driving cycle (B) as the major recombination cycle of CO (Yung and DeMore, 1982). The abundance of H_2 in the atmosphere appears to be unsettled at present. Measurements of the upper atmosphere detected a mass 2 ion which may be either H_2^+ (Kumar et al., 1981) or D^+ (McElroy et al., 1982). If H_2 exists in the upper atmosphere in substantial amounts (20 ppm from Kumar et al.) then it must be supplied in the mesosphere by photochemistry, as thermochemistry cannot supply the required amount (Yung and DeMore, 1982).

Regardless of the particular cycle that drives recombination of CO, the very low abundance of O_2 in the lower mesosphere cannot be explained by recombination of CO alone. If recombination of CO were the only sink for O_2, one would expect the ratio $[O_2]/[CO]$ to be $\sim \frac{1}{2}$. Based on the measurements of Connes et al. (1968) and Traub and Carlton (1974), the ratio $[O_2]/[CO]$ is < 0.02.

Using the more recent upper limit of $[O_2] < 5 \times 10^{-7}$ from Trauger and Lunine (1982), the ratio $[O_2]/[CO]$ becomes < 0.01.

Sze and McElroy (1975) simply assumed a very rapid sink of O_2 at the lower boundary of their photochemical model (62 km). They set the concentration of O_2 equal to zero at this boundary with the assumption that formation of H_2SO_4 provided an adequate sink for O_2 and determined a minimum value for the eddy diffusion coefficient (3×10^5 cm^2/sec) in the lower stratosphere of Venus based on the upper limit of O_2 from Traub and Carlton (1974).

Winick and Stewart (1980) attempted to photochemically model the sulfur chemistry of the lower mesosphere of Venus in addition to O, H, Cl and C chemistry. While Winick and Stewart adequately reproduced the SO_2 abundances measured by the Pioneer Venus UVS, they could not reproduce the rapid depletion of O_2 in the lower mesosphere of Venus. Yung and DeMore (1982) succeeded in modeling both the SO_2 and O_2 abundances (as measured by Traub and Carlton) by including the important O_2 bond breaking reactions

$$SO + HO_2 \rightarrow SO_2 + OH$$

$$COCl + O_2 \rightarrow CO_2 + ClO$$

Yung and DeMore also required increased eddy mixing below 90 km relative to the form

$$K \propto (\text{atmospheric number density})^{-\frac{1}{2}}$$

which was used by Winick and Stewart. Faster vertical mixing is required to transport O_2 down to the H_2SO_4 forming region of the atmosphere (60-70 km).

At present there remain three important unanswered questions regarding the photochemistry of the Venus mesosphere. Firstly, there is the lower limit for O_2 as determined by Trauger and Lunine (1982) which is still roughly a factor of 2 less than the O_2 abundances predicted by Yung and DeMore. Secondly, is Cl or OH the important catalytic reagent in the mesosphere of Venus? Finally, what are the constraints applied by CO mixing profiles and their variability as determined from microwave measurements? We will address the latter question in the following sections.

3. OBSERVATIONS AND ANALYSIS OF CO MICROWAVE SPECTRA

To date, upwards of 15 CO microwave spectra of Venus have been published or presented in some form. The majority of these spectra have been presented in talks, and there have been only limited efforts to intercompare the whole body of CO microwave data. In this part of the data analysis section we present and analyze our own spectra with the partial intent of elucidating the information available in CO microwave spectra. Subsequently (section 4), we compare the entire body of available microwave spectra of CO in the Venus mesosphere in order to study the temporal behavior of the distribution of CO in the mesosphere of Venus.

We have obtained measurements of six microwave spectra of CO in the mesosphere of Venus, taken between December 1978 and November 1982. Two of the spectra (Figures 2 and 3) are of the $J = 0 \rightarrow 1$ rotational transition of CO. The other four spectra (Figures 1, 4 and 5) measured the $J = 1 \rightarrow 2$ transition, for which the absorption coefficient is eight times increased over the absorption coefficient for the $J = 0 \rightarrow 1$ transition. Before proceeding with a discussion of the analysis of these spectra, we provide a brief description of each measurement and a description of the calibration of the spectra.

3.1 The Observations

3.1.1 December 1978 Spectrum

We obtained the first $J = 1 \rightarrow 2$ spectrum (230 gHz; 1.3 mm) of CO on Venus, which was observed for us by Dr. G.R. Knapp and Prof. T.G. Phillips. The spectrum (Figure 1) was measured on December 2, 1978 using a hot electron bolometer mixer receiver (Phillips and Jefferts, 1973) mounted on the first of the 10.4 meter telescopes at Owens Valley Radio Observatory (OVRO). Frequency

resolutions of 1 mHz and ½ mHz were achieved by stepping the variable width bandpass of the hot electron bolometer in frequency. The maximum total bandwidth for the spectrum was ± 16 mHz about the line center of the J = 1 → 2 transition for CO. Observing at 230 gHz, the OVRO millimeter telescope has a 30 arcsecond beamwidth (HPFW), compared to the 50 arcsecond diameter of Venus at the time of observation. The antenna beam was displaced by ~ 10 arcseconds east, west, north, and south (relative to the equator, central meridian of Venus) from the sub-Earth point on Venus in order to search for spatial variations of CO on Venus. No apparent differences in the spectra were noted, probably due to poor spatial resolution, saturation of absorption in the line center, and limited signal/noise, so that the spectra were averaged to form a single spectrum of higher signal/noise. At the time of the observations Venus was at a phase angle of 135°, approximately four weeks past inferior conjunction. The aspect of Venus was characterized by a bright morning crescent (relative to the retrograde motion of Venus) covering ~ 15% of the total disk area (see Figure 1).

3.1.2 May 1980 Spectrum

We observed the J = 0 → 1 transition of CO in the Venus mesosphere on May 28, 29 of 1980 using a room-temperature Schottky-diode receiver constructed by Prof. P. Wannier and mounted on the OVRO 10.4 meter antenna. A one-bit autocorrelator assembled by Prof. A. Moffet was used to produce the spectrum of Figure 2. The spectral resolution is 195 kHz with a total bandwidth of ± 20 mHz about the J = 0 → 1 line center frequency of 115 gHz. The first twenty channels are very noisy in the spectrum of Figure 2 due to erratic behavior of the baseline produced by the autocorrelator in this region of the spectrum. Observing at 115 gHz, the half power-full width (HPFW) of the

antenna beam was 60 arcseconds, compared to the 50 arcsecond diameter of Venus at the time of observation. The phase of Venus was 145°. Venus exhibited a narrow evening crescent of illumination covering ~ 10% of the visible disk.

3.1.3 December 1980 Spectrum

We measured the J = 0 → 1 transition of CO in the Venus atmosphere again on December 12, 1980, observing with the second 10.4 m OVRO antenna. The observed spectrum (Figure 3) was measured with a helium cooled SIS receiver (Phillips et al., 1980) and an acousto-optical spectrometer (Masson, 1982). The total bandwidth was ± 50 mHz about the line center frequency with a spectral resolution of 200 kHz. The antenna beam (~ 60 arcseconds) was substantially larger than the observed angular diameter of Venus (12 arcseconds). The phase angle of Venus was 40°, with the morning terminator visible and approximately 88% of the visible disk illuminated.

3.1.4 January 1982 Spectrum

Our most accurate measurement (in terms of signal-to-noise and baseline) of CO in the mesosphere of Venus was taken on January 24 and 25, 1982 at the NRAO 36 foot radio telescope at Kitt Peak National Observatory, Arizona. For detection purposes we used the NRAO 200-240 gHz mixer-receiver and two sets of 256 channel Kitt Peak filterbanks which were operated in parallel to produce the J = 1 → 2 spectra of Figure 4. Over the course of two observing days we obtained CO spectra of 1 and 1/2 mHz resolution with total bandwidths of ± 128, and ± 64 mHz, respectively. Operating at 230 gHz, the HPFW of the NRAO antenna was ~ 60 arcseconds, equal to the observed angular diameter of Venus (61 arcseconds). Venus was at a phase angle of 167-169°, just several days past inferior conjunction. Less than 2% of the observed disk of Venus was illuminated.

3.1.5 September, November 1982 Spectra

We obtained our most recent CO spectra of Venus from Dr. Edward Sutton who observed Venus on September 6 and November 4, operating with his newly developed 230 gHz SIS cooled receiver at OVRO. These J = 1 → 2 spectra have total bandwidths of 500 mHz (with 1 mHz resolution) obtained with a second acousto-optical spectrometer developed by Dr. Colin Masson. Hence these newest spectra contain the largest bandwidth so far measured for CO microwave spectra of Venus. Unfortunately integration times for these spectra were short so that signal-to-noise ratios are poor. A more serious problem is introduced by large residual standing waves of short (5-10 mHz) and long (200-500 mHz) periods which could not be removed from the spectra (see Figure 5). Nevertheless these September and November spectra are potentially important as they measure respective Venus phases of 15° and 0° (i.e. just before and directly at superior conjunction). At these phase angles, Venus is greater than 95% illuminated.

A summary of the important observational parameters pertaining to each of the above CO microwave measurements is presented in Table I.

3.2 Observing Procedure and Calibration

All of the above spectra were observed by position switching on Venus. Position switching is the standard observing procedure for absorption spectra (see Appendix I) as opposed to frequency switching for emission spectra. Spectra are alternately measured with the antenna beam centered on Venus and offset in azimuth from the position of Venus (offset = 5 arcminutes for our observations). These on-off pairs of spectra are differenced to form individual spectra which are in turn averaged to form the total spectra of Figures 1-5.

Table I. Observational Parameters for CO Microwave Spectra of Figures 1-5

Date	ν_o (GHz)	D (arcsec)	k (%)	α (degrees)	Term	B (MHz)	Δ (MHz)
Dec. 2, 1978	230	49.5	15	135	morning	32/16	1/.5
May 28-29, 1980	115	50	10	145	evening	20	.195
Dec. 12, 1980	115	11.8	88	40	morning	100	.2
Jan. 24-25, 1982	230	62	<2	168	morning	256/128	1/.5
Sept. 6, 1982	230	10.3	96	22	morning	500	1
Nov. 4, 1982	230	9.8	100	1		500	1

ν_o = centerline frequency, D = angular diameter of Venus, k = illuminated fraction of Venus, Term = visible terminator of Venus, B = total observed bandwidth, Δ = spectral resolution

FIGURE 1: The first J = 1 → 2 microwave spectrum of mesospheric CO on Venus taken on December 2, 1978. The phase angle (φ) of Venus was 135° and the illuminated fraction (k) of the Venus disk was 0.15. Spectra of 1 mHz and 1/2 mHz frequency resolution measured. The dots and the solid line indicate the measured and best fit synthetic spectra, respectively.

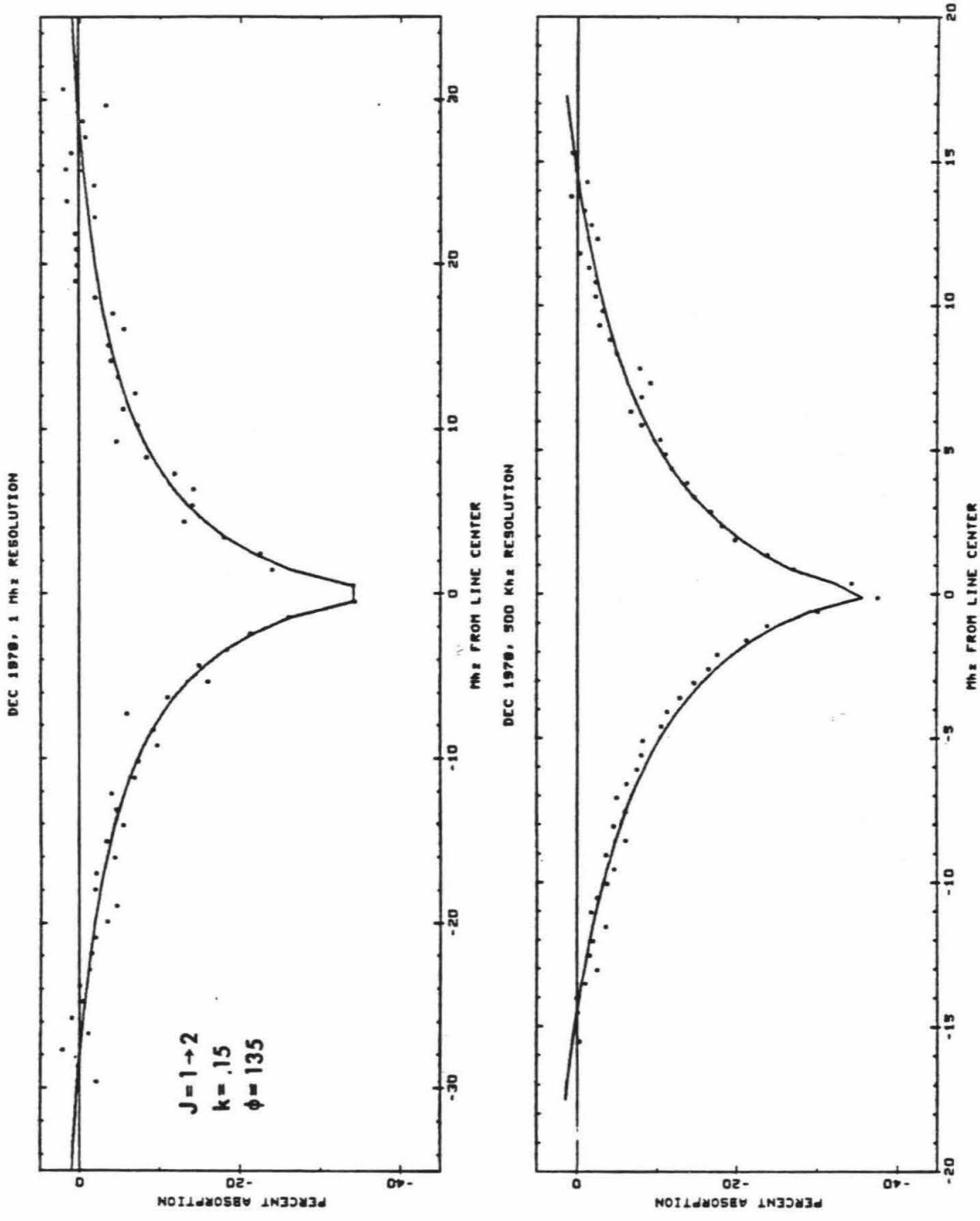
DEC 1978, 1 Mhz RESOLUTION
PERCENT ABSORPTION
0
-20
-40
Mhz FROM LINE CENTER
30
20
10
0
-10
-20
-30
J=1→2
k=.15
φ=135
DEC 1978, 500 Khz RESOLUTION
PERCENT ABSORPTION
0
-20
-40
Mhz FROM LINE CENTER
20
15
10
5
0
-5
-10
-15
-20

FIGURE 2: $J = 0 \rightarrow 1$ spectrum of Venus mesospheric CO measured on May 28 and 29, 1980. Description of figure symbols is the same as in Figure 1. Spectral resolution is 195 kHz.

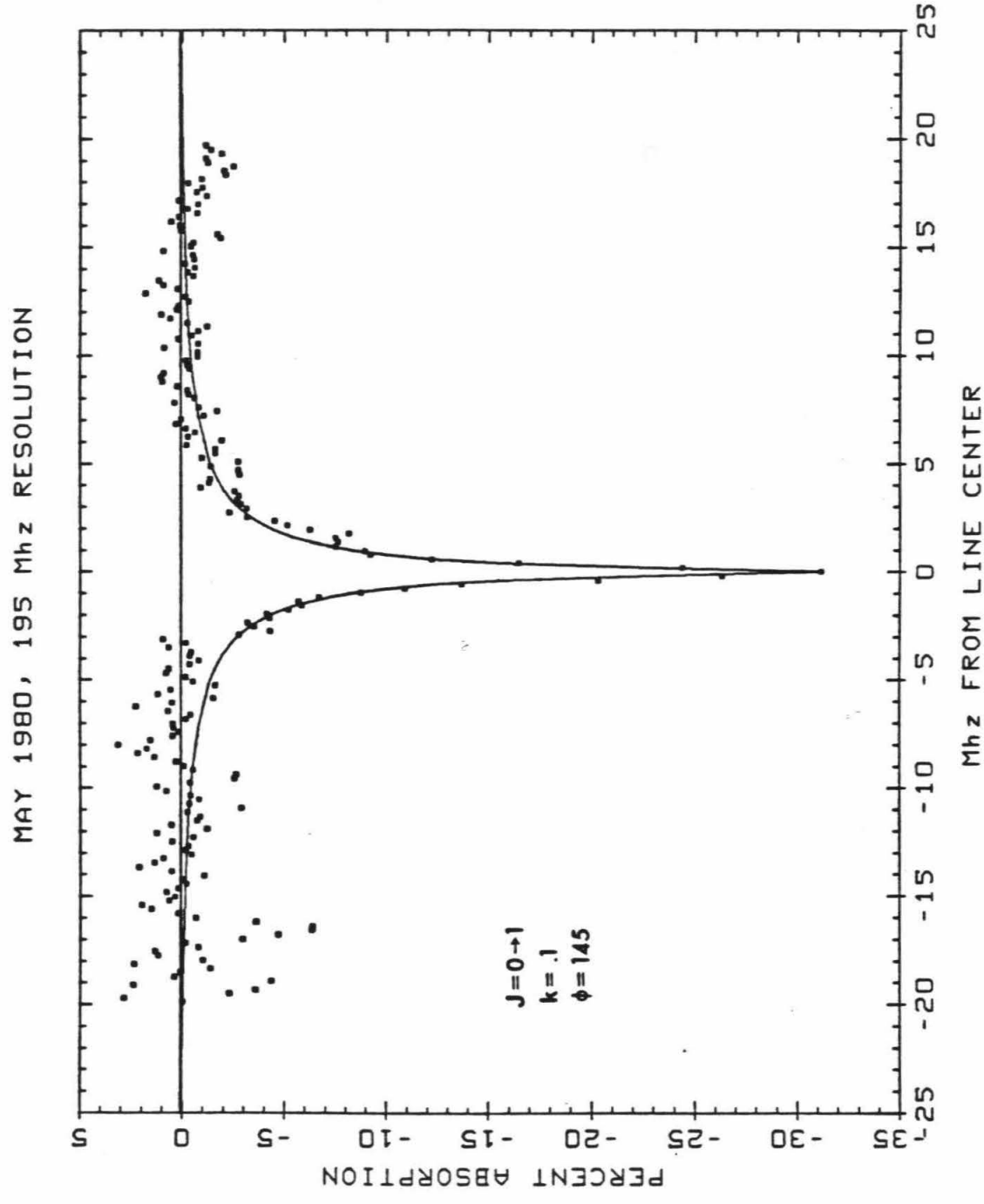
MAY 1980, 195 Mhz RESOLUTION
PERCENT ABSORPTION
Mhz FROM LINE CENTER
J=0→1
k=.1
φ=145
5
0
-5
-10
-15
-20
-25
-30
-35
25
20
15
10
5
0
-5
-10
-15
-20
-25

FIGURE 3: $J = 0 \rightarrow 1$ spectrum of Venus mesospheric CO measured on December 12, 1980. Description of figure symbols is the same as in Figure 1. Spectral resolution is 200 kHz.

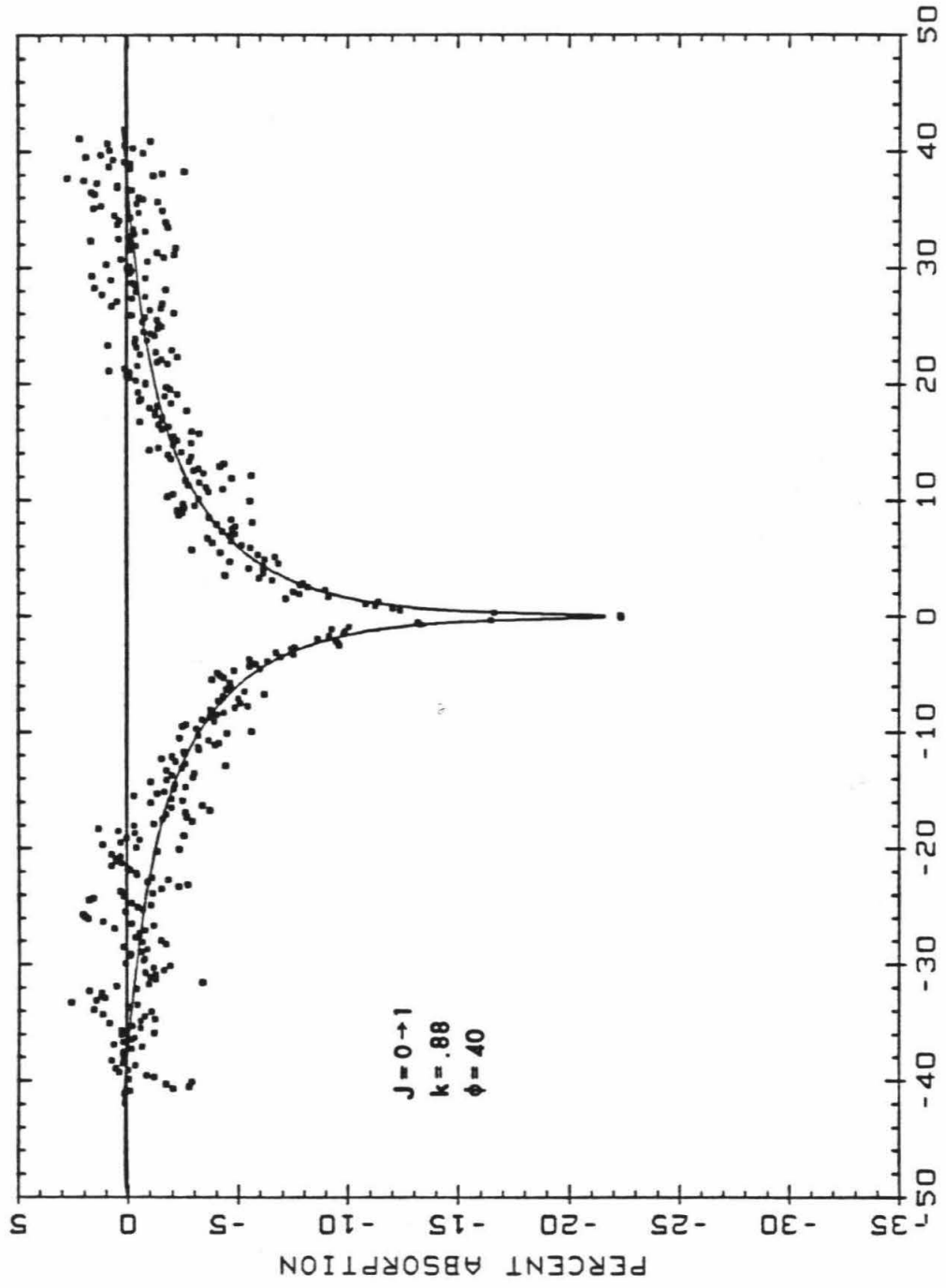
DEC 1980, 200 Khz RESOLUTION
PERCENT ABSORPTION
5
0
-5
-10
-15
-20
-25
-30
-35
J=0→1
k=.88
ϕ=40
-50
-40
-30
-20
-10
0
10
20
30
40
50
Mhz FROM LINE CENTER

FIGURE 4: Very high signal-to-noise ratio, J = 1 → 2 spectrum of Venus mesospheric CO measured on January 24 and 25, 1982. Description of figure symbols is the same as in Figure 1. Spectral resolutions of 1 and 1/2 Mhz were measured.

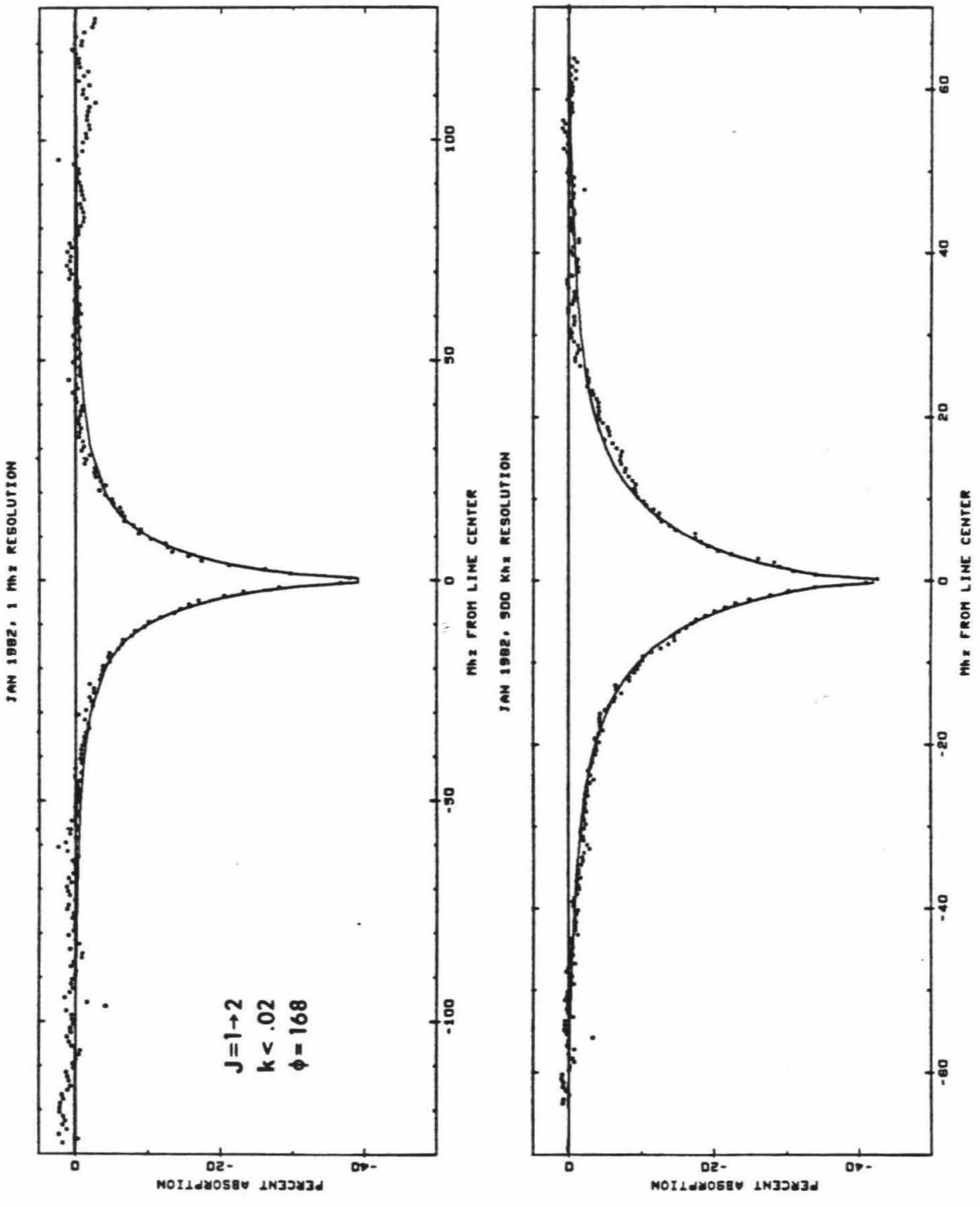
JAN 1982, 1 Mhz RESOLUTION
PERCENT ABSORPTION
0
-20
-40
-100
-50
0
50
100
Mhz FROM LINE CENTER
J=1→2
k < .02
φ = 168
JAN 1982, 500 Khz RESOLUTION
PERCENT ABSORPTION
0
-20
-40
-60
-40
-20
0
20
40
60
Mhz FROM LINE CENTER

FIGURE 5: J = 1 → 2 spectra of mesospheric CO on Venus taken on September 6 and November 4, 1982. Note that the measured spectra are indicated by the solid lines whereas the synthetic, fitted spectra are shown by the dotted lines. Spectral resolution is 1 mHz for both measurements. Both of these broad bandwidth (512 mHz) spectra are seriously affected by standing waves and low signal-to-noise ratios.

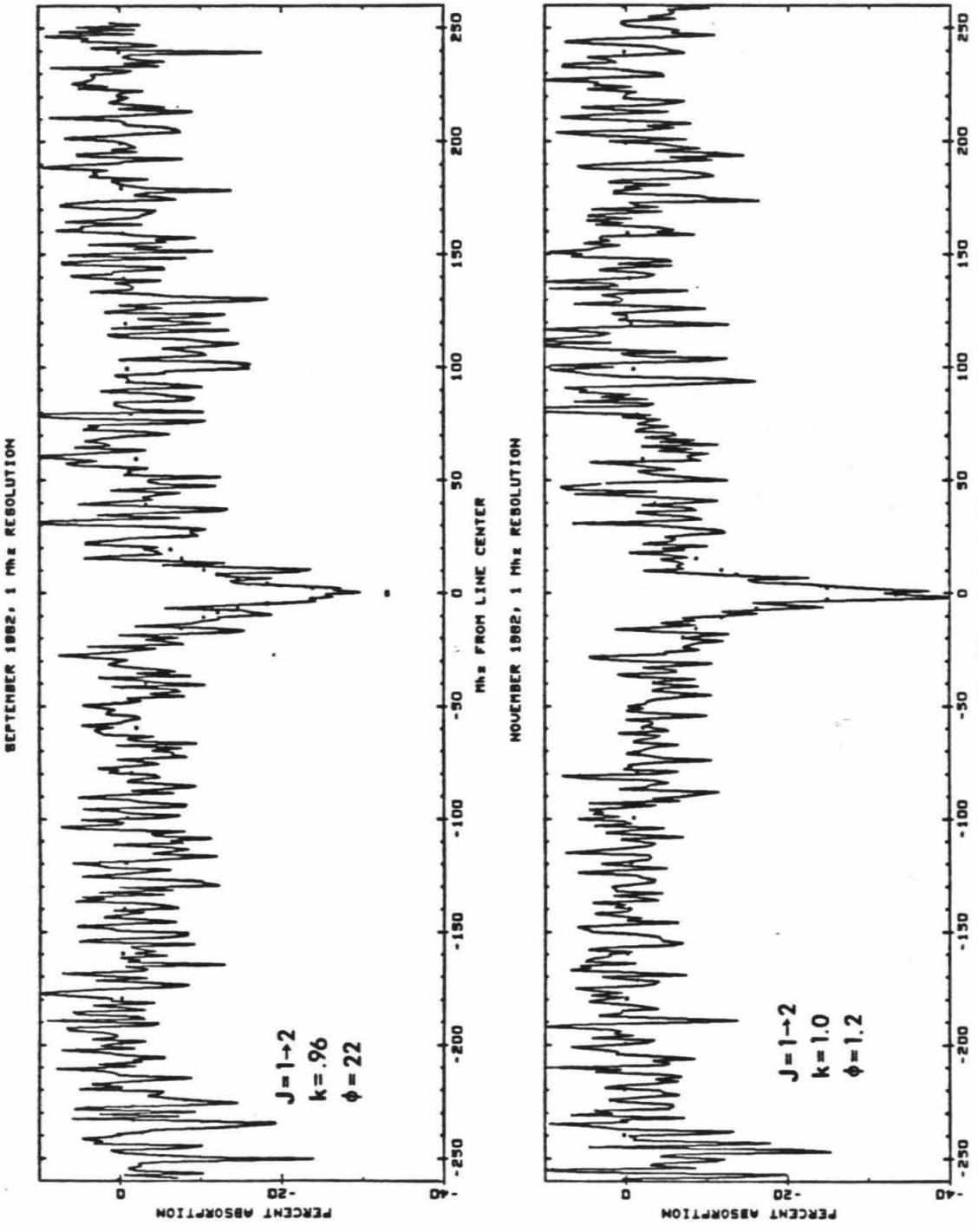
SEPTEMBER 1982, 1 Mhz RESOLUTION
J=1→2
k=.96
ϕ=22
PERCENT ABSORPTION
0
-20
-40
250
200
150
100
50
0
-50
-100
-150
-200
-250
Mhz FROM LINE CENTER
NOVEMBER 1982, 1 Mhz RESOLUTION
J=1→2
k=1.0
ϕ=1.2
PERCENT ABSORPTION
0
-20
-40
250
200
150
100
50
0
-50
-100
-150
-200
-250
Mhz FROM LINE CENTER

Position switching removes emission from the earth atmosphere and the system (antenna, spillover, receiver, etc.) so that the difference spectra are a direct measure of the continuum of Venus diminished by the frequency dependent absorption of CO in the atmosphere of Venus. One of the more important criteria for position switching is that the on and off source spectra sample nearly identical atmospheric and system conditions for adequate removal of their contributions to the detected power. For reasonable weather conditions alternating 30 second scans on and off source remove sky and system levels very effectively.

However, for strong continuum sources such as Venus one has the additional problem of the effect of standing waves within the antenna/receiver system that may not be adequately removed by position switching. Standing waves, which appear as periodic ripples in the baselines of the spectra, are generated by reflection of continuum radiation between the primary antenna dish and subreflector or subreflector supports. Strong continuum sources such as Venus enhance the power of standing waves in the on scans relative to the off scans. Such waves may be reduced by using several LO frequencies (which is not practical for the broad CO spectra of Venus), moving the subreflector over a $\lambda/4$ range, or by simple averaging in time of many spectra. If the phase of the standing wave drifts in time, averaging over a long period of time tends to beat down the standing waves.

The spectra of Figures 1-4 were not strongly affected by standing waves. The spectra of Figures 3 and 4 contained residual standing waves of order $< 5\%$ of the line-to-continuum depth. These residual standing waves were removed by choosing a single frequency (in units of the number of channels in the spectrum) and solving for the phase and amplitude of the standing wave, which was then subtracted from the spectrum. Only channels near the flat end regions of

the spectra were used to solve for the standing waves. One can still note residual ripples in the 1 mHz resolution spectrum of Figure 4, where the standing wave did not remain coherent across the bandwidth and, hence, was not effectively removed. The 1982 spectra of Figure 5 show substantial standing waves which could not be corrected for and which introduce serious limitations in the analysis of these spectra.

The spectra of Figure 4 required a special observing procedure due to the filter banks employed to measure these spectra. The strong continuum power of Venus leads to a substantial difference in the power levels of the on and off spectra. This difference is large enough to begin introducing non- linear response in the filter banks. Variable non-linear response in each of the channels effectively introduces artificial noise in the difference spectrum (Dr. R. Howard, personal communication, 1981). In order to avoid this problem, we used a gain modulator to match the power levels of the on and off spectra. The gain modulator removed much of the continuum level in the on spectra. Because the continuum level is required for calibration purposes, we frequently measured on-off pairs without the gain modulator to determine the continuum level. We found that this procedure optimized signal/noise for Venus spectra taken at Kitt Peak (e.g. see Clancy and Muhleman, 1982).

For analysis purposes, CO microwave absorption spectra of Venus need not be calibrated in absolute temperature or flux units. As long as the relative levels of the continuum and absorption line are retained, the spectra may be analyzed to determine profiles of CO mixing ratios in the Venus mesosphere. Absorption for the spectra of Figures 1-5 is given in units of fraction of the continuum.

1 – (measured spectrum/continuum)

where the continuum is taken as the average level over some portion of the wings of the measured spectrum. The units of the spectra are then fractional or percentage absorption of the continuum of Venus. We note that due to the finite bandwidth of the measurements, the level in the wings of the spectra is not actually the microwave continuum but includes absorption due to CO. For consistency in our analysis, we normalize our synthetic spectra to zero over the same frequency region of the wings as used for the measured spectra.

However, there is an additional complication in the handling of the measured spectra. One of the important features of heterodyne observations is the introduction of double side bands (see Appendix I). Basically, two bandpasses (sidebands) separated in frequency by twice the IF of the observation are folded together to constitute the single measured bandpass. Thus, the measured power spectrum includes the continuum roughly twice relative to the CO absorption line which is located in either the upper or lower sideband only. If the gain of the receiver and the opacity of the atmosphere are identical for both sidebands, then the true absorption spectrum is exactly twice as deep as the measured absorption. For our December 1978 measurement, the IF was essentially zero so that the receiver gain and atmospheric opacity for the two sidebands were identical. In fact, atmospheric opacity remains very constant over frequencies near 230 gHz (Figure B in appendix I) so that for all of the $J = 1 \rightarrow 2$ spectra (December 1978, January, September and November 1982), atmospheric opacity should be equal for the two sidebands. We further note that for all of our measurements, the receivers were tuned to maintain gain balance for the sidebands.

The main concern for sideband corrections is the considerable gradient in frequency for atmospheric opacity near the 115 gHz (J = 0 → 1) transition, which is located on the broad shoulder of the 118 gHz terrestrial O_2 line (Figure B in appendix I). For our J = 0 → 1 spectra (May, December 1980) we centered the upper sideband on 115 gHz in order to minimize the difference in atmospheric opacities between the two sidebands ($\tau_{\text{atmosphere}} < 0.3$ for our observations). The sideband correction factor is (Appendix I)

$$1 + \exp(-\Delta\tau/\mu) \qquad (1)$$

for equal receiver gains in the two sidebands. $\Delta\tau$ is the difference in atmosphere opacities for the two sidebands and μ is the cosine of the observing zenith angle. Using the theoretical O_2 opacities of Rosenkranz (1975) we find $\Delta\tau = 0.18$ for an average sideband correction factor of 2.3 for the J = 0 → 1 spectra. We note that the signal may be placed in the lower sideband so that the upper sideband falls on top of the terrestrial O_2 line (depending on the IF of observation). In this case $\Delta\tau \to \infty$ and the sideband correction factor approaches 1. The terrestrial O_2 line is effectively used as a sideband rejection filter for the sideband without the absorption line (e.g. Schloerb et al., 1980). We also note that sideband rejection filters may also be used, although we did not have access to one.

In any case, the form of (1) indicates that calibration of the spectra is not terribly sensitive to the variation of atmospheric opacity between the sidebands. The J = 1 → 2 spectra of Figures 1 and 4 are corrected for the double sideband to better than 5%. The calibration of the May 1980 spectrum (Figure 2) is more uncertain (± 15%) because both the continuum and the absorption line were calibrated separately in the style of emission measurements (e.g. Ulich and Haas, 1976). The relative differences in calibration for the continuum and

absorption lead to added uncertainty in their quotient, which is presented in Figure 2.

As a final note on the CO microwave observations we point out the variable apparent velocity of Venus with respect to the rest frame of the observations. Both the orbital motions of Venus and the Earth and the rotation of the Earth require Doppler tracking of the observed CO line frequency in order to avoid frequency smearing of the spectra during averaging (Appendix II). The Doppler shift of the CO line frequency is illustrated in the $J = 1 \rightarrow 2$ spectrum of Figure 1 by the ~ 7 mHz displacement of the weak terrestrial CO line from the line center of CO absorption on Venus.

3.3 Analysis

The spectra of Figures 1-5 are produced by absorption of microwave radiation emitted from the hot, lower atmosphere of Venus ($\lesssim 60$ km). The absorption occurs predominantly in the relatively cold atmospheric region of 80-100 km altitude, where photodissociation of CO_2 leads to large concentrations of CO (~ 200 ppm). The widths and depths of absorption spectra depend on the altitude distribution of CO relative to the pressure-temperature profile of the mesosphere of Venus.

The basic tools for analyzing CO microwave spectra are:

1. Lower boundary brightness temperatures to specify the continuum flux of Venus
2. Profiles of atmospheric temperatures and pressures throughout the mesosphere of Venus

3. A radiative transfer program including the proper pressure-temperature dependent absorption coefficient for the rotational transitions of CO.

With the above tools one may solve for the distribution of CO in the mesosphere of Venus either by non-linear least squares inversion of the data (e.g. Schloerb et al., 1980) or by trial and error fitting of the data with synthetic spectra (e.g. Gulkis et al., 1977). We have adopted the latter method partly because the inversion problem is very complicated and time consuming on a computer. More importantly, inversion techniques so far developed (Schloerb et al., 1980; Wilson et al., 1981) provide almost no error analysis. We found that trial and error analysis is particularly useful in determining upper limits for CO mixing ratios below 80 km and above 95 km altitude. As a working procedure we determined monotonically increasing CO mixing ratios (at a resolution of 2 km steps in altitude) between 68 and 120 km altitude that yield best fits to our spectra in a least squares sense (see Figure 10). Subsequently we perturbed our derived mixing ratios at each altitude in order to test the sensitivity of our fits to the mixing ratio of CO at each altitude. By such procedure we arrived at the CO mixing profiles and error bounds of Figures 6, 7 and 8. Before discussing these profiles, we outline the important assumptions and features of the synthetic line fitting analysis.

3.3.1 Continuum Brightness Temperature of Venus

In order to analyze CO microwave spectra for mixing ratios of CO, one must know the absolute temperature difference between the microwave continuum of Venus and the CO absorbing-emitting region of the Venus atmosphere. The microwave continuum of Venus is produced by thermal emission in the lower atmosphere of Venus where roughly half of the radio opacity is due to CO_2

FIGURE 6: Altitude profiles (solid lines) of the volumetric mixing ratio of CO in the Venus mesosphere as derived from the $J = 0 \rightarrow 1$ spectra of Figures 2 and 3. The uncertainties in each of these profiles are shown by the respective boundaries drawn in as broken lines.

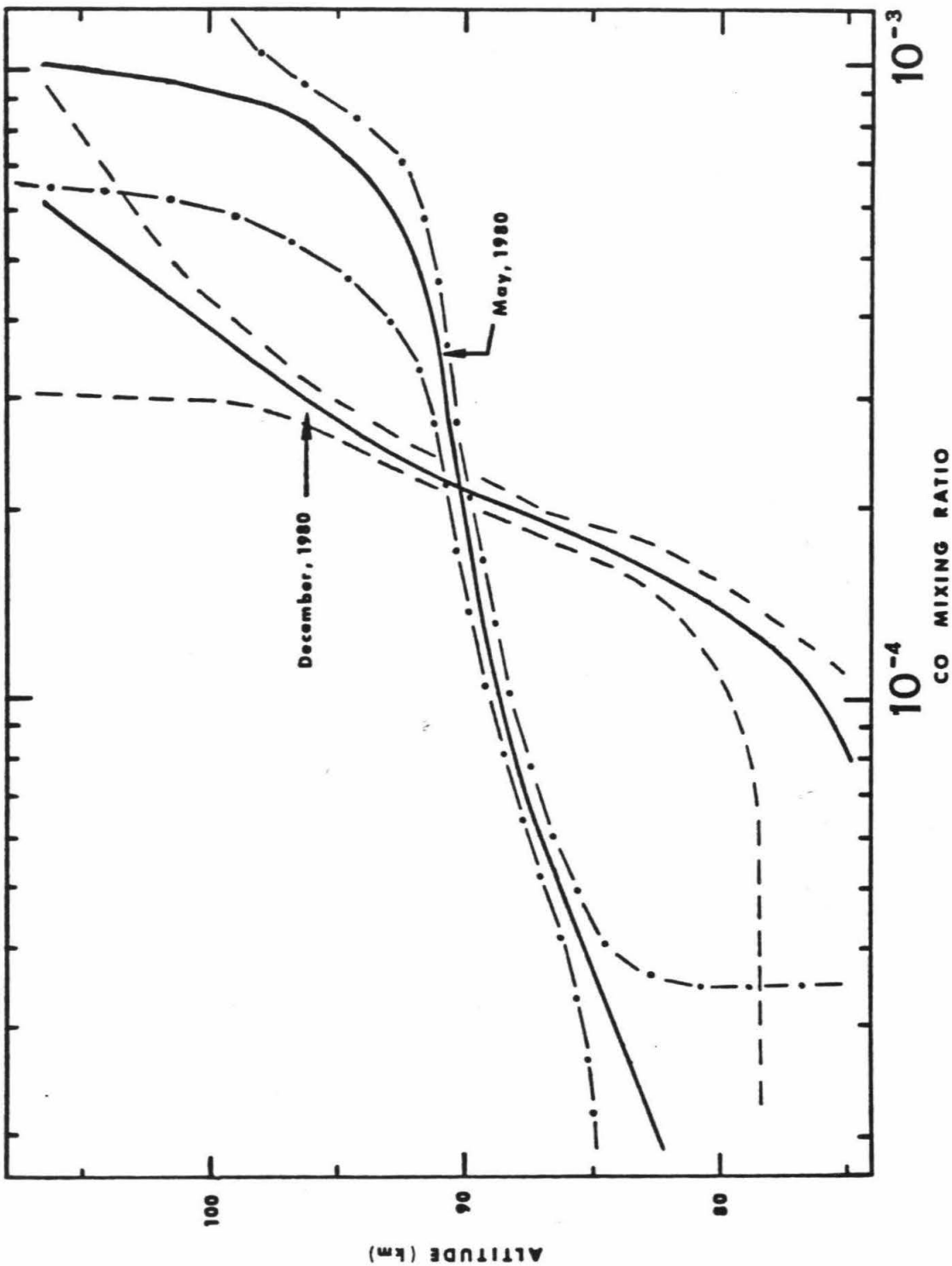
May, 1980
December, 1980
10^{-3}
10^{-4}
CO MIXING RATIO
ALTITUDE (km)
100
90
80

FIGURE 7: Altitude profiles (the solid and dotted lines) of the volumetric mixing ratio of CO in the Venus mesosphere as derived from the $J = 1 \rightarrow 2$ spectra of Figures 1 and 4. Uncertainty in the January 1982, profile is indicated by the dashed boundary lines. Uncertainty in the December 1978, profiles below 82 km altitude is shown by the dash-dotted boundary lines. Above ~ 87 km altitude uncertainty for both of these profiles is indicated by the dashed boundary lines.

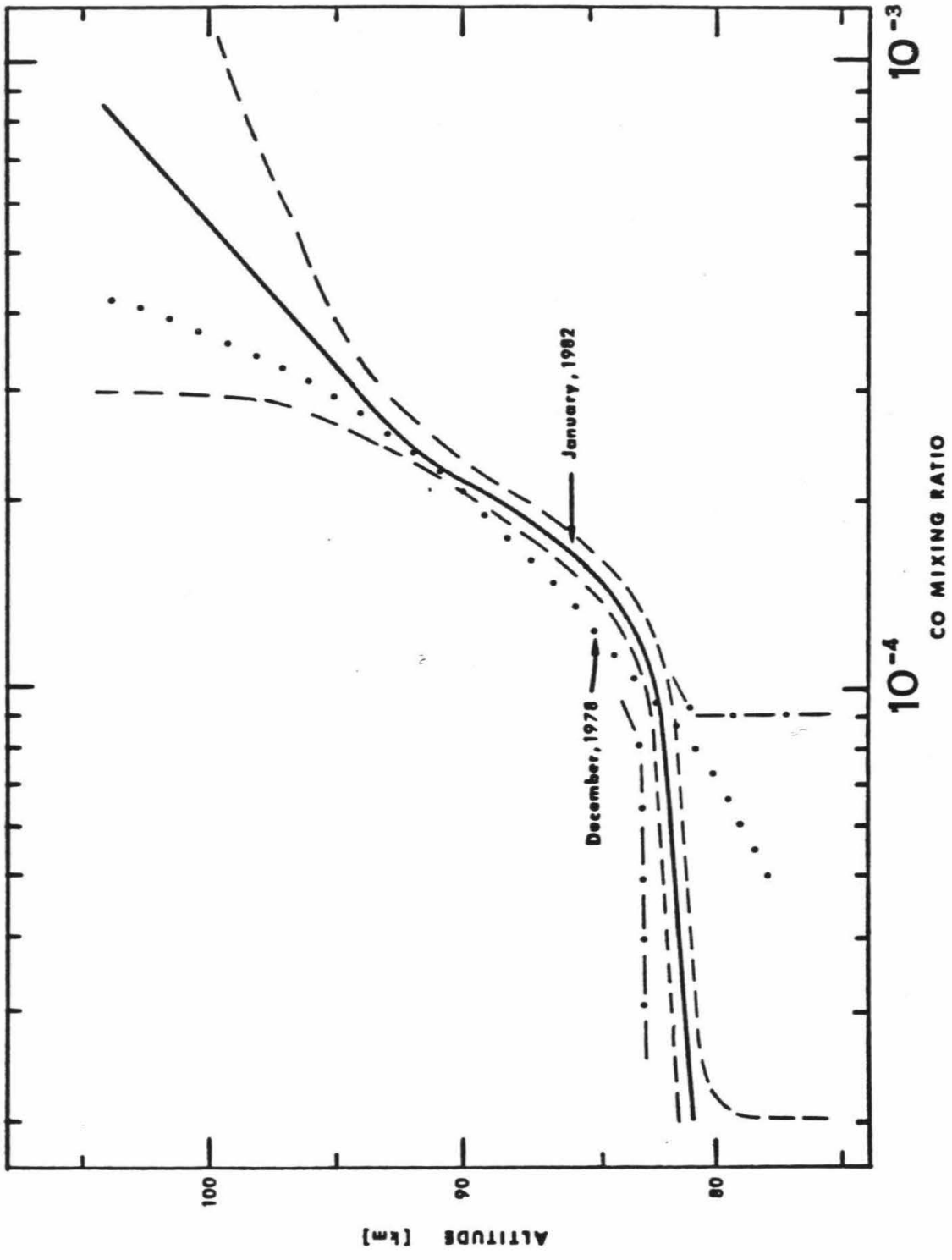
ALTITUDE [km]
100
90
80
10^{-4}
10^{-3}
CO MIXING RATIO
January, 1982
December, 1978

FIGURE 8: Altitude profiles (the solid and dotted lines, which overlap above ~ 87 km altitude) of the volumetric mixing ratio of CO in the Venus mesosphere as derived from the $J = 1 \rightarrow 2$ spectra of Figure 5. Uncertainty for both of these profiles is indicated by the dashed boundary lines.

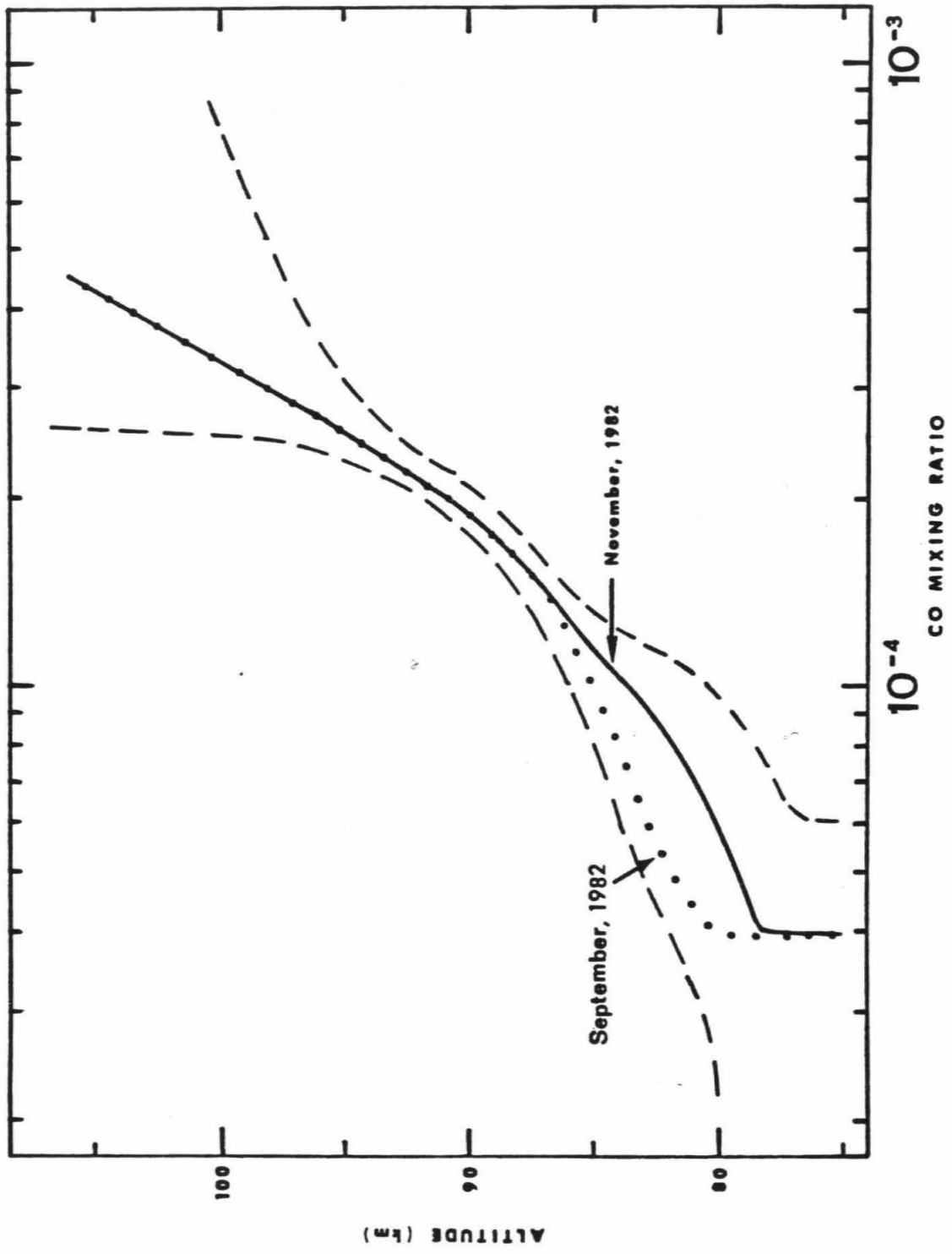
November, 1982
September, 1982
10^{-4}
10^{-3}
CO MIXING RATIO
ALTITUDE (km)
100
90
80

and another half to an as yet undefined absorber (Muhleman et al., 1979b). Muhleman et al. constructed a comprehensive radiative model of the atmosphere and surface of Venus that best fit a wide range of radio observations including radio brightness, spacecraft occultation, radar, and interferometric measurements. The model was constructed to agree with radio observations in the wavelength range of 1 to 78 cm but also provides consistent results down to a wavelength of 1 mm. We have used their model to specify 1.3 mm and 2.6 mm radio brightness temperatures over the disk of Venus. Model results indicate that, at normal incidence, continuum radiation at 1.3 mm (2.6 mm) decouples from the Venus atmosphere at an altitude of ~ 57 km (52 km) with a brightness temperature of 290 K (330 K). Corresponding disk brightness temperatures of 280 K (1.3 mm) and 318 K (2.6 mm) from the Venus model of Muhleman et al. are plotted against available microwave observations of Venus in Figure 8.

The uncertainties in these lower boundary continuum temperatures are less than ± 10% and introduce similar uncertainties in the CO mixing ratios determined from the spectra. The actual uncertainty introduced is a function of the assumed temperature-pressure profile of the atmosphere. We note that the very broad error bounds (Figure 6) below ~ 80-85 km and above 95 km are due to the specific nature of the radiative transfer. Uncertainties in assumptions for model continuum and atmospheric temperatures primarily introduce moderate (~ 20%) uncertainties in the absolute values of the CO mixing profiles.

3.3.2 Model Atmosphere

In order to calculate black body emission by mesospheric CO and the absorption coefficient of CO, which is pressure-temperature dependent, we must adopt a pressure-temperature profile for the mesosphere of Venus. Because the observations average over the observed hemisphere of Venus we should ideally

FIGURE 9: Microwave brightness temperatures of Venus at 0.41 mm (Lowenstein et al., 1977), 0.45 and 0.75 mm (Whitcomb et al., 1979), 1 mm (Werner et al., 1978), 1.4 mm (Rather et al., 1974), 1.7 mm (Rowan-Robinson et al., 1978), 2.1 and 3.5 mm (Ulich, 1974), 3.1 mm (Ulich et al., 1973), 8.6 mm (Kalaghan and Wulfsberg, 1968), and 9.55 mm (Hobbs and Knapp, 1971). The open circles at 1.3 and 2.6 mm represent model values from the atmospheric opacity model of Muhleman et al. (1979b).

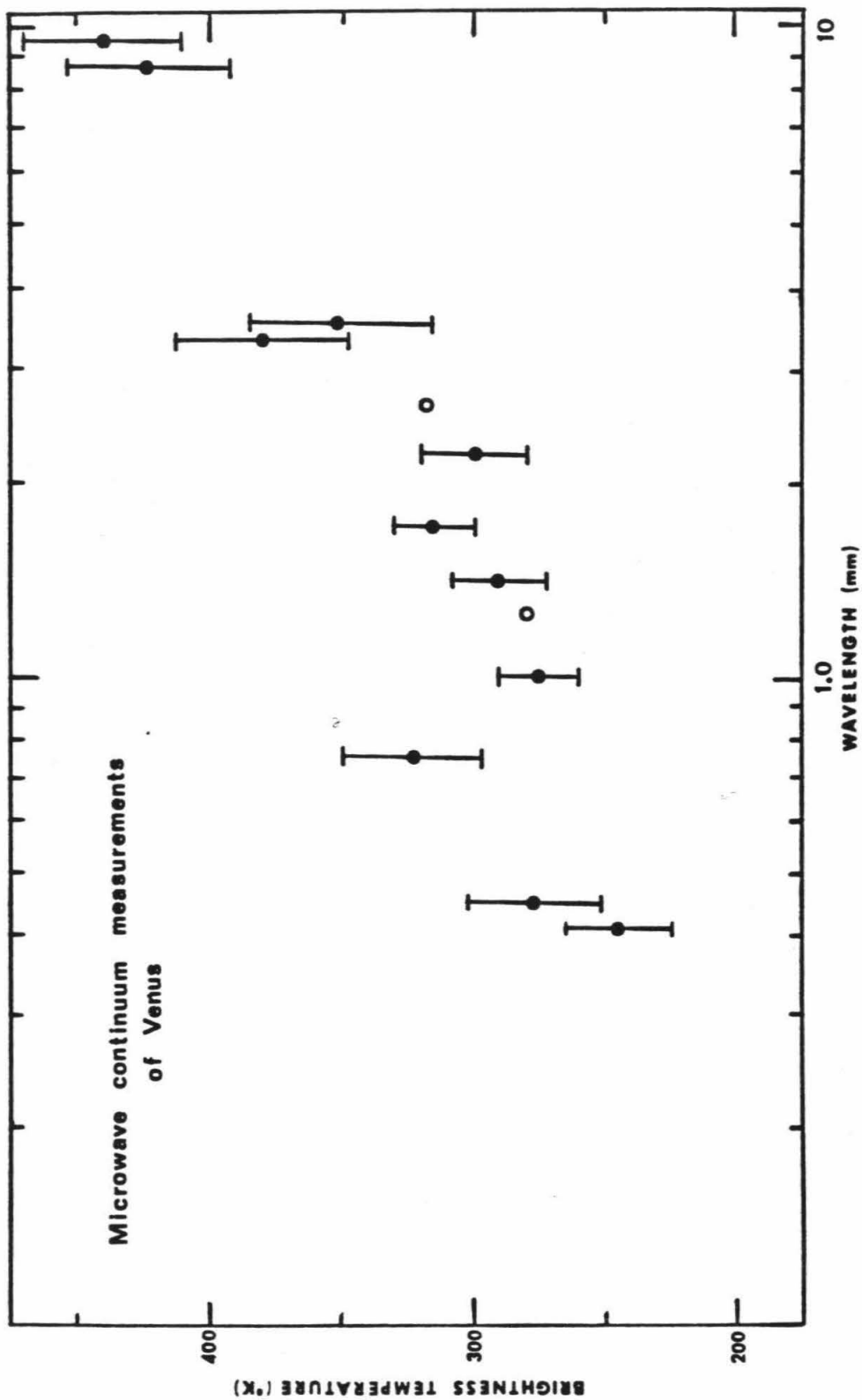
Microwave continuum measurements
of Venus
BRIGHTNESS TEMPERATURE (°K)
400
300
200
1.0
10
WAVELENGTH (mm)

specify the latitudinal and diurnal variation of atmospheric parameters over the disk of Venus. However, three important considerations allow us to analyze the spectra of Figures 1-5 with a single profile of atmospheric temperatures and pressures for the mesosphere of Venus.

Firstly, we note that analysis of CO microwave spectra of Mars proved that large spatial variations of surface and atmospheric temperatures affected the results very little as long as the disk average values of these parameters were not changed (see part III). The response of CO microwave spectra to these spatial variations appears very linear and averages out with whole disk integration. This feature of CO microwave spectra makes it very difficult to determine the specific variation of CO over the disk of Venus with single dish observations.

Secondly, we note that atmospheric temperatures and pressures below 100 km altitude do not vary much with latitude or local time of day on Venus. Comparison of entry profiles from the sounder (latitude = 4.4°N) and north (latitude = 59.3°N) probes of the Pioneer Venus spacecraft indicate temperature differences (at a given pressure level in the mesosphere) less than 10 K and generally less than 5 K (Seiff et al., 1980). The more global coverage of the Pioneer Venus OIR observations indicates a similar lack of diurnal contrast for global atmospheric temperatures between 70 and 100 km with a maximum equator to pole contrast of 10-20 K at ~ 80 km altitude (Taylor et al., 1980). Above 100 km, the day (local time = 6:46 a.m.) and night (local time = 0:07 a.m.) entry probes begin to show diurnal temperature contrast such that at 120 km altitude the measured temperature difference is ~ 80 K (Seiff and Kirk, 1982).

Finally, we point out that our spectra primarily measure dayside or nightside conditions on Venus. For analysis of the predominantly nightside

Table II. Dayside and Nightside (in parentheses) Model Atmospheres with Corresponding Collisional (pressure) and Doppler (thermal) Line Broadening Widths

Altitude (km)	Pressure (mbar)	Temperature (°K)	Collisional HPFW (MHz)	Doppler HPFW J = 0 -> 1 (MHz)	Doppler HPFW J = 1 -> 2 (MHz)
68	50.7 (50.7)	242 (242)	196.7 (196.7)	0.121 (0.121)	0.242 (0.242)
70	34.8 (34.8)	237 (237)	136.9 (136.9)	0.120 (0.120)	0.240 (0.240)
72	23.1 (23.1)	232 (232)	92.4 (92.4)	0.119 (0.119)	0.238 (0.238)
74	15.8 (15.8)	225 (225)	64.7 (64.7)	0.117 (0.117)	0.234 (0.234)
76	10.6 (10.6)	217 (217)	44.5 (44.5)	0.115 (0.115)	0.230 (0.230)
78	6.67 (6.52)	207 (207)	29.1 (28.5)	0.112 (0.112)	0.229 (0.224)
80	4.42 (4.37)	196 (196)	20.1 (19.9)	0.109 (0.109)	0.218 (0.218)
82	2.74 (2.66)	184 (184)	13.1 (12.7)	0.106 (0.106)	0.212 (0.212)
84	1.63 (1.77)	172 (172)	8.19 (8.89)	0.102 (0.102)	0.204 (0.204)
86	0.944 (0.942)	165 (165)	4.89 (4.93)	0.100 (0.100)	0.200 (0.200)
88	0.546 (0.609)	165 (165)	2.83 (3.16)	0.100 (0.100)	0.200 (0.200)
90	0.317 (0.381)	166 (166)	1.64 (1.97)	0.100 (0.100)	0.200 (0.200)
92	0.185 (0.229)	167 (167)	0.947 (1.18)	0.101 (0.100)	0.202 (0.200)
94	0.108 (0.130)	169 (167)	0.550 (0.666)	0.101 (0.101)	0.202 (0.202)
96	0.0638 (0.0680)	170 (167)	0.322 (0.349)	0.102 (0.101)	0.204 (0.202)
98	0.0379 (0.0305)	173 (166)	0.189 (0.157)	0.102 (0.100)	0.204 (0.200)
100	0.226 (0.0191)	176 (165)	0.112 (0.098)	0.103 (0.100)	0.206 (0.200)
102	0.136 (0.0118)	180 (164)	0.066 (0.061)	0.104 (0.100)	0.208 (0.200)
104	0.00839 (0.00682)	185 (162)	0.040 (0.036)	0.106 (0.099)	0.212 (0.198)
106	0.00521 (0.00332)	189 (159)	0.024 (0.018)	0.107 (0.098)	0.214 (0.196)
108	0.00326 (0.00231)	193 (153)	0.015 (0.013)	0.108 (0.096)	0.216 (0.192)
110	0.00206 (0.00125)	195 (145)	0.009 (0.007)	0.109 (0.094)	0.218 (0.184)
112	0.00130 (0.000731)	195 (135)	0.006 (0.004)	0.109 (0.090)	0.218 (0.180)

spectra (Figures 1, 2, 4) we used a smoothed version of the night probe entry profile. For the predominantly dayside spectrum of Figure 3 we used a smoothed version of the day probe entry profile. Both our day and night temperature-pressure profiles are presented in Table II.

3.3.3 Radiative Transfer

The fitted synthetic spectra, drawn in against the measured spectra in Figures 1-5, are calculated with a radiative transfer line synthesis program. The equation of radiative transfer for a non-scattering atmosphere is (Chandrasekhar, 1960)

$$I(z) = I(z_0)\, e^{-\tau(z,z_0)} + \int_{z_0}^{z} J(z')\, e^{-\tau(z,z')}\, k\, dz' \qquad (2)$$

$I(z)$ = intensity of radiation at altitude z

$J(z')$ = source function for radiation

k = absorption coefficient (per unit length)

$\tau(z,z_0 \text{ or } z')$ = opacity between level z and level z_0 or z' (given here for a normal path length)

z_0 = lower boundary for the problem (67 km altitude)

For our non-scattering case, the source function, $J(z')$, is the Planck function

$$B(\nu,T) = \frac{2h\nu^3}{c^2}\left[\frac{1}{e^{h\nu/kT}-1}\right] \frac{\text{erg}}{\text{cm}^2 \text{ Hertz steradian sec}}$$

which approaches the Rayleigh-Jeans approximation at microwave wavelengths

$$B(\nu,T) = \frac{2kT\nu^2}{c^2} \qquad (3)$$

h = Planck's constant

ν = frequency

k = Boltzmann constant

c = speed of light

T = temperature

We note that the submicron-size haze particles observed in the region of 80 km by Pioneer Venus polarimetry (Kawabata et al., 1980) do not effectively couple with microwave radiation due to the small particle size. Taylor et al. (1980) found that this haze did not measurably effect OIR data either, further evidence that scattering is not an important process for microwave observations of the mesosphere of Venus.

At the temperatures indicated in Table II, the Rayleigh-Jeans approximation overestimates radiation intensities at 2.6 mm and 1.3 mm by 2% and 4%, respectively. However errors in brightness ratios (such as $T_B(\nu_1)/T_B(\nu_2)$ where $T_B(\nu_2)$ is the continuum brightness temperature for our calculations) are second order. Thus computational errors caused by use of the Rayleigh-Jeans approximation are respectively 1% and 2% for 2.6 mm and 1.3 mm radiation.

Combining equations (1) and (2) results in

$$T_B(\nu,\mu) = T_0(\mu)\, e^{-\tau(\nu)/s(\mu)} + \int_{z_0}^{\infty} T(z)\, k(\nu,z)\, e^{-\int_z^{\infty} k(\nu,z')dz'/s(\mu)}\, dz/s(\mu) \qquad (4)$$

where we have introduced a slant path length, $dz'/s(\mu)$ (see Appendix VI) and allowed the upper limit of integration to approach infinity. T_B and T_0 are the observed and lower boundary brightness temperatures where brightness temperature is defined by

$$T = c^2 B / 2k\nu^2$$

$\tau(\mu)$ is defined as:

$$\int_{z_0}^{\infty} k(\nu,z')\, dz'$$

where $k(\nu,z)$ is the frequency and pressure-temperature dependent absorption coefficient for CO (per unit length).

Equation (3) refers to the brightness temperature for a particular position, μ, on the observed disk of Venus. We perform the integration of (3) for a distribution of points on the observed disk of Venus, corresponding to a distribution of path lengths through the Venus atmosphere (Figure 10). These individual spectra are averaged with appropriate weighting by area and the Gaussian beam pattern of the antenna.

$$T_B(\nu) = \frac{2}{A^2(1-e^{-1/A^2})} \int_0^1 T_B(\nu,\mu)\, \mu\, e^{-(1-\mu)^2/A^2}\, d\mu \qquad (5)$$

A = HWHP$/R\ln 2$

HWHP = half width half power of antenna beam (arcseconds)

R = angular radius of Venus (arcseconds)

$T_B(\nu)$ = disk brightness temperature of Venus

$T_B(\nu,\mu)$ = brightness temperature as a function of position on disk of Venus

μ = $\cos\vartheta$ where ϑ is the angular distance of the position from the sub Earth point on Venus (Figure 10).

3.3.4 Numerical Integration

The integrals of (3) and (4) must be calculated numerically. We discretized the altitude integral of (3) in 2 km steps over the altitude region 67-

FIGURE 10: Whole disk integration of Venus with the Gaussian beam of the observing antenna. The equally spaced vertical lines indicate ray paths of radiative transfer integration through the Venus mesosphere for calculation of synthetic spectra best fitting the measured spectra.

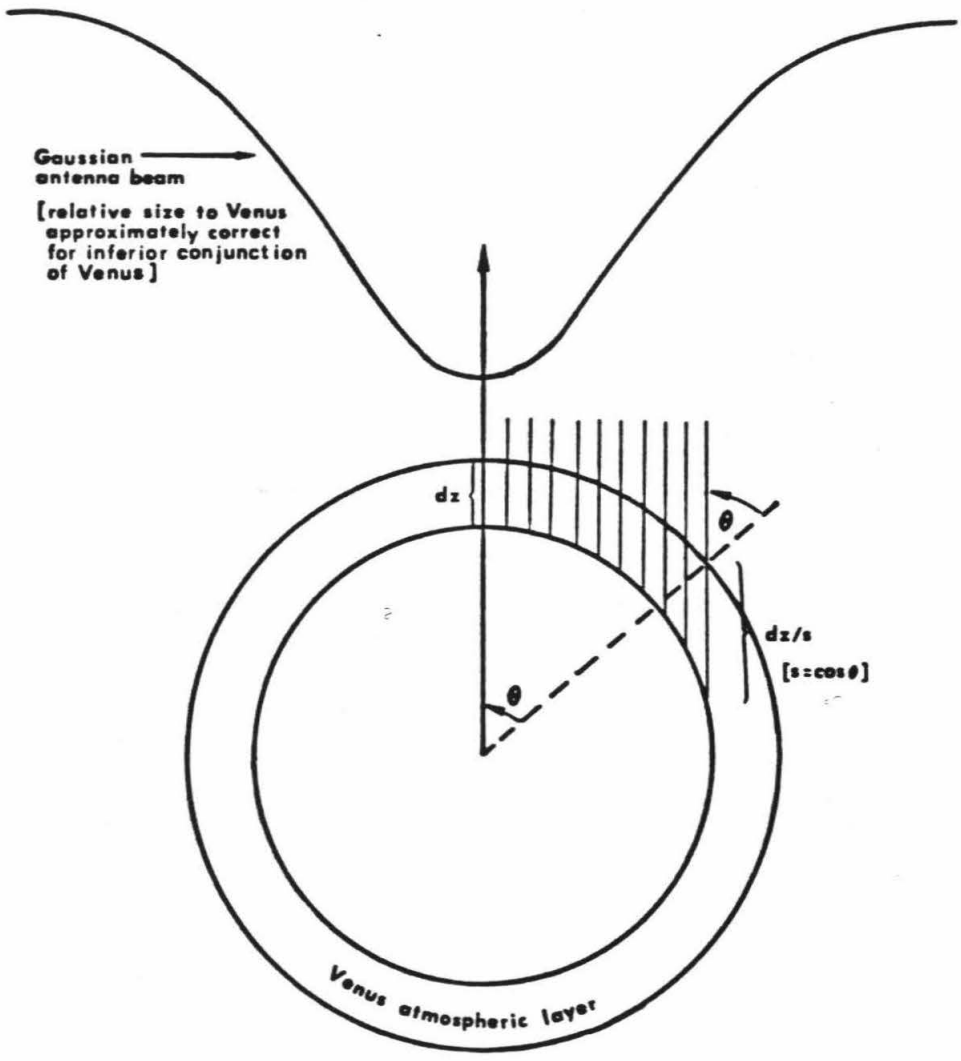
Gaussian
antenna beam
[relative size to Venus
approximately correct
for inferior conjunction
of Venus]
dz
θ
dz/s
[s=cosθ]
θ
Venus atmospheric layer

119 km. Contributions of CO opacity above 119 km and below 67 km were found to have negligible effects on the synthetic spectra due to the nature of the pressure dependent line shape of CO absorption (see following section). Thus (3) becomes:

$$T_B(\nu,\mu) = T_0(\mu) \prod_{n=1}^{u} e^{-\tau_n(\nu)\mathcal{S}(\mu)} + \sum_{n=1}^{u} T_n \, \tau_n(\nu)\mathcal{S}(\mu) \left[\prod_{i=n}^{u} e^{-\tau_i(\nu)\mathcal{S}(\mu)} \right] \qquad (6)$$

T_n = atmospheric temperature of layer n

u = upper most altitude interval (117-119 km)

$\tau_n(\nu)$ = opacity of layer n, $\int_{dz} k_n(\nu,z)\, dz_n$

dz_n = altitude interval, 2 km

$S(\mu)$ = slant path length factor ($\sim \mu$, see appendix VI)

$k_n(\nu,z)$ = absorption coefficient of CO in layer n

For the integration of $k(\nu,z)$ over each 2 km layer, atmospheric temperatures and the mixing ratio of CO were assumed constant. However, atmospheric pressure decreases by 40-80% for 2 km increments in depth in the Venus mesosphere. Fortunately, due to the particular form of $k(\nu,z)$, the altitude integral $\int_{dz} k_n(\nu,z)\, dz_n$ may be calculated analytically in atmospheric pressure coordinates (see Appendix IV). With such integration, 2 km increments provided a very accurate approximation to the exact integration of equation (3).

The finite spectral resolutions of the observations (i.e. channel widths) were also approximated in calculations for the fitted synthetic spectra. We used a single point (midpoint of the channel) value of $T_B(\nu)$ for frequencies in the linear wings of the spectra. For the central portion of the spectra we used three point trapezoidal integration of $T_B(\nu)$ over each channel. For the December 1978 (1/2 mHz resolution) and May 1980 observations, the middle channels of

the spectra were centered on the line center of absorption. We calculated the absorption in the line center for these spectra by averaging ten equally spaced values of $T_B(\nu)$ over the frequency range $\nu_0 \pm 1/2$ channel width. For all of the above calculations we assumed a step function for the bandpass of the channels. The actual shape of the bandpass within the channels is well approximated by a step function.

We performed the disk brightness temperature integration of (4) using Simpson rule integration for 10 points equally spaced from the center to the limb of the disk of Venus (see Figure 10). Circular symmetry is assumed. In order to test the accuracy of disk integration we doubled the number of integration points, which altered the disk integrated spectrum by less than 2%.

3.3.5 CO Absorption Coefficient

The microwave spectra of Figures 1-4 reflect dipole induced transitions between resonant rotational states of the linear CO molecule. The rotational energy, W, of a rigid, rotating molecule is quantitized into the discrete states (e.g. Townes and Schawlow, 1960):

$$W = \frac{h^2}{8\pi^2 I} J(J+1)$$

h = Planck's constant

I = principal moment of inertia

J = angular momentum quantum number

0, 1, 2, 3, ... (positive integer)

The selection rule for transitions between rotational energy levels is $\Delta J = \pm 1$. Thus allowed frequencies of radiation are

$$\nu = \frac{h}{8\pi^2 I}\left[J_2(J_2+1) - J_1(J_1+1)\right]$$

$$= \frac{2h}{8\pi^2 I}(J_1+1) \equiv 2B(J_1+1) \qquad (7)$$

where $B = (h/8\pi^2 I)$ is called the rotational constant. The above expressions are only approximately correct for the CO molecule which centrifugally stretches with rotation and simultaneously exists in a vibrational state. Both of these motions change the moment of inertia for CO so that B is a slight function of frequency.

The absorption coefficient, $k(\nu)$, for the transitions of equation (6) is partially derived in Appendix II, which includes a list of the important molecular parameters for CO absorption. We use the formulation of Waters (1976), corrected for a more recent determination of the dipole moment of CO (0.112 Debye, Kolbe et al., 1977).

$$k(\nu) = (7.99 \times 10^{-20})\nu^3\left[1 - \frac{h\nu}{kT}\right]\frac{N_{CO}}{T^2} f(\nu) \text{ cm}^{-1} \qquad (8)$$

N_{CO} = number density of CO molecules (cm^{-3})

$f(\nu)$ = the normalized frequency line shape function

Several important features of $k(\nu)$ are its inverse temperature squared dependence, its linear proportionality to the abundance of CO, and its frequency cubed dependence.

3.3.6 Spectral Line Shape Function

For purposes of analysis, the normalized line shape function, $f(\nu)$, is the essential feature of the absorption coefficient. We use the Voigt line shape, which is the convolution of collisional and thermal (Doppler) broadening.

$$f(\nu) = \int_{-\infty}^{\infty} \underbrace{\frac{1}{\pi} \frac{\Delta\nu_c}{(\nu - \nu_o - y)^2 + \Delta\nu_c^2}}_{\text{collisional}} \underbrace{\frac{e^{-\ln 2 (y/\Delta\nu_o)^2}}{\sqrt{\pi}\,\Delta \frac{\nu_o}{\sqrt{\ln 2}}}}_{\text{thermal}} dy \qquad (9)$$

Thermal broadening results from the Doppler shift of the line frequency due to the Boltzmann distribution of kinetic velocities for the CO molecules. The HPFW of the Doppler broadened line, is

$$\Delta\nu_D = (3.581 \times 10^{-7})\nu_o \sqrt{T/m_{CO}} \text{ Hertz}$$

where

ν_o = line center rest frequency

T = kinetic temperature of the CO molecules

m_{CO} = molecular weight of CO

The Doppler line width is a slowly varying function of altitude in the Venus mesosphere (see Table 2) due to the $\sqrt{T}$ dependence. As Table 2 indicates, the Doppler line width is always less than 250 kHz (125 kHz) for the $J = 1 \rightarrow 2$ ($J = 0 \rightarrow 1$) transition and thus is never adequately resolved by our measurements.

Equation (9) contains the Lorentz formulation for collisional (pressure) broadening line shape. Collisional broadening results from the random collisions of molecules with CO_2 molecules of the background atmosphere. Collisional broadening may be regarded quantum mechanically as the perturbation of the Hamiltonian of the rotating CO molecule caused by molecular collisions. In classical terms, the collisions smear the line center frequency over a range of frequencies which is roughly equal to the frequency of collisions (Waters, 1976).

The general collisional line shape was developed from classical mechanics by Van Vleck and Weisskopf (1946)

$$f(\nu) = \frac{1}{\pi}\left[\frac{\Delta\nu_c}{(\nu_o - \nu)^2 + \Delta\nu_c^2} + \frac{\Delta\nu_c}{(\nu_o + \nu)^2 + \Delta\nu_c^2}\right] \qquad (10)$$

The second term of (10) becomes exceedingly small for the lower atmospheric pressures of the mesosphere, (i.e. $\Delta\nu_c << \nu_o$). Hence we use the low pressure Lorentz line shape in (9). The HPFW of collisional broadening for CO in a CO_2 atmosphere is

$$\Delta\nu_c = 3300(300/T)^{0.75} \quad P \quad \text{Hertz} \quad \text{(Varanasi,1975)}$$

T = atmospheric temperature

P = atmospheric pressure (dynes/cm^2)

The pressure dependence of $\Delta\nu_c$ introduces a very sharp altitude gradient into the collisional line shape. An extrapolation for altitudes below 68 km in Table II indicates that the collisional line width exceeds the maximum bandwidth of our measurements (500 mHz) for altitudes below ~ 65 km. Above ~ 100 km the collisional line width becomes much smaller than the nearly constant Doppler line width. As Figure 11 schematically illustrates, higher layers of the atmosphere contribute narrower and narrower spectra until the Doppler line width is reached. Above this altitude spectra of roughly identical shape are contributed to the altitude-integrated spectrum we observe.

We are able to solve for the altitude profile of CO abundance due to the strong altitude dependence of the collisional line width parameter. The signal (i.e. absorption depth) at frequencies farther from the line center measures CO abundance at increasing depth in the Venus atmosphere. CO mixing ratios

FIGURE 11: Pressure dependence for line shape of CO absorption in the Venus mesosphere. Horizontal bars indicate successive layers in the atmosphere.

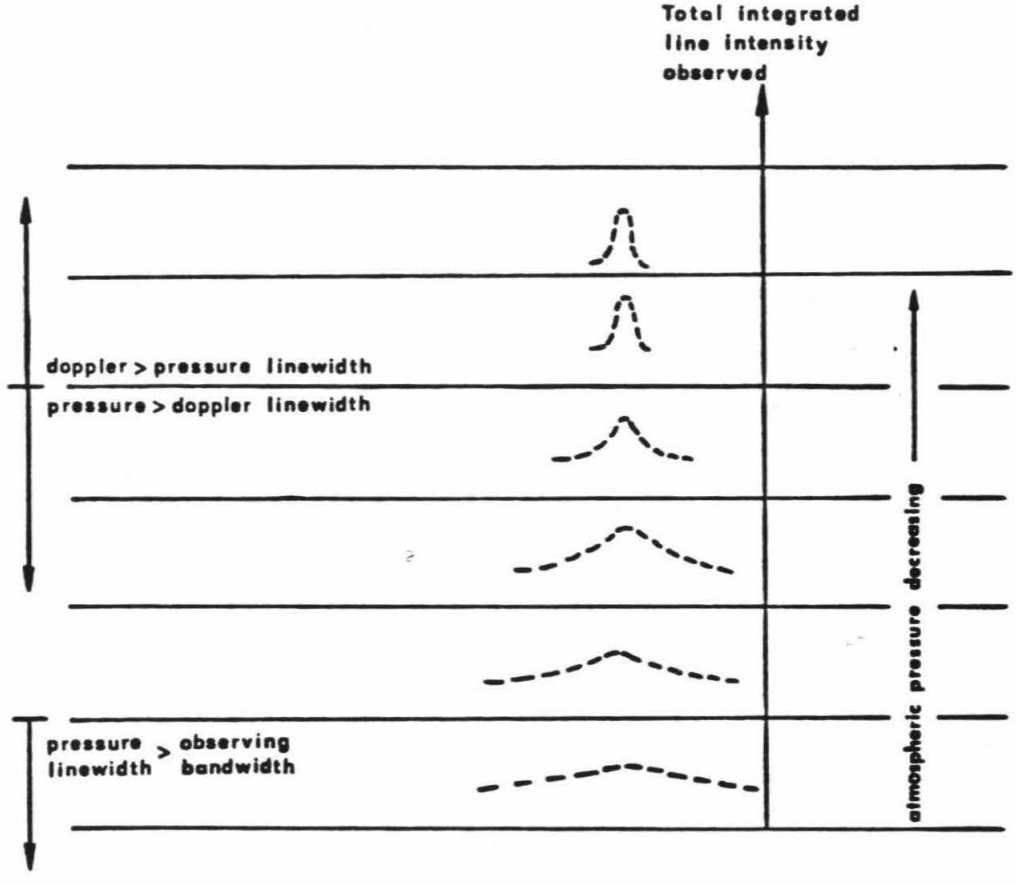
Total integrated
line intensity
observed
doppler > pressure linewidth
pressure > doppler linewidth
pressure
linewidth
>
observing
bandwidth
atmospheric pressure decreasing

between 85 and 95 km are well constrained by this technique (see Figure 6). Below 80-85 km the CO abundance falls sharply in the Venus mesosphere. Furthermore, the signal due to CO in this region becomes diminished due to extensive broadening in frequency such that the contributed line shape is no longer determined by the limited signal/noise and bandwidth of the measured spectrum. Above 95 km the line shape of CO absorption becomes constant and the number density of CO molecules, N_{CO} falls off rapidly. Thus the error bounds for CO mixing profiles from CO microwave measurements increase dramatically below 80-85 km and above 95 km (Figure 6).

3.3.7 The Line Forming Process

As indicated by equation (3), CO microwave spectra reflect both emission and absorption in the mesosphere of Venus. For insight into the relative contribution of emission and absorption we consider the simple case of continuum radiation of brightness temperature, T_0, passing through an atmospheric layer of constant temperature, T. Integration of (3) produces

$$T_0\, e^{-\tau(\mu)} + T(1 - e^{-\tau(\nu)})$$

normalizing by the continuum level, T_0, gives

$$\frac{T}{T_0} + \left[1 - \frac{T}{T_0}\right] e^{-\tau(\nu)}$$

Note that the baseline (i.e. far from line center, where $\tau \to 0$) of the spectrum approaches unity for large enough bandwidths. Thus for $T > T_0$ one observes an emission spectrum and for $T < T_0$ one observes an absorption spectrum. For CO spectra of the Venus mesosphere we may approximate $T \simeq 180$ K and $T_0 \simeq 300$ K. $T/T_0 \simeq 0.6$ so that the basic character of the spectra of Figures 1-5

is absorption. However, we note that there is still significant emission which cannot be neglected.

Both the competing influence of absorption and emission and the exponential dependence for CO abundance ($\tau \propto N_{CO}$) in equation (3) make it difficult to speak of a useful weighting function for CO abundance in the mesosphere of Venus. Wilson et al. (1981) defined an abundance weighting function, $W(\nu,z)$, for the emission term of (3) such that

$$T_{\text{emission}} = \int_{z_0}^{\infty} N_{CO}(z) W(\nu,z)\, dz$$

apparently with the assumption that $\tau(\nu) << 1$. We reproduce a graph of their weighting functions in Figure 12 for illustrative purposes. The most important feature is the altitude decreasing position of the weighting function maxima for increasing frequency offsets from the line center.

We note that the assumption $\tau << 1$ is good for $(\nu - \nu_0) \gtrsim 8$ mHz for the $J = 1 \rightarrow 2$ transition and $(\nu - \nu_0) \gtrsim 2$ mHz for the $J = 0 \rightarrow 1$ transition. These numbers are moderately dependent on the variable abundance of CO in the mesosphere of Venus. Table III presents microwave CO opacity as a function of $(\nu - \nu_0)$ for the CO mixing profiles of Figures 1-5.

3.4 CO Mixing Profiles

With the use of equations (5)-(8) and trial and error estimates of the CO mixing profile in the mesosphere of Venus, we calculated synthetic spectra which best fit the measured spectra (Figures 6, 7, and 8). We determined the best fit on the basis of minimizing the sum of the squared residuals between the synthetic and measured spectra. We reemphasize that the error bounds of the CO profiles in Figures 6-8 are due primarily to physical limitations in the meas-

FIGURE 12: Normalized weighting functions for the J = 0 → 1 transition of CO in the Venus mesosphere from Wilson et al. (1981a). The weighting functions peak at successively lower altitudes for increasing frequency offsets from line center.

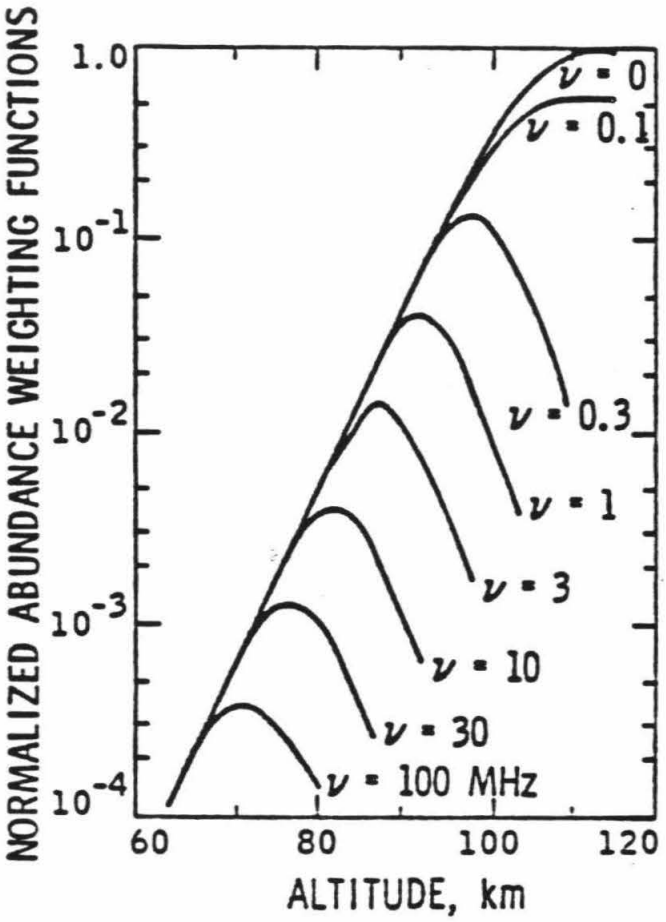
NORMALIZED ABUNDANCE WEIGHTING FUNCTIONS
1.0
10^{-1}
10^{-2}
10^{-3}
10^{-4}
60
80
100
120
ALTITUDE, km
ν = 0
ν = 0.1
ν = 0.3
ν = 1
ν = 3
ν = 10
ν = 30
ν = 100 MHz

Table III. CO Line Opacities from Derived CO Mixing Profiles

(MHz)°	J = 0 -> 1 May 80	Dec. 80	Dec. 78	J = 1 -> 2 Jan. 82	Sept. 82	Nov. 82
400	---	---	---	---	---	---
200	---	---	---	---	0.030	0.031
100	---	---	---	0.004	0.067	0.069
50	---	0.033	---	0.015	0.12	0.13
30	---	0.048	0.15	0.038	0.17	0.19
20	0.006	0.063	0.22	0.078	0.22	0.24
10	0.015	0.094	0.36	0.21	0.32	0.38
5	0.027	0.13	0.58	0.44	0.50	0.58
4	0.034	0.15	0.67	0.54	0.57	0.64
3	0.046	0.16	0.79	0.67	0.67	0.75
2	0.069	0.19	0.98	0.88	0.83	0.91
1	0.13	0.24	1.4	1.3	1.2	1.2
0.5	0.23	0.30	1.8	1.9	1.6	1.7
0.2	0.43	0.40	2.7	---	---	---
0.1	0.63	0.50	---	---	---	---
0.0	0.79	0.57	3.4	4.9	2.6	2.6

urements and the specific nature of the line formation rather than uncertainties in data calibration and analysis assumptions.

For a given distribution of CO abundance in the Venus mesosphere, the total measured bandwidth and noise level in the wings of the observed spectrum determine the depth to which the mixing ratio of CO may be derived. For example, we compare the J = 1 → 2 spectra of December 1978 and January 1982 in Figure 13, where we have used the average level of both the spectra at $\nu - \nu_o \simeq 26$ mHz to determine the baseline continuum (i.e. they are both normalized to zero at 26 mHz from line center). Note that the spectra have been folded about the line center to make the comparison clearer. The two spectra are remarkably similar other than the greatly extended bandwidth for the 1982 spectrum. The derived CO mixing profiles of Figure 7 are correspondingly similar except for the much stronger constraints of the 1982 spectrum on CO mixing ratios below 82 km. CO mixing ratios in the range of $5-10 \times 10^{-5}$ between 75 and 82 km were able to fit the December 1978 spectrum (Figures 1 and 7). This fitted synthetic spectrum is plotted against both of the J = 1 → 2 spectra in Figures 14. It clearly shows too much curvature beyond the limited bandwidth of the December 1978 spectrum to fit the very flat wings of the wide bandwidth January 1982 spectrum.

One might expect the very large bandwidths of our September-November 1982, J = 1 → 2 spectra to more closely constrain CO mixing ratios below 80 km altitude. Unfortunately these 500 mHz bandwidth spectra are seriously affected by very large levels of noise and standing waves (see Figure 5). The standing waves in particular introduce disappointingly high uncertainty for absorption in the broad wings of the spectra. Hence, CO mixing ratios below 85 km from these spectra are more poorly determined than those found from our January 1982,

FIGURE 13: A comparison of the J = 1 → 2 spectra of December 1978, (solid line) and January 1982 (dots). Both spectra measured a predominantly nightside of Venus and have been folded about line center for this comparison.

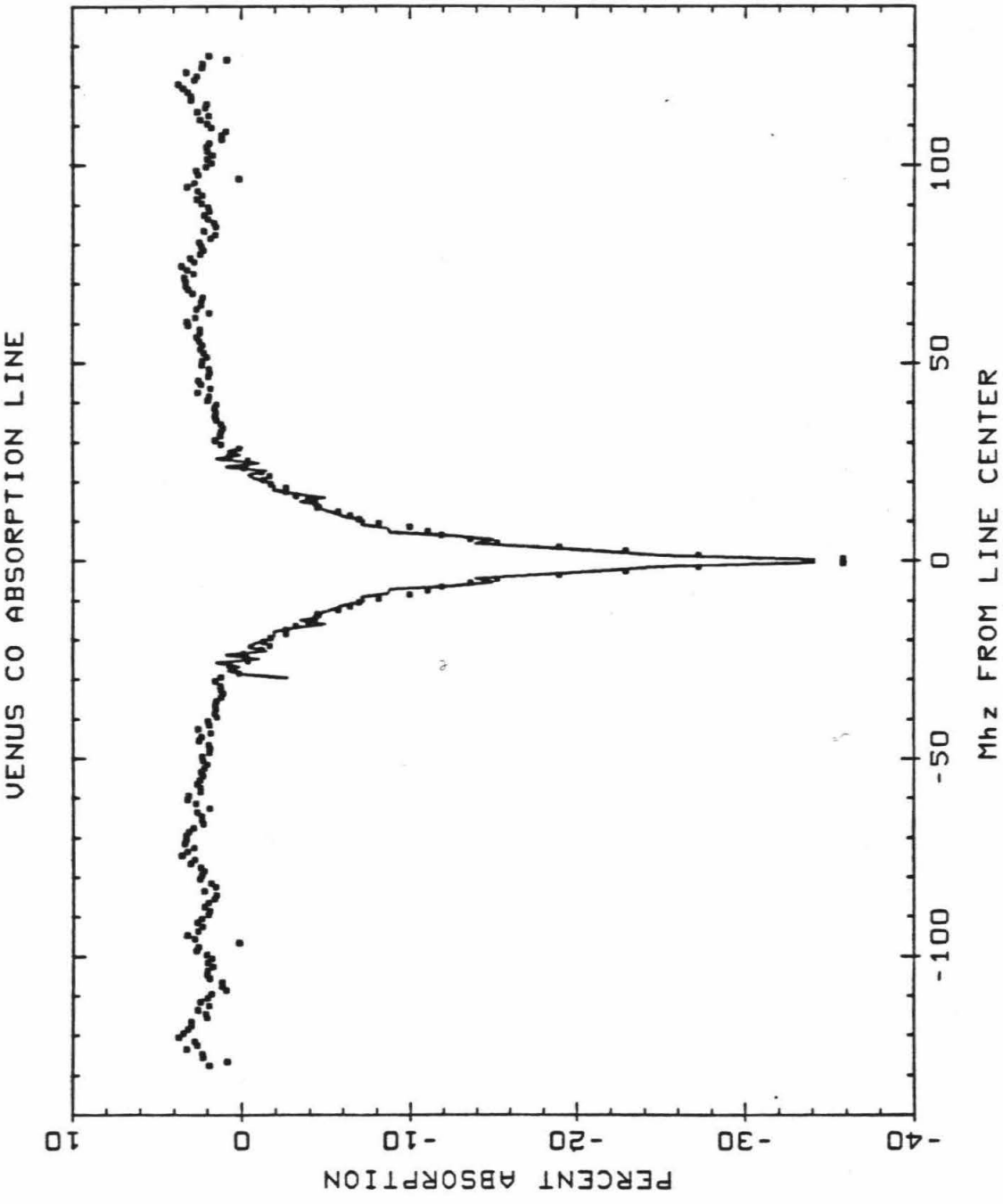
VENUS CO ABSORPTION LINE
PERCENT ABSORPTION
10
0
-10
-20
-30
-40
-100
-50
0
50
100
Mhz FROM LINE CENTER

FIGURE 14: The J = 1 → 2 spectra of December 1978, (solid line) and January 1982 (dots) are included with a full ± 128 mHz bandwidth synthetic spectrum (solid, smooth line). This synthetic spectrum was generated from the CO mixing profile found from the December 1978, narrow bandwidth (± 30 mHz) spectrum.

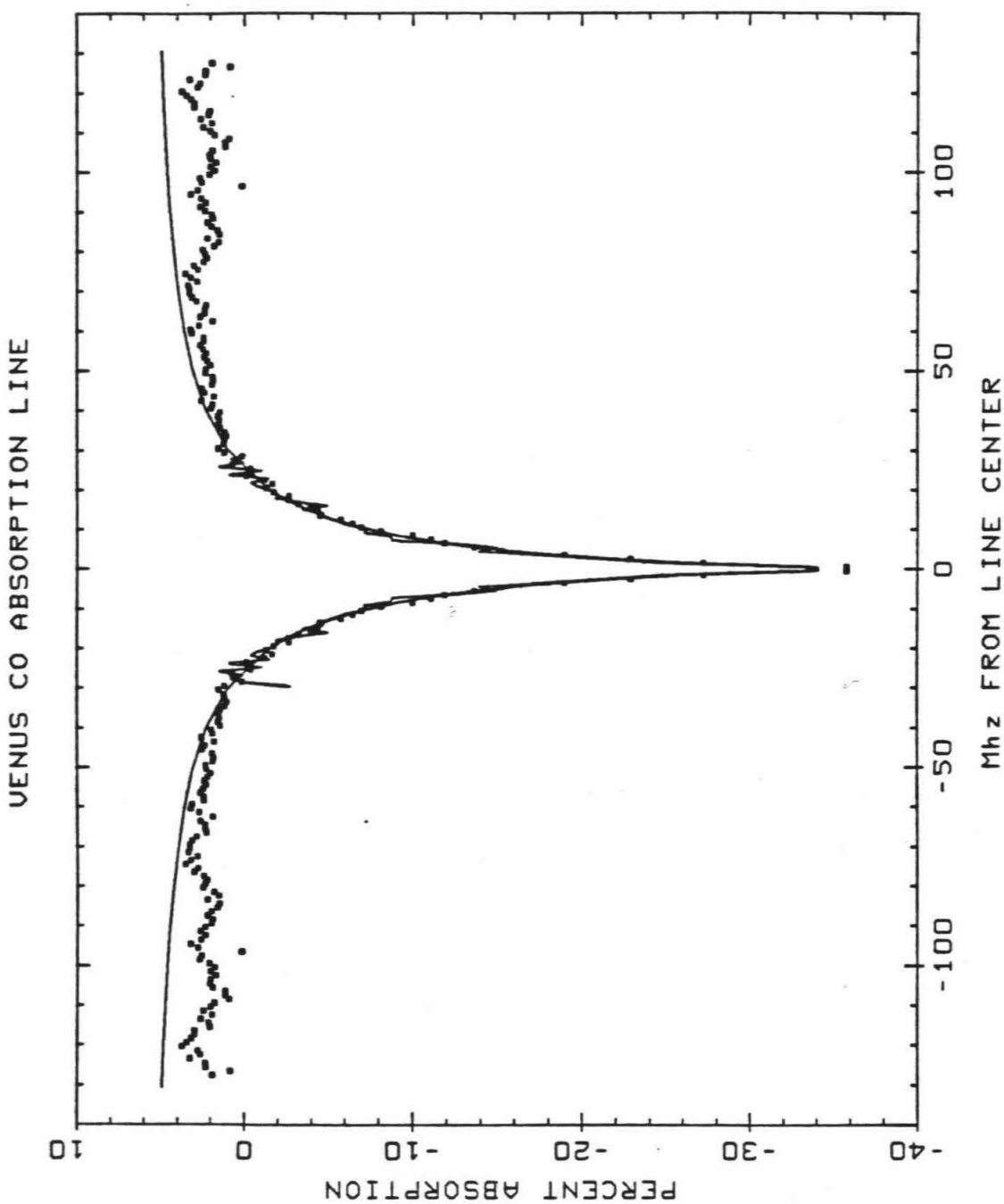
VENUS CO ABSORPTION LINE
PERCENT ABSORPTION
10
0
-10
-20
-30
-40
-100
-50
0
50
100
Mhz FROM LINE CENTER

$J = 1 \rightarrow 2$ spectrum (compare Figures 7 and 8).

The comparison between bandwidth and the depth to which CO mixing ratios may be determined becomes less clear if the mixing profile of CO varies between measured spectra. Direct comparison of the $J = 0 \rightarrow 1$ spectra (Figure 15) indicates considerable variation in the altitude distribution of CO. The nightside spectrum is narrow and deep relative to the very broad, shallow dayside spectrum. Figure 6 presents the indicated difference in CO mixing profiles for these two spectra. The dayside CO mixing ratios are 2-4 times those of the nightside between 88 and 80 km altitude. Above 92 km, the nightside CO abundance is 2-4 times the dayside CO abundance.

We present a comparison of all of the spectra in Figure 16. The folded May (line) and December (dots) 1980 spectra are presented directly in Figure 16. We show a synthetic $J = 0 \rightarrow 1$ spectrum (smooth line) calculated from the derived January 1982 CO mixing profile to represent the $J = 1 \rightarrow 2$ spectra. The limited bandwidth of the December 1978 spectrum and the poor baselines of the September, November 1982 spectra prevent the generation of separate $J = 0 \rightarrow 1$ comparisons for these spectra. The process of generating synthetic $J = 0 \rightarrow 1$ spectra from $J = 1 \rightarrow 2$ spectra is not accurate for frequencies near the line center ($\nu - \nu_o \lesssim 5$ mHz) where the opacity of the $J = 1 \rightarrow 2$ line is large. As can be seen in Figures 6-8, the $J = 1 \rightarrow 2$ spectra constrain the mixing ratio of CO above 95 km much more poorly than do the $J = 0 \rightarrow 1$ spectra. The $J = 1 \rightarrow 2$ spectra become opaque in the line center, where the line depth is determined by atmospheric temperatures above 95 km rather than the mixing ratio of CO. Above ~ 105 km, the diminished number density of CO molecules no longer allows significant contribution of absorption for either transition. Hence microwave spectra do not constrain the mixing ratio of CO at all well above

FIGURE 15: A comparison of the J = 0 → 1 spectra of May 1980, (solid line) and December 1980 (dotted line). The May spectrum measured the nightside of Venus (10% illuminated) whereas the December spectrum measured the dayside of Venus (88% illuminated). These two spectra reflect the basic distinction between day and nightside J = 0 → 1 CO spectra of Venus, a broader but less deep spectrum for the dayside relative to the nightside of Venus. Both spectra have been folded in this presentation.

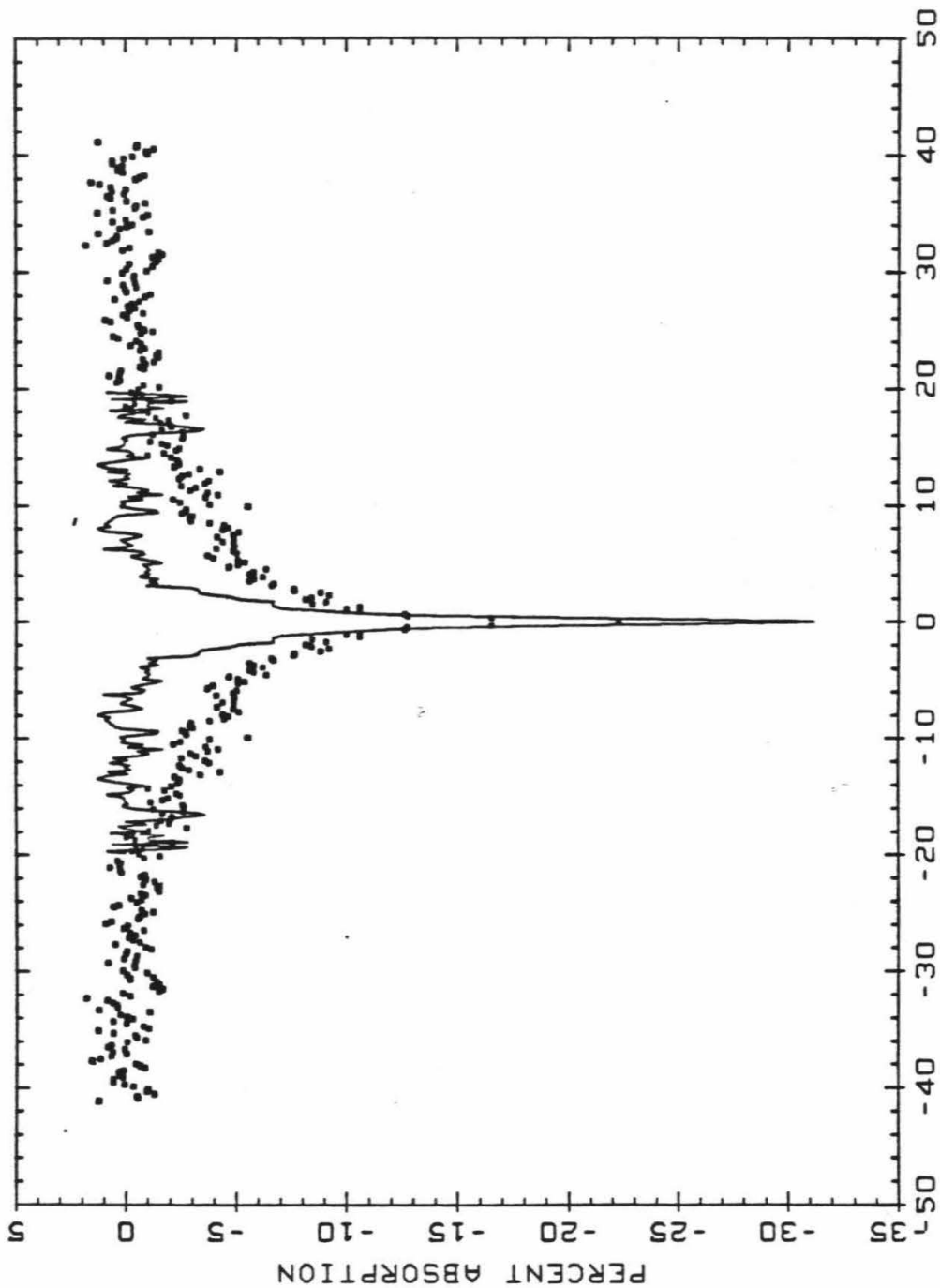
VENUS CO ABSORPTION LINE
PERCENT ABSORPTION
5
0
-5
-10
-15
-20
-25
-30
-35
50
40
30
20
10
0
-10
-20
-30
-40
-50
Mhz FROM LINE CENTER

FIGURE 16: Folded J = 0 → 1 spectra of May 1980, (solid line) and December 1980, (dotted line) compared to a synthetic J = 0 → 1 spectrum (smooth solid line). This synthetic spectrum is generated from the CO mixing profile as derived from our J = 1 → 2 January 1982, spectrum and allows an approximate comparison of all of the J = 1 → 2 spectra (Figures 1, 4, and 5) to our J = 0 → 1 spectra.

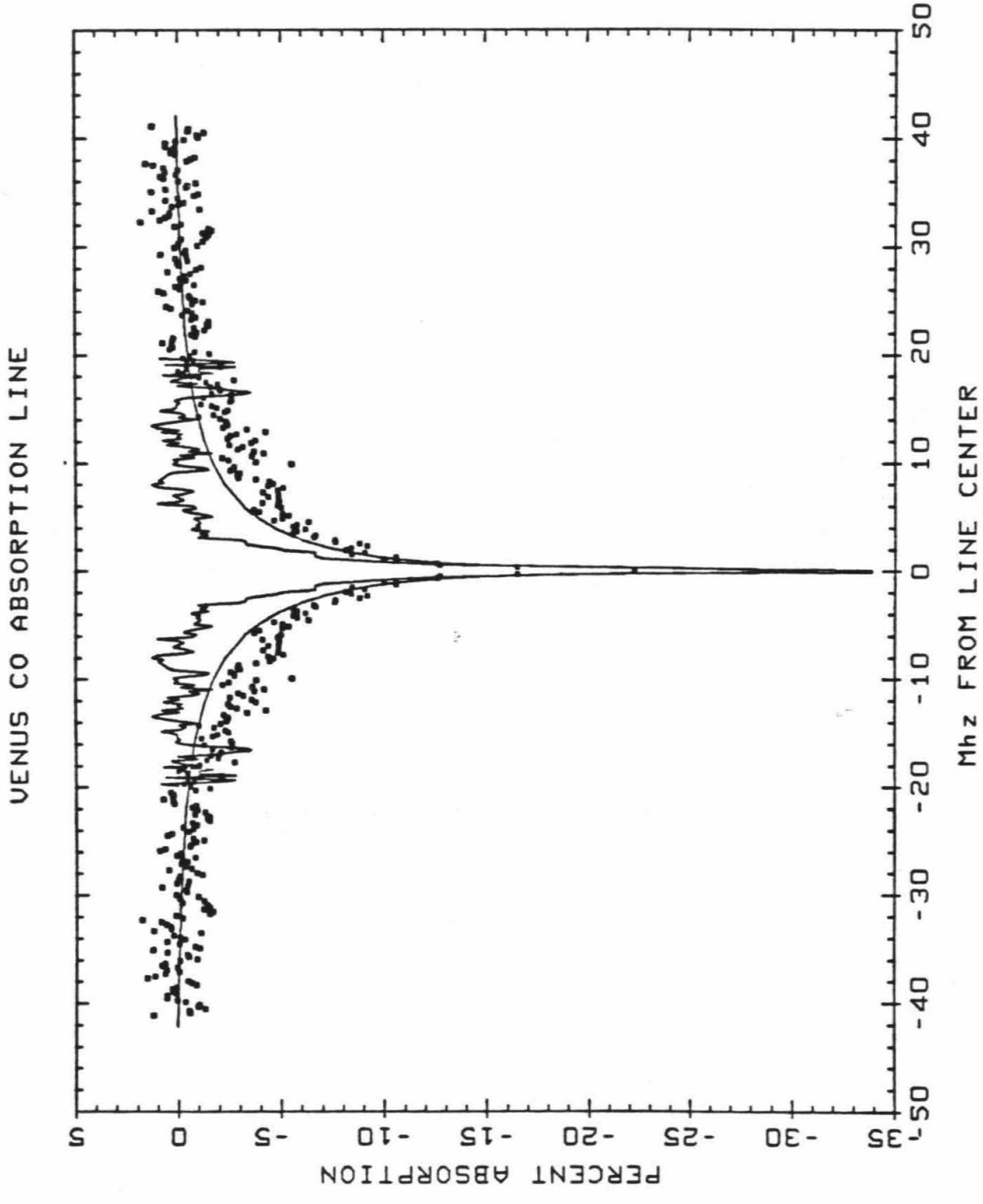
VENUS CO ABSORPTION LINE
PERCENT ABSORPTION
5
0
-5
-10
-15
-20
-25
-30
-35
Mhz FROM LINE CENTER
50
40
30
20
10
0
-10
-20
-30
-40
-50

~ 105 km altitude.

Figure 17 compares the CO mixing profiles derived from the May, December 1980 spectra and the January, November 1982 spectra. We omit profiles from our December 1978 and September 1982 spectra, which are similar to profiles derived from our January and November 1982 spectra, respectively. Note that we include only the altitude portions of the mixing profiles which are moderately well determined by the respective spectra. The May 1980 and January 1982 spectra suggest that a common feature of the CO mixing profile is an order of magnitude decline in CO mixing ratios over a 5-7 km region of the Venus mesosphere. This falloff of CO abundance begins at ~ 92 km for the May 1980 spectrum and at ~ 84 km for the January 1982 spectrum. Note that both of these spectra are of the nightside of Venus. At present we can only assume that such a cutoff occurs for the dayside of Venus. The December 1980 (dayside) spectrum constrains the sharp decline in CO mixing ratio to occur at or below ~ 80 km but does not convincingly require such a cutoff. Similarly, the November 1982 (dayside) spectrum constrains the cutoff to occur below ~ 85 km but does not determine the cutoff due to considerable uncertainty in the baseline for this spectrum. The large bandwidth November (and September) 1982 spectrum does provide stronger constraints for the dayside mixing ratio of CO below 80 km than does the December 1980 $J = 0 \rightarrow 1$ spectrum (see Figures 6 and 8). Still, until much better baselines can be obtained for these large bandwidth spectra, we cannot make comparisons between dayside and nightside CO mixing ratios below 80 km.

We point out that the upper bound for the mixing ratio of CO at 80 km as found from the January 1982 (nightside) spectrum is 2.0×10^{-5}. This is approximately a factor of three less than the value Connes et al. (1968) determined for

FIGURE 17: A comparison of all of the derived CO mixing profiles (Figures 6-8). Only the moderately well determined portions of each mixing profile are shown in this comparison.

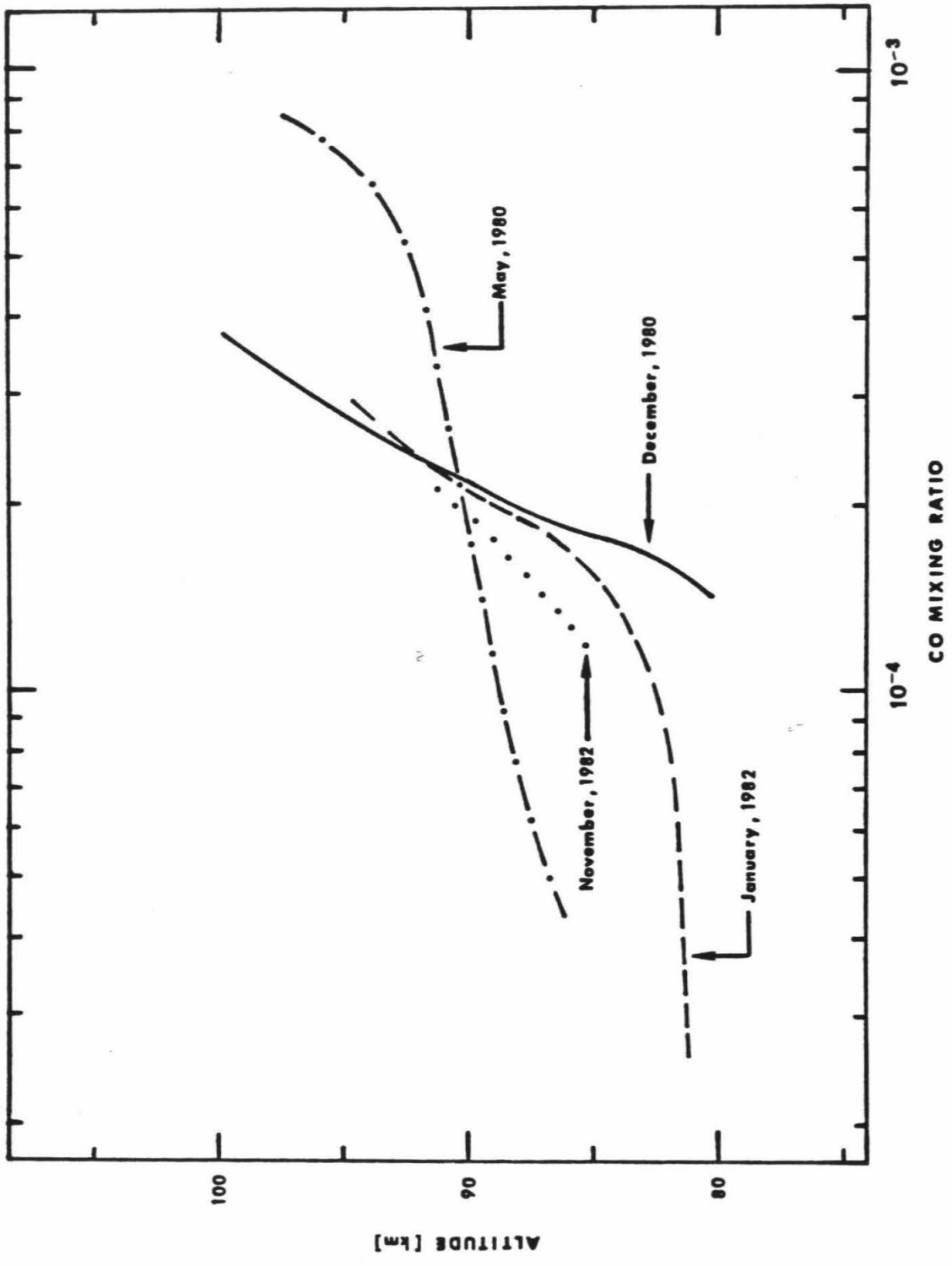
ALTITUDE [km]
100
90
80
10^{-4}
10^{-3}
CO MIXING RATIO
May, 1980
December, 1980
November, 1982
January, 1982

the 60-70 km region of the Venus atmosphere. Figure 18 represents the best fit found for the January 1982 spectrum using a lower limit of 4.5×10^{-5} (i.e., the Connes et al. value) for the mixing ratio of CO. There is clearly too much absorption in the wings of the synthetic spectrum to match the observed spectrum.

FIGURE 18: A best fit synthetic spectrum (solid smooth line) to the January 1982 J = 1 → 2 spectrum (dots). A constraint on the best fit synthetic spectrum is that the lower boundary value of the CO mixing ratio (below ~ 82 km altitude) in the Venus mesosphere is equal to the value derived by Connes et al. (1968) for 1967 (4.5×10^{-5}). The broader wings of the synthetic spectrum relative to the measured spectrum in 1982 indicate that the mixing ratio of CO in the lower boundary of the Venus mesosphere fell below 2×10^{-5} at the time of the 1982 measurement.

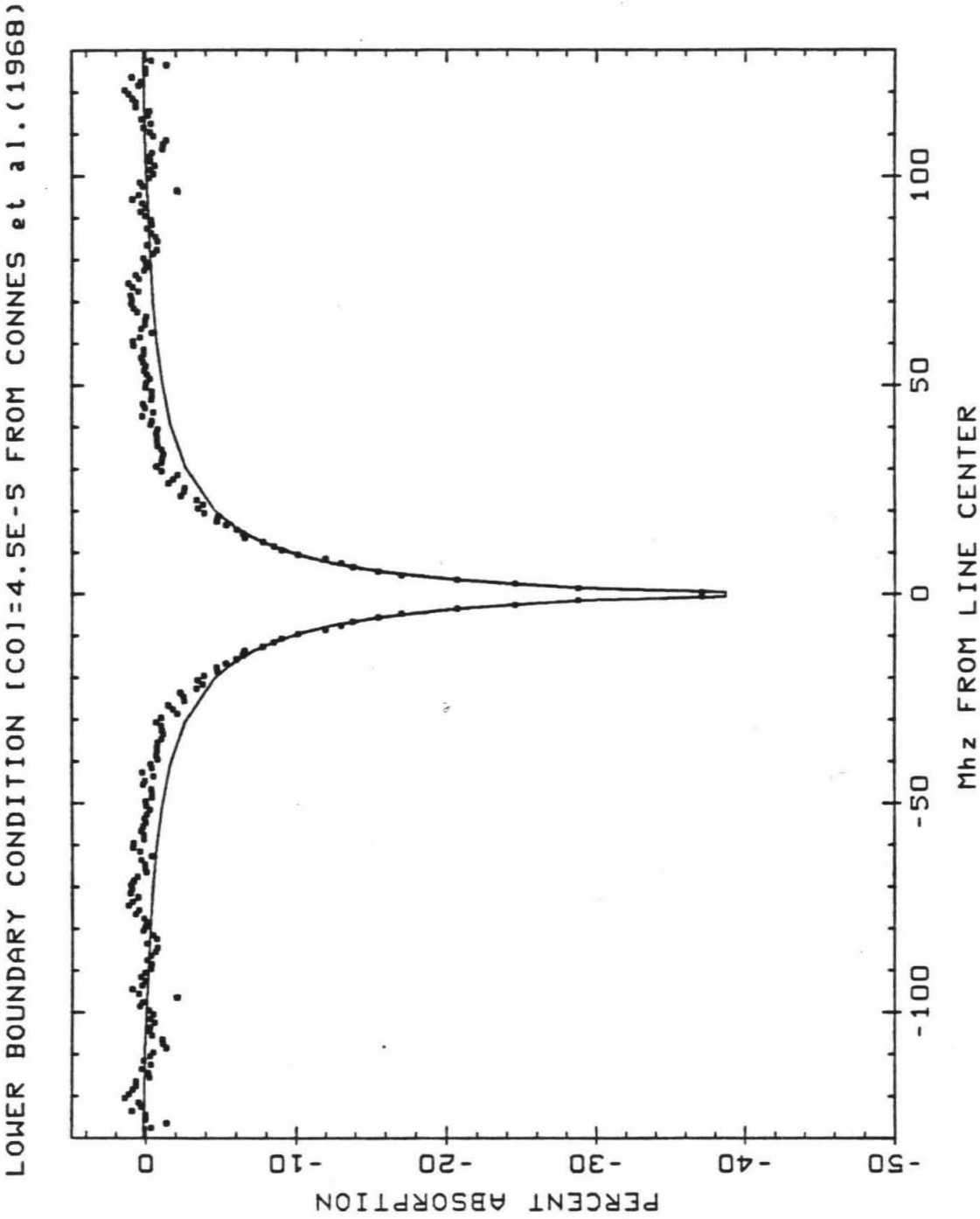
LOWER BOUNDARY CONDITION [CO]=4.5E-5 FROM CONNES et al.(1968)
PERCENT ABSORPTION
0
-10
-20
-30
-40
-50
-100
-50
0
50
100
Mhz FROM LINE CENTER

4. DIURNAL BEHAVIOR OF CO FROM MICROWAVE SPECTRA

The spectra of Figures 1-5 give evidence for variations of CO mixing ratios in the Venus mesosphere, but do not adequately define the pattern of variation. Ideally such definition requires simultaneous measurements which are spatially resolved over the globe of Venus. Spatial and temporal variations could thus be differentiated. However, present CO microwave measurements have not adequately resolved Venus, so that only disk average spectra taken for various phases of Venus are available. Under these conditions any variations observed are either temporal variations or hemispherically averaged diurnal variations.

4.1 Observations

In order to form a more complete picture of these observed variations, we compare the entire set of microwave CO spectra that have been presented by various workers to date. The most convenient form of direct comparison among the spectra is to consider the variation of the line depth at a given frequency offset from the line center. The offsets can be chosen to semi-quantitatively reflect the variation of CO mixing ratios at a particular altitude in the Venus mesosphere, due to the relationship between line width and pressure. We present (Figures 19-22) the variation of the spectral line depth versus Venus phase (and local solar time of the sub-Earth point on Venus) for line center frequency offsets of 0, 5, and 10 MHz. These frequency offsets correspond very roughly to the mixing ratio of CO at altitudes of $>$ 95, 85, and 80 kilometers, respectively (e.g. see Figure 12). Because the spectra do not have identical bandwidths, we reference the line depths at the 0, 5, and 10 MHz offsets to the signal at 30 MHz from line center. Hence the line depths plotted are the line depth at the given offset minus the line depth at 30 MHz from line center. The

data were taken between 1975 and 1982 by (W), Kakar et al. (1976), Gulkis et al. (1977) Wilson et al. (1981), and Wilson and Klein (1982); (S), Schloerb et al. (1980, 1981), Schloerb and Good (1982); and (P), ourselves. The ordinate presents the depth of absorption at a particular frequency relative to the depth at 30 MHz from line center. The abscissa is given in both local solar time of the sub-Earth point on Venus and the phase angle of Venus.

The measurements presented in Figures 19-22 cover 5 consecutive cycles of Venus phase (i.e., from superior to superior conjunction). We show the separate cycles by using different symbols for each apparition of Venus. The first microwave spectra of Venus were taken by Kakar et al. (1976) during the 1975-1976 apparition of Venus (symbol = □). Two more spectra were taken (Gulkis et al., 1977; Wilson et al., 1981) during the 1976-1977 apparition of Venus (symbol = *). The most comprehensive observations of the Venus phase cycle were taken during the 1978-1979 apparition of Venus with a total of 8 measurements (symbol = Δ) by Muhleman et al. (1979a), Schloerb et al. (1980), and Wilson and Klein (1981). Five more spectra were added during the 1979-1980 apparition of Venus (symbol = O) by Schloerb et al. (1981) and Clancy et al. (1981). Schloerb et al. measured a sixth spectrum near superior conjunction during the 1979-1980 apparition. We do not include that spectrum in our comparison as its signal-to-noise was very poor. Finally, we include our most recent January, 1982 measurement observed during the 1981-1982 apparition of Venus (symbol = ◊). Note that we do not include our September-November 1982 spectra due to their severe baseline limitations.

In principle, it is possible to partially separate temporal (cycle to cycle) and phase variations for the absorption depths of Figures 19-22. However, the phase coverage is limited for many of the individual cycles and there are

calibration biases among the different data sets. In particular, the handling of sidebands is not identical among the data sets of Wilson et al. (W), Schloerb et al. (S) and ourselves (P). Thus the relative absorption depths among these three data sets may be uncertain by ± 5%. This uncertainty makes it difficult to unambiguously demonstrate temporal variations of line center absorption depths among the 5 cycles of Venus that have been measured. We note that ± 5% uncertainty is a negligible error term for the very low absorption depths in the wings of the spectra.

The error bars shown in Figures 19-22 indicate uncertainty in the absorption depths due to system noise and systematic fluctuations in the baselines of the spectra. System noise is the most significant source of uncertainty only for the line center, narrow channel width absorption depths of Figure 19 (and, to a lesser extent, Figure 20). The absorption depths of Figure 19 are based upon signal in one or two channels and are thus strongly affected by channel-to-channel fluctuations.

The absorption depths of Figures 21 and 22 are measured in the nearly linear wings of the spectra and are thus determined from the signal in many channels. Uncertainty due to noise is subsequently smaller than the uncertainty introduced into the line center depths of Figure 19. However systematic baseline fluctuations in the spectra introduce proportionately large uncertainties in the low absorption wings of the spectra. We consider both standing waves and asymmetry in the spectra about the line center in our estimation of uncertainty due to systematic baseline fluctuation.

4.1.1 Offset = 0 MHz

Comparison of line center depths from different spectra requires special

care due to the steepness of the spectra in the line center. It is important to use equal filter widths (spectral resolution) when making such comparisons. We present line center depths with 200 kHz resolution in Figure 19 and 1 MHz resolution in Figure 20. Line center absorption depths from the $J = 1 \rightarrow 2$ spectra are not included in either Figure 19 or 20 because equivalent $J = 0 \rightarrow 1$ line center opacities cannot be reliably obtained from $J = 1 \rightarrow 2$ spectra, which are optically thick in the line center. The spectra of Schloerb et al. are not included in Figure 19 as these spectra were limited to 1 MHz filter resolution.

Although the data set is far from complete, a general relationship between line center depth and Venus phase is readily apparent in Figure 19. Line center absorption peaks near inferior conjunction of Venus (phase angle = 180°) when the sub-Earth point coincides with the antisolar point on Venus. The minimum line center absorption appears to occur near superior conjunction of Venus (phase angle = 0°) although the data do not extend to phase angles below 40°. There may be an asymmetry between observations covering the morning and evening faces of Venus but, again, the data are not good enough to define such an asymmetry. We note that all of the above conclusions were first made by Wilson et al. (1981) on the basis of their data set alone.

The behavior of the line center depth averaged over 1 MHz spectral resolution (Figure 20) is similar to the phase relationship of the narrow, 200 kHz resolution, line center depths but there are several significant differences. In general, the level of phase variation is smaller. A filter width of 1 MHz introduces much greater sensitivity of line center absorption depths to CO below 95 km. As Figures 21 and 22 show, absorption depths at 5 and 10 MHz from line center (and, hence, CO below 90 km) show a minimum near 180° phase and a maximum towards 0° phase. In other words, the phase variation of absorption

FIGURE 19: Line center absorption depths (referenced to a continuum level at 30 mHz from line center) versus Venus phase angle (or local solar time for the sub-Earth point on Venus) for J = 0 → 1 spectra from Wilson et al. [1981b (W)] and this work (P). Vertical bars indicate estimated error bars. The particular phase cycle of Venus for each measurement is indicated by the plotted symbols (1975-1976, □), (1976-1977, *), 1978-1979, Δ), (1979-1980, O), 1981-1982, ◊). The line center absorption depths are averaged over ± 100 kHz about line center. The solid curves indicate the predicted behavior of absorption depths for a particular diurnal model of CO distribution on Venus. The dashed line indicates the level of absorption depth variation for a diurnally invariant profile of CO. Vertical arrows near 3 and 4 a.m. local time on Venus indicate the position of hydrogen and helium bulges at ~ 160 km altitude (Mayr et al., 1980). Note that the implied CO bulge (~ 100 km altitude) is located near 0^{hr} local time.

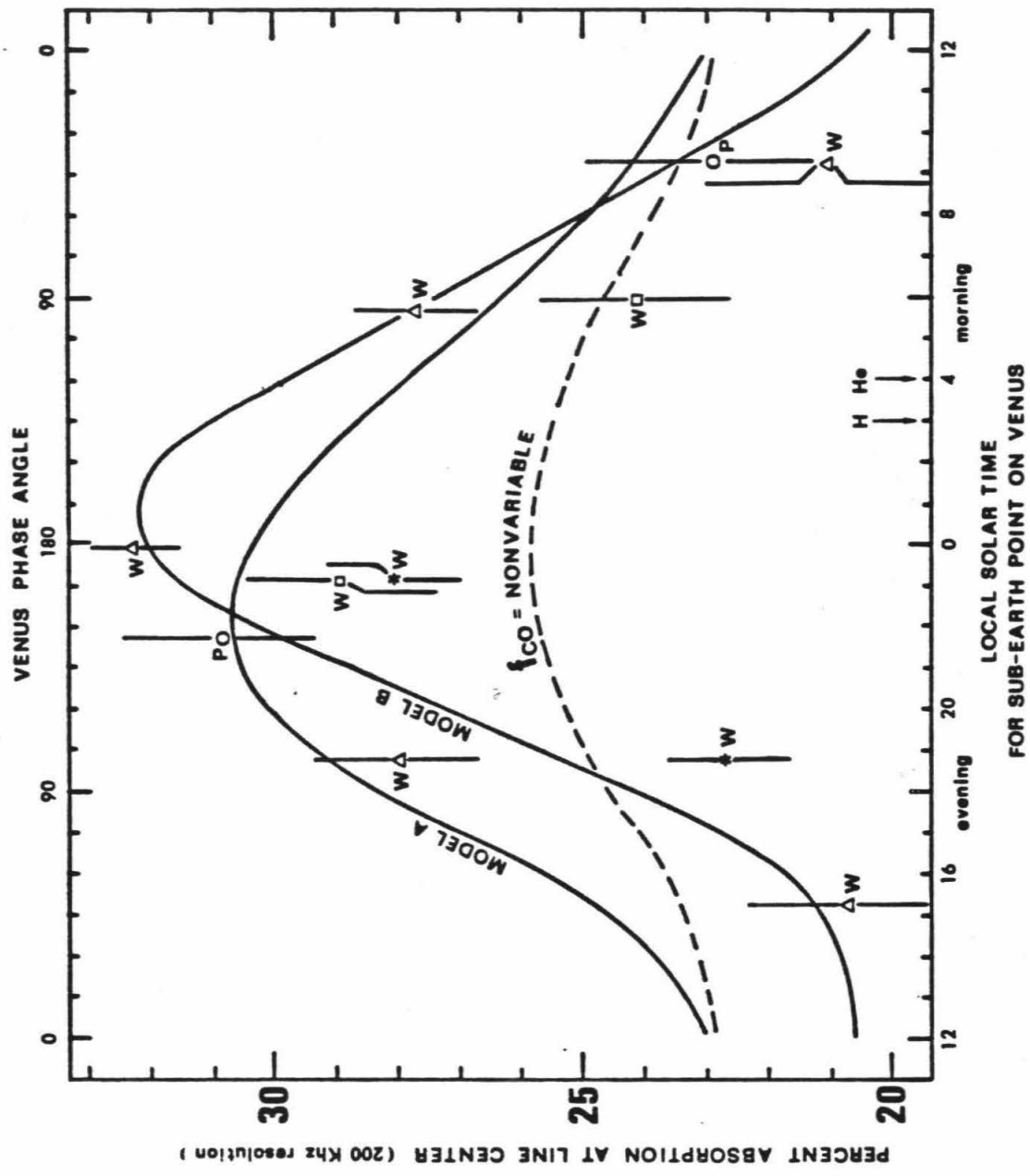
PERCENT ABSORPTION AT LINE CENTER (200 Khz resolution)
30
25
20
VENUS PHASE ANGLE
0
90
180
90
0
LOCAL SOLAR TIME
FOR SUB-EARTH POINT ON VENUS
12
16
evening
20
0
4
morning
8
12
MODEL A
MODEL B
f_{CO} = NONVARIABLE
H He
W
P
O

FIGURE 20: Description is identical to Figure 19 except that absorption at line center is averaged over ± 500 mHz about line center. Also included are measurements by Schloerb et al. (1980, 1981, S). The 1980 measurements of Schloerb et al. are drawn in lighter type (see text).

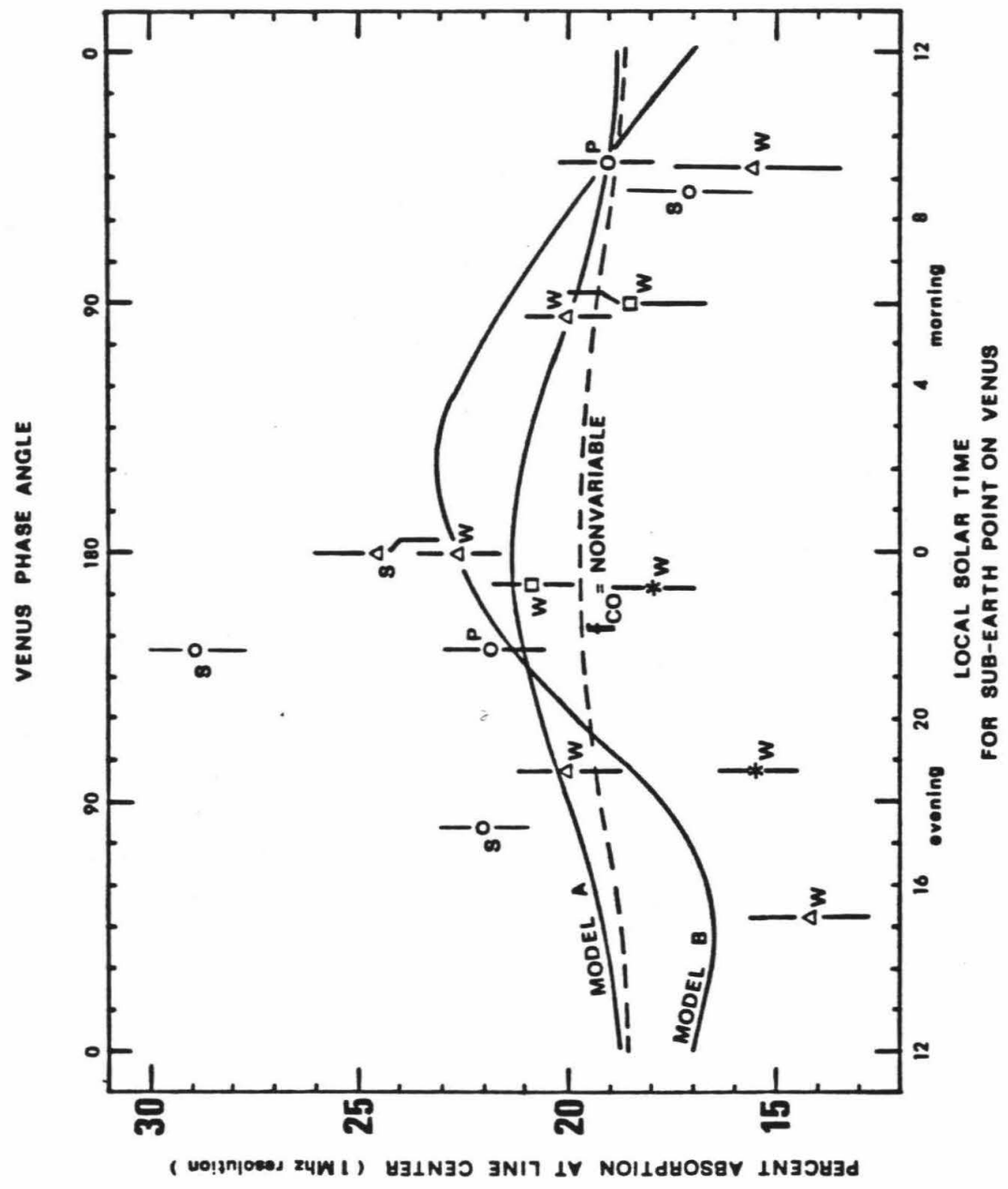
PERCENT ABSORPTION AT LINE CENTER (1Mhz resolution)
30
25
20
15
VENUS PHASE ANGLE
0
90
180
90
0
MODEL A
MODEL B
f_{CO} = NONVARIABLE
LOCAL SOLAR TIME
FOR SUB-EARTH POINT ON VENUS
12
16 evening
20
0
4 morning
8
12

depths reverses sign between the line center and 5 MHz from the line center. Thus the use of larger filter widths to measure line center absorption tends to dilute the effect of the strong phase variation of CO above 95 km. Furthermore, use of 1 MHz filter widths should lead to a shift towards 0° in the phase for maximum measured line center absorption depths. This shift is not clearly demonstrated in the data but is illustrated by the solid line model curves, which will be described shortly.

Finally, in Figure 20 we note the unusual behavior of line center depths measured by Schloerb et al. during the 1979-1980 apparition of Venus (the circles, drawn in with lighter lines). In particular, the Schloerb et al. observation near a phase angle of 140° exhibits considerably deeper absorption than any previous or subsequent measurements. We also point out the near coincidence in time between the 140° phase measurement of Schloerb et al. and our own 145° phase measurement, taken one day later in May of 1980 (the circle, labeled "P"). Yet the line center (1 MHz resolution) absorption depths for the two measurements are very different. In the following section we point out that absorptions depths in the wings of the spectra are also quite different for these nearly coincident observations.

Two important conclusions are: (1) The abundance of CO above ~ 95 km in the Venus atmosphere exhibits diurnal variation with average nightside abundance approximately a factor of 2-4 times greater than dayside abundance (e.g. Figure 6). (2) On the basis of a least squares $A\cos\vartheta + B\sin\vartheta$ fit to the line center absorption depths of Figure 19 (where ϑ is the local solar hour angle for the subearth point on Venus) the nightside CO bulge above ~ 95 km occurs at $0.6 \pm {}_{.6}{}^{.7}$ hr local solar time on Venus. This is in contrast to measurements (Niemann et al., 1980; Brinton et al., 1979) and models (Mayr et al., 1980) of H and He bulges

in the upper atmosphere of Venus (> 150 km altitude). As indicated in Figure 19, the observed H and He bulges are shifted from the antisolar point towards morning by 3-4 hr.

4.1.2 Offset = 5, 10 MHz

The trend for absorption depths at 5 and 10 MHz from line center is nearly opposite the behavior of line center absorption depths. As can be seen in Figures 21 and 22, maximum absorption occurs near the subsolar point on Venus. The maximum absorption level is not accurately constrained by the data, partly because there are no measurements between 0° and 40° phase. The minimum absorption depth appears to be offset a few hours before midnight (i.e. antisolar point) on Venus. This minimum is reliably repeated for four consecutive apparitions of Venus. On the basis of $A\cos\vartheta + B\sin$ fits to the data of Figures 21 and 22 we find maximum absorption depths in the wings of the spectra to occur at 8.5 ± 1.0 hr local solar time on Venus. There is, again, some indication of asymmetry between the morning and evening sides of Venus but coverage of the evening face of Venus is very limited.

The nature of the transition between the very narrow (i.e. low absorption depths at 5 and 10 MHz from line center) spectra measured near 180° phase and the broad spectra measured towards 0° phase is not well delineated by the data of Figures 21 and 22. The data may be taken to indicate either a sharp transition in spectral and line width after inferior conjunction (phase = 180°) or a more gradual transition between inferior and superior conjunction of Venus. Superimposed temporal variations, particularly between the different apparitions of Venus, further obscure the exact pattern of phase variation. The clearest indication of phase variations is obtained by comparing the absorption line depths for the 1978-1979 apparition of Venus (symbol = Δ), for which the

FIGURE 21: Absorption depths at 5 mHz from line center (referenced to a continuum level at 30 mHz from line center) versus Venus phase angle. Description of symbols is given in Figures 19 and 20. Maximum CO absorption falls near 9^{hr} local time versus $\sim 0^{hr}$ for line center absorption depths (Figures 19 and 20) indicating that the CO bulge at 80-85 km altitude is shifted towards the morningside of Venus.

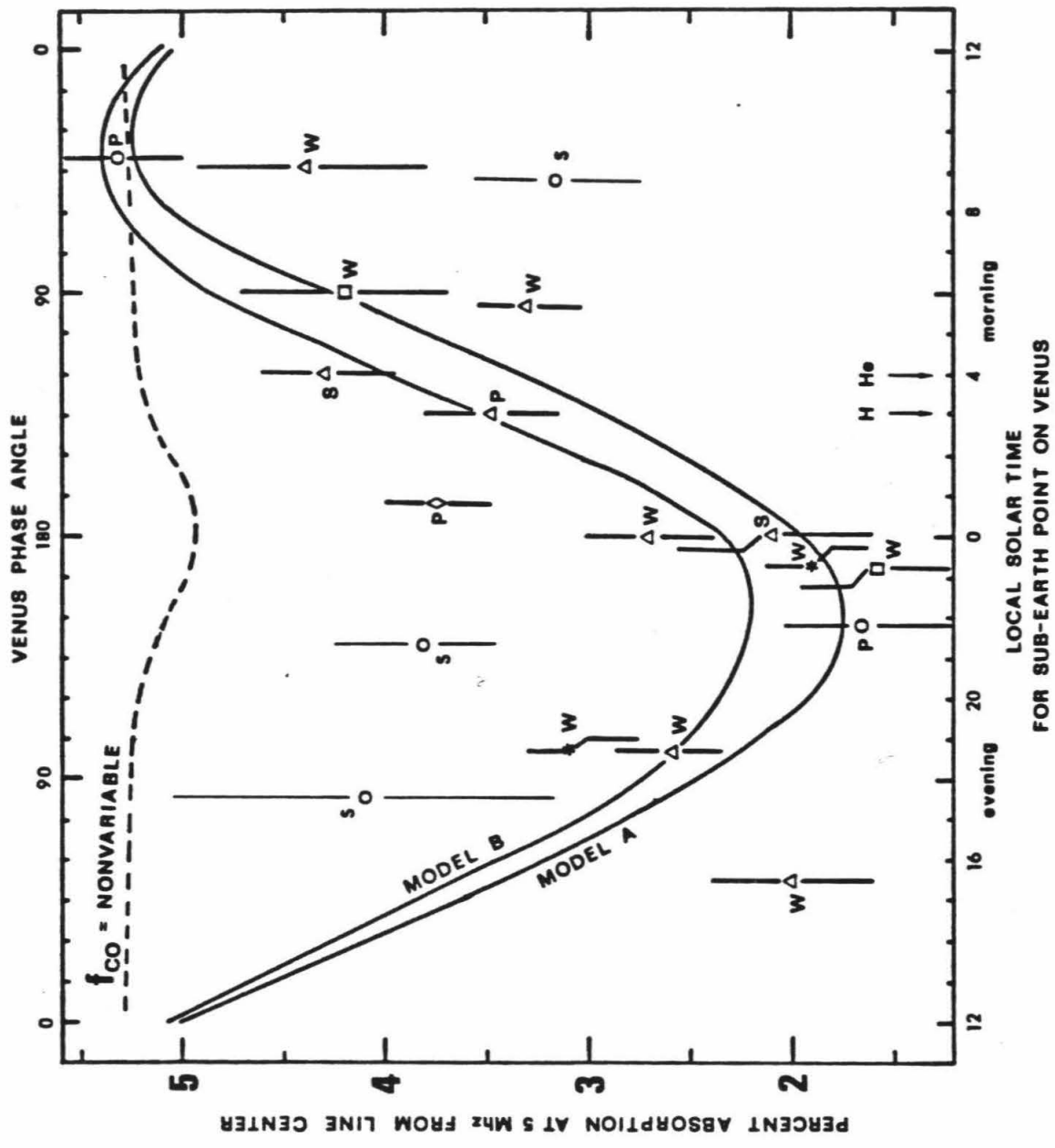
PERCENT ABSORPTION AT 5 Mhz FROM LINE CENTER
5
4
3
2
VENUS PHASE ANGLE
0
90
180
90
0
LOCAL SOLAR TIME
FOR SUB-EARTH POINT ON VENUS
12
16
evening
20
0
4
morning
8
12
MODEL A
MODEL B
f_{CO} = NONVARIABLE
H He

FIGURE 22: Absorption depths at 10 mHz from line center (referenced to continuum level at 30 mHz from line center) versus Venus phase angle. Description of symbols is given in Figures 19 and 20. Conclusions are identical to those from 5 mHz absorption depths in Figure 21.

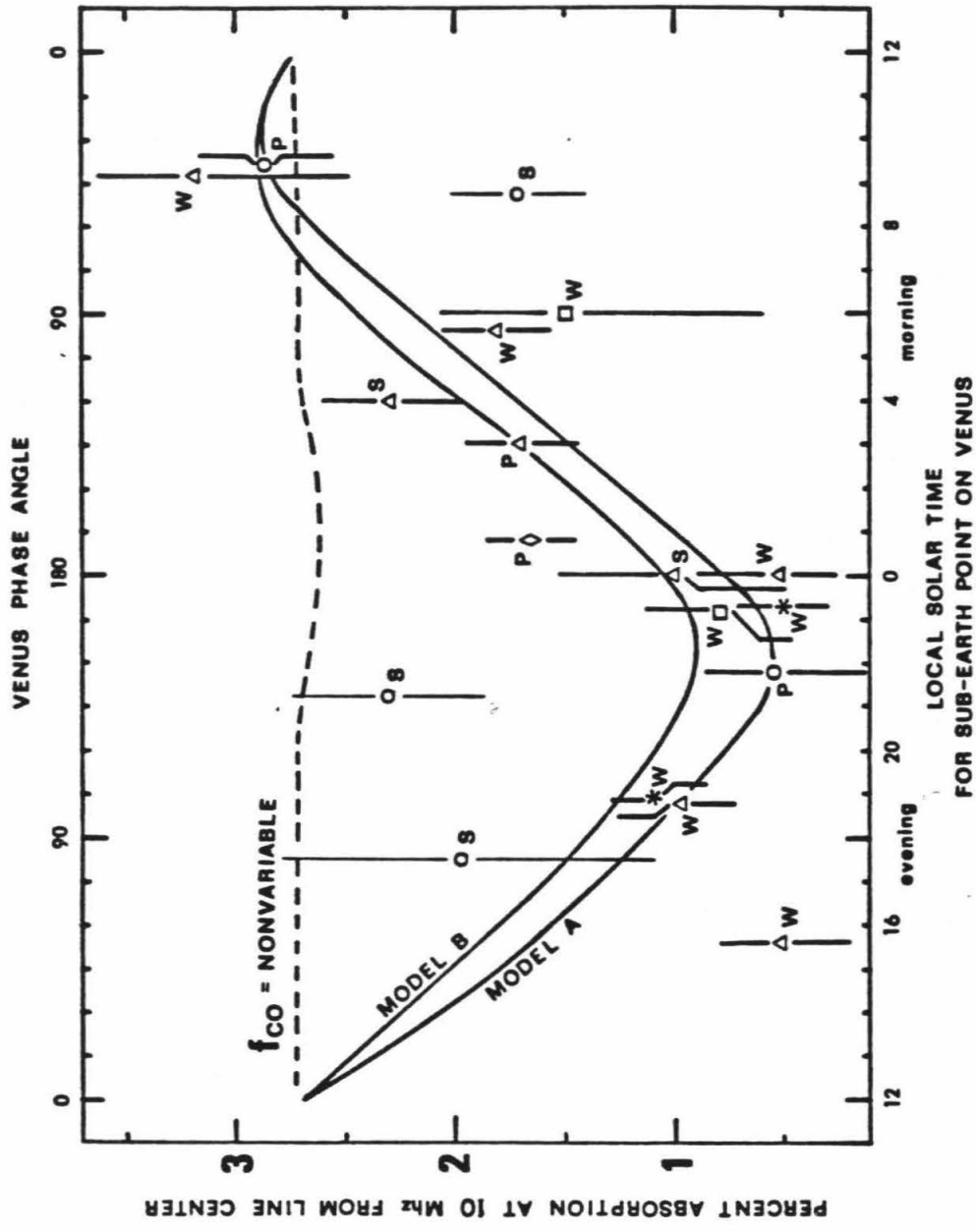
PERCENT ABSORPTION AT 10 MHz FROM LINE CENTER
VENUS PHASE ANGLE
LOCAL SOLAR TIME
FOR SUB-EARTH POINT ON VENUS
morning
evening
MODEL A
MODEL B
f_{CO} = NONVARIABLE

phase coverage is most complete.

We note that the most recent results of Schloerb et al. do not fall into the pattern of phase variation described above for 5 and 10 MHz offsets from line center. In fact, comparison of the 1980 observations of Schloerb et al. and ourselves indicates striking disagreement. Our May 1980 spectrum was taken one day after the May 1980 spectrum of Schloerb et al. (the points labelled "P" and "O" near the local solar time of 22 hr). Yet the May spectrum of Schloerb et al. implies 2 to 3 times greater CO abundance between 80 and 90 km altitude in the Venus mesosphere than our May spectrum. Furthermore, the November 1980 spectrum of Schloerb et al. implies a factor of two less CO abundance in the same altitude range than our December 1980 spectrum (the points labelled "P" and "O" near 10 hr local time). These two measurements were separated by three weeks in time but sample very similar phase angles.

As previously mentioned, the 1980 spectra of Schloerb et al. also show somewhat atypical line center absorption depths (Figure 20). At present the cause of these disagreements is unclear. Either the distribution of CO in the Venus mesosphere fluctuates on a timescale as short as ~ 1 day or there is inconsistency in the measurements. We note that we searched for variations in the CO spectrum of Venus during the 4 days of observation in January, 1982. We did not observe any significant variations. Still we have no idea what the time scale of such variations might be. It is interesting to note that for the 1981-1982 apparition of Venus, Schloerb measured ~ 15 $J = 0 \rightarrow 1$ spectra of Venus (Schloerb and Good, 1982) and found phase variations similar to the behavior shown in Figures 21 and 22. However, Schloerb finds maximum absorption in the spectral wings for local solar times of ~ 5 am on Venus (F.P. Schloerb, personal communication, 1982).

The principle conclusions to be drawn from Figures 21 and 22 are as follows. (1) The general trend for CO between 80 and 90 km is an approximately 2-4 times greater abundance on the dayside relative to the nightside of Venus. (2) There may be considerable fluctuations of the CO abundance between 80 and 90 km altitude on a timescale as small as one (Earth) day. (3) The maximum abundance for the diurnal trend of CO between 80 and 90 km altitude is shifted towards morning hours on Venus. The minimum abundance of CO in the same altitude region occurs 1-2 hours before midnight on Venus.

4.2 Models of the Diurnal Variation of CO in the Venus Mesosphere

The variation of absorption depths in Figures 19-22 indicates an average phase dependence for the distribution of CO in the Venus mesosphere. For phase angles near 0°, the altitude distribution of CO is similar to the CO mixing profile derived from our December 1980 spectrum (Figure 6). The mixing profile found from our May 1980 spectrum characterizes the mesosphere for phase angles near 180° (also Figure 6). We note that the observations presented in Figures 19-22 represent whole disk average measurements for Venus. The data do not distinguish the latitudinal distribution of CO because the latitudinal coverage of whole disk measurements does not change with the variation of the phase of Venus as viewed from the Earth. The observations measure changing phase within the ecliptic plane; i.e., the variation of local solar hour angle on Venus as seen from the Earth. Hence we describe and model the phase variations of Venus as diurnal variations.

In order to model the behavior of CO absorption depths as presented in Figures 19-22, we have constructed several basic models for the diurnal distributions of CO in the Venus mesosphere. Synthetic microwave spectra are gen-

erated in essentially the same manner as described in section 3 except that the altitude mixing profile of CO is not assumed constant over the disk of Venus. The radiative transfer problem is solved for a two-dimensional grid of ray paths (Figure 23) covering the observed hemisphere of Venus. We use two models for the longitudinal variation of the CO mixing profile. For both cases we assume constant CO profiles along constant lines of longitude. In addition we use the dayside atmosphere of Table II for illuminated portions of the observed disk of Venus and the nightside atmosphere of Table II for shadowed portions of the disk.

Before discussing the specific models of longitudinal variation, we point out that a small amount of phase variation for CO microwave spectra would occur even for a uniform global distribution of CO on Venus. A moderately important effect in the line center of CO microwave spectra is the day-night contrast in atmospheric temperatures above 100 km. Secondly, the relative sizes of the antenna beam and the disk of Venus change significantly between 0° phase and 180°. A result is that the longer path lengths (hence, deeper absorption) near the limb of Venus are partially excluded by the antenna beam when the angular dimension of Venus equals the beam size (near 180° phase). Hence, for a uniform global distribution of CO, spectra taken near 180° phase will show marginally decreased absorption relative to spectra taken near 0° phase (where the angular size of Venus is much smaller than the antenna beam and the beam samples evenly over the disk of Venus).

We show (dashed lines, Figures 19-22) the predicted phase variation for absorption depths, assuming uniform global distribution of CO on Venus. We assume the CO mixing profile found from our December 1980 spectrum for the calculation of absorption depths, so that the constant CO model (dashed lines)

FIGURE 23: Two dimensional grid (in latitude-longitude coordinates) used to generate synthetic spectra for model A and B diurnal distributions of mesospheric CO on Venus.

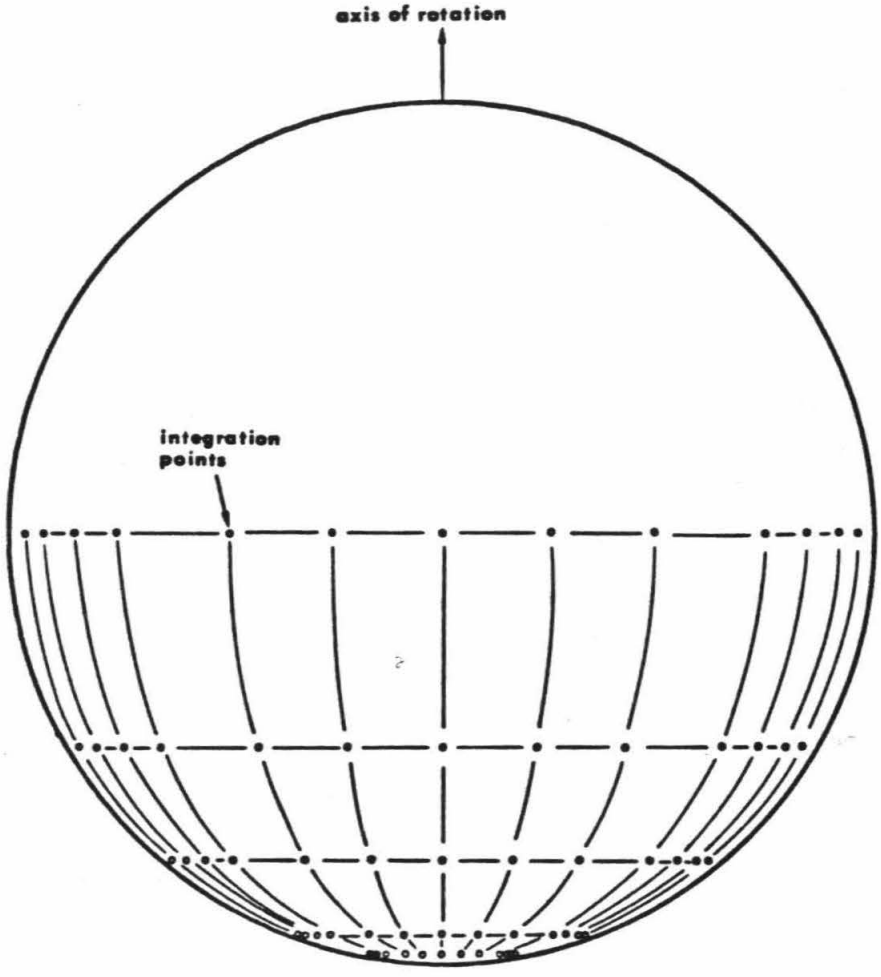
axis of rotation
integration
points

coincides with the data near 180° phase. One can see that the effects of the antenna beam and the diurnal variation of mesosphere temperatures on Venus cannot account for the phase variation of CO absorption spectra of Venus, although the effect is significant for line center absorption. We include both of these effects in synthetic spectra generated from our models of diurnal CO distribution in the Venus mesosphere.

4.2.1 Model A

The simplest model for global variation of CO in the Venus mesosphere is a bimodal distribution for the day and night hemispheres of Venus. We choose the CO profiles derived from our May 1980 and December 1980 spectra (Figure 6) to specify the altitude distribution of CO for the nightside and dayside mesospheres of Venus, respectively. The transition between these two mixing profiles is modeled as a sharp discontinuity (i.e. step function) offset 2 hours (30°) before the evening and morning terminators of Venus. The offset is chosen so that the model coincides, approximately, with the phase angle for the observed minimum absorptions depths at 5 and 10 MHz from line center (Figures 20 and 21). As a consequence, the maximum, line center absorption depth for model A (Figures 19 and 20) is also offset 2 hours prior to midnight on Venus.

The behavior of the synthetic absorption depths from model A versus Venus phase are presented as solid-line curves in Figures 19-22. The model curves agree with the absorption depths of the May 1980 and December 1980 spectra due to the use, in model A, of the CO profiles derived from these spectra. The synthetic absorption curves of model A are in approximate agreement with the observed behavior of absorption depths in the wings of measured spectra (Figures 21 and 22). There is some indication that absorption depths in the wings of the spectra increase more sharply after inferior conjunction than

predicted by model A. However, we reemphasize that the data are not continuous in time, but cover 5 apparitions of Venus. Inspection of absorption depths from the 1978-1979 apparition of Venus (symbol = Δ) indicates that the phase transition absorption depths at 5 and 10 MHz from line center may well be as gradual as depicted by the model A curve.

As shown in Figures 19 and 20, model A does not well describe the phase variation of CO line center depths for Venus. The maximum line center absorption for model A is offset 2 hours before midnight on Venus whereas the measured spectra appear symmetric about midnight (the antisolar point) on Venus. Note also the level of phase variation for 1 MHz resolution line center depths in Figure 20. Model A does not exhibit a sufficient amplitude of phase variation to match the observed behavior of the measurements.

4.2.2 Model B

The inadequacies of model A suggest that the global distribution of CO on Venus cannot be simply described by separate day and night CO mixing profiles for the Venus mesosphere. The phase offset of line center variations with respect to variation of absorption depths in the wings of the spectra indicates that the abundance of CO above 95 km does not vary in phase (or exactly out of phase) with CO abundance between 80 an 90 km. It is necessary to specify a diurnal variation of CO mixing ratios that allows maximum CO mixing ratios above 95 km to occur approximately 10^{hr} before maximum CO mixing ratios below 90 km. Furthermore it is useful to consider a smoothly varying longitudinal distribution of CO mixing profiles as opposed to the step function variation employed in model A. For model B we describe the longitudinal (diurnal) variation of the CO mixing profile in the form

$$f_{CO}(\varphi,z) = f_{CO}^{(1)}(z)\,\sin^2\left[\frac{\varphi}{2}+\Delta\right] + f_{CO}^{(2)}(z)\,\cos^2\left[\frac{\varphi}{2}\right] \qquad (1)$$

where φ is the longitudinal distance from the antisolar point on Venus. As with model A, we define the altitude mixing profile of CO in terms of the mixing profiles we derived from our day (December 1980) and night (May 1980) CO spectra of Venus. $f_{CO}^{(1)}(z)$ and $f_{CO}^{(2)}(z)$ are slightly modified day and night altitude mixing profiles derived from the day (December) and night (May) mixing profiles of Figure 6. We use a phase shift, Δ, of 30° in order to specify minimum CO abundance between 80 an 90 km to occur at 10 p.m. local solar time on Venus (i.e. to correspond roughly with the time of minimum absorption depths in Figures 21 and 22). The lack of a phase shift in the $\cos^2$ term assures that, to first order, maximum CO abundance above 95 km occurs at the antisolar longitude on Venus, although there is a slight shift due to the $\sin^2(\varphi/2 + \Delta)$ term. Figure 24 compares the bimodal distribution of CO mixing profiles from model A to the continuous longitudinal distribution of CO mixing profiles employed in model B. Note that the profiles are drawn as dashed lines above ~ 105 km and below ~ 85-80 km. The data of Figures 19-22 are not very sensitive to the mixing ratio of CO in these altitude ranges (e.g. Figures 6 and 7).

The agreement of model B with the data for line center absorption depths is considerably better than achieved with model A. The amplitude of phase variation for in line center absorption is greater for model B than model A. This is primarily because the May and December 1980 measurements (circles, labeled "P" in Figures 19 and 20) are constrained to fit the maximum and minimum line center absorption depths in model A, but represent only somewhat intermediate absorption depths in model B. The complete set of line center absorption measurements in Figures 19 and 20 indicates that the

FIGURE 24: Models of diurnally varying CO mixing profiles for the Venus mesosphere. Solid lines indicate the $\cos^2$, $\sin^2$ smoothed CO distribution of model B. The individual profiles are labeled by their appropriate local solar times on Venus. These profiles are represented by dashed lines where the data of the Figures 19-22 do not adequately define the CO mixing ratio (roughly below 80-85 km and above ~ 105 km). The two dotted profiles indicate the day-night bimodal distribution of model A.

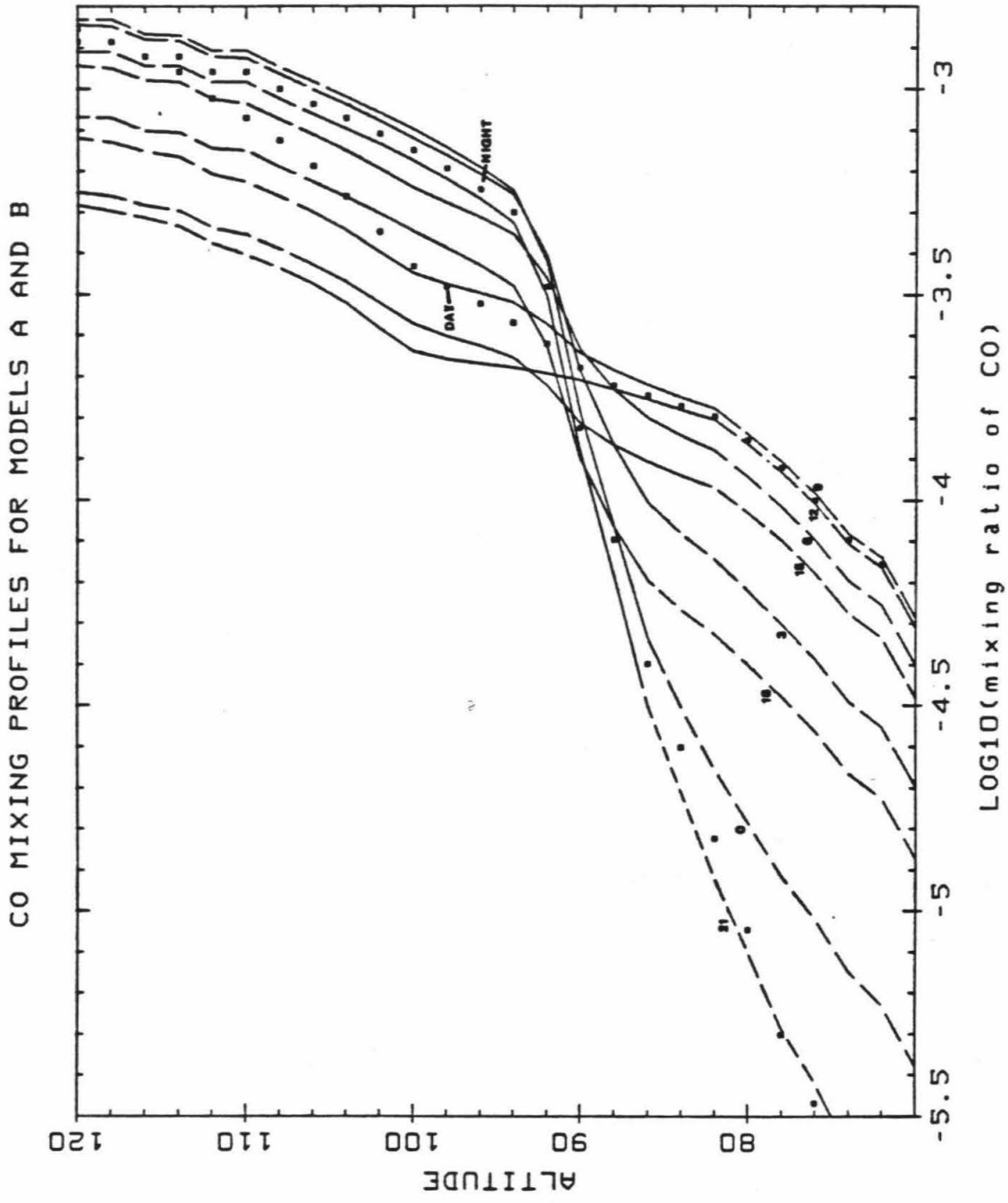
CO MIXING PROFILES FOR MODELS A AND B
ALTITUDE
120
110
100
90
80
LOG10(mixing ratio of CO)
-3
-3.5
-4
-4.5
-5
-5.5
DAY
NIGHT

assumptions of model B are more nearly valid.

The fit of model B for absorption depths in the wings of the spectra (Figures 21 and 22) differs from model A in one important respect. The $\sin^2$ term in model B for daytime CO mixing ratios does not fall off fast enough towards the nightside of Venus to allow sufficiently narrow spectra at phase angles of 180°. Thus the minimum absorption depths for model B in Figures 21 and 22 are larger than the minimum depths indicated by the data. This deficiency may be partly alleviated by reducing the dayside CO mixing ratios below 90 km for model B. Such a procedure would also lower the maximum absorption depths at 5 and 10 MHz from line center for model B. Alternatively, we could specify a larger gradient in dayside and nightside CO mixing profiles on Venus. For example, rather than the $\cos^2$ and $\sin^2$ dependence on φ in equation (1) we might use $|\cos^3|$ and $|\sin^3|$ dependence. The implication of higher powers of sin and cos in equation (1) is that the CO "bulges" near midnight (180° phase) above 95 km and near 10 a.m. between 90 and 80 km are more tightly confined in solar hour angle (basically φ in equation (1)) on Venus. Taking this argument one step further, we might specify different powers for the sin and cos terms of equation (1). There is no *a priori* reason to believe that the longitudinal confinement of the CO bulge above 95 km is identical to the longitudinal confinement of the CO bulge between 90 and 80 km.

At present these more detailed models of the diurnal distribution of CO in the Venus mesosphere are not justified by the data. Scatter in the measured absorption depths, particularly between phase cycles, does not allow adequate definition of the phase variation. One requires more extensive measurements within separate cycles of Venus phase, especially between local solar times of 10 a.m. and 10 p.m. on Venus, a region that is not well sampled by the data of

Figures 19-22.

5. CHEMICAL-DYNAMICAL MODELS OF THE VENUS MESOSPHERE

Both the altitude profile and the phase variations of CO mixing ratios in the Venus mesosphere can be used to place constraints on the chemistry and dynamics of the Venus mesosphere. In the first section of Chapter 5 we compare the predictions of Dickinson and Ridley's hydrodynamic modeling to the results of microwave observations of CO. We note that the nightside CO bulge above 90-95 km altitude as indicated by the microwave measurements is a primary characteristic of the Dickinson and Ridley models. The opposite phase behavior of CO between 80 and 90 km, as indicated by CO microwave spectra, is not predicted by the dynamical modeling of Dickinson and Ridley. These models do not extend below an altitude of ~95 km and, furthermore, do not consider the effect of zonal winds on the global distribution CO in the Venus mesosphere and thermosphere.

In the second and third sections of Chapter 5 we present the results of diurnal photochemical models for the Venus mesosphere. On the basis of photochemistry from Yung and DeMore (1982) we attempt to reproduce the phase behavior of CO between 80 and 90 km altitude in the Venus mesosphere. We consider possible diurnal variations due to chemistry and vertical eddy diffusion. In the final section of Chapter 5 we return to dynamical mechanisms for the phase variation of CO between 80 and 90 km altitude. Due to the extreme complexity of constructing a relevant dynamical model, we limit ourselves to heuristic arguments for these dynamical models.

5.1 Comparison of Microwave Observation with the Models of Dickinson and Ridley

As outlined in Chapter 1, the hydrodynamic models of Dickinson and Ridley show measures of success and failure in describing the chemical-physical

state of the upper atmosphere of Venus. The most serious failure is an inability to match the steep falloff in atmospheric density and temperature across the terminator from day to night in the Venus upper atmosphere. However this day-night density contrast can only enhance the predicted subsolar to antisolar transport velocities of Dickinson and Ridley's models (particularly vertical velocities in the Venus thermosphere). We note that differential vertical motions for the day and night sides of Venus are the primary cause for the CO nightside bulges predicted by Dickinson and Ridley. Hence it is still useful to compare the diurnal distribution of CO as determined from the microwave measurements to the predictions of Dickinson and Ridley.

As a preface to this comparison we caution that the altitude domain of the models of Dickinson and Ridley only marginally overlaps the uppermost altitude region sensed by the microwave observations. The lower boundaries for the Dickinson and Ridley models are at an atmospheric pressure level of ~ 0.1 mbar (approximately at 95 km altitude). As illustrated in Figures 6 and 7, CO mixing ratios derived from microwave spectra are poorly determined above ~ 105 km. We also note that the microwave measurements measure average altitude profiles of CO mixing ratios for the observed hemisphere of Venus and do not constrain the latitudinal variations of these profiles at all. Solutions for CO distributions from the microwave data do not assume latitudinal variations. The models of Dickinson and Ridley specify symmetry in solar zenith angle so that diurnal and latitudinal variations are derived. Hence comparison of CO profiles from Dickinson and Ridley models and CO profiles from microwave spectra cannot be made on a one-to-one basis.

These difficulties aside, we present the comparison of theory and observation in Figure 25. We show number density profiles derived from the May

FIGURE 25: A comparison of CO number density profiles from the J = 0 → 1 May and December 1980 spectrum to the theoretical models of Dickinson and Ridley, and various other measurements. The Dickinson and Ridley profiles are given for solar zenith angles of 30°, 120°, and 150°. Also included are the day (D) and nightside (N) values at ~ 150 km altitude from the Pioneer-Venus ONMS experiment (Niemann et al., 1980), morningside profile from the Pioneer-Venus BNMS experiment (Von Zahn et al., 1980), and a stratospheric value from the infrared spectra of Connes et al. (1968).

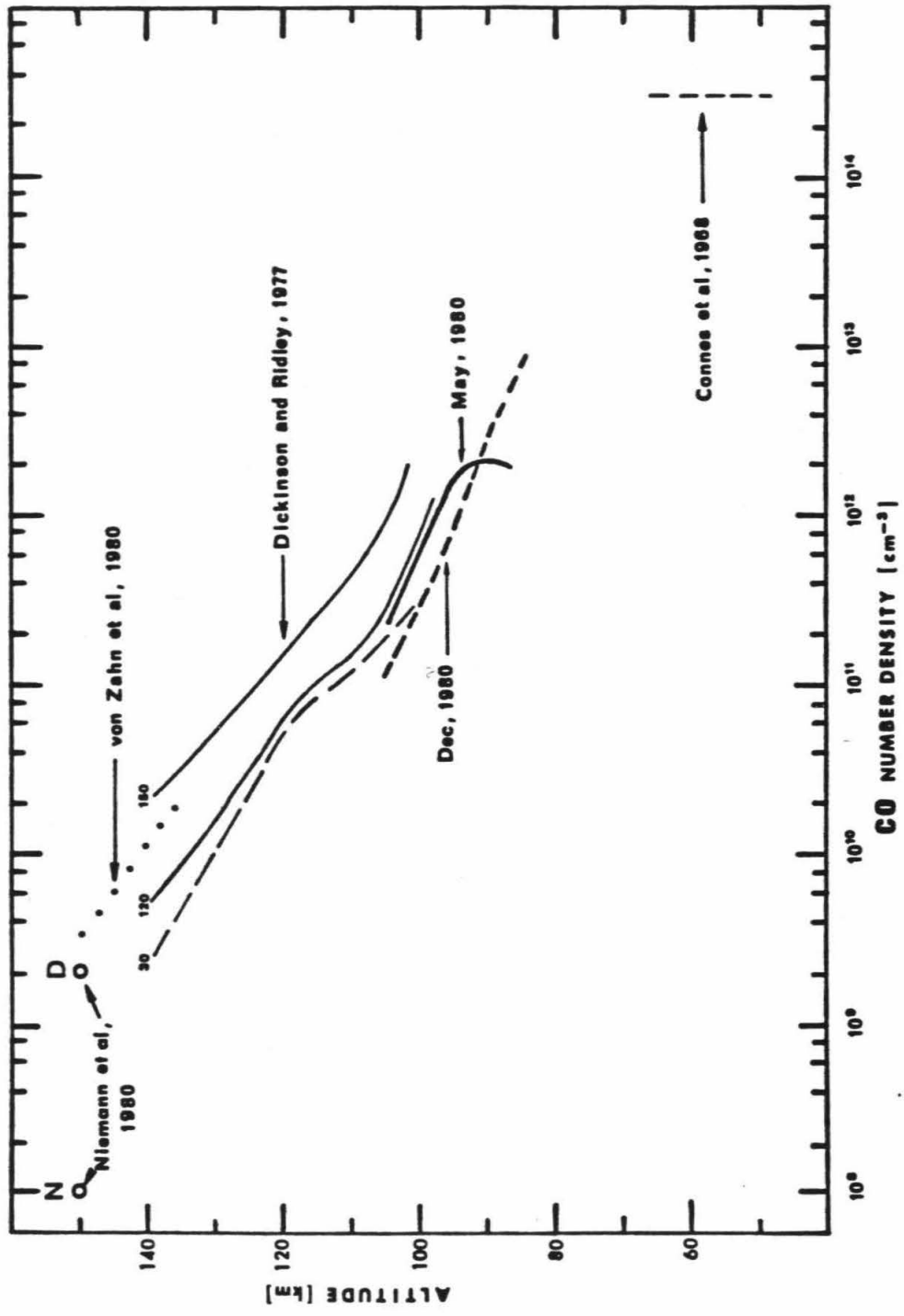
Niemann et al., 1980
N
O
D
O
von Zahn et al., 1980
180
120
90
Dickinson and Ridley, 1977
Dec, 1980
May, 1980
Connes et al, 1968
ALTITUDE [km]
140
120
100
80
60
CO NUMBER DENSITY [cm⁻³]
10⁸
10⁹
10¹⁰
10¹¹
10¹²
10¹³
10¹⁴

(nightside) and December (dayside) 1980 spectra, and profiles for solar zenith angles of 30°, 120° and 150° from the models of Dickinson and Ridley. Also included are CO number densities derived for the day (D) and nightside (N) of Venus above ~ 150 km from the orbiter neutral mass spectrometer (Niemann et al., 1980), and for the morning side (~ 7:40 a.m.) of Venus between 150 and 140 km altitude from the bus neutral mass spectrometer (von Zahn et al., 1980).

The agreement between the microwave results and the model results of Dickinson and Ridley is remarkably good given the before mentioned difficulties of the comparison. This agreement perhaps indicates that in the region 95-105 km altitude where day-night contrast in atmospheric temperatures and number densities is not large, the models of Dickinson and Ridley approximate the circulation of the Venus atmosphere moderately well. We point out that the Dickinson and Ridley model implicitly assumes zero zonal wind velocities so that the nightside CO bulge is centered at the antisolar point (i.e. midnight on Venus). The minimal offset of the CO bulge from midnight as determined from the CO microwave measurements (e.g. Figure 19) may indicate that zonal flow is indeed small in the 95-105 km altitude region of the Venus atmosphere.

Pioneer Venus CO measurements in the region of 140 km altitude and above do not compare well with results of the Dickinson and Ridley model. Apparently the failure of the Dickinson and Ridley models to account for vertical eddy diffusion forces their models to overestimate CO and O bulges in the night-side thermosphere of Venus (Schubert et al., 1980). Excessive buildup of O above ~ 140 km on the nightside thermosphere is the primary reason they do not reproduce the measured, large day-night contrast in atmospheric number density for the Venus thermosphere. Hence, the comparison of day and night CO number densities at 140-150 km for the measurements and models is poor.

Nevertheless, we point out that in terms of mixing ratios there is indeed an enhancement of O on the nightside relative to the dayside of Venus as measured near and above 160 km by the orbiter neutral mass spectrometer (Niemann et al., 1980). The CO/CO_2 ratio is also enhanced on the nightside in this region. Between 105 and 150 km there are no measurements for CO abundance on the dayside versus the nightside of Venus although, presumably, higher CO mixing ratios should also be found for the nightside in this altitude region.

The extension of the CO number density profiles below 90 km from the microwave data (Figure 25) indicates a shift in the CO bulge from the nightside towards the dayside of Venus in the altitude region 90-80 km. This behavior is not reproducible from the models of Dickinson and Ridley given the axisymmetric nature (in solar zenith angle) of their model. In the following several sections we consider important physical processes that may help to explain the phase behavior of CO in the lower (90-80 km) mesosphere of Venus.

5.2 Diurnal-Photochemical Modeling of the Venus Mesosphere

The depletion of CO between 90 and 80 km altitude in the nightside relative to the dayside Venus mesosphere indicates diurnal variation in the chemistry or dynamics of this region. One expects some diurnal variation given the fact that CO_2 is not photodissociated on the nightside of Venus. In order to analyze the magnitude of this effect, we must estimate recombination rates for CO in the nightside mesosphere and a residence timescale for CO molecules on the nightside (i.e., the rotation rate of the atmosphere in the altitude region of the mesosphere). The product of these two parameters allows an estimation of the depletion of CO on the nightside of the Venus mesosphere between 80 and

90 km due to photochemistry alone. One indication that recombination of CO on the nightside might be an important process below 90 km altitude is the altitude profile of CO recombination rates from photochemical models of Venus. Figures 26 and 27 (from Yung and DeMore, 1982) indicate that for schemes involving OH (Figure 26) or Cl (Figure 27), recombination of CO peaks sharply between altitudes of 70 and 90 km.

However, we should also point out several potential weaknesses of a photochemical explanation for the CO depletion on the nightside of Venus between 80 and 90 km altitude. At present it is not clear from the observations that CO below 80 km is depleted on the nightside relative to the dayside of Venus. This point alone does not rule out a photochemical explanation although a steep decline in CO mixing ratios for the dayside mesosphere below 80 km altitude (as suggested by the September 1982 spectrum) corresponding to the steep decline on the nightside below 90-85 km would appear to suggest a dynamical rather than photochemical explanation (see section 5.4). Furthermore, the microwave observations indicate a minimum (maximum) concentration of CO for the 80-90 km altitude region at local solar times before midnight (noon) on Venus. If recombination of CO on the nightside is the important process one might expect minimum (maximum) CO concentrations to be found after midnight (noon) on Venus. Nevertheless, it is important to consider the diurnal character of CO photochemistry in the Venus atmosphere.

5.2.1 The Photochemical Model

The photochemical model employed in this study is a modified version of Yung and DeMore's model C for the Venus mesosphere (1982). Their model C specifies only photochemically produced atmospheric H_2 through dissociation of HCl and H_2O. OH levels are, thus, very low and Cl reactions become the

FIGURE 26: Diurnally averaged profiles of CO recombination rates from model C of Yung and DeMore (1982) in which OH plays the major role for recombination of CO.

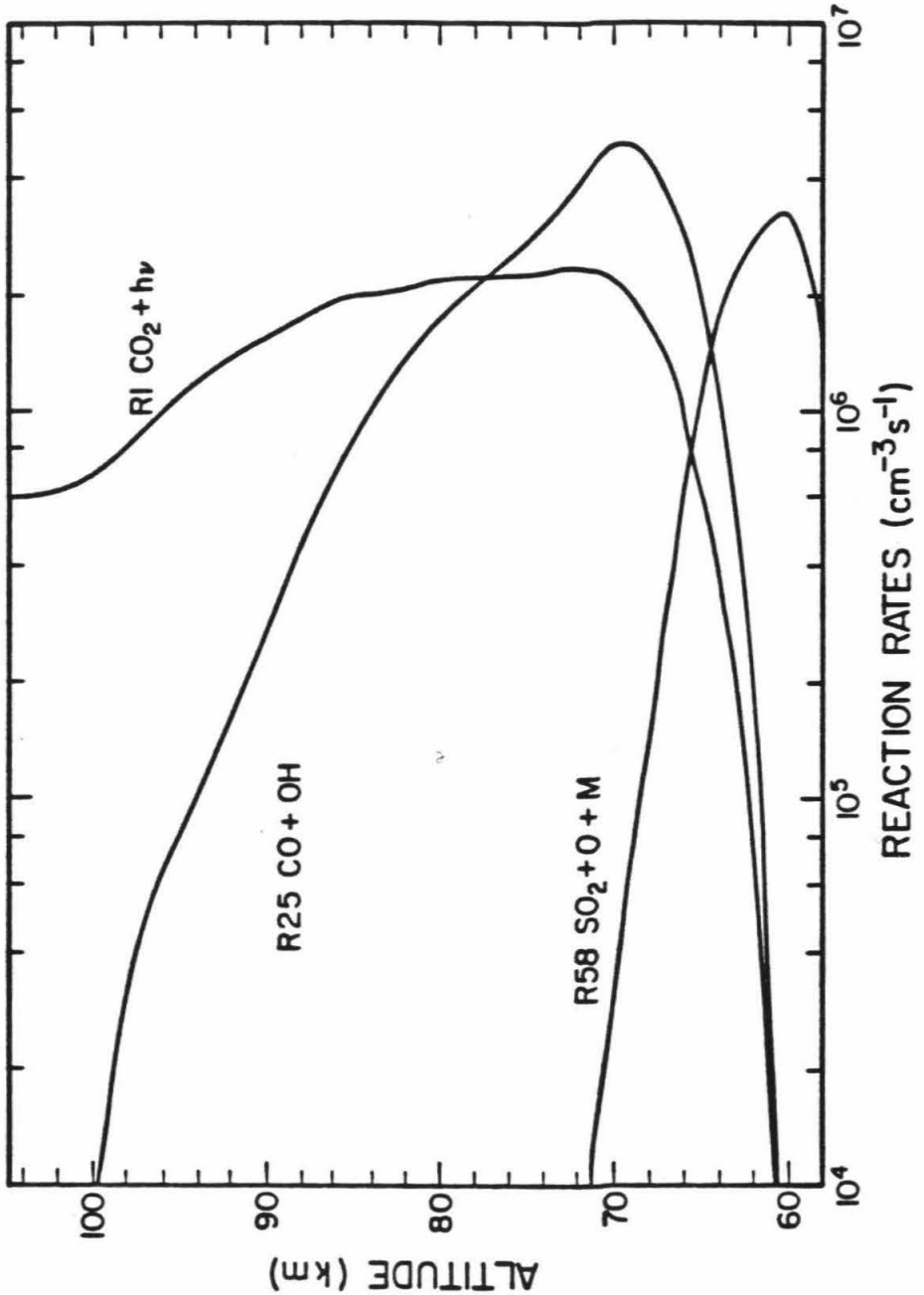
R1 $CO_2 + h\nu$
R25 CO + OH
R58 $SO_2 + O + M$
ALTITUDE (km)
REACTION RATES ($cm^{-3}s^{-1}$)
100
90
80
70
60
10^4
10^5
10^6
10^7

FIGURE 27: Diurnally averaged profiles of CO recombination rates from model C of Yung and DeMore (1982) in which Cl plays the major role for recombination of CO.

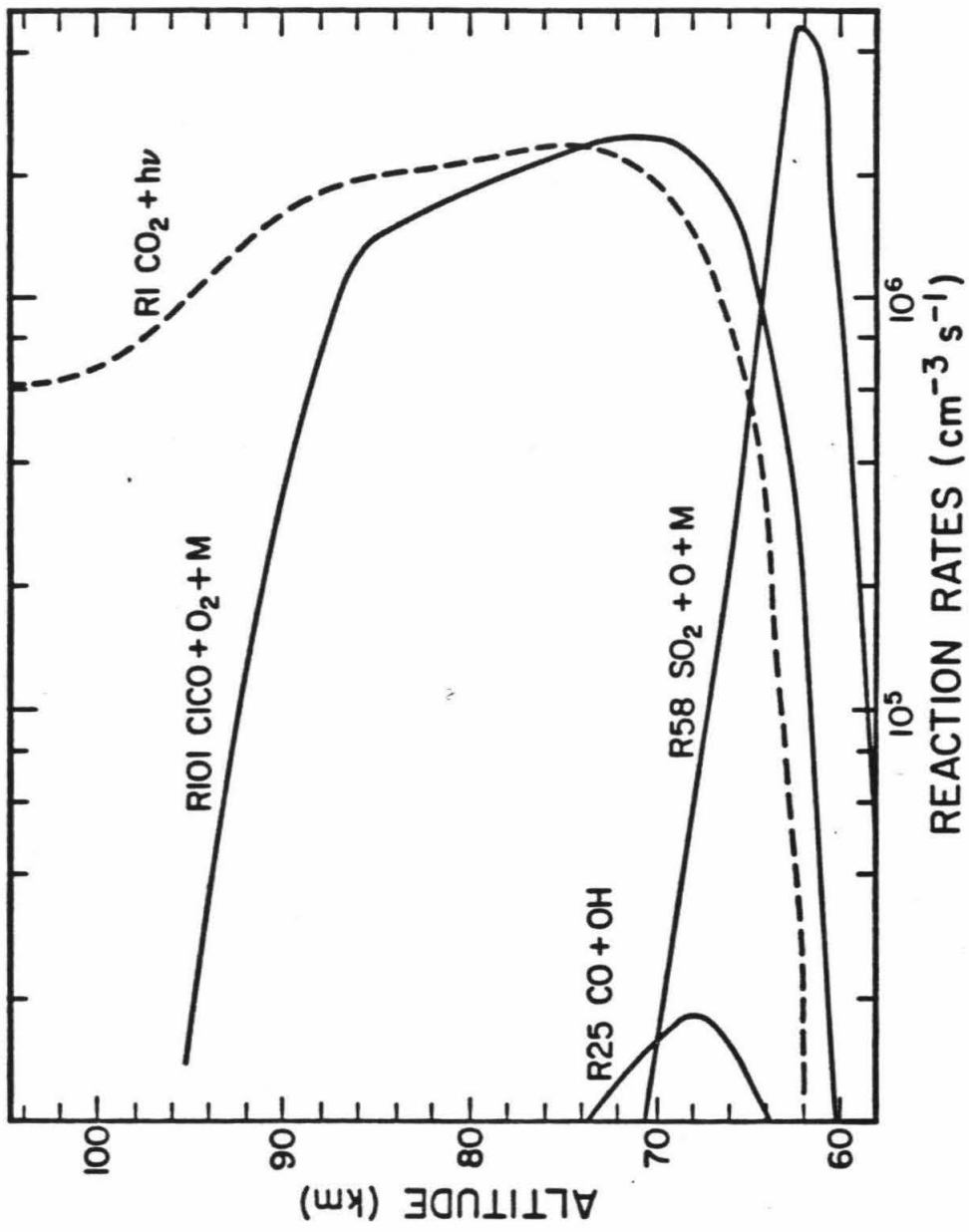
R1 $CO_2 + h\nu$
R101 $ClCO + O_2 + M$
R58 $SO_2 + O + M$
R25 $CO + OH$
ALTITUDE (km)
100
90
80
70
60
10^5
10^6
REACTION RATES ($cm^{-3}\ s^{-1}$)

predominant pathway to CO recombination. Cl is introduced through photodissociation of HCl, which is held constant at a mixing ratio of 10^{-7} (i.e. consistent with the measurement of Connes et al., 1967). The low levels of H_2 ensure sufficiently high levels of free Cl to drive the catalytic recombination of CO. We note that Yung and DeMore's model A, which specifies $[H_2] = 2 \times 10^{-5}$, is characterized by very low levels of free Cl. Recombination of CO is catalyzed by OH rather than Cl. We use model C rather than model A because of the somewhat arbitrary assumption of high levels of H_2 in model A. However both models produce similar recombination rates for CO in the Venus mesosphere (see Figures 26 and 27).

The model is one-dimensional, covering an altitude range of 70-90 km with 2 km altitude resolution. The continuity equation

$$\partial n_i/\partial t = P_i - L_i - \partial \varphi_i/\partial z$$

(where n_i, φ_i, P_i, and L_i are the concentration, vertical flux, production and loss rates of each chemical species, i, at altitude z) is solved with a time-dependent, diffusive-photochemical computer program developed by Mark Allen and Yuk Yung (see Allen et al., 1981; Yung and DeMore, 1982).

Vertical flux, φ_i, is primarily driven by eddy mixing in the mesosphere. We use a nearly constant value of 6×10^{-4} cm^2/sec for eddy diffusivity (K) that is roughly consistent with the altitude profile of K derived by von Zahn et al. (1979) for the upper atmosphere (~ 150-120 km) of Venus (see model I in Figure 29).

$$K(z) = 2 \times 10^{13} / \sqrt{M(z)} \text{ cm}^2/\text{sec}$$

where $M(z)$ is the atmospheric number density in molecules/cm^3.

The time dependence of the model (i.e. $\partial n_i / \partial t$) follows from the diurnal cycling of incident solar UV flux which drives photodissociation of CO_2, H_2O, CHl, ClO, and Cl_2. Short lived species such as H, Cl, OH, O and O_3 show very drastic diurnal variation. We are primarily interested in the diurnal variations of the longer life CO molecule which is in turn tied to abundances of the above, catalytic short lived species.

For further details of the specifics of the photochemical model we refer readers to Yung and DeMore (1982). The significant distinctions between this present work and the work of Yung and DeMore are: 1) the time- dependent nature of the present work versus the diurnal average nature of the Yung and DeMore model, 2) the present work contains only a limited subset of molecular species and reactions taken from the model of Yung and DeMore, 3) the altitude range of the present model (70-90 km) is limited in comparison to the altitude range of the Yung and DeMore model (58-110 km) as we do not treat sulfur chemistry and the cloud regions of the Venus atmosphere, 4) boundary conditions are somewhat modified, as will be described.

5.2.2 Chemistry

Our photochemical model involves 17 chemical species [three of which are held fixed ($[HCl] = 10^{-7}$, $[H_2O] = 2 \times 10^{-7}$, $[CO_2] = 0.95$)] and 29 reactions. The reactions and rate coefficients (Table IV) are taken from Yung and DeMore (1982). Only the atomic species C, H, O, and Cl are used in the present model. The reactions and species of Table IV were found to sufficiently model the altitude region 70-90 km by a comparison of diurnally averaged model results to

Table IV. Photochemical Model Reactions and Reaction Rate Coefficients (see Yung and DeMore, 1982)

	Reactions	Rate Coefficient
(1)	$CO_2 + h\nu \rightarrow CO + O$	
(2)	$H_2O + h\nu \rightarrow H + OH$	
(3)	$HCl + h\nu \rightarrow H + Cl$	
(4)	$ClO + h\nu \rightarrow O + Cl$	
(5)	$O + O_2 + M \rightarrow O_3 + M$	1.3×10^{-33}
(6)	$H + O_2 + M \rightarrow HO_2 + M$	$(3.6 \times 10^{-29})/T$
(7)	$H + O_3 \rightarrow OH + O_2$	$(1.4 \times 10^{-10}) \cdot e^{-480/T}$
(8)	$O + HO_2 \rightarrow OH + O_2$	3.1×10^{-11}
(9)	$CO + OH \rightarrow CO_2 + H$	1.4×10^{-13}
(10)	$H + HO_2 \rightarrow H_2O + O$	9.3×10^{-13}
(11)	$H + HCl \rightarrow H_2 + Cl$	$(2.44 \times 10^{-11}) \cdot e^{-1740/T}$
(12)	$OH + HCl \rightarrow Cl + H_2O$	$(3.0 \times 10^{-12}) \cdot e^{-425/T}$
(13)	$O + HCl \rightarrow OH + Cl$	$(1.1 \times 10^{-11}) \cdot e^{-3370/T}$
(14)	$Cl + H_2 \rightarrow H + HCl$	$(4.7 \times 10^{-11}) \cdot e^{-2340/T}$
(15)	$Cl + HO_2 \rightarrow HCl + O_2$	3.6×10^{-11}
(16)	$Cl + O_3 \rightarrow ClO + O_2$	$(2.8 \times 10^{-11}) \cdot e^{-257/T}$
(17)	$O + ClO \rightarrow Cl + O_2$	$(7.5 \times 10^{-11}) \cdot e^{-120/T}$
(18)	$CO + Cl + M \rightarrow COCl + M$	$(1.3 \times 10^{-34}) \cdot e^{1000/T}$
(19)	$COCl + M \rightarrow CO + Cl + M$	$(6.0 \times 10^{-11}) \cdot e^{-2250/T}$
(20)	$COCl + O_2 \rightarrow CO_2 + ClO$	$(1.0 \times 10^{-12}) \cdot e^{-500/T}$
(21)	$COCl + O \rightarrow CO_2 + Cl$	2.0×10^{-11}
(22)	$Cl + Cl + M \rightarrow Cl_2 + M$	$*1.0 \times 10^{-32}$
(23)	$Cl_2 + h\nu \rightarrow Cl + Cl$	
(24)	$H + Cl_2 \rightarrow HCl + Cl$	$(1.5 \times 10^{-10}) \cdot e^{-593/T}$

(25)	$Cl + HO_2 \rightarrow ClO + OH$		4.0×10^{-12}
(26)	$COCl + Cl \rightarrow CO + Cl_2$		1.0×10^{-12}
(27)	$COCl + COCl \rightarrow COCl_2 + CO$		1.0×10^{-12}
(28)	$COCl_2 + h\nu \rightarrow COCl + Cl$		
(29)	$ClO + ClO \rightarrow Cl + Cl + O_2$		$^{+}3.0 \times 10^{-12}$

the diurnally averaged results of the complete model (which includes sulfur and nitrogen chemistry) of Yung and DeMore. This is consistent with prior analysis of the Yung and DeMore model which indicated sulfur and nitrogen species do not play a significant role in photochemistry above 70 km altitude.

The important reactions for recombination of CO are

$$COCl + O_2 \rightarrow CO_2 + ClO \qquad R20$$

$$COCl + O \rightarrow CO_2 + Cl \qquad R21$$

The complex, COCl, reaches an equilibrium concentration through the reversible reaction

$$CO + Cl + M \iff COCl + M \qquad R18, R19$$

Thus the availability of free Cl drives recombination of CO. The concentration of free Cl is governed largely by the reactions

$$HCl + h\nu \rightarrow H + Cl \qquad R3$$

$$H_2 + Cl \rightarrow HCl + H \qquad R14$$

$$Cl + O_3 \rightarrow ClO + O_2 \qquad R16$$

$$ClO + O \rightarrow Cl + O_2 \qquad R17$$

$$Cl + Cl + M \rightarrow Cl_2 + M \qquad R22$$

$$Cl_2 + h\nu \rightarrow Cl + Cl \qquad R23$$

$$ClO + ClO \rightarrow 2\,Cl + O_2 \qquad R29$$

where R14 is slow due to the low levels of H_2 in the model. Although balance of reactions R3, R22, and R23 provide sufficiently rapid recombination rates for CO on the dayside of Venus (as shown by Yung and DeMore), we are primarily interested in CO recombination on the nightside of Venus, where reaction rates for R3 and R23 fall to zero. For our photochemical model, the stability of free Cl

on the nightside of Venus determines whether or not CO may be depleted by recombination on the nightside of Venus.

5.2.3 Boundary Conditions

For our study of the diurnal effects of photochemistry in the Venus mesosphere, we have generally retained the boundary conditions of Yung and DeMore (1982). That is: 1) zero flux at the boundaries for the short lived odd hydrogen and odd oxygen species, 2) a vertical velocity (-1×10^{-2} cm/sec) at 70 km and zero flux at 90 km for the longer lived Cl species (Cl_2, Cl, $COCl_2$, COCl) and H_2. As opposed to Yung and DeMore, we fixed the mixing ratio of CO at the top of our model to be consistent with the microwave observations (i.e $\sim 2 \times 10^{-4}$ at 90 km altitude). The lower boundary condition for CO is a bit more complicated and requires a short discussion.

Yung and DeMore fixed the mixing ratio of CO to 4.5×10^{-5} at the lower boundary of their model (58 km) on the basis of the 1967 observation of Connes et al. (1969). As we stated in section 3.4, our January 1982 CO spectrum places an upper limit of 1.5×10^{-5} for [CO] near 80 km altitude. Figure 28 compares the CO mixing profile derived from the diurnally averaged Yung and DeMore model C to the CO profile found from our January 1982 (predominantly night-side) spectrum. Also included in Figure 28 is a model profile from a specially modified version of Yung and DeMore's photochemical model A. For this model we artificially specified the same profile of CO recombination rates over the same altitude range (58-110 km) as in the Yung and DeMore model A. (We chose model A for this test because recombination rates of CO are most easily specified in this model. We point out that CO mixing profiles found for all three of the Yung and DeMore cases are nearly identical.) We also used the model A profile of eddy diffusivity from Yung and DeMore (see Figure 29). However,

FIGURE 28: A comparison of diurnally averaged CO mixing profiles from photochemical models of Yung and DeMore to the CO mixing profile derived from our $J = 1 \rightarrow 2$, January 1982 CO spectrum. Model C of Yung and DeMore was constrained to produce a CO mixing ratio of 4.5×10^{-5} at 60 km altitude. The modified version of model A specified a lower boundary vertical velocity for CO.

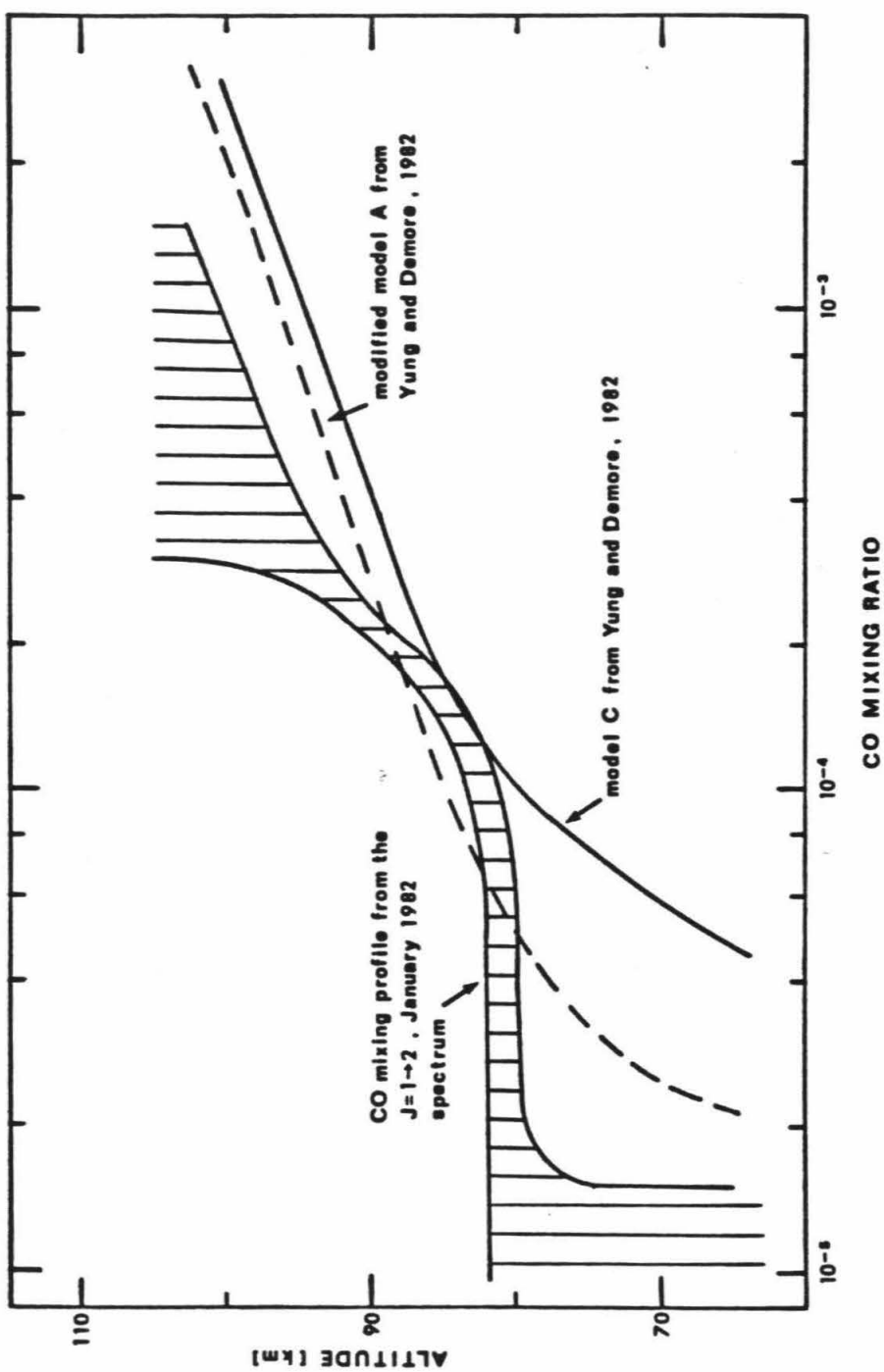
modified model A from
Yung and Demore, 1982
model C from Yung and Demore, 1982
CO mixing profile from the
J=1→2, January 1982
spectrum
ALTITUDE [km]
110
90
70
10⁻³
10⁻⁴
10⁻⁵
CO MIXING RATIO

FIGURE 29: Vertical profiles of eddy diffusivity for the diurnal photochemical models I, II, and III. Also included are model profiles from Yung and DeMore (1982).

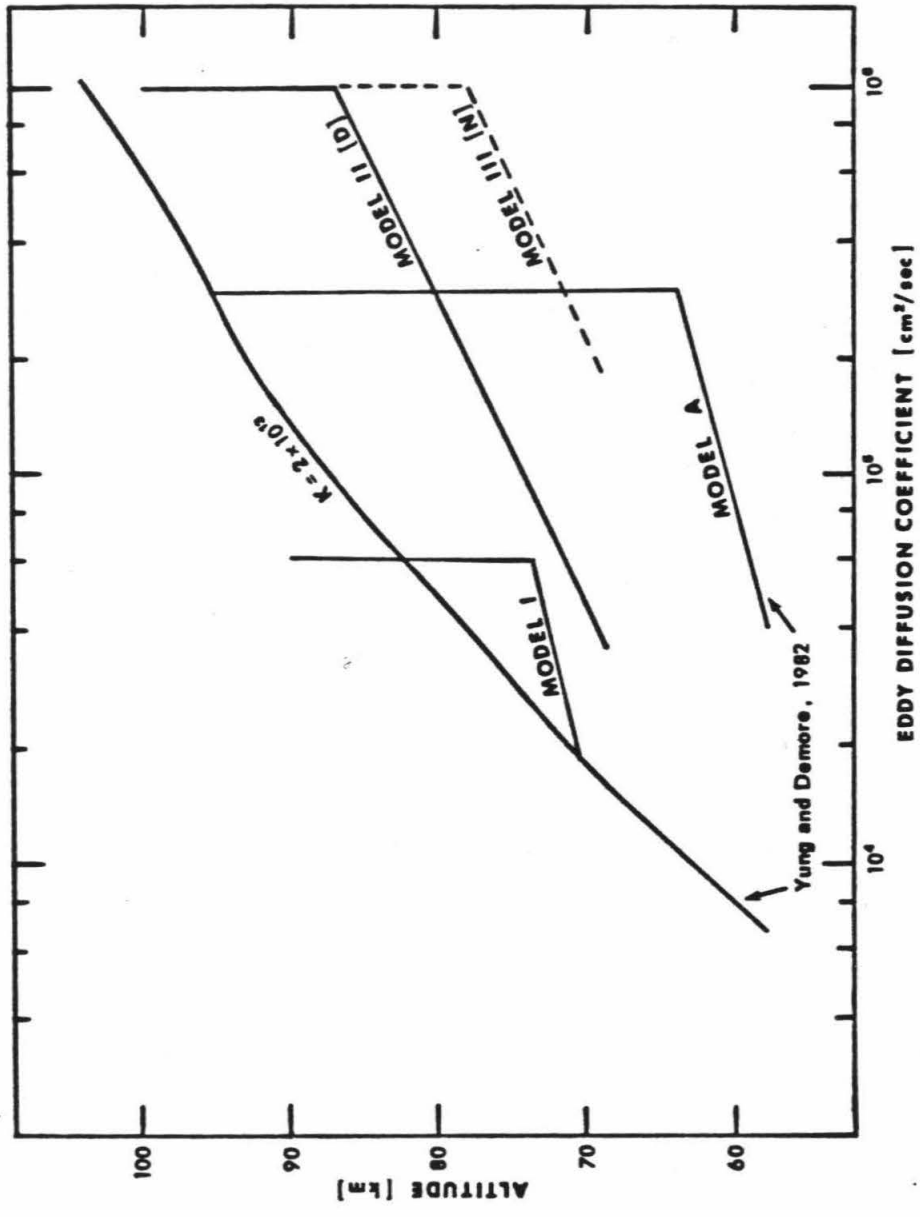
ALTITUDE [km]
100
90
80
70
60
EDDY DIFFUSION COEFFICIENT [cm²/sec]
10⁶
10⁷
10⁸
MODEL I
MODEL II [O]
MODEL III [N]
MODEL A
K=2×10⁷
Yung and Demore, 1982

instead of fixing the CO mixing ratio at the lower boundary, we used the same velocity boundary condition (-2×10^{-2} cm/sec) Yung and DeMore used for all of the other long lived chemical species in their models. The important conclusion is that the models of Yung and DeMore are quite consistent with lower stratospheric values of [CO] (i.e. $f_{CO} < 4.5 \times 10^{-5}$) when the lower boundary mixing ratio of CO is not held fixed.

This last point holds true only for models which span the entire altitude region of CO recombination, which is approximately 60-100 km (e.g. Figures 26 and 27). For the limited altitude domain of our diurnal models, CO mixing ratios between 70 and 80 km are far more sensitive to assumed boundary conditions and more poorly determined by model chemistry. We use a vertical velocity of -1×10^{-2} cm/sec for the lower boundary condition of CO which produces model CO mixing ratios of 7×10^{-5} at 70 km. For our study of the diurnal photochemistry of the Venus mesosphere, we were forced to choose a lower boundary of 70 km in order to avoid inclusion of sulfur and nitrogen chemistry, which would be prohibitively expensive (for instance, Yung and DeMore's model includes 114 reactions). Of course, the primary objective of the diurnal models is to look for diurnal variations due to photochemistry rather than an accurate absolute level for CO abundance. We chose an upper boundary of 90 km for our diurnal model because the CO microwave spectra indicate a relatively constant CO mixing ratio at this altitude (i.e., no diurnal variation). In section 5.3 we will study the possible effects of diurnal CO variations above 100 km on the model.

5.2.4 Diurnal Period for the Mesosphere of Venus

Finally, it is necessary to discuss the diurnal period or length of day for the Venus mesosphere. The solar period at the surface of Venus is 117 Earth days while the period defined by 100 m/sec zonal flow in the cloud regions of

Venus (50-60 km) is roughly 4 Earth days. Because our model is one-dimensional, we can only specify a single solar day or, in effect, a single value for zonal wind velocity in the Venus mesosphere (70-90 km). Given the uncertainty in zonal flow for the mesosphere (see section 2.1), any diurnal period between 4 and 117 days appears to be allowed. The length of the diurnal period determines the duration of nighttime in the Venus mesosphere and, hence, the timescale over which CO recombines without any offsetting production term on the nightside of Venus.

We note that if recombination of CO does produce a factor of two depletion in CO abundance on the nightside between 80 and 90 km then the residence time for CO on the nightside must be substantially greater than 2 days. This point can be seen from the following relation.

$$\text{timescale} \sim \Delta CO / (\text{loss rate})$$

If we consider an altitude of 85 km, the required loss of CO (ΔCO) is roughly 4×10^{12} molecules/cm^3. We can estimate the loss rate from the dayside recombination rate of CO at 85 km from Yung and DeMore (1982) which is roughly 3×10^6 molecule/cm^{3}sec. Hence, it would take on the order of 15 Earth days for CO on the nightside of Venus to be depleted by a factor of two, assuming that recombination of CO on the nightside proceeds as rapidly as it does on the dayside. We also point out that it takes roughly the same amount of time to reproduce the CO by photodissociation of CO_2 on the dayside of Venus.

From the above discussion it should be clear that any photochemical explanation for the diurnal CO variations below 90 km requires long diurnal periods ($\gtrsim$ 40 days) for the Venus mesosphere. The nominal period for our models is 58.5 days corresponding to a retrograde zonal wind velocity of

~5 m/sec. If the diurnal model produced a substantial depletion of nightside CO given the assumption of a 60 day diurnal period, we might argue that the microwave CO spectra suggest very low zonal velocities for the Venus mesosphere. However, as the model results indicate, photochemistry does not produce strong diurnal variations of CO even on timescales as large as 100 days.

5.2.5 Model I. Diurnal Photochemistry Model Results

The key to photochemically produced diurnal variations of CO in the Venus mesosphere is the retention of the CO recombining catalysts, Cl or OH, on the nightside of Venus. The results of our diurnal model indicate (Figure 30) that concentrations of odd oxygen species fall to zero approximately one hour after sunset in the Venus mesosphere. All of these species rely on photolysis for their production. As expected, OH cannot play an important role for recombination of CO on the nightside of Venus. Figure 30 also demonstrates that free Cl concentrations will decrease considerably (by a factor of 10-100) on the nightside of Venus. As can be seen, Cl is incorporated into Cl_2 (and, to some extent, ClO) on the nightside of Venus, where there is no efficient mechanism for dissociation of Cl_2. It is interesting to note that free chlorine does not disappear entirely on the nightside as do the odd hydrogen and oxygen species. This is because the primary sink for Cl on the nightside is the reaction

$$Cl + Cl + M \rightarrow Cl_2 + M \qquad R22$$

which is quadratic in [Cl] (i.e., the destruction rate of free Cl decreases as the square of free Cl concentration).

Nevertheless, the 10-100 fold decrease in free Cl on the nightside severely limits recombination of CO on the nightside. The peak-to-peak amplitude of model diurnal variation of CO abundance is less than 30% (as indicated in Figure

FIGURE 30: Diurnal variations in Cl, O and H chemistry from the diurnal photochemical model of this study. Cl provides the major recombinative path for CO in this model. The horizontal axis is referenced to local time of day in the Venus mesosphere with the assumption of a 58.5 day diurnal period. Both Cl and OH are reduced sharply on the nightside of Venus.

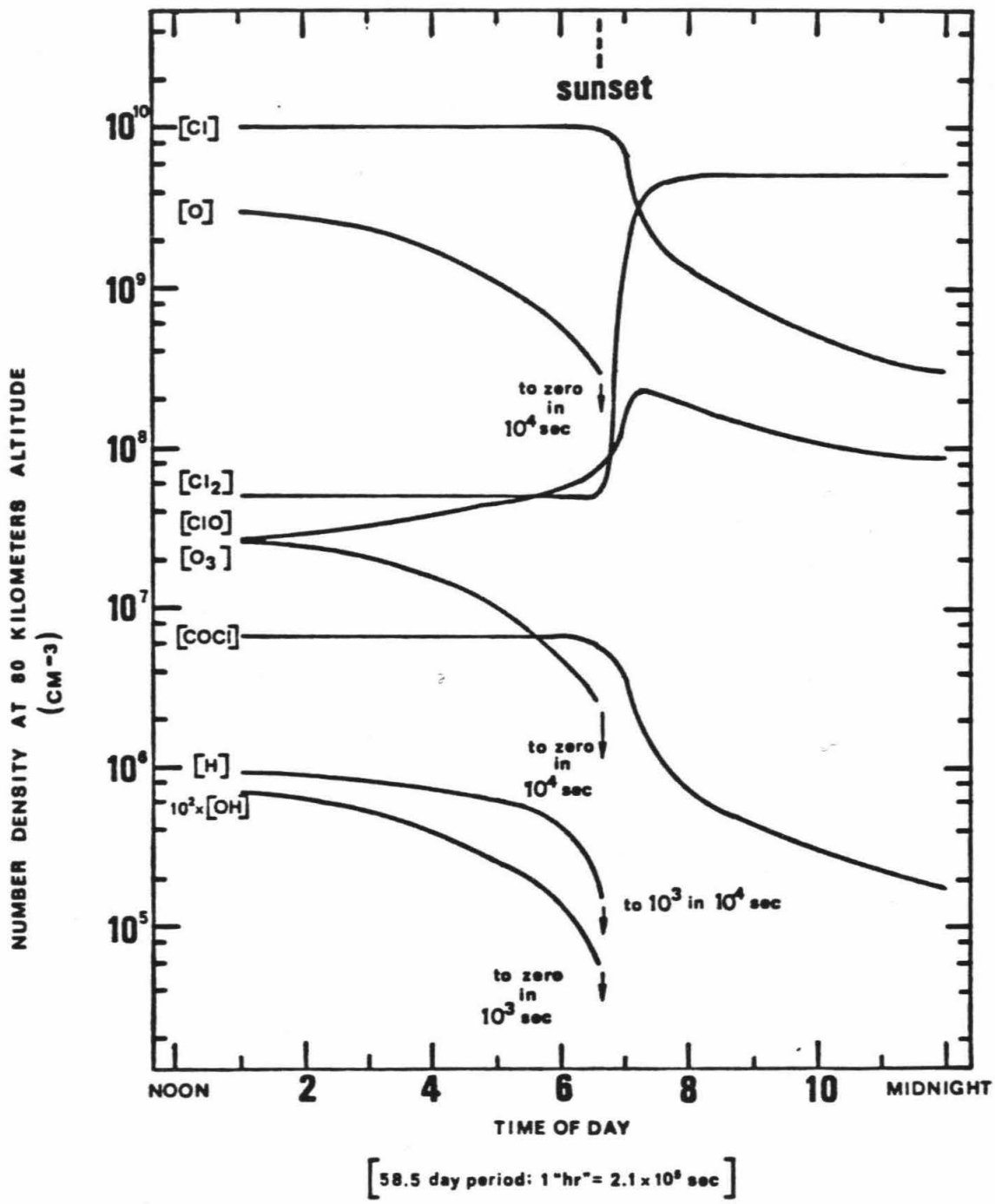
sunset
10^{10}
10^{9}
10^{8}
10^{7}
10^{6}
10^{5}
[Cl]
[O]
[Cl_2]
[ClO]
[O_3]
[COCl]
[H]
10^3x[OH]
to zero in 10^4 sec
to zero in 10^4 sec
to 10^3 in 10^4 sec
to zero in 10^3 sec
NOON
2
4
6
8
10
MIDNIGHT
TIME OF DAY
NUMBER DENSITY AT 80 KILOMETERS ALTITUDE (CM^{-3})
[58.5 day period: 1 "hr" = 2.1 x 10^3 sec]

31) and is predominantly an effect of eddy diffusive removal of CO on the nightside of Venus. The phase of the CO variations is also in disagreement with the diurnal variations implied by the microwave data. Maximum (minimum) model CO abundance at 85 km occurs at the evening (morning) terminator on Venus rather than just before noon (midnight) as required by the microwave data.

5.3 Vertical Transport as a Mechanism for Diurnal CO Variations between 80 and 90 km

As we noted at the end of the last section, eddy transport can contribute in some degree to depletion of CO on the nightside mesosphere below 90 km altitude. To properly model diurnal variations driven by eddy diffusion we include the observed diurnal CO variation above 90 km in the model. For this purpose we have extended the diurnal photochemical model to an altitude of 100 km and imposed, as a boundary condition, a diurnally varying mixing ratio for CO at 100 km altitude. We specify the diurnal variation of CO mixing ratios at 100 km according to the $\cos^2 H$ parameterization of model B in Figure 24 although we use a somewhat larger amplitude for the variation at 100 km (minimum f_{CO} (noon) = 1.5×10^{-4}, maximum f_{CO} (midnight) = 1.5×10^{-3}).

For our preceding study of diurnal chemistry in the mesosphere, we used moderately low values of eddy diffusivity which were based upon the extrapolated profile of von Zahn et al. (Figure 29). We consider larger values of eddy diffusion in this section partly because we wish to estimate the maximum effect CO mixing ratios at 100 km might have on CO abundances at 80-90 km altitude, through downward transport by eddy diffusion.

The level of eddy diffusivity in the mesosphere of Venus is not well constrained by observations. Woo and Ishimaru (1981) found a value of 4×10^4 cm^2/sec for eddy diffusivity in the vicinity of 60 km altitude from

FIGURE 31: Predicted diurnal variation in the CO mixing ratio at 85 km altitude from the diurnal photochemical models I, II, and III. Also shown is the observed diurnal variation as approximately defined by the diurnal variation of model B in Figure 24.

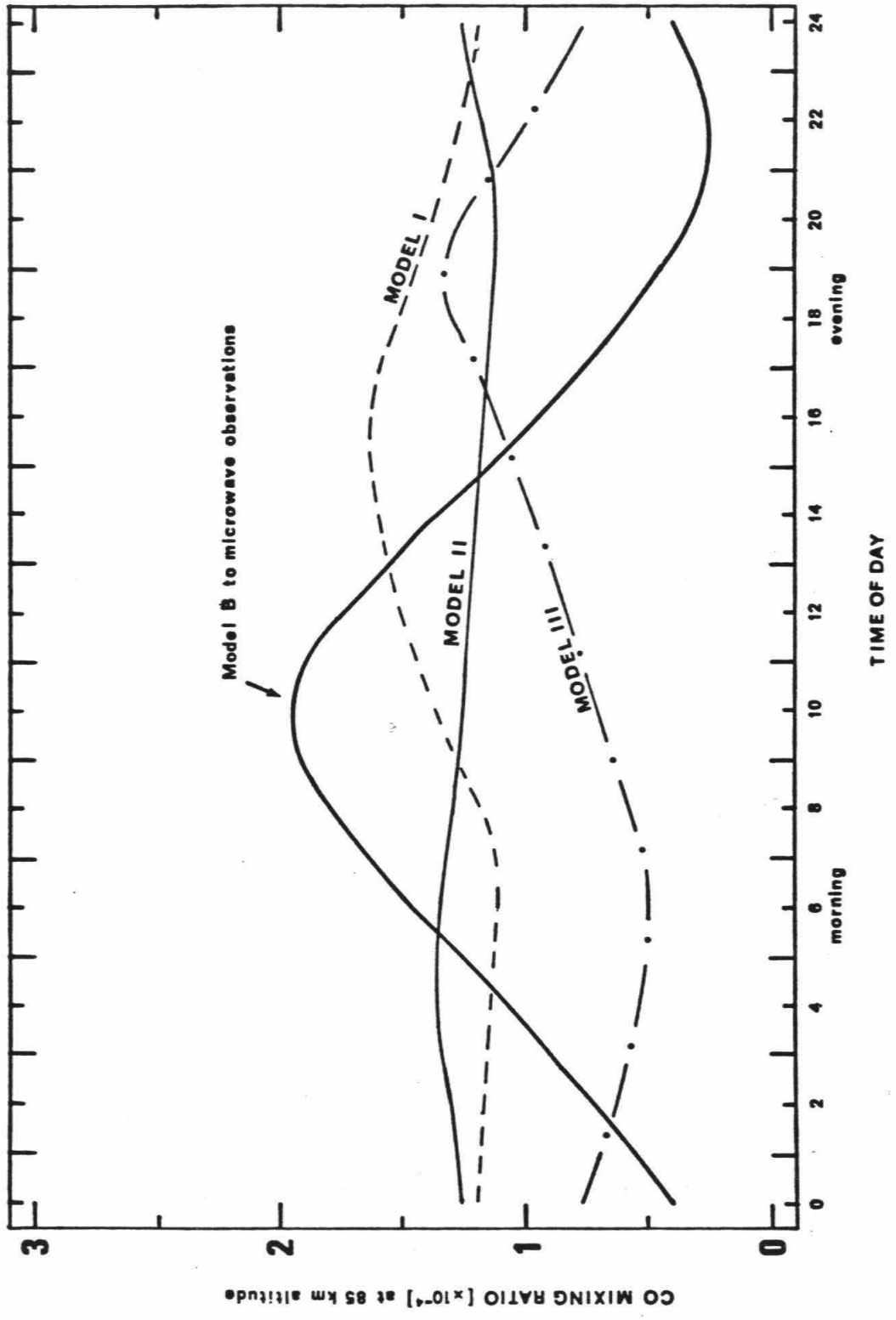
CO MIXING RATIO [×10⁻⁴] at 85 km altitude
3
2
1
0
0
2
4
6
morning
8
10
12
14
16
18
evening
20
22
24
TIME OF DAY
Model B to microwave observations
MODEL I
MODEL II
MODEL III

Pioneer Venus radio scintillation measurements. The stable lapse rate of the mesosphere may indicate that an extrapolation of the von Zahn et al. profile of eddy diffusivity is appropriate (Yung and DeMore, 1982). On the other hand, if 100 m/sec zonal flow diminishes to predominantly meridional flow in the mesosphere, as suggested by Elson in Taylor et al (1980), the implied shear may enhance vertical mixing in the mesosphere. We remark that eddy diffusivity profiles derived by Yung and DeMore to model the photochemistry of the Venus mesosphere considerably exceed the extrapolated eddy diffusivities of von Zahn et al. (see Figure 29). At present, values for eddy diffusivity in the mesosphere of Venus are simply not well determined.

Figure 29 presents the eddy diffusivity profile we use for our model (labeled model II). One important constraint for the level of eddy diffusivity at 100 km altitude is that the implied downward vertical flux of CO in the nightside atmosphere (where f_{CO} (100 km) reaches 1.5×10^{-3}) does not exceed the column production rate of CO above ~100 km on the dayside of Venus. An upper limit of $\sim 10^6$ cm^2/sec for eddy diffusivity at 100 km altitude is consistent with this constraint.

We have also fixed the mixing ratio of CO at the lower boundary of model II (70 km) to 10^{-5}. Our intent is to fix the boundaries of the model as close as possible to the constraints implied by the microwave results. As we found in the previous section, the limited altitude range of our models does not allow sufficiently low values of CO mixing ratios below 80 km to match upper limits set by the microwave spectra of January 1982 (nightside) and September 1982 (dayside). We do not assume a diurnal variation of the CO mixing ratio at the lower boundary partly because the microwave data do not specify such a variation. Furthermore, one expects less diurnal variability at lower altitudes in the Venus

mesosphere due to the increased atmospheric densities and shorter diurnal periods (i.e., substantial zonal flow probably extends to at least an altitude of 70 km).

Finally, we use the shorter diurnal period of 33 days for the mesosphere (70-100 km). A diurnal rotation period of 33 days roughly corresponds to 10 m/sec zonal flow, which is marginally more realistic than the 5 m/sec velocity of model I.

5.3.1 Model II. A Single Profile of Eddy Diffusivity for the Day and Nightsides of Venus

We initially specify a single profile of eddy diffusivity for both the day and nightsides of the Venus mesosphere. We are interested in the effects of downwards propagation of diurnal CO variations at 100 km altitude by eddy diffusion. The phase of diurnal variation at 100 km (extrema at the anti- and subsolar points) is offset with respect to diurnal variations driven by eddy diffusion when the mixing ratio of CO was held fixed at 90 km (extrema at the terminators, model I, Figure 31).

The results of model II are presented in Figure 31 against the results of model I. Again, the levels of CO abundance for models I and II are not identical due to the different lower boundary conditions and eddy diffusion profiles for the two models. As can be seen, the phase of diurnal CO variation at 85 km altitude is shifted by nearly 180° for model II with respect to model I. Also note that the amplitude of diurnal variation is considerably reduced in model II. The depletion of CO on the nightside by eddy diffusion is offset by higher mixing ratios at 100 km on the nightside so that the resulting amplitude of diurnal variation is very small.

Model I and model II effectively consider minimum (i.e., no effect) and

maximum effects of diurnal CO variation above ~ 90 km on diurnal CO variation below 90 km for the basic photochemical diffusive model. In neither case can model results approximate the observed CO variations between 80 and 90 km in the Venus mesosphere.

5.3.2 Model III. Separate Profiles of Eddy Diffusivity for the Day and Nightsides of Venus

We consider next the possibility of different eddy diffusivities for the day and nightsides of Venus. Justification for diurnal variability of eddy diffusion is rather weak, but there are several points which suggest that the attempt is worthwhile. At an altitude of 160 km, Niemann et al. (1980) find turbulence to be significantly greater on the nightside relative to the dayside of Venus. Niemann et al. speculate that the strong nightside turbulence is due to the Dickinson and Ridley flow field exceeding the Reynolds number on the nightside of Venus. However one would not expect stronger mixing at 160 km altitude on the nightside to necessarily imply stronger eddy mixing below 100 km for the nightside.

In fact, the most compelling motivation for changing eddy diffusion between the day and nightside of Venus mesosphere is the strong diurnal effect such a change can clearly have on CO mixing ratios below 90 km altitude. An important characteristic of altitude increasing eddy diffusivity profiles (as are all the eddy diffusivity profiles in Figure 29) is an effective bottleneck for downward transport of CO below 90 km altitude. If eddy diffusivity is increased below 90 km on the nightside of Venus, then CO below 90 km altitude can be transported downwards in a much shorter time scale. Very long diurnal periods would not be required to deplete CO on the nightside of Venus.

We propose a fairly simple form of diurnal variability for eddy diffusivity in the mesosphere of Venus for our model III. The eddy diffusivity profile of model II (Figure 29) is shifted downwards 10 km in altitude (dotted line in figure) to model eddy diffusivity in the nightside Venus mesosphere. We use the unchanged model II eddy diffusivity profile for the dayside of our model III. The consequence of increasing eddy diffusion below 90 km altitude for the nightside relative to the dayside of Venus is that CO abundance can build up below 90 km on the dayside, where eddy diffusion is slow, yet be quickly transported downwards on the nightside, where eddy diffusion is fast. Other than the diurnal variability of eddy diffusivity, we retain the model II parameters for our model III.

The results of model III are represented in Figure 31 by the diurnal variation of the CO mixing ratio at 85 km. The average level of CO abundance is lower for model III relative to models I and II because of the increased eddy diffusion below 90 km for the nightside of model III. The amplitude of diurnal variation is also greater for model III but is still not as large as required by the microwave observations. The limiting factor for the amplitude of diurnal variation in model III is not the time scale for removal of CO on the nightside, but rather the time scale for reproduction of CO by photodissociation of CO_2 on the dayside of the planet. Also note that the phase of the diurnal variation from model III is not consistent with the phase determined from the microwave observations.

Both of these weaknesses are intrinsic to photochemical-diffusive models for the diurnal variation of CO below 90 km in the mesosphere of Venus. Photodissociation rates of CO_2 on the dayside of Venus are well constrained and are the basic limiting rate for photochemical or diffusive models of diurnal variability of CO in the Venus mesosphere. Furthermore, any process which operates to remove CO on the nightside of Venus (where CO is not produced) will lead to

maximum (minimum) CO mixing ratios near the evening (morning) terminator of Venus. The observed opposite phase behavior of CO mixing ratios between 80 and 90 km altitude appears to reject a photochemical or diffusive transport explanation for the diurnal variability of CO in this altitude region.

5.4 General Circulation between 80 an 100 km in the Venus Mesosphere

All of the preceeding models for the lower Venus mesosphere suffer from the above-mentioned drawbacks. In this section we briefly argue possible effects on CO abundance between 80 and 90 km due to general circulation of the mesosphere in this region. The important elements of circulation we consider are vertical motions characterized by the Dickinson and Ridley sub-solar to anti-solar flow and horizontal motions characterized by the 4 day zonal rotation of the lower atmosphere. Our intention is to develop a qualitative model for the global distribution of CO that does not suffer the most serious problems of photochemical-diffusive models.

An important assumption for this discussion is that the mixing profile of CO on the day and nightsides of Venus is characterized by a sharp cutoff at a particular altitude in the Venus mesosphere. The variable location, in altitude, for this cutoff is assumed to produce the observed diurnal variation of CO between 80 and 90 km altitude. Figure 32 graphically illustrates this point. We note that CO mixing profiles derived from our May 1980 and January 1982 profiles indicate such a cutoff exists on the nightside of Venus. To a lesser extent the September, November 1982 spectra indicate such a cutoff for the dayside of Venus. Comparison of the May 1980 and January 1982 mixing profiles (Figures 6 and 7), convincingly demonstrate a temporal variability for the altitude of this cutoff. We assert that the phase dependence of absorption depths in

FIGURE 32: A schematic representation of day to night variation in the CO mixing profile for the Venus mesosphere. The day profile is assumed to be shifted ~10 km lower in altitude relative to the nightside profile. Both profiles are assumed to converge to some constant CO mixing ratio below an altitude of 80 km.

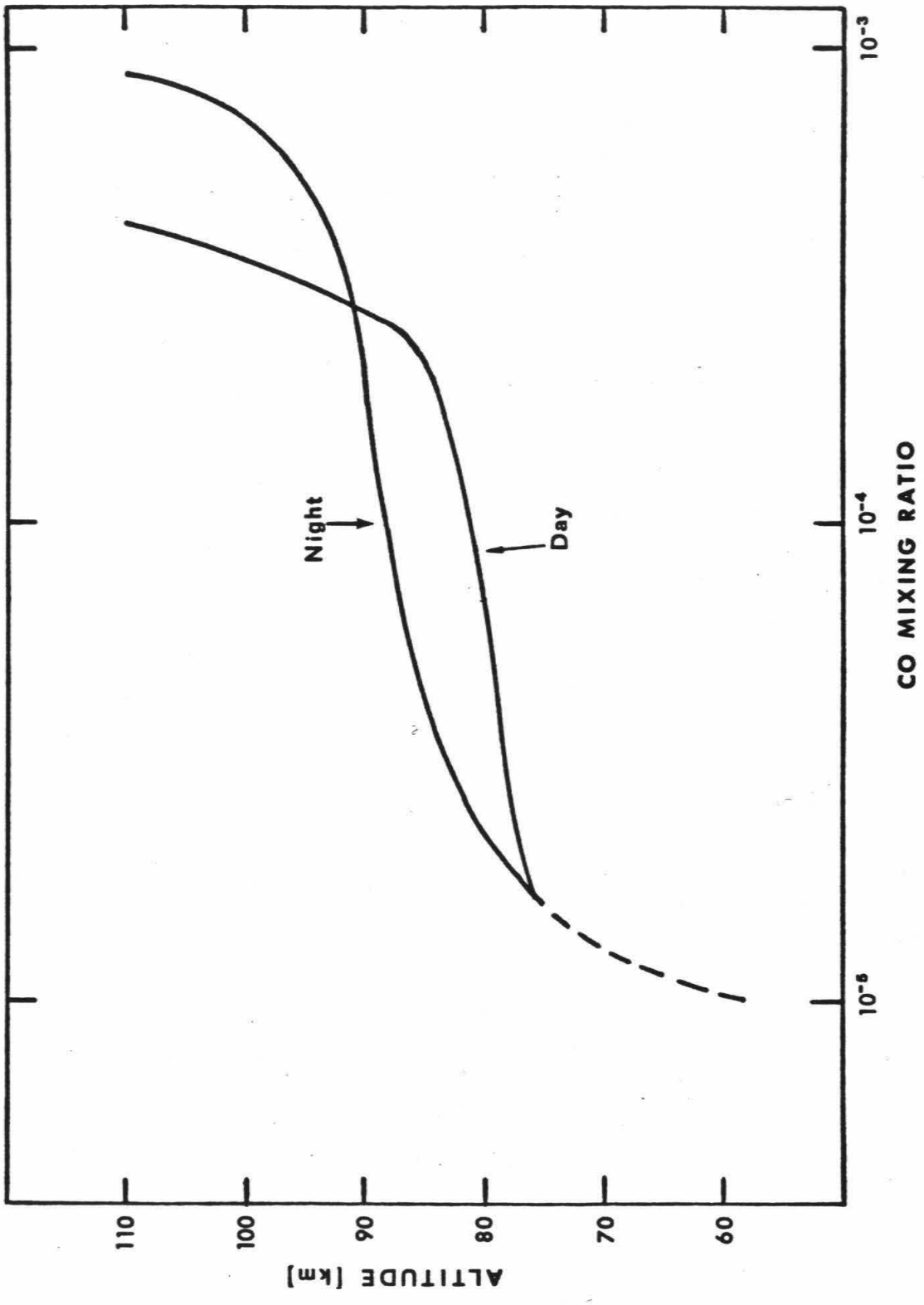
ALTITUDE [km]
110
100
90
80
70
60
Night
Day
10^{-5}
10^{-4}
10^{-3}
CO MIXING RATIO

the wings of microwave CO spectra (as shown in Figures 21 and 22) describes an average diurnal cycle for the altitude of the cutoff. However, we point out that the limited bandwidths of the spectra represented in Figures 21 and 22 do not determine a sharp cutoff in CO mixing ratios for the broad, dayside spectra. We rely on the 500 MHz bandwidth $J = 1 \rightarrow 2$ spectra taken in September-November 1982 to indicate a cutoff for the dayside CO mixing profile at an altitude near or below 80 km.

A sharp decline in CO mixing ratios with decreasing altitude is generally predicted by photochemical models (e.g. Yung and DeMore, 1982; Sze and McElroy, 1975). The fall-off of CO below a certain altitude follows from a corresponding cutoff in CO recombination rates above that same altitude. For example, Figures 26 and 27 (from Yung and DeMore, 1982) indicate that recombination of CO by OH or Cl falls off by nearly 2 orders of magnitude between 85 km and 95 km altitude, primarily because the catalyst species (Cl and OH) are strongly confined below ~ 90 km altitude. Hence, rapid recombination of CO below 90 km altitude leads to a strong decline in CO mixing ratios. Of course, the exact profile of CO mixing is affected by the profile of eddy diffusivity. An altitude increasing profile of eddy diffusion (such as the von Zahn et al. eddy diffusivity profile) tends to increase the gradient of CO mixing because downwards eddy transport of CO is diminished for lower altitudes. An altitude increasing profile of eddy diffusion in effect creates a bottleneck for downward transport of CO (as we noted in model III).

We schematically present our proposed model of zonal and vertical motions for the Venus mesosphere in Figure 33. Due to the latitudinally averaged nature of our observations we do not attempt to specify meridional circulation. Above ~ 90 km zonal flow is assumed to diminish to zero and the

Dickinson and Ridley model of rising motions on the dayside and sinking motions on the nightside is presumed to characterize vertical flow for the atmosphere. Both of these assumptions are borne out by the phase behavior of line center absorption depths for microwave CO spectra (Figures 19 and 20). Below ~ 90 km we assume zonal wind velocities become substantial (> several tens of meters/sec) and the pattern of rising and sinking vertical velocities below 90 km becomes shifted with respect to the day and nightsides of Venus. We can roughly estimate the magnitude of the phase shift at a given altitude by the following simple argument

$$\Delta l \sim u(\Delta z/\omega)$$

We assume a zonal wind velocity, u, and an average vertical velocity, ω, for the mesosphere below ~ 90 km. As an initial condition, maximum downward vertical velocities at 90 km altitude are centered at the antisolar point on Venus, as in the Dickinson and Ridley models. A parcel of atmosphere initially at the antisolar point sinks to a distance Δz below 90 km and is displaced horizontally by Δl. Hence, maximum downward velocities at Δz below 90 km are displaced with respect to the antisolar point on Venus. The minimum altitude for the cutoff in the CO mixing profile, which is roughly tied to maximum downward velocities, is similarly shifted in phase with respect to midnight on Venus.

The above model assumes that the vertical momentum of the atmosphere as set up by subsolar to antisolar flow above 90 km is transported horizontally without substantial modification by zonal rotation of the atmosphere below 90 km. It is difficult to assess the validity of such an assumption given the complexity of the complete circulation problem. However, it is important to note that a similar process is modeled to explain the 3-4 hr shift towards

FIGURE 33: Proposed general circulation for the Venus mesosphere. Vertical velocities are on the order of 2-10 cm/sec and horizontal velocities are on the order of 50-100 m/sec.

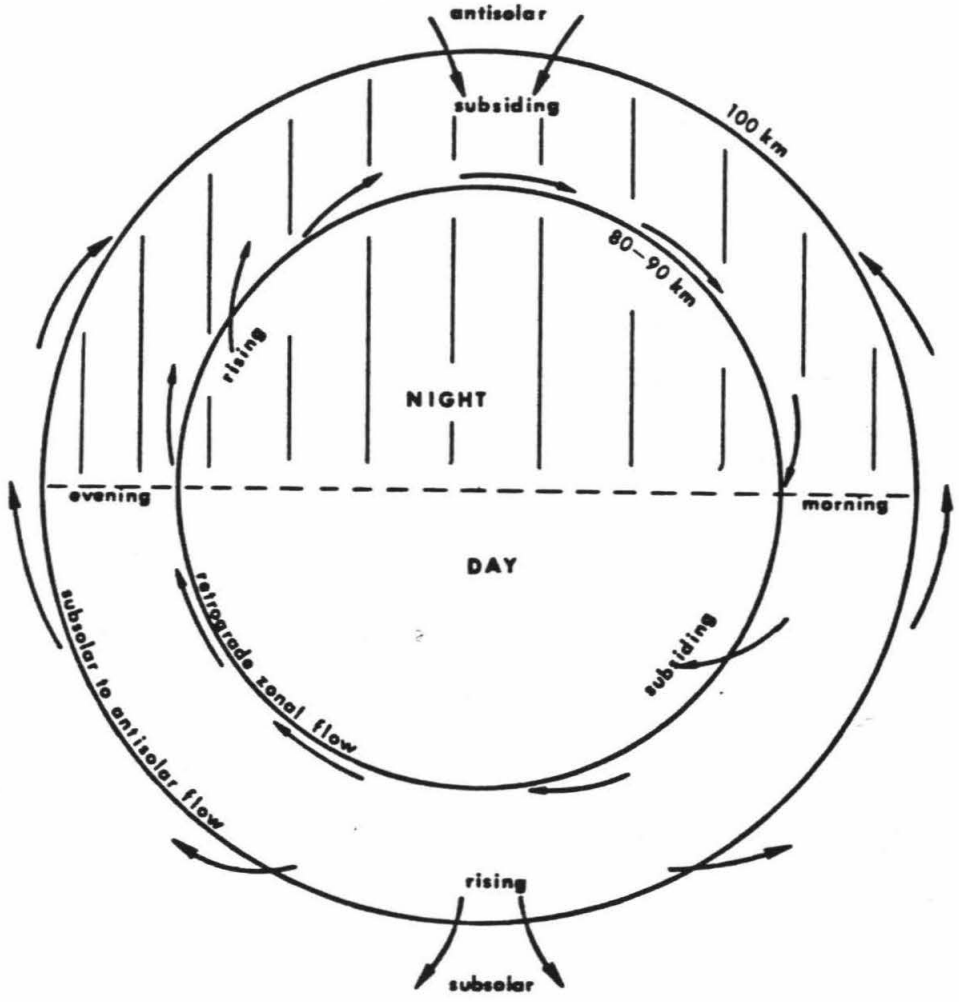
antisolar
subsiding
100 km
80–90 km
rising
NIGHT
evening
morning
DAY
retrograde zonal flow
subsiding
subsolar to antisolar flow
rising
subsolar

morningside for He and H bulges above 150 km on the Venus nightside thermosphere (Mayr et al., 1981).

Our circulation model also implies that the CO mixing profile is displaced vertically by vertical velocities without substantial modification in the process; at least to the extent that higher (lower) mixing ratios at higher (lower) altitudes are shifted downwards (upwards) for sinking (rising) motions. Dickinson and Ridley showed that this process should occur for the thermosphere of Venus, and the microwave CO observations appear to confirm that this aspect of their model also applies to the mesosphere. An important comparison to make is between the time scales of eddy diffusion and bulk transport in the mesosphere of Venus. If one assumes the extrapolated eddy diffusivity profile of von Zahn et al., then transport time scales for eddy diffusion are $\gtrsim 10$ times the 4 day period of rotation for the lower atmosphere. The model A profile of eddy diffusivity from Yung and DeMore (Figure 29) produces a factor of 3 times the 4 day rotation period of the lower atmosphere. In either case we might expect eddy diffusion to play a very limited role in the diurnal variability of the CO mixing profile if zonal flow on the order of tens of meters per second extends through the lower mesosphere.

If we consider reasonable (but fortuitously chosen) values of 10 km, 50 m/sec (retrograde), and 4 cm/sec for Δz, u, and ω, respectively, we find a phase shift for maximum downward vertical velocities of ~ 8 hr from midnight towards the morningside of Venus. A vertical displacement (Δz) of 10 km is roughly the diurnal amplitude for the altitude of the cutoff in CO mixing ratios as implied by the microwave data. A zonal wind on the order of 50 m/sec is consistent with mesospheric circulation models of Elson (in Taylor et al., 1981) and Seiff et al. (1981). Furthermore, the circulation models of Elson indicate a very sharp

decrease in zonal winds in the region of 85 to 90 km altitude which is generally consistent with the assumptions of our model. Finally, although there are no useful measurements of vertical velocities for the mesosphere of Venus, a value of 4 cm/sec would be a reasonable extrapolation of vertical velocities from the thermospheric models of Dickinson and Ridley. Vertical velocities of a few cm/sec are also consistent with the observed lack of diurnal contrast in atmospheric temperatures and pressures for the mesosphere of Venus.

The principal conclusion to be drawn is that global circulation in the mesosphere of Venus based on reasonable assumptions of vertical and horizontal motions can explain the pattern of diurnal CO variations found from microwave observations. Retrograde zonal flow below 90 km shifts the phase of diurnal CO variations produced by vertical motions associated with the subsolar to antisolar flow of Dickinson and Ridley. The shift in maximum CO abundance is towards the morningside of the Venus mesosphere and can be roughly the same amplitude as implied by the microwave observations (~ 8-10 hr).

One serious drawback for this model is the extreme complexity of a complete, quantitative analysis. Such an analysis (which is unfeasible at present and probably not justified by the present data set) could provide estimates of vertical velocities and zonal winds in the mesosphere of Venus through careful comparison with a more complete microwave data set.

The model is successful in that it reproduces the correct phase behavior for CO abundance between 80 and 90 km and does not require long diurnal periods for the Venus mesosphere. In fact, the implied time scale for diurnal variations is on the order of the 4 day rotation period of the cloud regions of Venus. The model also implies that temporal variations of microwave CO spectra

could be tied to the temporal variations of zonal flow reported by Traub and Carlton (1975), Boyer (1973), and Betz et al. (1976, 1977). We note that the most recent observations of Schloerb and Good (1982) indicate a CO bulge between 80 and 90 kilometers altitude that is centered near 5 a.m. local time on Venus compared to a local time of 8:30 am presented in the study. Changes in the mean zonal flow in this altitude region could well lead to such a change.

6. Conclusions

We have developed a fairly simple and consistent picture of general circulation in the Venus mesosphere based on the diurnal distribution of CO, which is in turn based upon analysis of CO microwave spectra. Antisolar to subsolar circulation dominates in the Venus atmosphere down to an altitude of ~ 90 km. This circulation also extends below 90 km altitude, but is strongly modified by rapid, retrograde zonal rotation of the atmosphere, which becomes the dominant pattern of circulation below 90 km altitude. The onset of zonal flow occurs quite abruptly near 90 km altitude. Such a pattern of circulation is proposed to explain a nightside CO bulge which is centered near the antisolar point at an altitude of 100 km, but becomes shifted to near or past the morning terminator at altitudes between 90 and 80 km. We also note the similarity of our proposed circulation model to the results of Betz et al. (1979), and Seiff (1982) [see section 2.1].

At present, available microwave spectra of CO do not place adequate constraints on CO mixing ratios below 80 km altitude. An implicit prediction of our circulation model is that day-night contrast in CO mixing ratios should approach zero below ~ 80 km altitude. The vertical motions that are associated with subsolar to antisolar motion and produce enhancement of nightside CO abundances should decrease with depth in the Venus mesosphere as atmospheric density increases and the effects of day-night temperature and pressures contrast in the thermosphere decrease. Hence, we assume that the higher dayside values of CO abundance at 80 km altitude decrease with depth in the Venus mesosphere to match the lower nightside values found at 80 km altitude.

Furthermore, if there is indeed no substantial CO production in the

lower atmosphere of Venus (as indicated by Yung and DeMore, 1982), then the mesospheric minimum value of the CO mixing ratio determined from microwave spectra places an upper limit on the lower atmospheric abundance of CO. Our present minimum value for the mixing ratio of CO is found from our nightside, January 1982, spectrum which constrains the mixing ratio of CO to be less than 2×10^{-5} at ~ 82 kilometers altitude. We note that this upper limit is a factor of 2-3 less than the Venus stratospheric CO mixing ratio determined by Connes et al. (1968, for the year 1967). This discrepancy may indicate a long term variation in CO abundance of the lower atmosphere (and presumably the mesosphere of Venus). One major uncertainty is the dayside CO mixing ratio below 80 km altitude, which can be determined by very broad bandwidth spectra $J = 1 \rightarrow 2$ (that are not seriously affected by baseline problems such as our September, November 1982, spectra) or by infrared transitions such as the 2.35 μ CO band observed by Connes et al. (1968).

References

Ainsworth, J.E., and J.R. Herman, Venus wind and temperature structure: The Venera 8 data, *J. Geophys. Res.* **80**, 173-179, 1975.

Allen, M., Y.L. Yung, and J.W. Waters, Vertical transport and photochemistry in the terrestrial mesosphere and lower thermosphere (50-120 km), *J. Geophys. Res.* **86**, 3617-3627, 1981.

Barker, E.S., Observations of Venus water vapor over the disk of Venus: The 1972-74 data using the H_2O lines at 8197 Å and 8176 Å, *Icarus* **25**, 268-281, 1975.

Barker, E.S., Detection of SO_2 in the UV spectrum of Venus, *Geophys. Res. Lett.* **6**, 117-120, 1979.

Betz, A.L., M.A. Johnson, R.A. McLaren, and E.C. Sutton, Heterodyne detection of CO_2 emission lines and wind velocities in the atmosphere of Venus, *Ap. J. (Letters)* L141-L144, 1976.

Betz, A.L., E.C. Sutton, R.A. McLaren, and C.W. McAlary, Laser heterodyne spectroscopy, *Proc. Symp. Planet. Atmos.* **61**, 29-33, 1977.

Boyer, C., and H. Camichel, Observations photographiques de la planete Venus, *Ann. Astrophys.* **24**, 531-535, 1961.

Boyer, C., and P. Guerin, Etude de la rotation retrograde, en 4 jours, de la couche exterieure naugeuse de Venus, *Icarus* **11**, 338-355, 1969.

Boyer, C., The 4-day rotation of the upper atmosphere of Venus, *Planet. Space Sci.* **21**, 1559-1561, 1973.

Brinton, H.C., H.A. Taylor, Jr., H.B. Niemann, and H.G. Mayr, Venus night time hydrogen bulge, *Bull. Amer. Astron. Soc.* **11**, 538, 1979.

Chamberlain, J.W., *Theory of Planetary Atmospheres: An Introduction to Their Physics and Chemistry*, Academic Press, N.Y., p. 330, 1978.

Chandrasekhar, S., *Radiative Transfer*, Dover Publications, Inc., N.Y., p. 393, 1960.

Clancy, R.T., D.O. Muhleman, and G.L. Berge, Mesospheric photochemistry and circulation from CO microwave measurements, presented at an International Conference on the Venus Environment, NASA/Ames, 1981.

Clancy, R.T., and D.O. Muhleman, A measurement of the $^{12}CO/^{13}CO$ ratio in the mesosphere of Venus, submitted to *Ap. J.*, 1982.

Connes, P., J. Connes, W.S., Benedict, and L.D. Kaplan, Traces of HCl and HF in the atmosphere of Venus, *Ap. J.* (Letters to the Editor), **147**, 1230-1237, 1967.

Connes, P., J. Connes, L.D. Kaplan, and W.S. Benedict, Carbon monoxide in the Venus atmosphere, *Ap. J.* **152**, 731-743, 1968.

Connes, J., P. Connes, and J.P. Maillard, *Atlas de spectres infrarouges de Venus, Mars, Jupiter et Saturne* (Paris, France: Editions due Centre National de la Recherche Scientifique), 1969.

Conway, R.R., R.P. McCoy, and C.A. Barth, IUE detection of sulfur dioxide in the atmosphere of Venus, *Geophys. Res. Lett.* **6**, 629-631, 1979.

Counselman, III, C.C., S.A. Gourevitch, R.W. King, and G.B. Loriot, Zonal and meridional circulation of the lower atmosphere of Venus determined by radio interferometry, *J. Geophys. Res.* **85**, 8026-8030, 1980.

Dickinson, R.E., Circulation and thermal structure of the Venusian thermosphere, *J. Atmos. Sci.* **28**, 885-894, 1971.

Dickinson, R.E., and E.C. Ridley, A numerical model for the dynamics and composition of the Venusian thermosphere, *J. Atmos. Sci.* **32**, 1219-1231, 1975.

Dickinson, R.E., and E.C. Ridley, Venus mesosphere and thermosphere temperature structure II. Day-night variations, *Icarus* **30**, 163-178, 1977.

Elson, L.S., Preliminary results from the Pioneer Venus orbiter infrared radiometer: Temperature and dynamics in the upper atmosphere, *Geophys. Res. Lett.* **6**, 720-722, 1979.

Esposito, L.W., J.R. Winick, and A.I. Stewart, Sulfur dioxide in the Venus atmosphere: Distribution and implications, *Geophys. Res. Lett.* **6**, 601-604, 1979.

Esposito, L.W., and L.J. Gates, Horizontal and vertical distribution of sulfur dioxide on Venus, *EOS* **62**, 321, 1981.

Fink, U., H.P. Larson, G.P. Kuiper, and R.F. Poppen, Water vapor in the atmosphere of Venus, *Icarus* **17**, 617-631, 1972.

Gordy, W., and R.L. Cook, *Microwave Molecular Spectra*, Interscience Publishers (John Wiley and Sons), New York, 1970.

Gulkis, S., R.K. Kakar, M.J. Klein, and E.T. Olsen, Venus: Detection of variations in stratospheric carbon monoxide, *Proc. Symp. Planet. Atmos.* **61**, 61-65, 1977.

Hobbs, R.W., and S.LKnanapp, Planetary temperatures at 9.55 mm wavelength, *Icarus*, **14**, 204-209, 1971.

Hoffman, J.H., R.R. Hodges, T.M. Donahue, and M.B. McElroy, Compositions of the Venus lower atmosphere from the Pioneer Venus mass spectrometer, *J. Geophys. Res.* **85**, 7882-7890, 1980.

Kalaghan, P.M., and K.N. Wulfsberg, Radiometric observations of the planets Jupiter, Venus, and Mars at a wavelength of 8.6 mm, *Ap. J.* **154**, 771-773, 1968.

Kakar, R.K., J.W. Waters, and W.J. Wilson, Venus: Microwave detection of carbon monoxide, *Science* **191**, 379-380, 1975.

Kawabata, K., D.L. Coffeen, J.E. Hansen, W.A. Lane, Makoto, Sato, and L.D. Travis, Cloud and haze properties from Pioneer Venus polarimetry, *J. Geophys. Res.* **85**, 8129-8140, 1980.

Keating, G.M., J.Y. Nicholson, III, and L.R. Lake, Venus upper atmosphere structure, *J. Geophys. Res.* **85**, 7941-7956, 1980.

Keldysh, M.V., Venus exploration with the Venera 9 and Venera 10 spacecraft, *Icarus* **30**, 605-625, 1977.

Krasnopolsky, V.A., and V.A. Parshev, Chemical composition of the atmosphere of Venus, *Nature* **292**, 610, 1981.

Kumar, S., D.M. Hunten, and H.A. Taylor, Jr., H_2 abundance in the atmosphere of Venus, *Geophys. Res. Lett.* **8**, 237, 1981.

Limaye, S.S. and V.E. Suomi, Cloud motions on Venus: Global structure and organization, *J. Atmos. Sci.* **38**, 1220-1235, 1980.

Loewenstein, R.F., D.A. Harper, S.H. Moseley, C.M. Telesco, H.A. Thronson, R.H. Hildebrand, S.E. Whitcomb, R. Winston, and R.F. Steining, Far-infrared and submillimeter observations of the planets, *Icarus* **31**, 315-324, 1977.

Marov, M.Ya., V.S. Avduevsky, V.V. Kerzkanovich, M.K. Rozhdestvensky, N.F. Borodin, and O.L. Ryabov, Venera 8: Measurements of temperature, pressure and wind velocity on the illuminated side of Venus, *J. Atmos. Sci.* **30**,

1210-1214, 1973.

Masson, C., A stable acousto-optical spectrometer for millimeter radio astronomy, *Astron. Astrophys.*, in press, 1982.

Mayr, H.G., I. Harris, H.B. Niemann, H.C. Brinton, N.W. Spencer, H.A. Taylor, Jr., R.E. Hartle, W.R. Hoegy, and D.M. Hunten, Dynamic properties of the thermosphere inferred from Pioneer Venus mass spectrometer measurements, *J. Geophys. Res.* **85**, 7841-7847, 1980.

McElroy, M.B., and T.M. Donahue, Stability of the Martian atmosphere, *Science* **177**, 986-988, 1972.

McElroy, M.B., M.J. Prather, and J.M. Rodriguez, Escape of hydrogen from Venus, *Science* **215**, 1614-1615, 1982.

Muhleman, D.O., R.T. Clancy, G.R. Knap, and T.G. Phillips, The carbon monoxide distribution in the Venus atmosphere from 230 GHz spectral measurements, *Bull. Amer. Astron. Soc.* **11**, 540, 1979a.

Muhleman, D.O., G.S. Orton, and G.L. Berge, A model of the Venus atmosphere from radio, radar, and occultation observations, *Ap. J.* **234**, 733-745, 1979b.

Niemann, H.B., W.T. Kaprzak, A.E. Hedin, D.M. Hunten, and N.W. Spencer, Mass spectrometric measurements of the neutral gas composition of the thermosphere and exosphere of Venus, *J. Geophys. Res.* **85**, 7817-7827, 1980.

Phillips, T.G., and K.B. Jefferts, A low temperature bolometer heterodyne receiver for millimeter wave astronomy, *Rev. Sci. Instrum.* **44**, 1009-1014, 1973.

Phillips, T.G., D.P. Woody, T.J. Dolan, R.E. Miller, and R.A. Linke, Dayen-Martin (SIS tunnel junction) mixers for low noise heterodyne receivers, *IEEE Trans.*

Magnet. MAG-17, 684-689, 1981.

Pollack, J.B., O.B. Toon, R.C. Whitten, R. Boese, B. Ragent, M. Tomasko, L. Esposito, L. Travis, and D. Wiedman, Distribution and source of the UV absorption in Venus' atmosphere, *J. Geophys. Res.* **85**, 8141-8150, 1980.

Prinn, R.G., Photochemistry of HCl and other minor constituents in the atmosphere of Venus, *J. Atmos. Sci.* **28**, 1058-1068, 1971.

Rather, J.D.G., B.L. Ulich, and P.A.R. Ade, Planetary brightness temperature measurements at 1.4 mm wavelength, *Icarus* **22**, 448-453, 1974.

Rosenkranz, P.W., Shape of the 5 mm oxygen band in the atmosphere, *IEEE Trans. Antennas Propagat. AP-23*, 498-506, 1975.

Rossow, W.B., A.D. Del Genio, S.S. Limaye, and L.D. Travis, Cloud morphology and motions from Pioneer Venus images, *J. Geophys. Res.* **85**, 8107-8128, 1980.

Rossow, W.B., and E. Kinsella, Variations of winds on Venus, *Bull. Amer. Astron. Soc.* **14**, 740, 1982.

Rowan-Robinson, M., P.A.R. Ade, E.I. Robson, and P.E. Clegg, Millimeter observations of planets, galactic and extragalactic sources, *Astron. Astrophys.* **62**, 249-254, 1978.

Schloerb, F.P., S.E. Robinson, and W.M. Irvine, Observation of CO in the stratosphere of Venus via its J = 0 → 1 rotational transition, *Icarus* **42**, 121-128, 1980.

Schloerb, F.P., and J.C. Good, Temporal monitoring of the J = 1 → 0 CO line in the atmosphere of Venus, presented at the 13th annual DPS/AAS meeting, 1981.

Schloerb, F.P., and J.C. Good, Temporal monitoring and spatial mapping of millimeter CO lines on Venus during the 1982 conjunction, *Bull. Amer. Astron. Soc.* **14**, 744, 1982.

Schubert, G., C.C. Counselmann III, J. Hansen, S.S. Limaye, G. Petingill, A. Seiff, I.I. Shapiro, V.E. Suomi, F. Taylor, L. Travis, R. Woo, and R.E. Young, Dynamics, winds, circulation and turbulence in the atmosphere of Venus, *Space Sci. Rev.* **20**, 357-387, 1977.

Schubert, G., C. Covey, A. Del Genio, L.S. Elson, G. Keating, A. Seiff, R.E. Young, J. Apt, C.C. Counselman III, A.J. Kliore, S.S. Limaye, H.E. Revercomb, L.A. Sromovsky, V.E. Suomi, F. Taylor, R. Woo, and U. von Zahn, Structure and circulation of the Venus atmosphere, *J. Geophys. Res.* **85**, 8007-8025, 1980.

Scott, A.H., and E.J. Reese, Venus: Atmospheric rotation, *Icarus* **17**, 589-601, 1972.

Seiff, A., D.B. Kirk, R.E. Young, R.C. Blanchard, J.T. Findlay, G.M. Kelly, and S.C. Sommer, Measurements of thermal structure and thermal contrasts in the atmosphere of Venus and related dynamical observations: Results from the four Pioneer Venus probes, *J. Geophys. Res.* **85**, 7903-7933, 1980.

Seiff, A., and D.B. Kirk, Structure of the Venus mesosphere and lower thermosphere from measurements during entry of the Pioneer Venus probes, *Icarus* **49**, 49-70, 1982.

Seiff, A., Dynamical implications of the observed thermal contrasts in Venus' upper atmosphere, *Icarus* **52**, 574-592, 1982.

Smith, B.A., Rotation of Venus: Continuing contradictions, *Science* **158**, 114-116, 1967.

Stewart, A.I., D.E. Anderson, L.W. Esposito, and C.A. Barth, Ultraviolet spectroscopy of Venus: Initial results from the Pioneer Venus orbiter, *Science* **203**, 777, 1979.

Sze, N.D., and M.B. McElroy, Some problems in Venus' aeronomy, *Planet. Space Sci.* **23**, 763-786, 1975.

Taylor, F.W., R. Beer, M.T. Chahine, D.J. Diner, L.S. Elson, R.D. Haskins, D.J. McCleese, J.V. Martonchik, P.E. Reichley, S.P. Bradley, J. Delderfield, J.T. Schofield, C.B. Farmer, L. Froidevaux, J. Leung, M.T. Coffey, and J.C. Gille, Structure and meteorology of the middle atmosphere of Venus: Infrared remote sensing from the Pioneer orbiter, *J. Geophys. Res.* **85**, 7962-8006, 1980.

Townes, C.H., and A.L. Schawlow, *Microwave Spectroscopy*, Dover Publications, Inc., N.Y., p. 698, 1975.

Traub, W.A., and N.P. Carleton, Observations of O_2, H_2O and HD in planetary atmospheres, in *Exploration of the Planetary System* (ed. A. Woszczyk and C. Ivaniszewska), D. Reidel, Hingham, Mass., p. 223-229, 1974.

Traub, W.A., and N.P. Carleton, Spectroscopic observations of winds on Venus, *J. Atmos. Sci.* **32**, 1045-1059, 1975.

Trauger, J., and J.I. Lunine, in preparation, 1982.

Ulich, B.L., J.R. Cogdell, and J.H. Davis, Planetary brightness temperature measurements at 8.6 mm and 3.1 mm wavelengths, *Icarus* **19**, 59-82, 1973.

Ulich, B.L., Absolute brightness temperature measurements at 2.1-mm wavelength, *Icarus* **21**, 254-261, 1974.

Ulich, B.L., and R.W. Haas, Absolute calibration of millimeter-wavelength spectral lines, *Ap. J. Supple. Ser.* **30**, 247-258, 1976.

Van Vleck, J.H., and V.F. Weisskopf, On the shape of collision-broadened lines, *Rev. Modern Phys.* **17**, 227-236, 1946.

Varanasi, P., Measurement of line widths of CO of planetary interest at low temperatures, *J. Quant. Spectrosc. Radiat. Transfer* **15**, 191-196, 1975.

von Zahn, U., D. Krankowsky, K. Mauersberger, A.O. Nier, and D.M. Hunten, Venus thermosphere: In situ composition measurements, the temperature profile and the homopause altitude, *Science* **203**, 768, 1979.

von Zahn, U., K.H. Ficke, D.M. Hunten, D. Krankowsky, K. Mauersberger, and A.O. Nier, The upper atmosphere of Venus during morning conditions, *J. Geophys. Res.* **85**, 7829-7840, 1980.

Waters, J.W., Absorption and emission by atmospheric gases, in *Methods of Experimental Physics*, vol. **12, Astrophysics, Part B**, Academic Press, N.Y., p. 142-176, 1976.

Whitcomb, S.E., R.H. Hildebrand, J. Keene, R.F. Stiening, and D.A. Harper, Submillimeter brightness temperatures of Venus, Jupiter, Uranus, and Neptune, *Icarus* **38**, 75-80, 1979.

Werner, M.W., G. Neugebauer, J.R. Houck, and M.G. Hauser, One-millimeter brightness temperatures of the planets, *Icarus* **35**, 289-296, 1978.

Wilson, W.J., M.J. Klein, R.K. Kakar, S. Gulkis, E.T. Olsen, and P.T.P. Ho, Venus I. Carbon monoxide distribution and molecular-line searches, *Icarus* **45**,

624-637, 1981a.

Wilson, W.J., and M.J. Klein, Venus: Observed variations in the carbon monoxide distribution, presented at an International Conference on the Venus Environment, NASA/Ames, 1981b.

Winick, J.R., and A.I.F. Stewart, Photochemistry of SO_2 in Venus' upper cloud layers, *J. Geophys. Res.* **85**, 7849-7860, 1980.

Woo, R., and A. Ishimaru, Eddy diffusion coefficient for the atmosphere of Venus from radio scintillation measurements, *Nature* **289**, 383-384, 1981.

Yung, Y.L., and W.B. DeMore, Photochemistry of the stratosphere of Venus: Implications for atmospheric evolution, *Icarus* **51**, 199-247, 1982.

PART II

A Measurement of the $^{12}CO/^{13}CO$ Ratio in the Mesosphere of Venus

R. Todd Clancy and Duane O. Muhleman

(Submitted to Astrophysical Journal)

Introduction

In this paper we report our attempts to measure the isotropic ratio $^{12}C^{16}O/^{13}C^{16}O$ in the mesosphere of Venus, i.e. from about 80 km to 110 km above the Venus surface. This ratio was measured near the cloud tops (~ 60 km) by Connes et al. (1968) who obtained a value of 100:1, using infrared spectroscopy. The carbon dioxide isotope ratio was determined from Pioneer Venus Mass Spectrometer measurements by Hoffman et al. (1980). They interpreted their measurement as the ratio $^{12}C/^{13}C \geq 84$, a value that they refer to as a lower limit due to ambiguities among several mass peaks. This result comes from the lower atmosphere below 30 km. These results are fairly consistent with the $^{12}C/^{13}C$ ratio for the earth of 89.

The column content of CO on Venus can be determined from microwave measurements of the rotational spectrum of CO which appears as a strong absorption line created in the relatively cool layers of CO above the warm atmosphere of Venus. In practice, the isotope ratio can be estimated from the measurements of the ^{12}CO and ^{13}CO spectra in either the (0–1) rotational transitions (115.27 and 110.2 GHz) or the (1–2) transitions (230.5 and 220.4 GHz). However, the (0–1) ^{13}CO line in the Venus atmosphere is extremely weak (~ eight times weaker than the (1-2) line) and nearly impossible to measure with currently available instrumentation. Nevertheless, Wilson et al. (1981) did detect the depth of the (0–1) ^{13}CO line center which, when combined with their ^{12}CO measurements, yielded a value of $^{12}CO/^{13}CO = 85 \pm 15$. This result was presented without any discussion and we feel that the uncertainty may be underestimated.

Our measurements of the spectra for the two isotopes were done

utilizing the (1–2) transitions with the NRAO 36 foot telescope (as did Wilson et al.) at 230 and 220 GHz. The absorption in the ^{13}CO line is about a factor of ten stronger than that obtained by Wilson et al. for the lower transition.

Our formal result for the $^{12}CO/^{13}CO$ isotope ratio in the mesosphere of Venus is 185 ± 69. If this result is correct, significant isotopic fractionation takes place in the upper atmosphere of Venus. Most of the text that follows focuses on the error analysis of our determination which is as complete as we can make it. Although our result is marginal we believe that it does point to a fractionation process in the mesosphere of Venus or, much less likely, a slight but significant difference in the $^{12}C/^{13}C$ ratio on Venus with respect to that for the earth. We are presenting this preliminary report at this time since the measurements cannot be repeated until the next inferior conjunction of Venus, i.e. the fall of 1983.

Observations

Our observations were carried out on January 24, 25, and 27, 1982 at the NRAO 36 foot radio telescope at Kitt Peak National Observatory, Arizona. We employed the NRAO 200-240 gigahertz mixer-receiver which operated with a single side band noise temperature of 1100 K. For spectral analysis, the NRAO facility operates a variety of 256 channel filterbanks, two of which may be used in parallel producing pairs of spectra with different resolution. Over the course of three observing days we obtained ^{12}CO (ν_0 = 230.538 gHz) spectra of 1000, 500 and 250 kilohertz resolution; and ^{13}CO (ν_0 = 220.399 gHz) spectra of 500, 250 and 100 Kilohertz resolution.

We achieved maximum sensitivity for the experiment by observing Venus just several days after inferior conjunction when its apparent diameter was

61 arcseconds. This was approximately the same size as the HPFW of the antenna beam. It was particularly important to measure the $J = 1 \rightarrow 2$ transition as it provides a gain of a factor of eight over the $J = 0 \rightarrow 1$ transition with a corresponding decrease of about 60 in integration time required to obtain a given signal-to-noise ratio. A ^{12}CO spectrum was measured on three separate days within a six day period. Since no day-to-day variations in the spectra were noted they were averaged to form a single spectrum with a very high signal-to-noise ratio. In Figure 1 we present the 1 megahertz resolution spectrum containing a total bandwidth of 256 megahertz. The spectrum is given in units of fraction of the Venus 230 gHz continuum, i.e. the signal in each channel is divided by the signal/channel averaged over the 256 megahertz bandwidth.

It is important to note that by presenting the spectrum in units of fraction of continuum, we are left with a spectrum that is essentially self-calibrated. Measured "raw" spectra of the Venus CO line consist of a continuum level in arbitrary units that is diminished (absorbed) by the frequency (channel) dependent absorption of CO in the Venus mesosphere. For single side band observations, the absorption line depth scales exactly with the continuum level (i.e., terrestrial atmospheric absorption, antenna efficiency, gain, etc., produce identical scaling factors in the continuum level and depth of the absorption line). Hence by dividing the spectrum, channel by channel, with the continuum level, one is left with an internally calibrated spectrum in units of fraction of continuum. This resultant spectrum can be analyzed for the mixing profile of CO in the Venus mesosphere without any further calibration (e.g., see Gulkis et al., 1977; Schloerb et al, 1980). One consequence of this method is that no information can be found for the Venus atmosphere below a certain altitude since the CO absorption below this

Figure 1. Rotational $J = 1 \rightarrow 2$ spectrum of ^{12}CO in the Venus mesosphere. The data are presented as filled circles. Before fitting this spectrum the slight linear baseline was removed by folding the data. The solid line is a synthetic spectrum generated with a radiative transfer program. The ^{12}CO mixing profile of Figure 4 was derived to obtain a fit of the synthetic spectrum with the data.

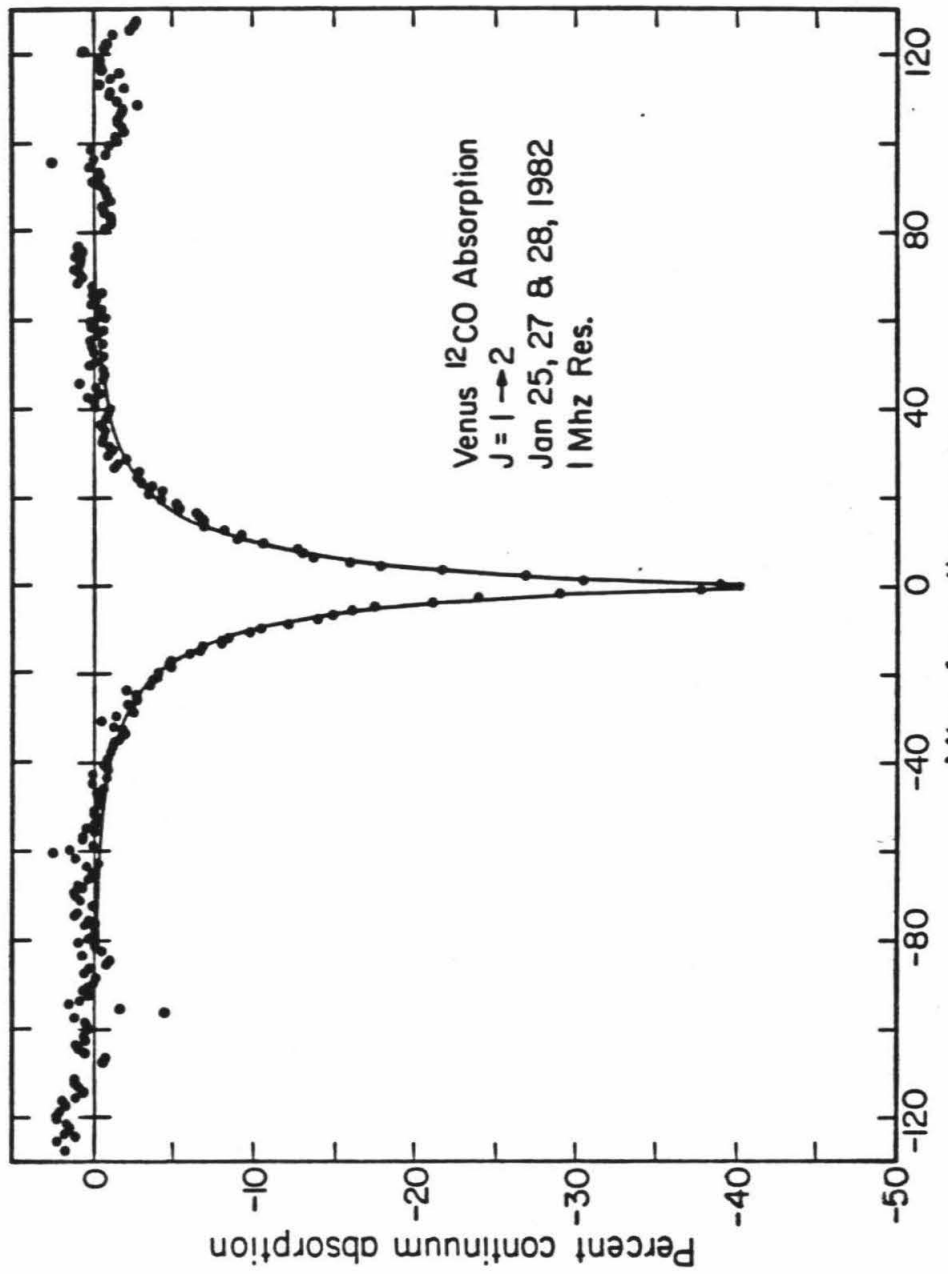
Venus ^{12}CO Absorption
J = 1 → 2
Jan 25, 27 & 28, 1982
1 Mhz Res.
Percent continuum absorption
0
-10
-20
-30
-40
-50
-120
-80
-40
0
40
80
120
Mhz from line center

altitude is pressure broadened beyond the measured bandwidth. The greater the total bandwidth of the spectrum, the lower the altitude for which CO mixing ratios may still be determined. For the case of the ^{12}CO spectrum in figure 1, information on CO mixing ratios is available down to an altitude of approximately 75 km in the Venus mesosphere.

We point out two important caveats to the internal calibration of our spectra, as described above (and in Appendix I). Firstly, our observations were double sideband rather than single sideband. The CO absorption line was present only in the upper sideband, whereas the Venus continuum was present in both sidebands. The resultant spectrum, which is the sum of the two sidebands, required rescaling in order to present the absorption line in units of fraction of the continuum. We have assumed that both the system gain and the terrestrial atmospheric opacity are identical for the two sidebands. Thus, we rescaled the absorption line by a factor of two after subtracting off the continuum level channel by channel. Subsequently we divided the spectrum, channel by channel, by the continuum level. For an estimate of the error in this rescaling factor, we rely on sideband balance measurements by Richard Howard in November of 1981 which suggest 5-10% level sideband balance for the receiver at both the ^{12}CO and ^{13}CO $J = 1 \rightarrow 2$ frequencies. We also include in this error term the very small ($\sim 1\%$) difference in atmospheric opacities for the two sidebands.

A second source of potential error in the internal calibration was introduced because the continuum levels for the spectra were not measured simultaneously with the spectra. The data of figures 1, 2, and 3 were taken using a gain modulator to remove the continuum of Venus. This was necessary because of mismatch between power levels in 'on' and 'off' scans

(introduced by the continuum level of Venus in the 'on' scans) which induced nonlinear response in the filter banks. This nonlinearity effectively appears as enhanced noise in the on-off spectra and is particularly destructive when trying to measure the weak ^{13}CO line. Every third spectrum was measured without the gain modulator in order to determine the continuum level. From day-to-day variation in the ^{12}CO absorption line depths, we estimate that the maximum calibration uncertainty introduced by the nonsimultaneous measurement of the continuum and line spectra is ~ 3% which, due to high opacity of the ^{12}CO line, introduces and 11% uncertainty in our derived $^{12}CO/^{13}CO$ ratio (see Table 2).

The ^{12}CO spectrum of Figure 1 was obtained with a total of 45 minutes of integration of on-source (Venus) and off-source (5 arcminute offset in azimuth) scans. A total of 5 hours of on-off source pairs were taken to produce the ^{13}CO spectrum of Figure 2 (250 kHz resolution) and a total of 2 hours integration for the ^{13}CO spectrum of Figure 3 (100 kHz resolution). Note that the total bandwidth of the spectrum in Figure 2 is 128 megahertz, and, correspondingly, 64 megahertz for the spectrum of Figure 3. Also note the much reduced signal for the ^{13}CO spectrum.

Although the CO signal is clearly evident in several channels at the proper Doppler frequency, an immediate concern for the ^{13}CO spectra is the unfortunate double spike on the left-hand side (-8 to -4 mHz from line center) which was apparently introduced in the mixer-receiver. The width and position of this "glitch" is stationary in frequency in the spectra of both Figures 2 and 3. The presence of this feature introduces considerable uncertainty in determination of the $^{12}CO/^{13}CO$ ratio.

Figure 2. Rotational $J = 1 \rightarrow 2$ spectrum of ^{13}CO in the Venus mesosphere. The data are presented as a solid line. The best fit synthetic spectrum is the dotted line and corresponds to a constant ratio of $^{12}CO/^{13}CO = 185$. The dashed line synthetic spectrum employs a ratio of $^{12}CO/^{13}CO = 89$, corresponding to the earth $^{12}C/^{13}C$ ratio. For both synthetic spectra the altitude dependence of ^{12}CO is taken from Figure 4.

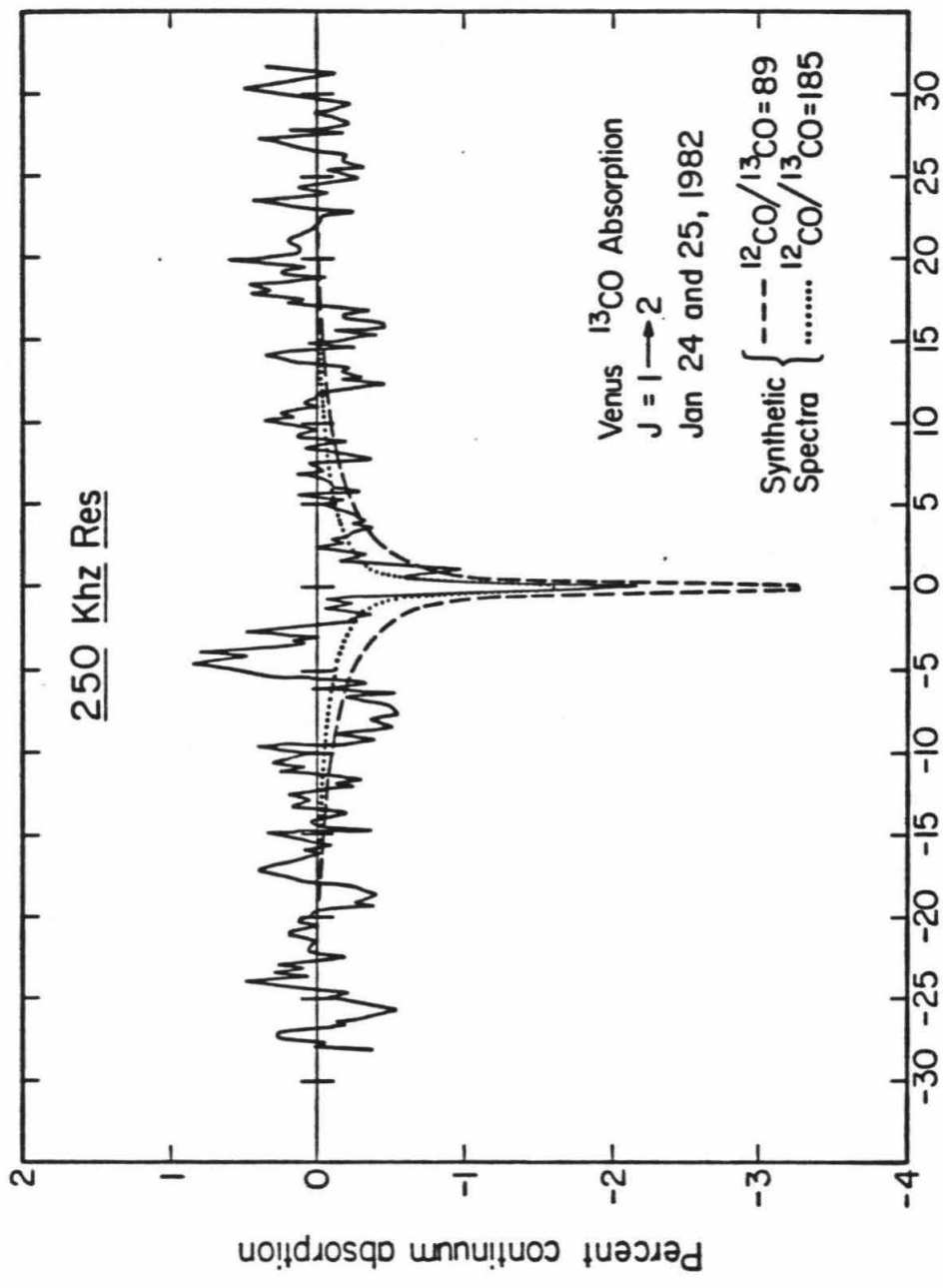
250 Khz Res
Venus ^{13}CO Absorption
J = 1 → 2
Jan 24 and 25, 1982
Synthetic Spectra
$^{12}CO/^{13}CO$=89
$^{12}CO/^{13}CO$=185
Percent continuum absorption
Mhz from line center
2
1
0
-1
-2
-3
-4
-30 -25 -20 -15 -10 -5 0 5 10 15 20 25 30

Figure 3. High frequency resolution of the ^{13}CO spectrum in the Venus mesosphere. Explanation is the same as for Figure 2.

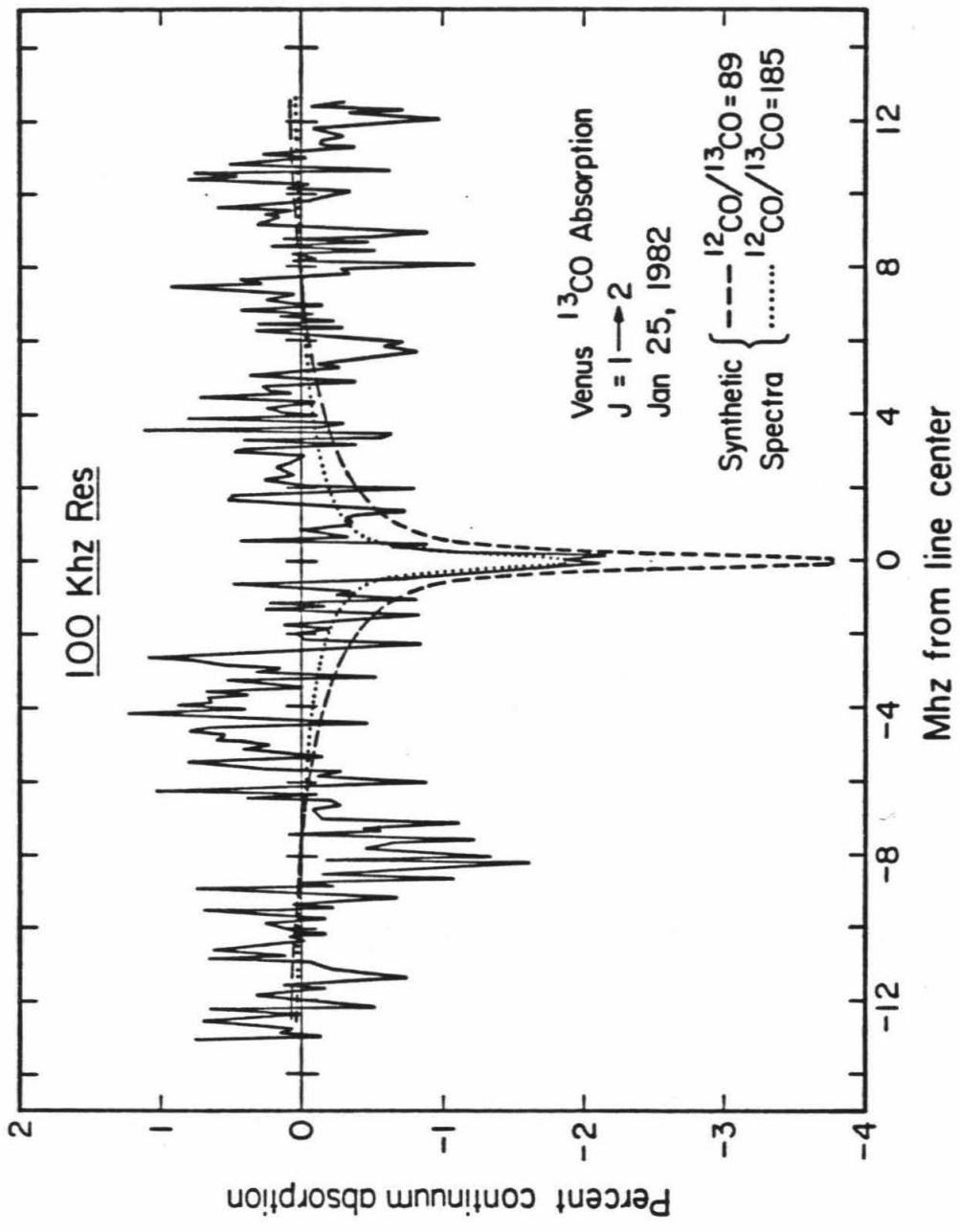
100 Khz Res
Venus ^{13}CO Absorption
J = 1 → 2
Jan 25, 1982
Synthetic Spectra
$^{12}CO/^{13}CO = 89$
$^{12}CO/^{13}CO = 185$
Percent continuum absorption
Mhz from line center
2
1
0
-1
-2
-3
-4
-12
-8
-4
0
4
8
12

Analysis

The optimum method by which a $^{12}CO/^{13}CO$ ratio may be calculated from the spectra of Figures 1, 2 and 3 is determined in part by limitations of the line forming process and in part by limitations of our particular data set. Neither ratios of spectral line areas or spectral line depths are applicable, primarily because the ^{12}CO line is optically thick in the center part of the spectrum. We point out that even the very thin ^{13}CO line is part emission, part absorption, a fact that makes the line area difficult to use.

We settled on a two part method which exploits the high signal-to-noise of our ^{12}CO data and avoids most of the ambiguities of the complicated line forming process. As a first step, we fit the folded ^{12}CO spectrum with synthetic spectra from a spectral line synthesis program (see Part I and Appendix IV). By trial and error, a ^{12}CO mixing ratio profile was determined along with upper and lower error bounds on this profile. The final fit spectrum is drawn against the data in Figure 1. For line synthesis we employed the nightside P,T model of Seiff et al. (1982). We have also analyzed the spectra using an earlier nightside model from Pioneer Venus probe data. Lines synthesized with the two atmospheres give an estimate of the sensitivity of our results on the assumed model atmosphere. We note that because we are solving for the ratio of ^{12}CO and ^{13}CO, our results are not very sensitive to the choice of a model atmosphere. The derived ^{12}CO mixing profile, presented in Figure 4, has several important features. The profile is well determined between 80 and 95 kilometers. Below 80 kilometers the limited bandwidth (and, ultimately, signal-to-noise ratio) allows only upper limits to be set on the ^{12}CO mixing ratio. Above 95 kilometers we lose resolution of the ^{12}CO mixing ratio because the opacity in the line center of the spectrum has become large and that part of the

Figure 4. A profile of ^{12}CO volume mixing ratios in the mesosphere of Venus. This profile was derived from the Venus ^{12}CO spectrum in Figure 1. The dashed boundaries about the solid line, best fit profile indicate the uncertainty in the ^{12}CO mixing profile as derived from the data.

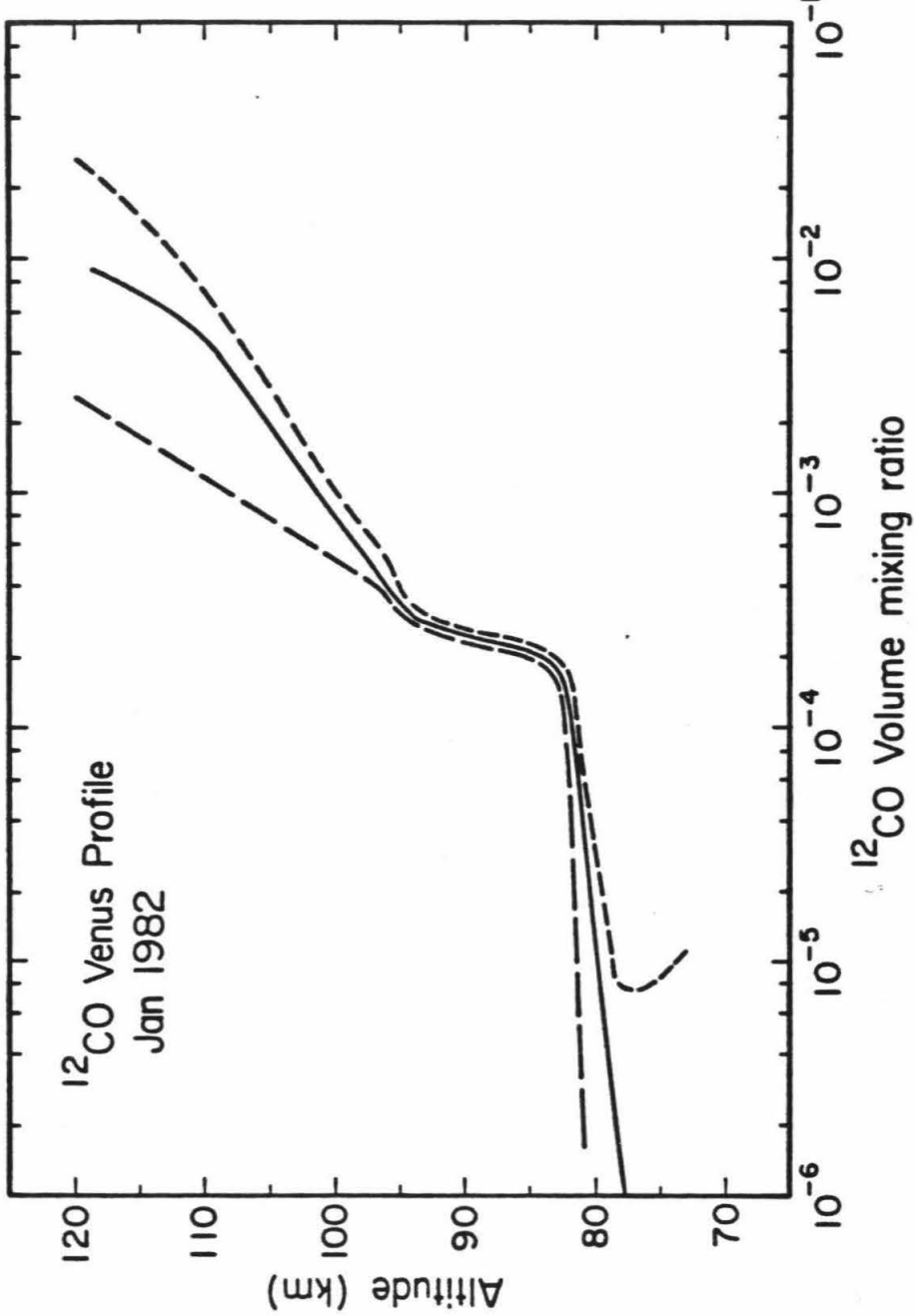
^{12}CO Venus Profile
Jan 1982
Altitude (km)
120
110
100
90
80
70
10^{-6}
10^{-5}
10^{-4}
10^{-3}
10^{-2}
10^{-1}
^{12}CO Volume mixing ratio

spectrum is saturated. The uncertainty in the mixing ratio of ^{12}CO between 95 and 100 kilometers is another important source of uncertainty in the determination of the $^{12}CO/^{13}CO$ ratio. The CO above 100 km is unimportant in this study.

As the second step in the process of deriving a value for $^{12}CO/^{13}CO$, we synthesized ^{13}CO spectral lines using the same model atmosphere and a ^{13}CO mixing profile which is some constant fraction of the derived ^{12}CO profile. The isotope fraction was varied in discrete steps and the sum of squares of the residuals for each synthesized spectrum was computed. A value for the constant ratio $^{12}CO/^{13}CO$ was found by finding the value which yielded minimum variance in the post-fit residuals. This process was repeated using the upper and lower bounds (Figure 4) found for the ^{12}CO mixing profile. The variation in the least squares value of $^{12}CO/^{13}CO$ found for these separate ^{12}CO mixing profiles was used to estimate an error in the $^{12}CO/^{13}CO$ ratio due to the uncertain ^{12}CO profile above 95 kilometers (Table I). The most probable value found for $^{12}CO/^{13}CO$ is 185.

As a final step in the error analysis, we considered a worst possible case for the receiver "glitch" in the ^{13}CO spectra of Figures 2 and 3. The concern in this case is not simply the effect of the very evident spike, which is included in the error from the least squares analysis. The main problem is that we cannot assume that the "glitch" did not persist into the line center of the spectrum. We have tested the pathological case that a spike of the same size and shape and of a direction such that it would *reduce* our measured ^{13}CO line has occurred at line center frequency. To do this we synthesized a ^{13}CO spectrum using the ^{12}CO mixing profile from Figure 4 and the nominal value of 89 for $^{12}CO/^{13}CO$. We then added our hypothetical spike to the synthesized spectrum and proceeded via

Table I. Minimum variance values for $^{12}CO/^{13}CO$ with formal error bounds. A range of $^{12}CO/^{13}CO$ is found due to uncertainty in the ^{12}CO mixing profile.

^{12}CO Mixing Profile	Lower Bound	Best Fit	Upper Bound
250 KHz (Figure 2)	159 ± 24	182 ± 30	212 ± 45
100 KHz (Figure 3)	165 ± 42	196 ± 42	233 ± 60

brute force least squares to determine a new value for $^{12}CO/^{13}CO$ from this spike-altered spectrum. We found the $^{12}CO/^{13}CO$ ratio had risen to 105, suggesting the worst-case error that the IF spike may have given us.

We summarize the results of our analysis in Table II. We have shown a standard deviation attributed to each error source except for the pathological IF spike hypothesis. Its error allotment of ± 20% is not really statistical but we will treat it as a standard deviation. Thus, the quadrature sum of the 7 error terms yields a conservative statistic which we interpret to be one standard deviation on our estimate of the isotope ratio, i.e., 185 ± 65. Also, on Figures 2 and 3 we have drawn in both the best fit synthesized spectrum for the isotope and the spectrum which we would have measured if the ratio was indeed 89 (dashed curve). It is obvious with out any analysis that the measured ^{13}CO absorption is about a factor of two less than the dashed line both in the center channels and, more importantly, in the spectral wings.

Discussion

As we have stated in the introduction, our value for $^{12}CO/^{13}CO$ is not an expected value. It is in direct conflict with the determination of Wilson et al. We should point out that Wilson et al. measured the $J = 0 \rightarrow 1$ transition of ^{13}CO arriving at a 4σ detection in the line center channel, compared to our 10σ measurement of Figure 2. They were, in effect, forced to estimate the $^{12}CO/^{13}CO$ ratio from the line centers of their spectra. Although the $J = 0 \rightarrow 1$ transition is not as optically thick as the $J = 1 \rightarrow 2$ transition, the $J = 0 \rightarrow 1$ transition is not optically thin. In fact, their derived CO mixing profile indicates a line center opacity greater than 1.0 for the $J = 0 \rightarrow 1$ transition. From the discussion of Wilson et al. (1980) on their line searches and estimates of upper bounds for

Table II. Summary of error analysis for $^{12}CO/^{13}CO$

Source of Error	Induced Error in $^{12}CO/^{13}CO$
Uncertainty in model atmosphere	<2%
Uncertainty in lower boundary brightness temperature of synthetic spectra program	<4%
Uncertainty in double sideband correction for spectra	<8%
Uncertainty in the relative continuum flux of Venus	11%
Uncertainty in ^{12}CO mixing ratios above 95 km	20%
Possibility of IF spike occurring at line center	20%
Formal error in least square fitting analysis	20%
	$^{12}CO/^{13}CO = 185 \pm 69.$

various molecular species, it is apparent that they have assumed an optically thin line center ^{12}CO opacity. It also appears that they have derived their $^{12}CO/^{13}CO$ ratio by the same method, ratioing ^{13}CO and ^{12}CO line center intensities. For such a case, the $^{12}CO/^{13}CO$ ratio may be seriously underestimated because the relative abundance of ^{12}CO is considerably underestimated.

The discrepancy between our measurement and Connes et al.'s measurement may possibly be explainable although a specific mechanism is not yet apparent. There is, for example, fractionation of ozone isotopes in the Earth's atmosphere. Cicerone and McCrumb (1980) predicted an enhancement of heavy ozone in the Earth's stratosphere due to a higher dissociation rate for $^{18}O^{16}O$ than for $^{16}O^{16}O$. This effect was subsequently measured by Mauersberger (1981) who showed that the enhancement (about 50%) decreased to zero at an altitude of 25 kilometers in the earth's atmosphere. We are, however, *suggesting* a reduction in the heavy isotope ^{13}CO over ^{12}CO. In addition, the doubling of the dissociation rate for $^{18}O^{16}O$ is due primarily to the resulting asymmetry in the oxygen molecule (Cicerone and McCrumb, 1980). No such obvious alteration occurs from $^{12}CO_2$ to $^{13}CO_2$. Any change in dissociation rates for $^{13}CO_2$ over $^{12}CO_2$ is thought to be slight (William DeMore, personal communication, 1982).

A potential mechanism for separation of CO isotopes in the upper atmosphere of Venus is some form of mass fractionation. The mass of ^{13}CO is 3.5% greater than the mass of ^{12}CO. At first glance this mass difference appears too small to explain a factor of two depletion of ^{13}CO relative to ^{12}CO. Furthermore, gravitational separation of atmospheres begins above the homopause, which occurs at ~ *130*–140 kilometers altitude on the dayside of Venus (von Zahn et al., 1980).

However, an important feature of CO in the mesophere of Venus is its striking diurnal variation . Microwave observations indicate factors of two to four greater abundance of CO on the nightside relative to the dayside of Venus between altitudes of 90 and 110 kilometers (Gulkis et al., 1977; Schloerb et al., 1980; Wilson et al., 1981). Dickinson and Ridley (1975, 1977) predicted such a nightside CO bulge on the basis of hydrodynamic numerical modeling of the upper atmosphere of Venus (~ 100-200 kilometers). Solar heating of the dayside atmosphere leads to steep subsolar to antisolar gradients of upper atmospheric temperatures which in turn lead to strong subsolar to antisolar mass transport. Lighter molecules such as CO become enriched on the nightside of Venus. Measurements made by pioneer Venus instruments (e.g., Niemann et al., 1979) indicate even larger day to night temperature gradients than those calculated by Dickinson and Ridley. The additional discovery of a sharp gradient in atmospheric density across dawn and dusk terminators would support wind velocities approaching sound velocities across the terminators.

We raise the possibility that transport of CO in the upper atmosphere of Venus may lead to fractionation of CO isotopes in the nightside upper atmosphere. The dynamics of day to night circulation in the upper atmosphere of Venus are still poorly understood, but it is possible that such transport may be significantly more efficient for the lighter ^{12}CO isotope relative to ^{13}CO. Still, at present it remains far from clear that dya-to-night transport in the upper atmosphere of Venus can fractionate CO isotopes to anywhere near the level our measurement requires. As direct mass transport from day to night should not significantly distinguish ^{12}CO and ^{13}CO, some form of diffusive separation would appear to be required.

Finally we note that equilibrium partitioning of ^{13}C into CO_2 will always segregate ^{13}C into CO_2 to some degree. From the formulation of isotope partition studies by Urey (1946), we found that the ratio $(^{13}CO_2/^{12}CO_2)$ / $(^{13}CO/^{12}CO)$ increases from 1.09 to 1.25 between 300 K and 120 K. Assuming equilibrium partioning of ^{13}C, the cold nightside of Venus upper atmosphere would be depleted ~ 25% in ^{13}CO relative to the dayside atmosphere. We note that rapid photodissociation of CO_2 would tend to drive the ratio $(^{13}CO_2/^{12}CO_2)$ $/(^{13}CO/^{12}CO)$ towards 1.0 on the dayside, assuming there are no substantial differences in photodissociation rates for $^{13}CO_2$ and $^{12}CO_2$. Whether or not ^{13}C equilibrium partioning is reached in the nightside atmosphere depends on the number density of CO^+ ions, which permit exchange of ^{13}C between CO_2 and CO^+ due to ion-molecular reaction (S. Epstein, personal communication, 1982). The Pioneer Venus ion mass spectrometer indicated peak CO^+, N_2^+ concentrations (the spectrometer could not distinguish CO and N_2) of $\sim 10^4\ cm^{-3}$ near 140 kilometers altitude on the nightside of Venus (Taylor et al., 1980; see also Nagy et al., 1980). Unfortunately, rate coefficients of ^{13}C exchange between CO_2 and CO, and the residence time of CO on the nightside of Venus are unknown. Without knowledge of these parameters, we cannot estimate the likelihood of equilibrium partitioning of carbon isotopes in the nightside upper atmosphere of Venus. Thus, we have at present no clear mechanism for depleting ^{13}CO in the Venus mesosphere.

As a final caveat we offer the following. A major weakness in the microwave spectral technique is the uncertainty in the flatness of the baseline across the entire spectrum. It is possible but unlikely that our baselines in the ^{13}CO spectra have a gentle curvature which effectively removed about half the area under the spectra. It is not possible to estimate the likelihood of such a

circumstance. However, no such curvatures were suggested in many other measurements using this system during the observing run.

References

Cicerone, R.J., and J.L. McCrumb, Photodissociation of isotopically heavy O_2 as a source of atmospheric O_3, *Geophys. Res. Lett.* **7**, 251-254, 1980.

Clancy, R.T., D.O. Muhleman, and B.M. Jakosky, Variability of carbon monoxide in the Mars atmosphere, submitted *Icarus*, 1983.

Connes, P., J. Connes, L.D. Kaplan, and W.S. Benedict, Carbon monoxide in the Venus atmosphere, *Astrophys. J.* **152**, 731-743, 1968.

Dickinson, E.D. and E.C. Ridley, A numerical model for the dynamics and composition of the Venusian thermosphere, *J. Atmos. Sci.* **32**, 1219-1231, 1975.

Dickinson, E.D. and E.C. Ridley, Venus mesosphere and thermosphere temperature structure II. Day-night variations, *Icarus* **30**, 163-178, 1977.

Gulkis, S., R.A. Kakar, M.J. Klein and E.T. Olsen, Venus; Detection of variations in stratospheric carbon monoxide, *Proc. Symp. Planet. Atmos.* **61**, 61-65, 1977.

Hoffman, J.H., R.R. Hodges, T.M. Donahue, and M.B. McElroy, Composition of the Venus lower atmosphere from the Pioneer Venus mass spectrometer, *J. Geophys. Res.* **85**, 7882-7890, 1980.

Mauersberger, K., Measurement of heavy ozone in the stratosphere, *Geophys. Res. Lett.* **8**, 935-937, 1981.

Nagy, A.F., T.E. Cravens, S.G. Smith, H.A. Taylor, and H.C. Brinton, Model calculations of the dayside ionosphere of Venus: ionic composition, *J. Geophys. Res.* **85**, 7795-7801, 1980.

Schloerb, F.P., S.E. Robinson, and W.M. Irvine, Observation of CO in the stratosphere of Venus via its $J=0\rightarrow 1$ rotational transition, *Icarus* **42**, 121-128, 1980.

Seiff, A. and D.B. Kirk, Structure of the Venus mesosphere and lower thermosphere from measurements during entry of the Pioneer Venus probes, *Icarus*, **49**, 49-70, 1982.

Taylor, Jr., H.A., H.C. Brinton, S.J. Bauer, R.E. Hartle, P.A. Cloutier, and R.E. Daniell, Jr., Global observations of the composition and dynamics of the ionosphere of Venus: implications for the solar wind interaction, *J. Geophys. Res.* **85**, 7763-7777, 1980.

Urey, H.C., The thermodynamic properties of isotopic substances, *J. Chem. Soc.* April, 562-581, 1946.

Wilson, W.J., M.J. Klein, R.K. Kahar, S. Gulkis, E.T. Olson, and P.T.P. Ho, Venus carbon monoxide distribution and molecular-line searches, *Icarus* **45**, 624-637, 1981.

von Zahn, U., K.H. Fricke, D.M. Hunten, D. Krankowsky, K. Mauersberger, and A.L. Nier, The upper atmosphere of Venus during morning conditions, *J. Geophys. Res.* **85**, 7829-7840, 1980.

PART III

Variability of Carbon Monoxide in the Mars Atmosphere

R.T. Clancy, D.O. Muhleman and B.M. Jakosky

(Submitted to Icarus)

INTRODUCTION

Measurements of carbon monoxide in the atmospheres of Mars and Venus have provided one of the more difficult challenges to modern photochemical modeling of planetary atmospheres. Simple photochemical models of pure CO_2 atmospheres predict equilibrium states substantially photodissociated into CO and O_2 (Donahue, 1968; McElroy and Hunten, 1970; McElroy and McConnell, 1971). Three body recombination of CO ($CO + O + M \rightarrow CO_2 + M$) is forbidden by angular momentum conservation and, hence, proceeds at a very slow rate. Yet infrared and microwave observations of Venus (Connes et al., 1968; Waters et al., 1976) and Mars (Kaplan et al., 1969; Kakar et al., 1977; Good and Schloerb, 1981) reveal CO abundances orders of magnitude below predicted levels. The apparent resolution of this disagreement between modeling and observations requires catalytic recombination of CO and O. Atmospheric trace constituents such as OH (McElroy and Donahue, 1972; Parkinson and Hunten, 1972) and Cl (Prinn, 1971; Krasnopolsky and Parshev, 1981; Yung and DeMore, 1982) must play critical roles in the overall chemical composition of these planetary atmospheres.

Unfortunately, investigation of the important processes requires extremely difficult measurements due to the trace levels of the catalysts. Present knowledge of the photochemistry of the lower atmosphere of Mars (< 100 km) rests upon atmospheric column density measurements of O_2 (Carlton and Traub, 1972; Barker, 1972; Trauger and Lunine, 1982) and CO (Kaplan et al., 1969; Kakar et al., 1977; Good and Schloerb, 1981). Yet even this limited data set has provided both insight and controversy. The very low levels of O_2 observed require either high rates of eddy diffusion (McElroy and Donahue, 1972) or very high levels of odd hydrogen (Parkinson and Hunten, 1972) in the Martian atmosphere. Hunten (1974) has described both cases as somewhat

extraordinary and unstable, with the consequence that CO and O_2 should be variable on a timescale of $\gtrsim 1$ year in the Martian atmosphere.

Total O_2 abundance appears to show negligible variation as determined from measurements in 1972 and 1982. Carlton and Traub (1972), and Barker (1972) determined respective values of 10.4 ± 1.0 and 9.5 ± 0.6 cm amagat of O_2 in the Martian atmosphere in 1972. Recent measurements of Trauger and Lunine (J. Trauger, personal communication), are consistent with these earlier results. On the other hand, measurements of CO appear to show significant variability of CO abundance in the atmosphere of Mars. Good and Schloerb (1981) reported a four-fold increase in CO abundance between 1967 and 1980. Assertion of this large variation was based upon the initial measurement of CO by Connes et al. (1969) in 1967, as analyzed by Kaplan et al. (1969), and microwave observations of Good and Schloerb, taken in 1980.

The question arises, how can CO abundance increase by a factor of four while O_2 abundance shows no apparent variation. Higher levels of CO imply a greater release of O which quickly recombines to form O_2. A lack of correlation between CO and O_2 variations in the Martian atmosphere would suggest that the photochemistry of Mars is not well understood. In an effort to further constrain the behavior of CO in the atmosphere of Mars we obtained a microwave spectrum of Martian CO in January of 1982. Our spectrum is of the $J = 1 \rightarrow 2$ rotational transition of CO, which is eight times stronger than the $J = 0 \rightarrow 1$ transition measured by Good and Schloerb. We have also reanalyzed the data of Good and Schloerb and Kakar et al. (1977) in an attempt to determine consistency among CO abundances from CO microwave spectra of Mars and the initial measurement of Connes et al. (1969).

PREVIOUS OBSERVATIONS

Before proceeding with a discussion of our own measurement of Martian CO, we should begin with a brief history of preceding observations and analyses.

The discovery of CO in the Martian atmosphere was made some 15 years ago when Connes et al. (1969) measured infrared absorption spectra of reflected solar radiation from both Mars and Venus. Kaplan et al. (1969) published the initial analysis of the Martian spectra, reporting a total CO column density of $1.5 \pm 0.3 \times 10^{20}$ molecules/cm^2. From spectra of CO_2 in the same data set, Kaplan et al. determined a CO/CO_2 mixing ratio of $8 \pm 3 \times 10^{-4}$. Although there were no subsequent infrared measurements of Martian CO, several reanalyses of the Connes et al. spectra were published in the 1970's. Young (1971) published the first such reanalysis which produced CO abundances about twice those reported by Kaplan et al. Young also significantly broadened the error bars of the CO abundance, reporting an uncertainty of a factor of four in the CO column density due to uncertainties in Martian surface pressure, pressure broadened half width of CO, and systematic measurement errors. Carlton and Traub (1972) reanalyzed the Connes et al. spectra using CO lines less sensitive to uncertainties in CO pressure broadened line widths and also using recent laboratory measurements of these line widths. The authors published a value of $2.0 \pm 0.3 \times 10^{20}$ molecules/cm^2 for the column density of CO. Finally, the most recent reanalysis of the original Connes et al. spectrum was published by Young and Young (1977), reporting a "very conservative estimate of the CO abundance" (i.e., in terms of uncertainty) equal to $2.0 \pm 0.8 \times 10^{20}$ molecules/cm^2.

It was not until 1975 that a second measurement of CO in the atmosphere of Mars was obtained. Kakar et al. (1977) observed the microwave

$J = 0 \rightarrow 1$ rotational transition of atmospheric CO as an absorption feature against the continuum emission of the surface of Mars. The authors obtained a best fit of their spectrum with a constant CO mixing ratio of 1.9×10^{-3} in the Martian atmosphere, corresponding to an approximate CO column density of 4.4×10^{20} molecules/cm^2. Although this value is more than a factor of two greater than the best estimate from the Connes et al. infrared spectra, the Kakar et al. determination is uncertain by more than ± 70%. The large error bars are primarily due to the extreme sensitivity of the analysis to the 10% uncertainty in the 2.6 millimeter radio brightness temperature of the Mars continuum rather than noise in the data. Uncertainty in the relative temperature difference between the Martian atmosphere and continuum is the main error term in the analysis of CO microwave spectra of Mars.

Good and Schloerb (1981) obtained the most recent published measurement of CO in the Martian atmosphere in 1980. Their $J = 0 \rightarrow 1$ spectrum (Figure 5) included a much larger bandwidth than Kakar et al.'s spectrum (Figure 7) and revealed emission wings peaking some 20 megahertz from line center. From fitting synthetic spectra to their data, they obtained a CO mixing ratio of $3.2 \pm 1.1 \times 10^{-3}$, yielding an approximate column density of $7.4 \pm 2.6 \times 10^{20}$ molecules/cm^2. Their error analysis included several models of atmospheric temperature profiles but did not include any uncertainty in the continuum brightness temperature of Mars. Based on the CO mixing ratio of 8×10^{-4} from Kaplan et al. (1969) and their own value, Good and Schloerb concluded that a four fold increase in CO occurred between 1967 and 1980.

OBSERVATION OF THE $J = 1-2$ TRANSITION

From the 24th to the 27th of January 1982, we observed the $J = 1 \rightarrow 2$

rotation transition (at 230.538 gigahertz; 1.3 mm) of CO in the atmosphere of Mars. We used the 36 foot, millimeter radio telescope of the NRAO at Kitt Peak, Arizona and the NRAO 200-240 gigahertz mixer receiver, which operated with a single sideband noise temperature of 1100 K. For spectral analysis, we used two sets of NRAO filter banks, each set consisting of 256 channels. The individual channel widths were 1 megahertz and ½ megahertz, allowing spectra of 256 and 128 megahertz total bandwidth. The observing procedure was standard position switching with the on position centered on Mars and the off position separated by 5 arcminutes in azimuth from the position of Mars. Differencing the on and off measurements provided the basic, uncalibrated spectrum of Mars, although the quantity actually stored for each channel was this signal minus the average signal per channel. The average signal per channel (called BL) was stored with each on-off pair so that the basic spectrum could be reproduced.

While the spectra proved to be remarkably free of standing waves, we were warned (Richard Howard, personal communication, 1981) that strong continuum sources introduced non-linear response due to mismatch in power levels between on and off source spectra in the filter banks. Subsequent tests proved that noise levels in spectra of Mars and Venus were abnormally high unless a gain modulator was used to remove the average continuum level (BL) of Mars in the on scans before detection in the filter banks. During the observations we measured spectra of Mars with the gain modulator and separate spectra without the gain modulator for a determination of BL. With this procedure we obtained spectra which were reproducible to within 5% from day to day.

We did not attempt to calibrate our spectra in absolute temperature units. For the purpose of inverting microwave absorption spectra it is not generally necessary to calibrate the spectra (although such calibration does provide

further information). As long as the continuum level is retained in the absorption spectrum, one can invert the data for mixing ratios of the observed species. Still, an essential requirement for this procedure is that one know the relative temperatures of the background continuum (the surface of Mars) and the absorbing medium (the atmosphere of Mars). The closer these temperatures are to one another, the more accurately their difference must be known. We will return to this point in the discussion of our analysis.

One other caveat in the calibration of our spectra is the double sideband correction. The essential point here is that we measured the continuum of Mars in two bandpasses (sidebands) that were separated in frequency by ~ 4 gHz. The CO line transition was contained in only one of these bandpasses. In order to represent the absorption in fraction of the continuum we must reduce the continuum level by roughly a factor of two relative to the line absorption level. This factor becomes exactly two if the terrestrial atmospheric opacity is the same for the two sidebands (which is true to within ~ 1% for an observing frequency of 230 gHz) and if the system gain is identical for the two sidebands. We rely on sideband balance measurements by Richard Howard in November of 1981 which indicate 5-10% level sideband balance for the NRAO ^{12}CO J = 1 → 2 observing system at Kitt Peak. Hence we feel that the absorption depths of Figures 1 and 2 are accurately calibrated to within the 5-10% level.

At the time of our observations, Mars was 9 arcseconds in diameter. We found that observing at 1.3 mm wavelengths, the half power full width of the 36 foot NRAO telescope beam was ~ 60 arcseconds indicating that our spectra sampled evenly over the entire disk of Mars. Other important aspects of Mars were the latitude (24°N) and local time (2:30 p.m.) for the sub-Earth point on Mars. At Mars transit the range of central meridian longitudes for our

observations was 130-105°W, approximately the position of the Tharsis plateau. Efforts to model the effects of Martian topography on synthesized $J = 1 \rightarrow 2$ spectra showed remarkable insensitivity, although we note that average hemispheric temperatures of the Mars continuum and lower atmosphere (< 10 km) are very similar. Our spectra do not strongly constrain CO abundance in this altitude region.

We present our total averaged spectra of Mars with 1 megahertz resolution in Figure 1, and ½ megahertz resolution in Figure 2. Included in the figures are fitted synthetic spectra from our model line fitting analysis.

I. ANALYSIS OF THE 1982 $J = 1 \rightarrow 2$ SPECTRUM

The essential component for analysis of our spectra of Figures 1 and 2 is a radiative transfer program which computes synthetic CO spectra. We refer readers to Waters (1976) for a good description of microwave spectroscopy and the physics of microwave line formation in planetary atmospheres. The central process producing our spectra is pressure broadened, resonant absorption of microwave continuum by atmospheric CO over a generally warmer, solid surface. Appendix IV contains a description of the radiative transfer equation and the absorption coefficient of CO.

Schematically, we subdivided the Martian atmosphere into a set of discrete horizontal layers and traced, as a function of frequency, the microwave radiation from the Martian surface upward through these layers. The relevant characteristics of each layer are its temperature, atmospheric pressure, and mixing ratio of CO. Each layer effectively adds an emission and absorption spectrum to the upwelling radiation. The net effect of the layer is proportional to the mixing ratio of CO and to the difference between the brightness temperature

Figure 1. Rotational $J = 1 \rightarrow 2$ spectrum of CO in the Martian atmosphere. The measured spectrum (represented by a solid line) was taken in January 1982 with a full bandwidth of ± 128 MHz and a spectral resolution of 1 MHz. The dotted line is the best fit synthetic spectrum (using model E) for a constant CO mixing ratio in the Martian atmosphere. The dashed line is the best fit synthetic spectrum for an altitude varying CO mixing ratio (see Figure 4).

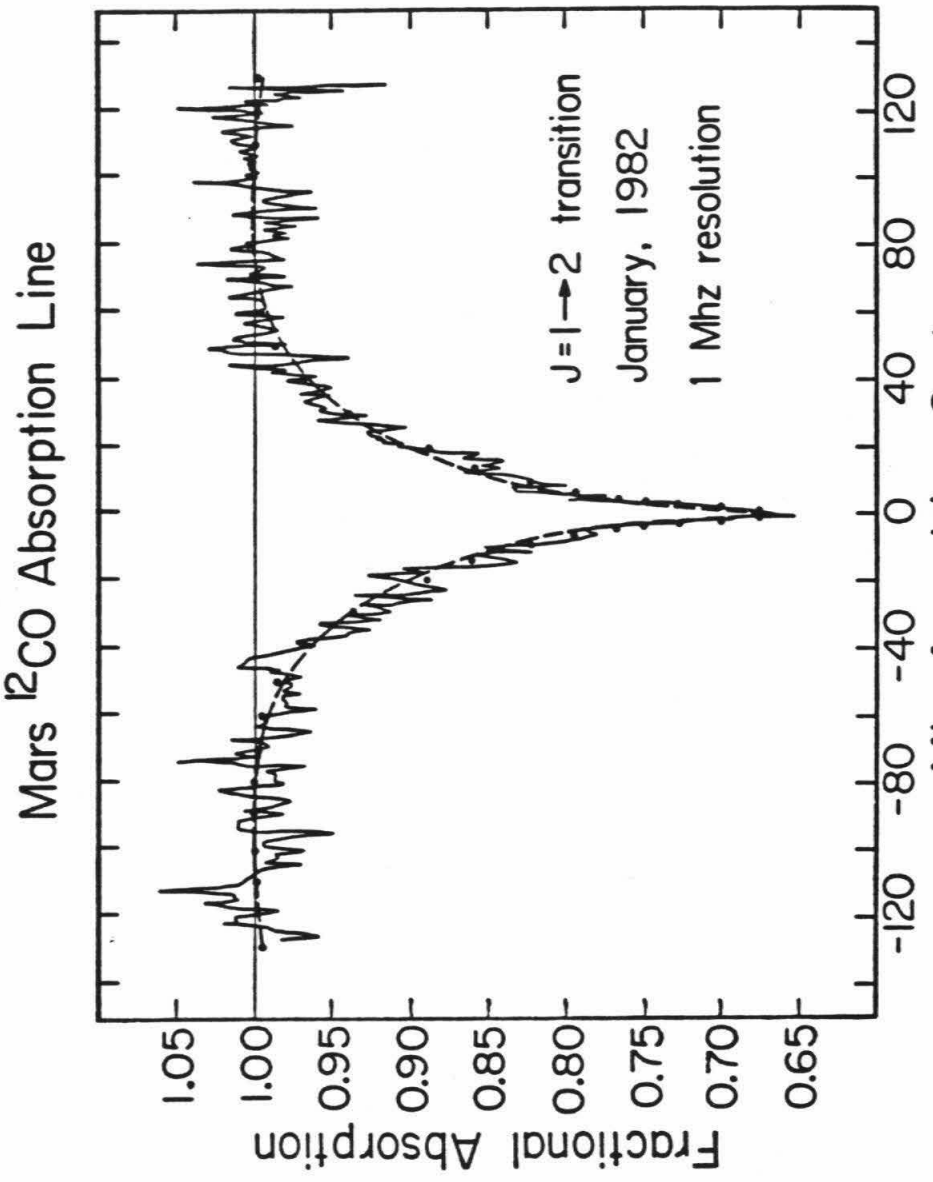
Mars ^{12}CO Absorption Line
J=1→2 transition
January, 1982
1 Mhz resolution
Fractional Absorption
1.05
1.00
0.95
0.90
0.85
0.80
0.75
0.70
0.65
-120
-80
-40
0
40
80
120
Mhz from Line Center

Figure 2. Rotational $J = 1 \rightarrow 2$ spectrum of CO in the Martian atmosphere with ± 64 MHz bandwidth and spectral resolution of ½ MHz. Explanation is same as for Figure 1.

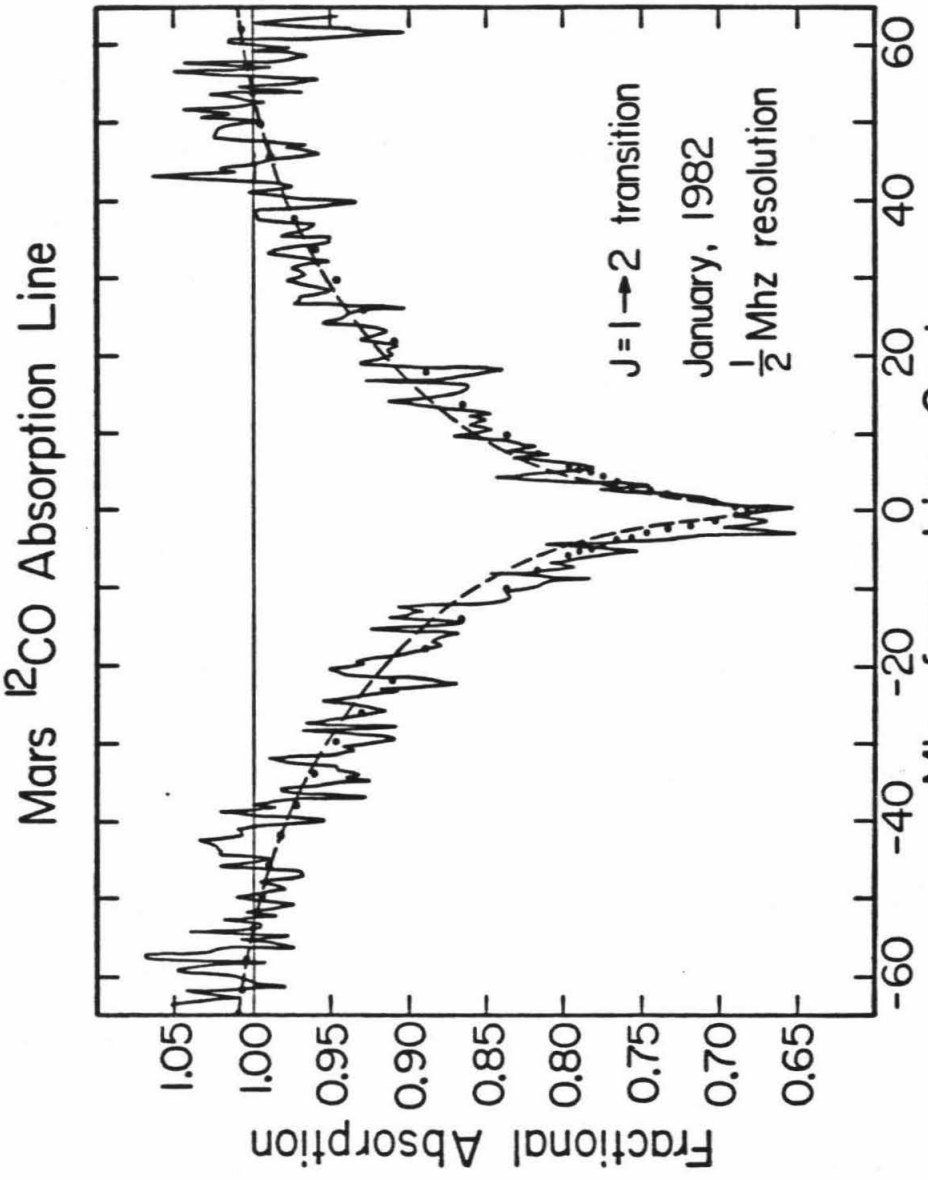
Mars ^{12}CO Absorption Line
Fractional Absorption
1.05
1.00
0.95
0.90
0.85
0.80
0.75
0.70
0.65
-60
-40
-20
0
20
40
60
Mhz from Line Center
J=1→2 transition
January, 1982
½ Mhz resolution

of the upwelling radiation and the atmospheric temperature of the layer. If the temperature of the layer is greater (less) than the brightness temperature of the upwelling radiation, the net effect of the layer is emission (absorption). This holds true separately at each frequency. The width in megahertz of the spectrum contributed by each layer is proportional to the atmospheric pressure of the layer. This pressure dependence of the spectral line width allows the possibility of determining the mixing ratio of CO as a function of altitude in the atmosphere of Mars.

The entire process of tracing the CO spectrum through a column of atmospheric layers was repeated at 132 separate horizontal positions on the disk of Mars. This allowed the inclusion of horizontal variations in surface brightness temperature, atmospheric temperature, topography, and path length of the received radiation through the Martian atmosphere. We formed the final synthetic spectrum by averaging the 132 individual spectra with proper weights.

Model Surface Temperatures

As we have noted, an important element in the analysis of CO microwave spectra of Mars is the assumption for the lower boundary brightness temperature of Mars. Radio observations of the Martian brightness temperature at millimeter wavelengths are few in number and limited by 10-15% uncertainties in calibration (Epstein et al., 1970; see also Cuzzi and Muhleman, 1972). Martian surface temperatures are much better determined from measurements made by the Viking Infrared Thermal Mapping (IRTM) experiment (Kieffer et al., 1977; Palluconi and Kieffer, 1981). However, a necessary and difficult effect to include is the depth in the Martian regolith to which 1.3 mm ($J = 1 \rightarrow 2$) and 2.6 mm ($J = 0 \rightarrow 1$) radiation penetrate. Scattering and microwave absorption proper-

ties of the Martian surface are poorly defined (Jakosky and Muhleman, 1981) but the effect of a finite radio skin depth is significant (Cuzzi and Muhleman, 1972). Average dayside temperatures at a depth of 2 cm can be 20 K cooler than average dayside surface temperatures. One must also consider the effect of the large variation of surface temperatures on Mars (~ 100 K). We note that Good and Schloerb used a single surface temperature (220 K) for a dielectric sphere (dielectric constant = 2.5) to estimate their microwave continuum of Mars. (It turns out that this procedure is surprisingly accurately.) In an effort to treat the lower boundary continuum more accurately, we modeled Martian surface and subsurface temperatures as a function of local time and latitude on Mars. We provide a brief discussion of our thermal modeling and assumptions in appendix VII.

Our models of local surface and subsurface temperatures on Mars are particularly useful in allowing an accurate comparison among the different microwave observations of Mars. The centimeter radio brightness temperature of Mars exhibits a 5-10 K rotational variation due to longitudinal variations in Martian surface properties (Jakosky and Muhleman, 1980; Andrew et al., 1977; Doherty et al., 1979). Furthermore, the average disk temperature of the surface of Mars as seen from Earth varies by ± 15 K as the sub-Earth point on Mars moves from afternoon (pre-opposition) to morning (post-opposition) hours and from mid to equatorial latitudes. At the time of Good and Schloerb's 1980 observation, the local time of the sub-Earth point on Mars was 10:10 a.m. (latitude, 25°N), compared to 2:30 p.m. for our observations. From our thermal modeling we found that the average surface temperature of Mars for our observations was 10 K warmer than for Good and Schloerb's 1980 observation. On the other hand, we found that the average surface temperature for Kakar et al.'s

1975 observation was 10 K warmer than our own. The sub-Earth point for their apparition of Mars was near the equator of Mars (local time ~ 2 p.m.). We summarize the important observational parameters of Mars for all three of the microwave observations in Table I.

Model Atmosphere

Uncertainty in the disk average atmospheric temperatures of Mars may also introduce large uncertainties in the analysis of microwave CO spectra. We note that, at altitudes above a few kilometers, variations of atmospheric temperatures across the dayside of Mars are generally less than 15 K (e.g., Pollack et al., 1981). Variations of observed, hemispheric average temperatures due simply to the changing aspect of Mars should be less than 10 K. A more difficult problem to consider is actual temporal variability of average atmospheric temperatures on Mars. In particular, global dust storms on Mars may raise atmospheric temperatures by as much as 20-40 K globally (Pollack et al., 1979; Martin et al., 1979). The Martian atmosphere appears to have the least amount of suspended dust between solar longitudes (L_s) of 30 and 150° (Pollack et al., 1979). It may be argued that the safest microwave observations to compare should be taken between these solar longitudes. In any case variability of atmospheric temperatures among the different CO observations must be considered as an uncertainty when making comparisons. L_s for our 1982 observation, Good and Schloerb's 1980 observation, and Kakar et al.'s 1975 observations were 77°, 86°, and 340°, respectively. We might expect the 1982 and 1980 observations to be most easily compared with a bit more reservation in comparison with the 1975 observation.

We rely on the atmospheric measurements taken by the Viking space-

1975 observation was 10 K warmer than our own. The sub-Earth point for their apparition of Mars was near the equator of Mars (local time ~ 2 p.m.). We summarize the important observational parameters of Mars for all three of the microwave observations in Table I.

Model Atmosphere

Uncertainty in the disk average atmospheric temperatures of Mars may also introduce large uncertainties in the analysis of microwave CO spectra. We note that, at altitudes above a few kilometers, variations of atmospheric temperatures across the dayside of Mars are generally less than 15 K (e.g., Pollack et al., 1981). Variations of observed, hemispheric average temperatures due simply to the changing aspect of Mars should be less than 10 K. A more difficult problem to consider is actual temporal variability of average atmospheric temperatures on Mars. In particular, global dust storms on Mars may raise atmospheric temperatures by as much as 20-40 K globally (Pollack et al., 1979; Martin et al., 1979). The Martian atmosphere appears to have the least amount of suspended dust between solar longitudes (L_s) of 30 and 150° (Pollack et al., 1979). It may be argued that the safest microwave observations to compare should be taken between these solar longitudes. In any case variability of atmospheric temperatures among the different CO observations must be considered as an uncertainty when making comparisons. L_s for our 1982 observation, Good and Schloerb's 1980 observation, and Kakar et al.'s 1975 observations were 77°, 86°, and 340°, respectively. We might expect the 1982 and 1980 observations to be most easily compared with a bit more reservation in comparison with the 1975 observation.

We rely on the atmospheric measurements taken by the Viking space-

Table 1. Observational Parameters of Mars for CO Microwave Observations

	Kakar et al., 1977	Good and Schloerb, 1981	This Paper
Microwave transition	$J = 0 \rightarrow 1$	$J = 0 \rightarrow 1$	$J = 1 \rightarrow 2$
Date of observation	November 9, 1975	March 29-April 1, 1980	January 24-27, 1982
L_s for Mars	340°	86°	77°
Central meridian longitude on Mars at observed transit	10°W	290-320°W	105-130°W
Latitute of sub-Earth point on Mars	4°N	25°N	21°N
Time of day for sub-Earth point on Mars	2 p.m.	10 a.m.	2 30 p.m.

craft for our model atmosphere of Mars, which is based upon the Viking entry probe data of Seiff and Kirk (1977). Model pressure and temperature profiles (Figure 3) are based upon smoothed averages of the profiles measured by Viking 1 (L_s = 97°) and Viking 2 (L_s = 117°) entry probes. The pressure-temperature profile of Figure 3 agrees with the average of the two Viking entry profiles to within ± 2 K at and below an altitude of 40 km in the Mars atmosphere (see *The Mars Reference Atmosphere*, COSPAR, published by JPL, 1978). We also made an attempt to include the solar zenith angle dependence of atmospheric temperatures on Mars. 15 μm brightness temperatures (Martin and Kieffer, 1979) and Viking lander temperature sensors (Hess et al., 1977) indicate significant diurnal variation of atmospheric temperatures with highest temperatures near 2 p.m. local time. The large variations measured by the landers (± 25 K) are likely to converge rapidly (within the first few kilometers of altitude) to the more moderate variations (± 10 K) at 20-30 kilometer altitudes (Pollack et al., 1979) measured by the 15 micron channel of the IRTM (Martin and Kieffer, 1979). We chose to model atmospheric temperature variations according to the diurnal-latitudinal behavior of 15 μm temperatures determined by Martin and Kieffer (1979).

For analysis of our CO spectra we computed least-squares fit synthetic spectra using successively complex models of the Martian surface and atmosphere. This procedure allowed us to selectively determine aspects of the model that seriously affected our derived column density and latitude profile of CO. Before discussing the results, we describe the models separately in ascending order of complexity.

Figure 3. Pressure-temperature profile of Martian atmosphere employed for spectral line analysis. The profile is obtained from a smoothed average of the Viking 1 and 2 descent profiles (Seiff and Kirk, 1977) and is used to specify the average atmospheric state for models A and B. For globally varying temperature profile of models C-G, the above profile represents the atmospheric state for a local solar hour angle of 3 hr at subsolar latitudes on Mars.

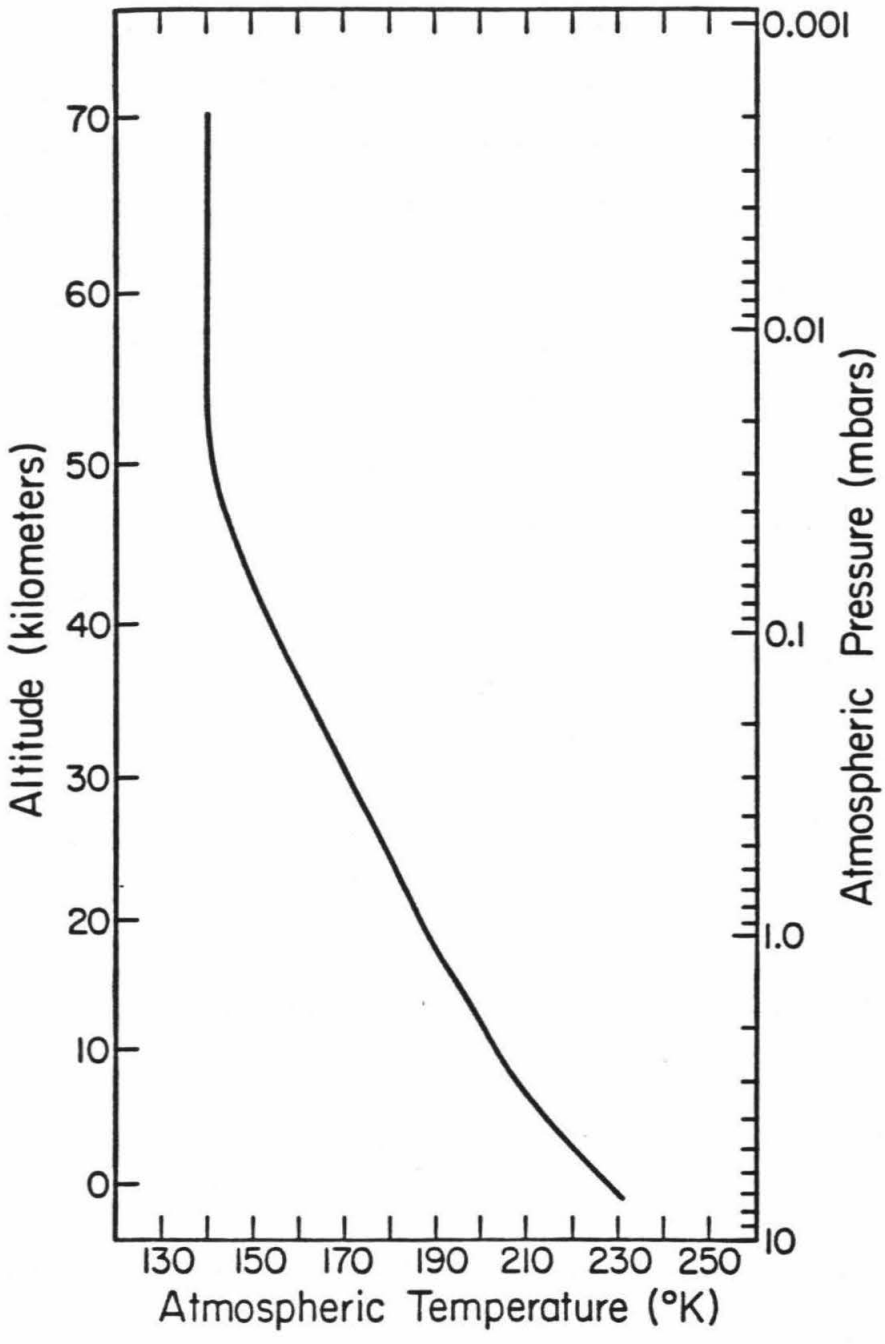
Altitude (kilometers)
70
60
50
40
30
20
10
0
130
150
170
190
210
230
250
Atmospheric Temperature (°K)
0.001
0.01
0.1
1.0
10
Atmospheric Pressure (mbars)

Model A

For our simplest case we adopted model assumptions similar to those of Good and Schloerb. The lower boundary was treated as a dielectric sphere of constant surface temperature and zero radio skin depth. On the basis of our thermal models, we found an average surface temperature of 232 K for our apparition of Mars. We chose a dielectric constant, ε, of 2.5 although at millimeter wavelengths this parameter is not well known. The resulting disk brightness temperature of Mars was 208.5 K. Uncertainty in the dielectric constant produces approximate $\pm 3\%$ and ± 6 K uncertainties in surface emissivity and brightness temperature, respectively. (For all of our models we calculated emissivity from the average of the two polarizations.) For model A, a single profile of atmospheric temperature (Figure 3) was used for the entire hemisphere of Mars.

Model B

Our second case tested sensitivity of our spectra to the large variation of surface temperatures on Mars. At the time of our observations the visible hemisphere of Mars included the very cold temperatures of the north polar cap ($\sim$ 150 K) and the much warmer temperatures (250 K) of lower latitudes in the afternoon hours. We used the results of our thermal modeling to specify surface temperatures across the visible disk of Mars. As in model A, radio brightness temperatures were calculated treating Mars as a dielectric sphere ($\varepsilon = 2.5$) of zero radio skin depth. The disk-average surface and brightness temperatures of model B and model A were identical. Modeling of the Martian atmosphere was also identical for the two cases.

Model C

Model C incorporated variability of atmospheric temperatures across the visible hemisphere of Mars. We used a simple parameterization of the latitudinal and diurnal temperature variations measured by the 15 μm channel of the Viking orbiters (Martin and Kieffer, 1979). These model temperature variations were assumed constant in altitude. We note that the local times sampled by the Viking 1 and 2 entry probes ($\sim$ 4:10 p.m. and 10:00 a.m.) reflect intermediate temperatures of the Martian atmosphere. The addition of diurnal-latitudinal variability lowered the average atmospheric temperatures of our model by approximately 2 K. Surface brightness temperatures were calculated as in model B.

Model D

We allowed for the effect of surface topography in model D. This was done by choosing the appropriate lower boundary of the atmosphere for each of our 132 points on the disk of Mars. The central meridian longitude of Mars rotated by about 120° during each of our $\sim$ 8 hour observation periods. The range of observed longitudes also shifted by about 25° during the four days of our observations. For the boundary conditions of model D we used the average Mars longitudes of our observations to specify surface elevations. All other parameters for model D are identical to those of model C. We note that our observations could have been binned to separate the observed longitudes of Mars but the effect of Martian surface elevations on our spectra proved to be negligible. The $J = 1 \rightarrow 2$ CO spectrum of Mars is less sensitive to CO below 10 kilometers, due to nearly equal atmospheric and Mars continuum temperatures in this region. The signature of CO below 10 km is also spread out in fre-

quency by pressure broadening due to exponentially increasing atmospheric pressures. We found that our $J = 1 \rightarrow 2$ spectrum is most sensitive to CO between 10 and 50 kilometers in altitude.

Model E

For our fifth case we considered the effect of a non-zero radio skin depth. Radio waves penetrate homogeneous media to a depth that is roughly proportional to the wavelength of radiation (e.g., Muhleman, 1972). Radio absorption properties of the lunar regolith indicate penetration depths (opacity = 1) of approximately seven wavelengths (Muhleman, 1972). We applied this rough scaling analysis to estimate the radio skin depth for the microwave continuum of Mars at 1.3 and 2.6 mm radio wavelengths. We note that the effects of surface scattering tend to diminish the depth of radio penetration. Surface roughness on the order of the wavelength of observation tends to dilute contribution of subsurface temperatures in favor of surface temperatures. However, the relative importance of surface scattering is not well known, particularly at millimeter radio wavelengths. We used a 1.3 mm radio skin depth of 1.0 cm, subsurface temperature profiles from our thermal modeling, and the emissivity of a dielectric sphere ($\varepsilon = 2.5$) to specify the lower boundary brightness temperatures of model E. Because temperatures at depth are cooler than surface temperatures on the Earth-facing dayside of Mars, the disk average brightness temperature for model E was 5 K cooler than for models A-D. The atmospheric temperature variations of model C were retained in model E.

Models F and G

Models A-D investigated the sensitivity of our synthetic spectra to variations of surface temperature, atmospheric temperatures, and topography

across the visible hemisphere of Mars. We generally found (see Table II) our $J = 1 \rightarrow 2$ spectra to be insensitive to these variations as long as the average value of each of the parameters over the disk of Mars was not changed significantly. In model E we measured the effect of 5 K cooler lower boundary temperatures in an attempt to include the effect of finite radio skin depths at 1.3 millimeter wavelengths.

In order to derive the sensitivity of our analysis to assumptions of atmospheric temperatures, we perturbed our model atmospheric temperature profiles and refit our spectra. These perturbations can be considered as uncertainties in the difference between atmospheric and lower boundary temperatures on Mars. In model F we added 10 K to atmospheric temperatures of model D. For model G we subtracted 10 K from the atmospheric temperatures of model D.

Model Results

For all of the above models we computed synthetic spectra that minimized the sum of the squared residuals of fitting against the measured spectra (abbreviated as $\sum r^2$). In each case we solved for both a constant and altitude varying profile of CO mixing ratio in the atmosphere of Mars. The results of our line fitting analysis are presented in Table II. $\sum r^2$ and total CO column density are given for the two CO profiles of each model. CO column densities were calculated from our derived CO mixing ratio profiles, using a base surface pressure of 6.5 mbar. From measurements of noise in the wings of our spectra, we found that fitting the spectra to the noise level should produce $\sum r^2$ of 470 and 870 for 1 and ½ megahertz resolution spectra, respectively. The results in Table II suggest that for all models (with the possible exception of model F) we adequately

Table II. Sum of the squared residuals of fitting ($\sum r^2$) to 1 MHz and ½ MHz resolution measured spectra. $\sum r^2$ and total CO column density are given for solutions of constant and altitude varying CO profiles for Models A-G.

	CO Mixing Ratio Constant in Altitude with Altitude			CO Mixing Ratio Variable		
Models	$\sum r^2$ (1 MHz spectrum)	$\sum r^2$ (½ MHz spectrum)	CO Column Density (molecules/cm^2)	$\sum r^2$ (1 MHz spectrum)	$\sum r^2$ (½ MHz spectrum)	CO Column Density (molecules/cm^2)
A	546	1059	5.0×10^{20}	482	896	3.4×10^{20}
B	526	1000	4.6×10^{20}	487	914	3.4×10^{20}
C	542	1053	4.3×10^{20}	476	913	3.3×10^{20}
D	544	1037	4.4×10^{20}	478	963	3.5×10^{20}
E	571	1137	5.8×10^{20}	487	945	4.4×10^{20}
			For Error Analysis Only			
F	668	1373	8.3×10^{20}	534	974	6.3×10^{20}
G	512	982	2.5×10^{20}	515	940	2.0×10^{20}

fitted our data, particularly when we used altitude varying profiles of CO. Profiles of constant CO mixing ratio generally gave 10% higher $\sum r^2$ for models A-E. The increased atmospheric temperatures of model F more strongly favored altitude varying over constant CO profiles. However, the lower atmospheric temperatures of model G allowed our spectra to be fitted equally well by both CO profiles.

Solutions with constant CO mixing ratios also produced CO column densities which were an average (models A-F) of 30% higher than those for solutions of altitude varying CO mixing ratios. Figure 4 presents both profiles of CO mixing ratios for each of our models. For models A-G the derived, altitude varying profiles have a similar shape, with CO mixing ratios falling off by a factor of 4-10 below 20 kilometers altitude. This fall-off accounts for the lower CO column densities of the altitude varying CO profiles. We again point out that our spectra are less sensitive to CO below 10 kilometers and, hence, do not adequately constrain this fall-off of CO mixing ratios below 20 kilometers. In Figures 1 and 2 we have drawn synthetic spectra (from model E) for constant (dotted spectra) and altitude varying (dashed spectra) CO profiles. One can see that the fit with constant CO mixing ratios is poorer although the difference between the two is slight, as suggested by comparison of $\sum r^2$. We feel that improvement of a factor of 2 in signal-to-noise ratios for the measured spectra is necessary before we can convincingly distinguish the altitude dependent profile of CO mixing ratios in the atmosphere of Mars.

For all our models, with the possible exception of model F, we found CO mixing ratios to fit the data equally well. The fits of models F and G indicate that our $J = 1 \rightarrow 2$ spectra do not adequately discriminate surface and atmospheric temperatures on Mars, and that analysis is very sensitive to these

Figure 4. Altitude profiles of CO mixing ratios in the Martian atmosphere derived from the microwave spectra of Figures 1 and 2. Mixing profiles of CO are found for models A-G for both constant CO mixing (dashed lines) and altitude-variable CO mixing (solid lines).

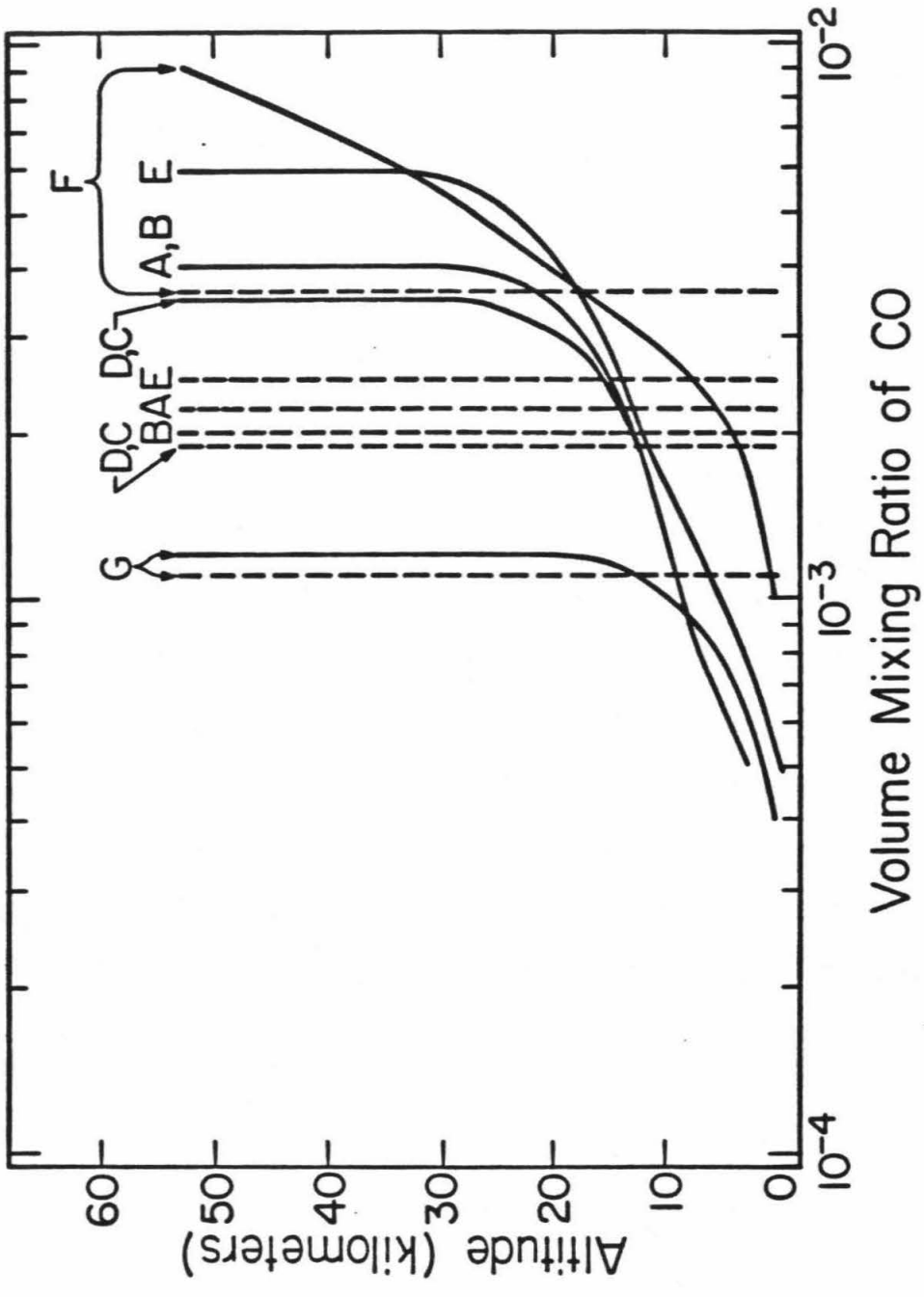
Altitude (kilometers)
0
10
20
30
40
50
60
10^{-4}
10^{-3}
10^{-2}
Volume Mixing Ratio of CO
F
A,B
E
D,C
D,C
BAE
G

parameters. From the analysis of models A-G we estimate the column density of CO on Mars to be $4.6 \pm 2.0 \times 10^{20}$ molecules/cm^2. This estimate is based on a constant mixing profile of CO as there is insufficient evidence to suggest an altitude varying CO mixing ratio. The large error bars are primarily due to the sensitivity of our measurement to model assumptions of atmospheric temperatures.

II. ANALYSIS OF THE 1980 $J = 0 \rightarrow 1$ SPECTRUM

We first point out that our own analysis of Good and Schloerb's 1980 spectrum produced a discordance with the original results of Good and Schloerb (1981). Our reanalysis suggested that they overestimated their CO mixing ratio by approximately a factor of 2 which, if correct, would considerably weaken evidence for CO variability on Mars. Good and Schloerb (P. Schloerb, personal communication, 1982) have since discovered a minor numerical error which produced a 30% overestimation of the CO mixing ratio on Mars. We arrive at an abundance of CO that is yet another 50% lower because we adopt different surface and atmospheric temperatures from those of Good and Schloerb. We present our reanalysis briefly in order to compare CO column abundances indicated by our spectrum, Good and Schloerb's spectrum and Kakar et al.'s 1975 spectrum, using a global model of surface and atmospheric temperatures that is self consistent among the observations.

Features of the $J = 0 - 1$ Transition

The $J = 0 \rightarrow 1$ spectrum of Good and Schloerb (Figure 5) is different from our $J = 1 \rightarrow 2$ in several important respects. At a given frequency, $J = 0 \rightarrow 1$ opacities are a factor of eight less than $J = 1 \rightarrow 2$ opacities. Consequently, at each frequency, the weighting function of the $J = 0 \rightarrow 1$ transition

Figure 5.

Rotational $J = 0 \rightarrow 1$ spectrum of CO in the Martian atmosphere (from Good and Schloerb, 1981) measured in March-April of 1980 with ±110 MHz bandwidth and 1 MHz resolution. Best fit synthetic spectra for the present reanalysis of the Good and Schloerb spectrum are drawn in for derived constant (dashed line, model 1) and altitude-variable CO mixing profiles (dotted line, model 2).

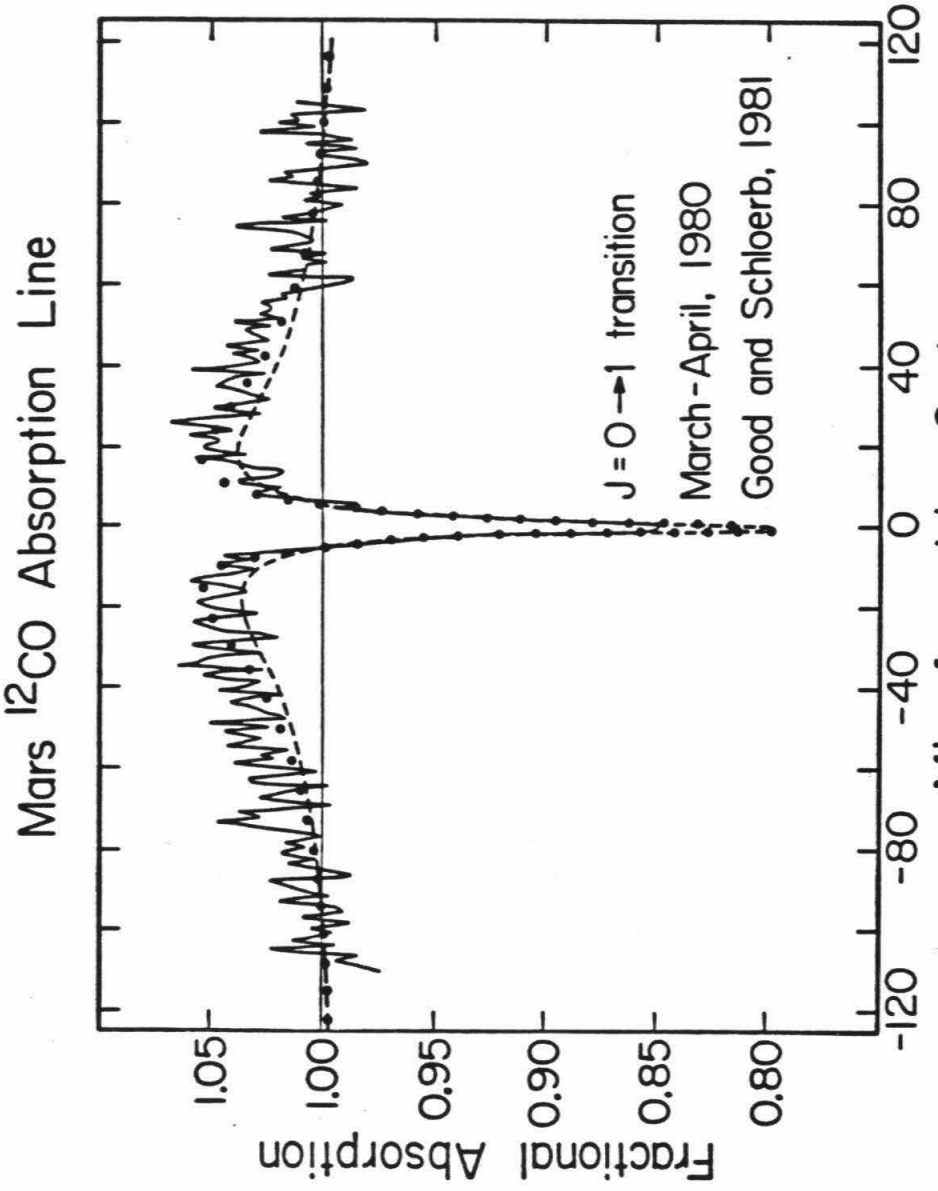
Mars ^{12}CO Absorption Line
Fractional Absorption
1.05
1.00
0.95
0.90
0.85
0.80
-120
-80
-40
0
40
80
120
Mhz from Line Center
J = 0 → 1 transition
March-April, 1980
Good and Schloerb, 1981

compared to the $J = 1 \rightarrow 2$ transition peaks about 20 kilometers lower in the atmosphere of Mars. With reasonable bandwidths (~ 200 megahertz) both transitions can be used to measure CO between 10 and 30 kilometers altitude in the Martian atmosphere. Given measurements of equal signal-to-noise ratios, the $J = 0 \rightarrow 1$ transition is more sensitive than the $J = 1 \rightarrow 2$ to CO below 10 kilometers altitude. However, $J = 1 \rightarrow 2$ spectra place constraints on CO mixing ratios up to altitudes of 50 kilometers compared to 30 kilometers for $J = 0 \rightarrow 1$ spectra.

The above relations are very dependent on the atmospheric and continuum brightness temperatures of Mars. If Martian atmospheric temperatures below 10 kilometers altitude are equal to the continuum brightness temperature of Mars, spectra of neither transition will be sensitive to CO below 10 kilometers altitude. If (as is generally the case) temperatures of the lower atmosphere are warmer than the continuum brightness temperature of Mars, the CO spectrum becomes a broad emission line with a central absorption peak. The cooler, low pressure atmospheric layers above 10 kilometers lead to reabsorption near the center of the spectral line. This central core of absorption extends much further in frequency from line center for the optically thick $J = 1 \rightarrow 2$ transition (50-100 megahertz) than for the $J = 0 \rightarrow 1$ transition (10 megahertz). Hence, the broad emission wings of the CO microwave spectrum are much more apparent with the lower opacities of the $J = 0 \rightarrow 1$ transition. This point is evident in the comparison of Figures 1 and 5.

Another factor which affects the strengths of the emission wings in particular is the variable continuum brightness temperature of Mars as observed from the Earth. At the time of Good and Schloerb's observation, the continuum brightness temperature of Mars was near a minimum. They observed the cool

morning hours of the northern hemisphere of Mars ($L_s \sim 90°$, pre-opposition). Assuming that observed atmospheric temperatures were not equally reduced, Good and Schloerb's observation measured the maximum contrast between surface and lower atmospheric temperatures on Mars. (As the latitudinal-diurnal variations of atmospheric temperatures above ~ 2 km are only ± 10 K compared to the large latitudinal-diurnal variations in surface temperatures (± 50 K), changes in disk average surface temperatures are much larger than corresponding changes in disk averaged atmospheric temperatures.) The spectrum of Good and Schloerb (Figure 5) may represent the maximum intensity of the emission wings for CO microwave spectra of Mars. One should see a gradual decrease (~ over 3 months) in the level of emission as Mars moves through opposition. Another interesting point to consider is the effect of atmospheric warming by global dust storms. If such storms produce an isothermal warming of the Martian atmosphere (Pollack et al., 1979), one should expect to measure nearly pure emission spectra of microwave CO transitions during global dust storms. Microwave CO observations should in fact be ideal for studying atmospheric temperatures of Mars during global dust storms. Of course, it is useful to determine the distribution of CO in the atmosphere of Mars beforehand.

Models and Results

We analyzed the Good and Schloerb spectrum using two models of lower boundary and atmospheric temperature conditions on Mars. We did not attempt to specify the topography of Mars for our $J = 0 \rightarrow 1$ analysis. However, we extended the lower boundary of our model atmosphere by 1 kilometer to approximate the effect of the generally lower regions of Mars observed during Good and Schloerb's observations (see Table I). The resulting 8% increase in atmospheric surface pressures did not affect our $J = 0 \rightarrow 1$ synthetic spectra

significantly. One further point regarding surface pressures is the seasonal variation of surface pressure due to condensation of CO_2 at the polar caps of Mars. We do not attempt to model this phenomenon primarily because the column abundance of CO should not be strongly affected by seasonal condensation of CO_2.

Models 1 and 2 of our $J = 0 \rightarrow 1$ analysis correspond roughly to models D and E of our $J = 1 \rightarrow 2$ analysis. We calculated the 2.6 mm continuum brightness temperature of Mars assuming a radio skin depth of zero (model 1) and 2.0 cm (model 2). For both cases we used our thermal models to specify surface and subsurface temperatures across the observed hemisphere of Mars. Treating Mars as a dielectric sphere ($\varepsilon = 2.5$), we arrived at whole disk brightness temperatures of 198.6 K (model 1) and 187 K (model 2). Atmospheric temperatures of models 1 and 2 followed the procedure of model C of our $J = 1 \rightarrow 2$ analysis. We note that peak atmospheric temperatures of Mars were offset from the center of the Mars hemisphere observed by Good and Schloerb. The morning sub-Earth point of Good and Schloerb's 1980 observation had the effect of decreasing average model continuum and atmospheric temperatures by about 10-15 K and 4 K, respectively, compared to our 1982 observation. Other variations in these model parameters which could not be estimated from the changing apparition of Mars must remain as uncertainties in the comparison of the 1980 and 1982 spectra.

Table III presents the results of our model fits to Good and Schloerb's 1980 spectrum. For model 2 we found constant and altitude varying CO mixing profiles (Figure 6) which fitted the spectrum equally well. The best fit of model 1 (assuming constant CO profile) did not adequately fit the spectrum (see Figure 5). The high continuum brightness temperatures of model 1 prevented

Table III. Sum of the squared residuals of fitting ($\sum r^2$) to the $J = 0 \rightarrow 1$ spectra of Kakar et al. (1977) and Good and Schloerb (1981). $\sum r^2$ and total CO column density are given for solutions of constant and altitude varying CO profiles for Models 1 and 2.

	CO Mixing Ratio Constant in Altitude		CO Mixing Ratio Variable in Altitude	
Models	$\sum r^2$	CO Column Density (molecules/cm^2)	$\sum r^2$	CO Column Density (molecules/cm^2)
Good and Schloerb (1981)				
1 (radio skin depth = 0)	583	1.8×10^{20}	—	—
2 (radio skin depth = 2.0 cm)	483	3.0×10^{20}	457	2.6×10^{20}
Kakar et al. (1977)				
1 (radio skin depth = 0)	112	1.1×10^{20}	—	—
2 (radio skin depth = 2.0 cm)	97	1.7×10^{20}	102	1.2×10^{20}

Figure 6. Altitude profiles of CO mixing ratios in the Martian atmosphere derived from the $J = 0 \rightarrow 1$ spectra of Good and Schloerb (Figure 5, labeled *GS*) and Kakar et al. (Figure 7, labeled *K*). Constant (dashed lines) and altitude-variable (solid lines) profiles are found for both spectra using two models for the 2.6 mm brightness temperatures of Mars (e.g. K1 versus K2).

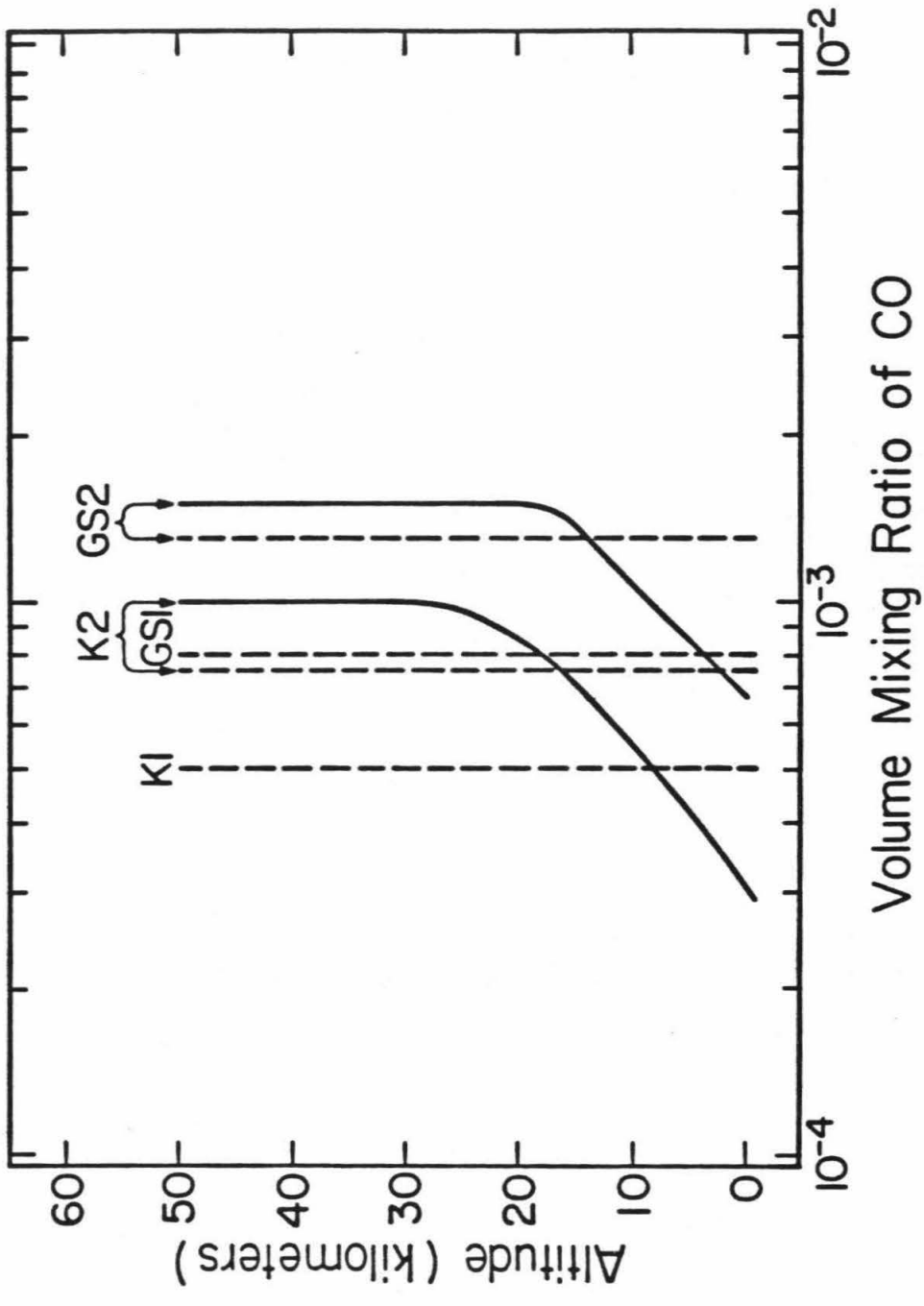
Altitude (kilometers)
0
10
20
30
40
50
60
10^{-4}
10^{-3}
10^{-2}
Volume Mixing Ratio of CO
K1
K2
GS1
GS2

sufficient emission in the wings of the synthetic spectrum. However, an increase in atmospheric temperatures of ~ 5 K would allow a fit of the data with model 1. We also note that all of our $J = 0 \rightarrow 1$ synthetic spectra are ~ 6 K too deep at line center, as shown by the model spectra in Figure 5. A better fit of the line center would require either an altitude decreasing CO mixing ratio or an increase of ~ 6 K in model atmospheric temperatures above ~ 25 km. The latter is much more plausible physically.

Rather than adopt separate models of atmospheric temperatures for analysis of the individual microwave spectra, we quote error bars for the effect of ± 10 K uncertainty in atmospheric temperatures on each of the microwave measurements. From the 1980 spectrum of Good and Schloerb, we found a best estimate of the CO column density on Mars (assuming a constant CO mixing ratio above the 6.5 mbar reference pressure) to be $3.0 \pm 1.0 \times 10^{20}$ molecules/cm^2.

III. ANALYSIS OF THE 1975 $J = 0 \rightarrow 1$ SPECTRUM

The Kakar et al. $J = 0 \rightarrow 1$ spectrum (Figure 7) differs in two important aspects from the Good and Schloerb $J = 0 \rightarrow 1$ spectrum. As pointed out by Good and Schloerb (1981), the limited bandwidth of the Kakar et al. spectrum prevented detection of the broad emission wings of the CO $J = 0 \rightarrow 1$ transition on Mars. Hence, the Kakar et al. spectrum is less sensitive than the Good and Schloerb spectrum to CO in the lower 10 kilometers of the Martian atmosphere. Secondly, the sub-Earth point for Kakar et al.'s observation fell in mid-afternoon hours and equatorial latitudes on Mars (Table I). Our thermal models indicated 20 K higher continuum brightness temperatures for Mars at the time of the Kakar et al. observation compared to the Good and Schloerb observation. Any

Figure 7. Rotational $J = 0 \rightarrow 1$ spectrum of CO in the Martian atmosphere (from Kakar et al., 1977) measured in November of 1975 with ± 32 MHz bandwidth and a maximum resolution (near line center) of ½ MHz. The best fit synthetic spectrum (dashed line) is for model 1 with a constant CO mixing ratio in the Martian atmosphere.

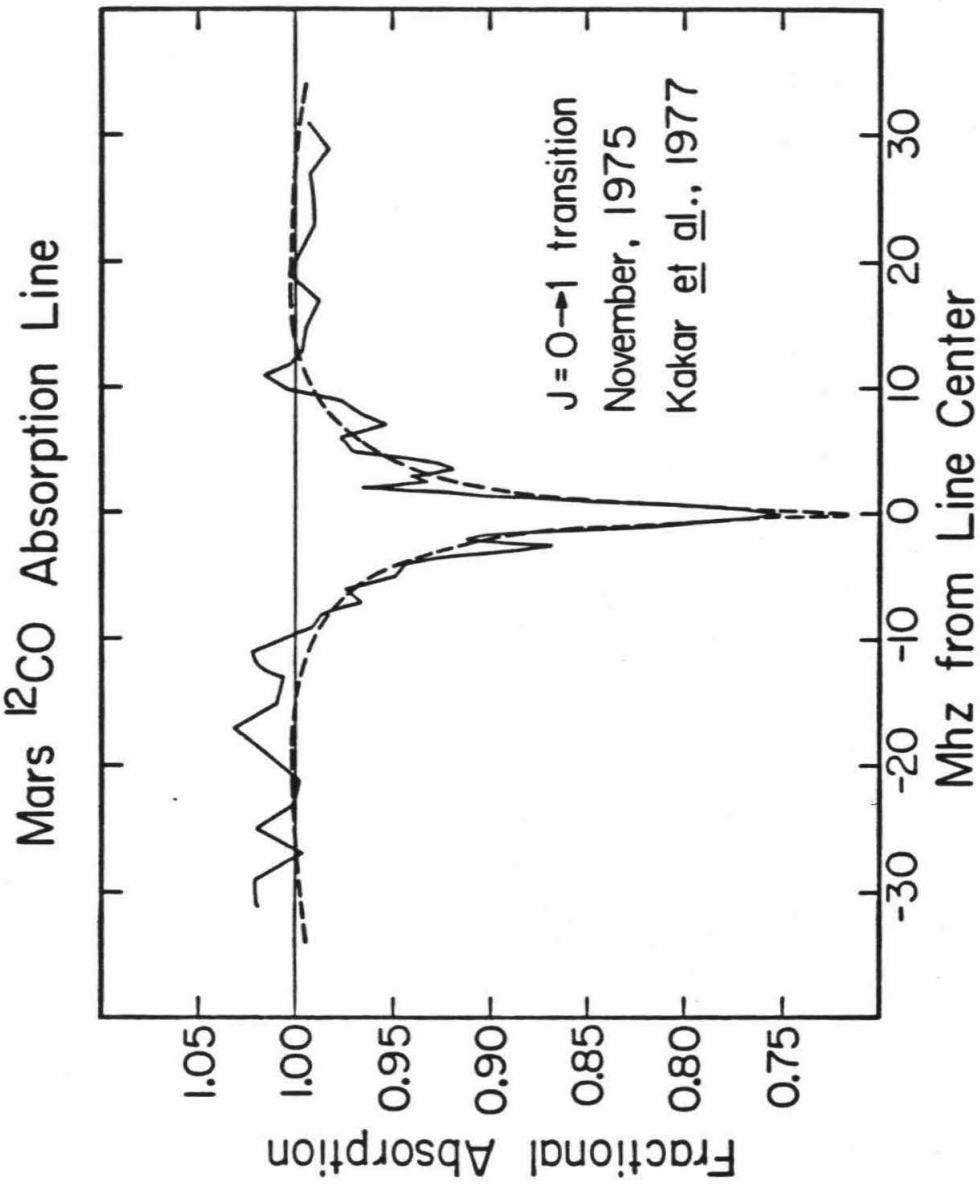
Mars ^{12}CO Absorption Line
J = 0→1 transition
November, 1975
Kakar et al., 1977
Fractional Absorption
1.05
1.00
0.95
0.90
0.85
0.80
0.75
-30
-20
-10
0
10
20
30
Mhz from Line Center

emission in the Kakar et al. spectrum would be correspondingly weaker.

Models and Results

Our analysis of Kakar et al.'s spectrum followed closely our analysis of Good and Schloerb's spectrum. Due to the similar Martian longitudes observed by both measurements (Table I), we retained the increased surface pressures used in the analysis of the Good and Schloerb spectrum. Our thermal models determined continuum brightness temperatures of 218.5 K for zero radio skin depth (model 1) and 205.7 K for a radio skin depth of 2.0 cm (model 2). The sub-Earth point on Mars during Kakar et al.'s observation coincided with peak atmospheric temperatures on Mars (as it did for our $J = 1 \rightarrow 2$ observation). Based on our model of diurnal-latitudinal variation of atmospheric temperatures on Mars, we found that average atmospheric temperatures sampled by Kakar et al.'s observations were ~ 5 K warmer than those sampled by Good and Schloerb's observation.

Table III includes the results of our model fits to the Kakar et al. spectrum (also Figure 7). As with the spectra of Figures 1 and 5, we could not distinguish constant and altitude varying profiles of CO mixing ratios. The $\sum r^2$ seem to indicate a slight preference for the lower continuum brightness temperatures of model 2 (or, alternatively, a warmer model atmosphere). Profiles of CO mixing ratios derived from the Kakar et al. spectrum are presented in Figure 6.

Allowing an uncertainty of ± 10 K in model atmospheric temperatures, we determined a CO column density of $1.7 \pm 0.9 \times 10^{20}$ molecules/cm^2 (above 6.5 mbar) from analysis of the 1975 Kakar et al. spectrum. This result is consistent with the value of $\sim 2.2 \times 10^{20}$ molecules/cm^2 for a Martian continuum temperature of 207.5 K, as indicated in the original analysis of Kakar et al.

(1977).

DISCUSSION

A summary of our microwave analysis is presented in Table IV. Here we compare CO column densities in the Martian atmosphere (assuming an altitude constant CO mixing ratio) as derived from the CO microwave spectra of 1975, 1980, and 1982. If we allow for an altitude varying CO mixing ratio, the derived values of CO column density are roughly 30% lower than those of Table IV. We again note the correction for CO abundance from Good and Schloerb's 1980 spectrum. A value from the 1967 infrared observation of Connes et al. (1969) as most recently interpreted by Young and Young (1977) is also included.

The large error bars listed in Table IV are the effect of uncertainty in the difference between continuum and atmospheric temperatures on Mars. We believe that we have specified relative continuum temperatures among the microwave observations to a precision of 5 K. However, while we may adequately model the variation of the continuum temperature of Mars as seen from the Earth, we cannot estimate temporal variation of global atmospheric temperatures on Mars. We used a single model of global atmospheric temperatures, based on Viking measurements in 1976, to fit all three of the microwave spectra; taken in 1975, 1980, and 1982. In order to estimate the sensitivity of the CO microwave measurements to possible variations of global atmospheric temperatures, we perturbed the average level of our global model of atmospheric temperatures $\pm$ 10 K and refit each of the microwave spectra. The large error bars of Table IV are primarily a result of the sensitivity of the CO microwave spectra to these $\pm$ 10 K perturbations. This sensitivity makes comparison of the infrared and microwave observations very difficult. CO column densities derived

Table IV. Summary of CO column abundances from our reanalyses of 1975, 1980 microwave spectra and analysis of our 1982 spectrum. These column densities assume an altitude-constant CO mixing ratio. CO column densities derived for altitude increasing CO mixing profiles are roughly 30% lower in value. Also included is the reanalysis by Young and Young (1977) of the 1969 infrared spectrum from Connes et al. (1969).

Measured Spectrum	CO Column Density above 6.5 mbar Pressure Level (molecules/cm^2)
Connes et al. (1969) as reanalyzed by Young and Young (1977) (measured in 1967)	$2.0 \pm 0.8 \times 10^{20}$
Kakar et al. (1977) (measured in 1975)	$1.7 \pm 0.9 \times 10^{20}$
Good and Schloerb (1981) (measured in 1980)	$3.0 \pm 1.0 \times 10^{20}$
This work (measured in 1982)	$4.6 \pm 2 \times 10^{20}$

from infrared spectra are far less sensitive to assumptions of atmospheric temperatures.

Assuming that global atmospheric temperatures did not change significantly (i.e., less than 5 K) among the microwave observations, Table IV would indicate a significant increase of CO in the atmosphere of Mars between 1975 and 1982. On the other hand, the apparent increase may be explained by ± 10 K variations in global average atmospheric temperatures on Mars. The 1975 observation of Kakar et al. was taken during winter of the northern hemisphere of Mars, a time when considerable dust is usually suspended in the atmosphere of Mars (Pollack et al., 1979). In contrast, the 1980 and 1982 observations were taken during the typically minimum dust conditions of late spring in the northern hemisphere of Mars. Radiative models indicate that the dust observed in the atmosphere of Mars can lead to considerable warming of the atmosphere. Atmospheric temperatures may vary by as much as 40 K between minimum and maximum dust conditions in the atmosphere of Mars (Pollack et al., 1979). Global insolation on Mars is also ~ 40% increased during winter relative to summer season in the northern hemisphere of Mars due to the ellipticity of the orbit of Mars. Both factors would indicate warmer atmospheric temperatures for the 1975 compared to the 1980, 1982 observations. Hence, the most appropriate comparison of CO column densities in Table IV may be between the upper limit for the 1975 observation and the lower limits of the 1980, 1982 observations.

The apparent 50% increase in CO column densities between the 1980 and 1982 observations may indicate a real change of CO abundance in the atmosphere of Mars. The two measurements were both taken during late spring in the northern hemisphere of Mars when atmospheric dust is at a minimum. One

might expect global atmospheric temperatures to be nearly identical for these two measurements. Yet we find that global atmospheric temperatures are required to be 10 K warmer for the 1980 observation relative to the 1982 observation in order to fit both spectra with the same CO abundance on Mars. Alternatively, we require a 10 K greater contrast in continuum temperatures between the two observations in order to fit both with a single profile of CO mixing ratios. It is hard to estimate the likelihood of either of these possibilities although we feel it would be difficult to increase the contrast of model continuum temperatures for the two observations. By assuming finite radio skin depths we have probably calculated the maximum contrast in continuum brightness temperatures between the 1980 and 1982 observations. Still, the sensitivity of the calculations for CO column abundance to model temperatures makes unambiguous comparison of the 1980, 1982 observations very difficult. As variability of global atmospheric temperatures on Mars is no less plausible than variability of CO abundance, we cannot conclude that CO abundance is indeed variable on Mars.

In summary we do not find sufficient evidence for temporal variability of CO abundance in the Martian atmosphere. Due to uncertainties in temporal variations of global average atmospheric temperatures, the data allow a range of CO variability from 0-100%. If the Martian CO abundance is indeed variable, we may still face the contradiction of CO variability without corresponding variations in O_2. Present theory indicates that any variation of O_2 is likely to be about one half the variation of CO and in phase with variations of CO abundance (e.g. McElroy and Donahue, 1972). Column abundances of O_2 and CO are roughly equal and the production of O_2 requires the photodissociation of two CO_2 molecules. However, we note that measurements of CO column abundance on Mars have now been made in 1967, 1975, 1980, and 1982; in comparison to

measurements of O_2 column abundance taken in 1972 and 1982. Taking into consideration the $\gtrsim 1$ year timescale for large variation (factors of two or more) of O_2 and CO suggested by Hunten (1974), the abundances of O_2 and CO may be inadequately sampled in time to observe correlated variations, particularly given the measurement uncertainties. Thus, at present, substantial correlated year-to-year variation of CO and O_2 cannot be entirely ruled out.

A best estimate of the average CO column abundance on Mars from analysis of available microwave spectra is $2–5 \times 10^{20}$ molecules/cm^2. The sensitivity of our analysis to atmospheric temperatures on Mars suggests that individual microwave spectra of CO are not the best tool for measuring variations of CO abundance on Mars. However, simultaneous measurement of the $J = 0 \rightarrow 1$ and $J = 1 \rightarrow 2$ transitions could provide much stronger constraints on both CO abundance and atmospheric temperatures of Mars. Such measurements could also determine the altitude distribution of CO in the atmosphere of Mars, as the two transitions are sensitive to CO and atmospheric temperatures at different altitudes in the atmosphere of Mars.

CO microwave spectra of Mars should be most useful in measuring changes of atmospheric temperatures during global dust storms on Mars. In this case, the sensitivity of the spectra to atmospheric temperatures is an advantage. The time constant for changes in global atmospheric temperatures (months) is relatively short compared to the time constant of possible CO variability ($\gtrsim 1$ year; Hunten, 1974) on Mars.

REFERENCES

Andrew, B.H., G.A. Harvey, and F.H. Briggs, Rotational variations in the radio brightness of Mars, *Ap. J. (Letters)* **213**, L131-L134, 1977.

Barker, E.S., Detection of molecular oxygen in the Martian atmosphere, *Nature (Letters)* **238**, 447-448, 1972.

Carlton, N.P. and W.A. Traub, Detection of molecular oxygen on Mars, *Science* **177**, 988-992, 1972.

Christensen, P.R., Martian dust mantling and surface composition: Interpretation of thermophysical properties, *J. Geophys. Res.*, in press, 1982.

Connes, P., J. Connes, L.D. Kaplan, and W.S. Benedict, Carbon monoxide in the Venus atmosphere, *Ap. J.* **152**, 731-743, 1968.

Connes, J., P. Connes, and J.P. Maillard, *Atlas de spectres infrarouges de Venus, Mars, Jupiter et Saturne* (Paris, France: Editions due Centre National de la Recherche Scientifique), 1969.

Cuzzi, J.N. and D.O. Muhleman, The microwave spectrum and nature of the subsurface of Mars, *Icarus* **17**, 548-560, 1972.

Doherty, L.H., B.H. Andrew, and F.H. Briggs, Confirmation of the longitudinal dependence of the radio brightness of Mars, *Ap. J. (Letters)* **233**, L165-L168, 1979.

Donahue, T.M., The upper atmosphere of Venus: A review, *J. Atmos. Sci.* **25**, 568-, 1968.

Epstein, E.E., M.M. Dworetsky, J.W. Montgomery, and W.G. Fogarty, Mars, Jupiter, and Uranus: 3.3-mm brightness temperatures and a search for variations with time or phase, *Icarus* **13**, 276-281, 1970.

Good, J.C. and F.P. Schloerb, Martian CO abundance from the $J = 0 \rightarrow 1$, rotational transition: Evidence for temporal variations, *Icarus* **47**, 166-172, 1981.

Hess, S.L., R.M. Henry, C.B. Leovy, J.A. Ryan, and J.E. Tillman, Meteorological results from the surface of Mars: Viking 1 and 2, *J. Geophys. Res*, **82**, 4559-4574, 1977.

Hunten, D.M., Aeronomy of the lower atmosphere of Mars, *Rev. of Geophys. and Space Phys.* **12**, 529-535, 1974.

Jakosky, B.M. and D.O. Muhleman, The longitudinal variation of the thermal inertia and of the 2.8 centimeter brightness temperature of Mars, *Ap. J.* **239**, 403-409, 1980.

Jakosky, B.M. and D.O. Muhleman, A comparison of the thermal and radar characteristics of Mars, *Icarus* **45**, 25-38, 1981.

Kakar, R.K., J.W. Waters, and W.J. Wilson, Mars: Microwave detection of carbon monoxide, *Science* **196**, 1090-1091, 1977.

Kaplan, L.D., J. Connes, and P. Connes, Carbon monoxide in the Martian atmosphere, *Ap. J. (Letters)* **157**, L187-L192, 1969.

Kieffer, H.H., T.Z. Martin, A.R. Peterfreund, B.M. Jakosky, E.D. Miner, and F.D. Palluconi, Thermal and albedo mapping of Mars during Viking primary mission, *J. Geophys. Res.* **82**, 4249-4291, 1977.

Kieffer, H.H., Soil and surface temperatures at the Viking Lander sites, *Science* **194**, 1344-1346, 1976.

Kolbe, W.F., H. Buscher, and B. Leskovar, Microwave absorption coefficients of atmospheric pollutants and constituents, *J. Quant. Radiat. Transf.* **18**,

47-64, 1977.

Krasnopolsky, V.A. and V.A. Parshev, Chemical composition of the atmosphere of Venus, *Nature* **292**, 610, 1981.

Martin, T.Z. and H.H. Kieffer, Thermal infrared properties of the Martian atmosphere, 2, the 15 μm band measurements, *J. Geophys. Res.* **84**, 2843-2852, 1979.

Martin, T.Z., A.R. Peterfreund, E.D. Miner, H.H. Kieffer, and G.E. Hunt, Thermal infrared properties of the Martian atmosphere, 1, global behavior at 7, 9, 11 and 20 μm, *J. Geophys. Res.* **84**, 2830-2842, 1979.

McElroy, M.B. and D.M. Hunten, Photochemistry of CO_2 in the atmosphere of Mars, *J. Geophys. Res.* **75**, 1188-1201, 1970.

McElroy, M.B. and J.C. McConnell, Dissociation of CO_2 in the Martian atmosphere, *J. Atmos. Sci.* **28**, 879-884, 1971.

McElroy, M.B. and T.M. Donahue, Stability of the Martian atmosphere, *Science* **177**, 986-988, 1972.

Muhleman, D.O., Microwave emission from the Moon, in *Thermal Characteristics of the Moon* (J.W. Lucas, Ed.), MIT Press, 51-81, 1972.

Palluconi, F.D. and H.H. Kieffer, Thermal inertia mapping of Mars from 60°S to 60°N, *Icarus* **45**, 415-426, 1972.

Parkinson, T.D., and D.M. Martin, Spectroscopy and aeronomy of O_2 on Mars, *J. Atmos. Sci.* **29**, 1380-1390, 1972.

Piddington, J.H., and H.C Minnert, Microwave thermal radiation from the Moon, *Australian J. of Sci. Res. Series A2* **63**, 1949.

Pollack, J.B., D.S. Colburn, F.M. Flasar, R. Kahn, C.E. Carlston, and D. Pidek, Properties and effects of dust particles suspended in the Martian atmosphere. *J. Geophys. Res.* **84**, 2729-2945, 1979.

Pollack, J.B., C.B. Leovy, P.W. Greiman, and Y. Mintz, A Martian general circulation experiment with large topography, *J. Atmos. Sci.* **38**, 3-29, 1981.

Prinn, R.G., Photochemistry of HCl and other minor constituents in the atmosphere of Venus, *J. Atmos. Sci.* **28**, 1058-1068, 1971.

Seiff, A. and D.B. Kirk, Structure of the atmosphere of Mars in summer at mid-latitudes, *J. Geophys. Res.* **82**, 4364-4378, 1977.

Trauger, J., and J. Lunine, in preparation, 1982.

Varanasi, P., Measurement of line widths of CO of planetary interest at low temperatures, *J. Quant. Spectrosc. Radiat. Transfer* **15**, 191-196, 1975.

Waters, J.W., Absorption and emission of atmospheric gases, in *Methods of Experimental Physics*, vol. 12, *Astrophysics*, Part B, *Radio Telescopes*, edited by M.L. Meeks, Academic, New York, 142-176, 1976.

Young, L.D.G., Interpretation of high resolution spectra of Mars. III. Calculations of CO abundance and rotational temperature, *J. Quant. Spectrosc. Radiat. Transfer* **11**, 385-390, 1971.

Young, L.D.G. and A.T. Young, Interpretation of high-resolution spectra of Mars. IV. New calculations of the CO abundance, *Icarus* **30**, 75-79, 1977.

Yung, Y.L., and W.B. DeMore, Photochemistry of the stratosphere of Venus: Implications for atmospheric evolution, *Icarus* **51**, 199-247, 1982.

PART IV

Microwave Spectra of Terrestrial Mesospheric CO

R. Todd Clancy, Duane O. Muhleman and Glenn L. Berge

(Published in Journal of Geophysical Research)

Introduction

In this paper we present measurements and interpretation of terrestrial carbon monoxide microwave absorption spectra taken in early December for the consecutive years 1979 and 1980 and in late January 1982. The spectra are primarily sensitive to the total CO column density in the earth's mesosphere above ~65 km but also provide limited information on the mixing profile of CO between 65 and 75 km altitude. We provide analysis of the spectra and a comparison with previously reported mesospheric CO microwave spectra in order to constrain possible yearly and/or seasonal variations of mesospheric CO.

The physical processes governing the vertical distribution of CO in the earth's mesosphere are photodissociation of CO_2 (at altitudes $\gtrsim 55$ km, Allen et al., 1981; Waters et al., 1976) balanced by chemical recombination (via $CO + OH \rightarrow CO_2 + H$) and vertical eddy diffusion of CO. This is in contrast to CO abundance in the troposphere which is believed to be controlled by oxidation of biologically produced methane (Wofsy et al., 1972). The mesosphere and troposphere are separated by the 20-60 km altitude region which is characterized by very low CO mixing ratios ($\lesssim 10^{-8}$) due to rapid recombination of CO and slow vertical eddy diffusion (Wofsy et al., 1972).

Individual microwave spectra of mesospheric CO can be used to place constraints on both recombination rates for CO and eddy diffusion rates in the altitude range of roughly 60-80 km (e.g., Allen et al., 1981). For this purpose we feel our January 1982 emission spectrum may provide the best constrained mesospheric mixing profile of CO reported to date. We are further interested in possible temporal variations of CO abundance in the earth's mesosphere. Due to the limited signal-to-noise for our December observations we cannot provide an

accurate comparison of mixing profiles but we can provide a useful comparison of spectral line areas (and hence CO column density above ~ 65 km) including a comparison with other reported spectra.

Although there are no reported seasonal variations of chemical constituents in the earth's mesosphere (other than ozone which is influenced by the seasonal dependence of solar insolation, M. Allen, personal communication, 1982), there are observations of seasonal variations for O (Mauersberger et al., 1976; Mayr et al., 1976; Hedin et al., 1977), O_2 (Roble and Norton, 1972; Noxon and Johanson, 1972; Alcayde et al., 1974; Scialom, 1974), and N_2 (Offerman, 1974; Waldteufel, 1970; Alcayde et al., 1974) in the terrestrial thermosphere. The seasonal variation of these constituents may be explained by global circulation between the northern and southern hemispheres (Kasting and Roble, 1981). Furthermore, stratospheric ozone exhibits seasonal and latitudinal varibility (Newell, 1963; Dutsch, 1971) which is well modeled by global circulation (Cunnold et al., 1974). We intend to show strong seasonal variability of mesospheric CO for northern midlatitudes. All of the microwave spectra we include in this comparison were taken between 30° and 40° north latitudes.

Observational Method

All three of the observations are of mesospheric CO in absorption against the Moon. We also measured a mesospheric emission spectrum of CO in January 1982. The 1979 spectrum is due to the $J = 1 \rightarrow 2$ rotational transition (230 GHz) and employed the Bell Telephone Laboratories hot electron bolometer receiver (Phillips and Jefferts, 1973) mounted at the Cassegrain focus. The 1980 spectrum measured the $J = 0 \rightarrow 1$ transition (115 GHz) a factor of eight weaker than the $J = 1 \rightarrow 2$ transition) using an SIS receiver (Phillips et al., 1981) mounted off axis of the telescope. Both the 1979 and 1980 observations were taken with the

10.4 meter, millimeter wavelength telescope at the Owens Valley Radio Observatory. The January 1982 observations were of the $J = 1 \rightarrow 2$ transition both in emission and in absorption against the Moon. These spectra were taken with the millimeter NRAO telescope at the Kitt Peak Observatory using the NRAO 200-240 GHz mixer-receiver.

The spectrographic methods of the three systems are also distinctly different. The bolometer receiver is essentially a single channel device; the local oscillator was stepped across the desired bandwidth (10 MHz) with steps or channels corresponding to the spectral resolution (195 KHz). The SIS receiver was employed with an acousto-optical spectrometer (AOS) backend (Masson, in preparation). The total bandwidth was fixed at 100 MHz with a spectral resolution of 200 KHz. For the 1982 Kitt Peak observations we used two parallel sets of NRAO filter banks with resolutions of 250 and 100 KHz and respective total bandwidths of 64 and 25.6 MHz. The Doppler widths of the $J = 0 \rightarrow 1$ and $J = 1 \rightarrow 2$ lines are $\sim$ 100 KHz and $\sim$ 200 KHz, respectively.

For the purposes of intercomparison among the spectra absorption rather than emission measurements were chosen, primarily because the absorption technique is self-calibrating. On-and off-source (Moon) spectra, taken with 30 second integration intervals, were differenced. The difference spectra were divided by the power level far in the wings of the on-source spectra, after which linear baselines were fit to these normalized spectra. With the condition that the vertical opacity in the line, $\tau_{CO} << 1$, one is left with spectra of $\frac{\tau_{CO}}{\mu}$ (μ = cos (zenith angle)) which may be averaged with the proper correction for zenith angle. One further correction regarding the double sideband image was necessary for the 1980 and 1982 spectra. The spectra were scaled by the factor

$\left[1 + \frac{G^-}{G^+} e^{(\tau^+ - \tau^-)/\mu}\right]$ where $G^+(G^-)$ and $\tau^+(\tau^-)$ are the gain and atmospheric opacity for the upper (lower) sideband (see Appendix I). If the gains and opacities for the two sidebands are equal, the factor is simply 2. The gains were in fact tuned to be equal during operation of the receiver. For the J = 0 → 1 1980 spectrum the lower sideband was at a frequency of 112.4 GHz on the sky. We adopted a difference in opacity for the two sidebands of $\tau^+ - \tau^- = 0.18$ based on theoretical zenith opacities due to the 118 GHz O_2 line (Rosenkranz, 1975; Waters, 1976). The correction factor is, in fact, not very sensitive to these assumptions. In the extreme case $\tau^+ - \tau^- = \tau^+ (\tau^+ < 0.3$ for our observations), our calibration will be in error by 10% on the low side. The December 1979 J = 1 → 2 observation did not require a double sideband correction as the IF of the hot electron bolometer receiver is essentially zero. For the 1982 J = 1 → 2 spectra we use a sideband correction factor of 2. At 230 GHz atmospheric opacity remains constant over the separation between the two sidebands. Receiver gain for the two sidebands was balanced to within 5-10% (R. Howard, personal communication, 1982).

At this point, we would like to reemphasize the value of absorption measurements. The main advantage of such observations is that, with proper handling of the sidebands, the spectra are completely self-calibrating. No assumptions of antenna efficiency, ground spillover, or atmospheric extinction are necessary. One simply requires the continuum and atmospheric line absorption for a background source. The Moon is a particularly good background source due to its large angular extent and relatively moderate brightness temperature.

For our on-source spectra the antenna beam was placed on the center of the illuminated portion of the Moon. In all cases, the beam was much smaller

than the Moon's disk. All of the observations were taken at half moon, the 1979 spectra at past full moon and the 1980, 1982 spectra at past new moon (i.e., morning *vs.* evening moon). The off-source positions were offset 30 arcminutes in azimuth from the center of the Moon.

The emission spectrum taken during the January 1982 observations was calibrated with the standard emission method as outlined by Ulich and Haas (1976). Receiver signal levels are measured while pointing at the sky and a hot load. Given assumptions for antenna efficiency and atmospheric temperature, one may solve for atmospheric opacity and an absolute scale for receiver signal level versus antenna temperature. Equal sideband gains and atmospheric opacities are assumed in the calibration. The resulting units for the emission spectra are degrees Kelvin, which may be converted to spectral line opacities through division by an average atmospheric temperature for the line emitting region of the mesosphere.

We observed the emission spectrum of mesospheric CO in part because we wished to compare line opacities derived from the emission technique to line opacities found from the self-calibrating absorption measurement. We found that the two methods produced comparable results to within ~20% from our January 1982 observations. We also found emission spectra to have one important advantage over absorption spectra. The ~300 K continuum level of the background source (the Moon) introduced standing waves in the spectra which effectively increased the noise temperature for the absorption measurement (the standing waves showed a multiplicity of periods and did not generally remain coherent across the bandpass). For observations with the NRAO filter banks at Kitt Peak an additional source of system noise is introduced in absorption measurements. The strong continuum level of the Moon produced a

significant mismatch in the power levels between the off and on scans. This imbalance introduced additional noise in the spectra due to nonlinear behavior of the filter bank detectors (R. Howard, personal communication, 1981). We partially offset this problem in our January 1982 absorption measurement by using a gain modulator to reduce the signal level in the on-spectra to the signal level in the off-spectra. This effectively removed the continuum level of the spectra (called BL), which had to be measured separately without the gain modulator.

An important consequence of the additional noise sources for absorption spectra is that much cleaner spectra may be obtained by the emission technique for equal integration times. Hence our January 1982 emission spectrum contains by far the best signal-to-noise ratios of any of our spectra (and any mesospheric CO spectrum so far published). Although its calibration is poorer than the absorption spectra, this emission spectrum constrains the altitude distribution of CO in the mesosphere better than our absorption spectra.

For the purposes of convenience, description of the 1979, 1980, and 1982 spectra are presented separately. Despite differences in observational methods, the three data sets allow fairly straightforward comparison which is reserved for the discussion section.

December 1979 Observations

The 1979 spectra were obtained on December 12, following the Moon from a zenith angle of 54° (3:45 am) to a minimum of 35° (6:45 am) and back to a maximum of 67° (11:00 am). There is an unfortunate gap in data between 7:00 am and 9:00 am during which other observations were conducted. The most immediate purpose of observation was twofold: to determine the vertical profile of CO mixing ratios in the Earth's mesosphere, and to constrain a possible day-

night variation in the CO abundance. On the basis of estimated CO lifetimes such a variation should not be discernible (Allen, Yung, and Waters; 1981).

The spectral resolution of the $J = 1 \rightarrow 2$ measurement, 195 KHz, was comparable to the doppler half power width of CO at 200 K (220 KHz). The width of the mesospheric CO line is not much larger than this doppler halfwidth as was known from a previous measurement of the $J = 1 \rightarrow 2$ transition (Goldsmith *et al.*, 1979) and several measurements of the $J = 0 \rightarrow 1$ transition (Waters et al., 1976; Goldsmith *et al.*, 1979).

The total, day-night average spectrum is presented in Figure 1. As no physical effects are expected to create a significant asymmetry in the spectrum, it was folded about the center channel. The $\pm 1\sigma$ error bars are shown in the figure; the larger error bars about the center channel reflect the differential effect of folding on noise for the center channel.

The area under the curve in Figure 1 can be calculated to give the total column density of CO in the mesosphere (since $\tau_{CO} << 1$) above approximately 65 km.

$$\text{(Dec. 12, 1979)} \qquad \int_{\sim 65\text{km}}^{\infty} N_{CO} dz = 0.90 \pm 0.07 \times 10^{16}\ \text{cm}^{-2}$$

The quoted error is formal, derived from noise fluctuations in the baseline of the spectrum. There were no significant errors associated with handling of the spectrum, which was self-calibrating. All previously published column densities have larger uncertainties, due mainly to the requirement of uncertain calibrations. The column density calculation does depend on the true temperature of the absorbing region. The above result assumes a linear temperature gradient of 210 to 200° K, which approximates the temperatures of the main line

Figure 1. Total folded spectrum of the $J = 1 \rightarrow 2$ transition of mesospheric CO in absorption against the Moon taken on December 12, 1979. Total bandwidth was 10 MHz, channel width was 195 KHz. Error bars are calculated from noise in the wings of the line. τ_0 is the normal optical depth, ν_0 is the center line frequency of 230.538 GHz.

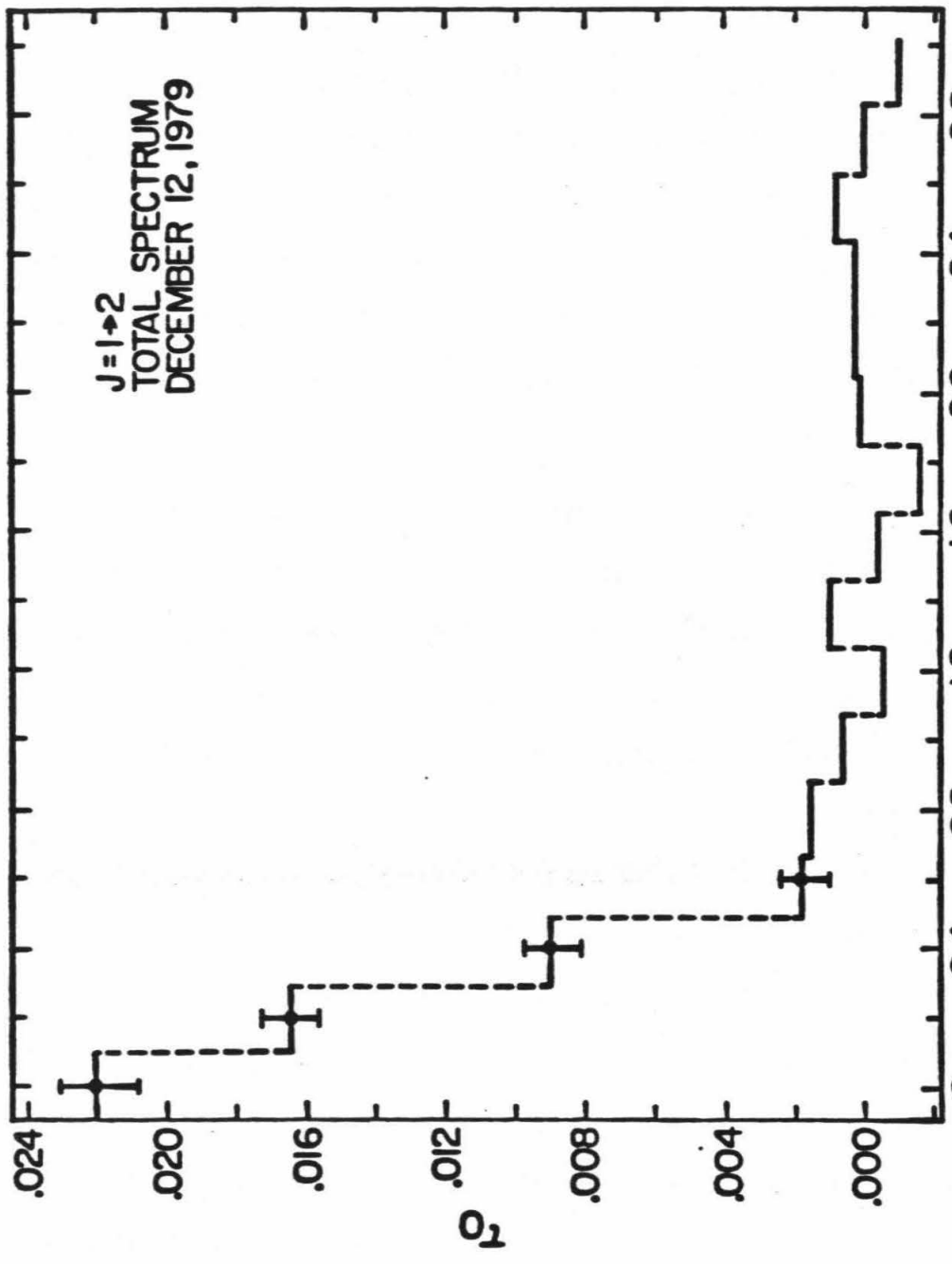
J=1→2
TOTAL SPECTRUM
DECEMBER 12, 1979
τ_0
.024
.020
.016
.012
.008
.004
.000
0
0.4
0.8
1.2
1.6
2.0
2.4
2.8
$\nu-\nu_0$ (Mhz)

forming region (65-90 km). A +10 K temperature error throughout the line forming region results in $\sim +0.1 \times 10^{16}$ cm^{-2} column density bias. The choice of the lower boundary of 65 km is somewhat arbitrary due to the finite bandwidth and due to the baseline fitting procedure, which removes signal beyond 3 MHz from line center. In the line forming process all altitudes contribute in some degree to the signal at all frequencies. Cutting off the signal to within a particular frequency interval does not correspond to a distinct altitude range of observation. For the case of the Earth's mesosphere, the total column density of CO proves to be fairly insensitive to the lower boundary because CO number density falls rapidly in the altitude range 50-65 km (as evidenced by the narrowness of the line).

Due to altitude dependent pressure broadening of the line, the CO absorption spectrum of Figure 1 also contains information on the vertical distribution of CO in the mesosphere. In principle, one can invert the spectrum of optical depth to obtain the vertical mixing profile of the absorber in the atmosphere. Such a procedure works quite well for ozone in the stratosphere and mesosphere (Penfield *et al.*, 1976; Shimabukuro et al., 1977). However, one is ultimately limited by signal-to-noise ratio. For the spectrum of Figure 1, signal level falls below noise level in the region of 800 KHz from line center (400 KHz for the 1980 data). As a consequence, only upper bounds for CO mixing ratios can be placed for altitudes below ~65 km. Above 65 km (69 km) the 230 (115) GHz Doppler halfwidth is equal to or greater than the pressure broadening halfwidth and, as a result, inversion for mixing ratios above 65 km is very nonunique. Doppler broadening is a function of temperature which does not exhibit the large vertical gradient of pressure. Nevertheless, there is limited vertical information available from the data due to pressure broadening in the region of

65-75 km.

The spectrum of Figure 1 has been inverted for CO mixing profiles using several different methods of parameterization. The most straightforward solution is a linearization of signal, τ_i, in terms of constant CO volume mixing ratios, ξ_n, for n layers contributing to the opacity τ_i at frequency ν_i.

$$\tau_i = \sum_n P_{in}\, \xi_n \tag{1}$$

where the P_{in} are functions of the pressure and temperature in the n^{th} layer. This requires $\tau_i << 1$ for all i and careful integration of P_{in} over pressure within each layer for adequate accuracy of the line shape function, i.e., the Voigt shape. The P_{in}'s are constructed from atmospheric parameters of the December 40° N Cospar (1972) tables and are values of opacity at frequency ν_i, in a height interval, n, per volume mixing ratio of CO (see Appendix V). The most basic features of these coefficients are an inverse temperature squared dependence and a pressure dependence through the Voigt line shape, for which the width of the absorption line increases linearly with the atmospheric pressure of the line forming region.

Equation (1) also requires the obvious constraints $\xi_n > 0$ for all n and, as such, its inversion is not a linear problem. A simple method to include these constraints in nearly equivalent nonlinear equations is to solve for $\xi_n = e^{z_n}$

$$\tau_i = \sum_n P_{in}\, e^{z_n} \tag{2}$$

The amount of information inherently contained in the data will determine the number of layers, n, for which ξ_n may be found. As previously mentioned, the CO profile is essentially indeterminant above 80-90 km and only upper limits for ξ can be placed for layers below 65 km. Furthermore, we find

that solutions of equation (2) do not converge for $n > 2$ unless artificial constraints are introduced into the solution. The solutions are very dependent on the choice of layers. The layers are required to be contiguous with one another and span the line forming region (~ 60-105 km). For reasonable representation of temperature and pressure in the mesosphere, the coefficients, P_{in}, are calculated at two kilometer intervals from 50 to 106 km in altitude. The layers are formed by summing these two kilometer slabs in appropriate groups. Table 1 illustrates the sensitivity of solutions to choices of layers. ξ has been estimated for only the upper two layers while the lower layer was constrained near an upper limit.

Having established that only a very few parameters may be derived from the data, we were persuaded towards simple parameterizations of the mixing ratio profile. Several methods were tried, two of which are presented here. The logarithm of the CO mixing ratio is parameterized as a linear and parabolic function of altitude.

$$\ln\xi = A + B(z - z_0)$$

$$\ln\xi = A + B(z - z_0) + C(z - z_0)^2 \qquad (3)$$

where z = altitude and the constants A and B are estimated from the nonlinear set of equations,

$$\tau_i = \sum_s P_{is}\, e^A\, e^{B(z_s - z_0)}$$

$$\tau_i = \sum_s P_{is}\, e^A\, e^{B(z_s - z_0)}\, e^{C(z_s - z_0)^2} \qquad (4)$$

For all parameterized cases $s = 1,28$ corresponding to 2 km steps between $z_0 = 50$ km and $z = 106$ km. The difficulty encountered in the solution of eq. (4)

TABLE I. CO Mixing Profiles Constant over Layers

December 1979

layers (km)	CO	layers (km)	CO	layers (km)	CO
50-60	2.0×10^{-7}	50-64	2.0×10^{-7}	50-60	2.0×10^{-7}
60-80	2.6×10^{-6}	64-84	5.2×10^{-6}	60-70	2.0×10^{-6}
80-106	1.3×10^{-5}	84-106	2.8×10^{-6}	70-106	6.3×10^{-6}

December 1980

layers (km)	CO	layers (km)	CO	layers (km)	CO
50-60	2.0×10^{-7}	50-70	2.0×10^{-7}	50-70	2.0×10^{-7}
60-80	3.1×10^{-7}	70-90	4.8×10^{-6}	70-80	3.4×10^{-6}
80-106	3.7×10^{-5}	90-106	9.2×10^{-5}	80-106	2.5×10^{-5}

January 1982

layers (km)	CO	layers (km)	CO	layers (km)	CO
50-60	8.6×10^{-8}	50-64	1.0×10^{-7}	50-70	2.0×10^{-7}
60-70	9.3×10^{-7}	64-84	2.9×10^{-6}	70-80	8.7×10^{-6}
70-80	5.3×10^{-6}	84-106	3.8×10^{-5}	80-106	1.3×10^{-5}
80-106	1.9×10^{-5}				

was found to be consistent with all attempts to invert the data; only two parameters could be obtained for the converging solution. Consequently, $A = \ln\left[\xi(50\text{ km})\right]$ was constrained in the quadratic parameterization.

The parabolic fits of $\ln\xi$ are presented in Figure 2 for the 1979 and 1980 observations. The linear fits of $\ln\xi$ are shown in Figure 3. Dashed curves give the range of fits for the 1979 spectrum as A is varied for the quadratic parameterization. The residuals after fitting increased by ~ 20%, proceeding from the double valued left hand limit to the right hand limit of Figure 2.

The residuals for all attempted methods of inversion described here are comparable within 10-20%, the parabolic parameterization giving marginally lower residuals. As a result of this indeterminancy, only in mixing ratios between 65-80 km are moderately well determined by the data. The shaded area of Figure 2 indicates, qualitatively, the uncertainty in the CO mixing profile as derived from the data.

Day-night Differences for the 1979 Observations

Day-night contrast was not expected to be seen and, in fact, was not conclusively detected. There are, however, some indications of variability that should be mentioned. Figure 4 illustrates the behavior of the integrated line intensity with time or sun angle. There appears to be an anomalous, ~ 20% rise in CO line intensity centered on sunrise as is also indicated in the day (after 15:00 UT) and night (before 15:00 UT) spectra shown in Figure 5. Gaps in the observations and limited signal-to-noise ratios leave the observation of this morning terminator CO line intensity "bulge" very tentative. If it is real, this increase in the morning terminator CO line intensity probably indicates an ~ 10% change in mesospheric teperatures near the morning terminator.

Figure 2. Mixing ratio profiles of CO derived from the total December spectra of 1979 and 1980. A parabolic logarithmic parameterization of ξ was used with the mixing ratio at 50 km (e^A) constrained. B and C were determined in a least squares inversion of the spectra of Figures 1 and 5. The shaded area about the 1979 profile indicates a range of profiles found to fit the data with similar residuals after fitting. A was varied to produce this range. A similar range of uncertainty surrounds the 1980 profile. The inverted mixing profiles for 1979 and 1980 exaggerate the difference between the spectra, which are quite similar to the level of noise (see Figure 6).

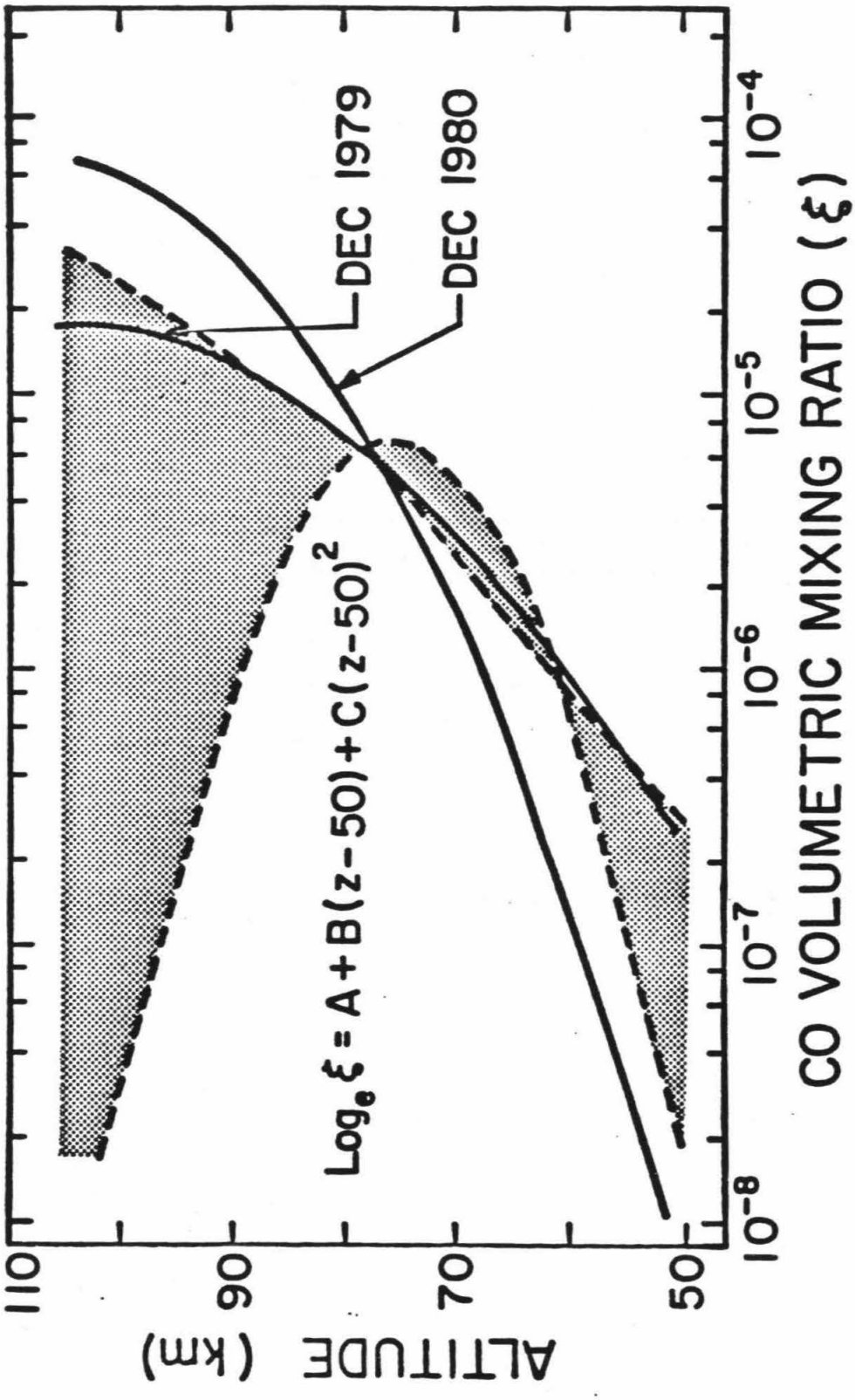
ALTITUDE (km)
110
90
70
50
10^{-8}
10^{-7}
10^{-6}
10^{-5}
10^{-4}
CO VOLUMETRIC MIXING RATIO (ξ)
DEC 1979
DEC 1980
$\text{Log}_e \xi = A + B(z-50) + C(z-50)^2$

Figure 3. Mixing ratio profiles of CO derived from the 1979, 1980, and 1982 microwave spectra. A linear logarithmic parameterization of ξ was used and does not represent a unique CO mixing ratio profile. A and B were determined in a least squares inversion of the spectra. Due particularly to the poor signal-to-noise ratios for the December spectra, a clear distinction among the three derived profiles is not definitive.

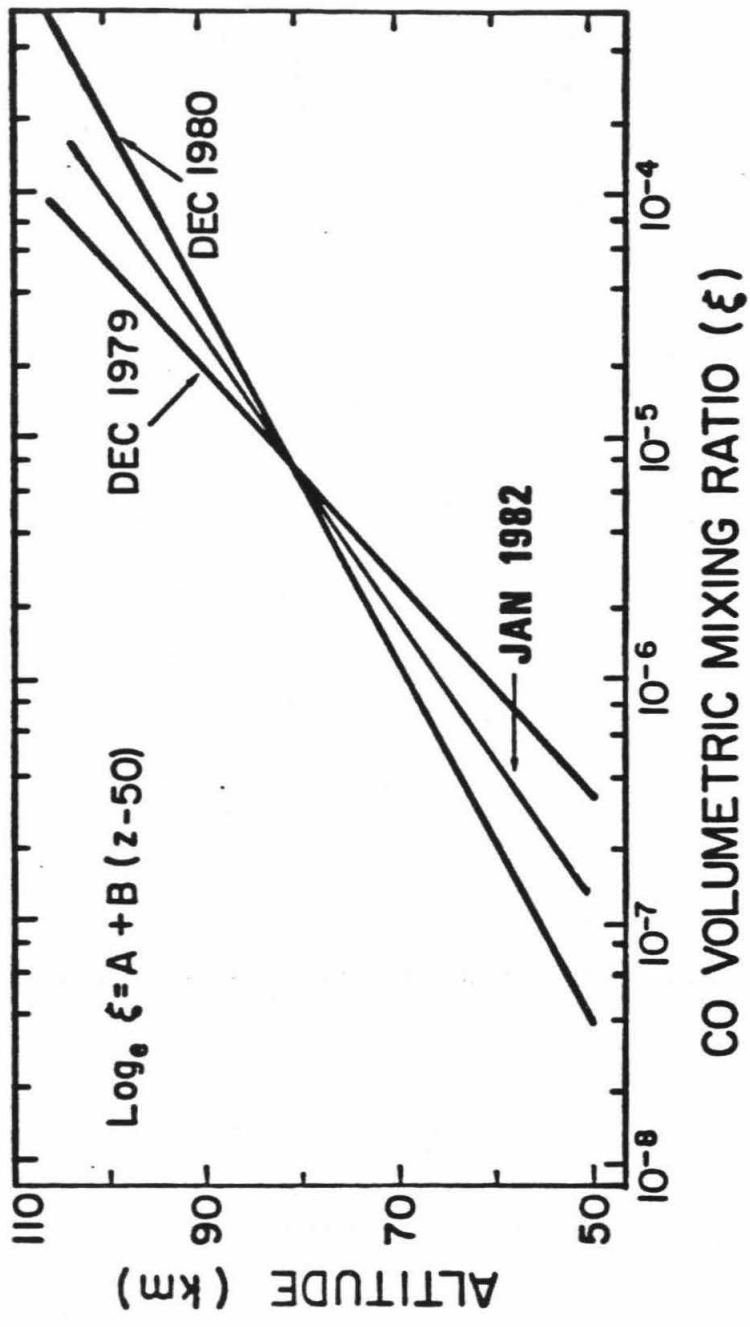
ALTITUDE (km)
110
90
70
50
10^{-8}
10^{-7}
10^{-6}
10^{-5}
10^{-4}
CO VOLUMETRIC MIXING RATIO (ξ)
$\text{Log}_e\ \xi = A + B\,(z-50)$
DEC 1979
DEC 1980
JAN 1982

Figure 4. The dependence of vertical CO column density above ~65 km with time or hour angle. Time of sunrise at an altitude of 80 km is indicated by a dashed vertical line. CO column density was determined from 20 minute averaged spectra with the assumption of a 210-200 K temperature of the absorbing region (~70-100 km).

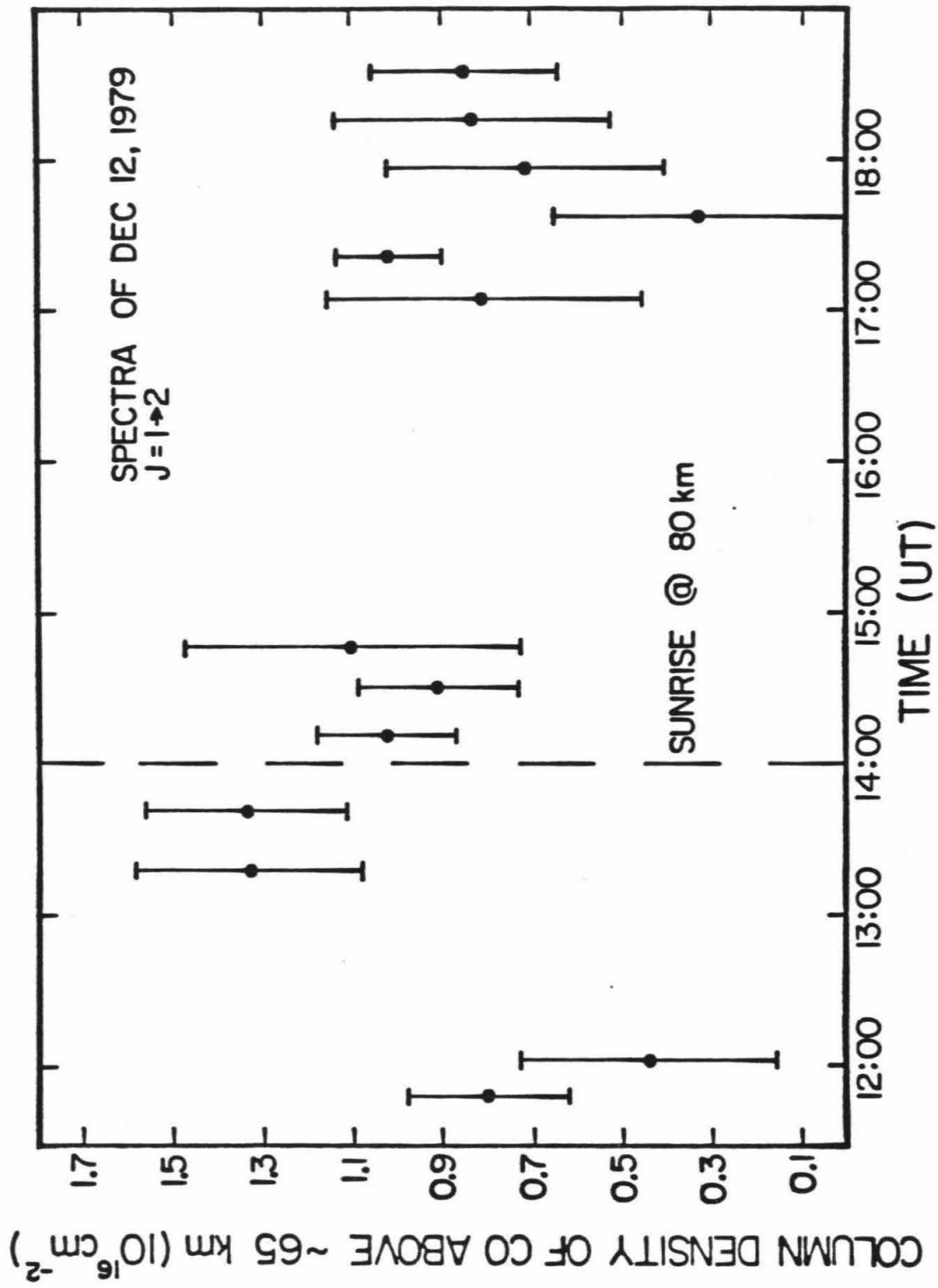
SPECTRA OF DEC 12, 1979
J=1→2
SUNRISE @ 80 km
TIME (UT)
12:00
13:00
14:00
15:00
16:00
17:00
18:00
0.1
0.3
0.5
0.7
0.9
1.1
1.3
1.5
1.7
COLUMN DENSITY OF CO ABOVE ~65 km (10^{15} cm^{-2})

Figure 5. Comparison of averaged day (after 15:00 UT) and night (before 15:00 UT) spectra. The night spectrum shows a somewhat deeper, broader line. However, differences are very close to noise levels of the measurements.

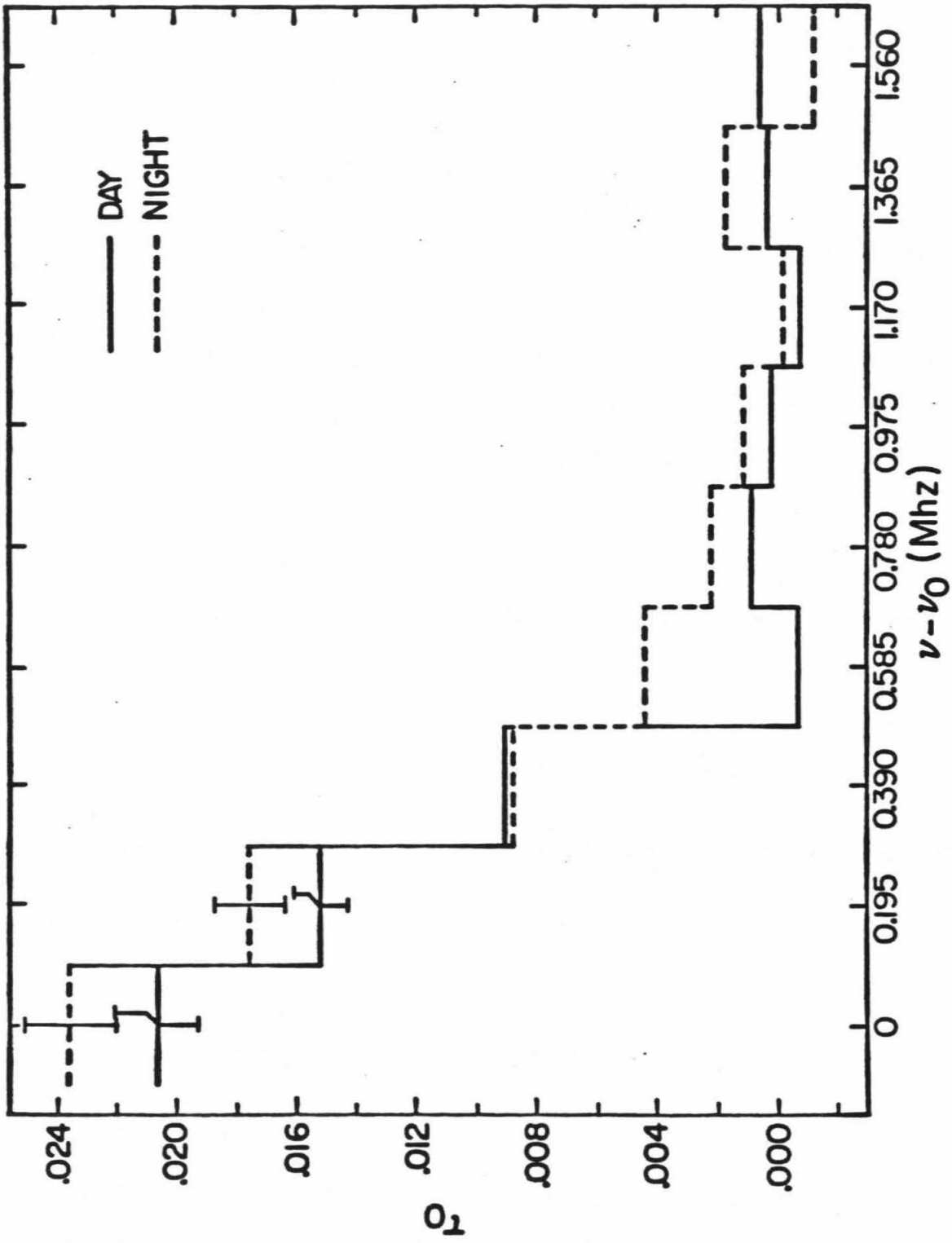
DAY
NIGHT
.024
.020
.016
.012
.008
.004
.000
τ_0
0
0.195
0.390
0.585
0.780
0.975
1.170
1.365
1.560
$\nu - \nu_0$ (Mhz)

Photochemical and diffusive time scale for CO in the terrestrial mesosphere are considerably longer than a few hours (M. Allen, personal communication, 1981). Further observations of high signal-to-noise ratio are necessary to confirm this effect.

December 1980 Observations

The 1980 spectra were taken on December 13, 14 and 15. The Moon was followed from early afternoon (~2:30 pm) until early evening (~8:00 pm). Expectations for a day-night difference were less for the evening terminator and, more importantly, signal-to-noise ratio for the 1980 data was lower by nearly a factor of two over that of the 1979 observations. Although the total integration time for the 1980 observations was longer than that of the 1979 observations, the 0-1 transition is eight times weaker than the 1-2 transition. Hence no attempt was made to separate day and night spectra. The total integrated spectrum is presented in Figure 6. Inversion for CO mixing profiles followed the procedures described for the 1979 observations. The various fits are found in Table 1 and Figures 2 and 3. Again, only two parameters could be derived from the data. The column density of CO is found with the same considerations as mentioned for the 1979 observations. The error bars are larger due to poorer signal-to-noise ratio, and uncertainty in the upper and lower sideband relative power levels for the 1980 observations.

$$(\textit{Dec. } 1980) \quad \int_{\sim 65\,\mathrm{km}}^{\infty} N_{CO}\, dz = 0.79 \pm 0.1 \times 10^{16}\ \mathrm{cm}^{-2}$$

The 1980 spectrum appears to be an intrinsically narrower line than the 1979 spectrum (i.e., narrower than accounted for by the reduced Doppler halfwidth of the 0-1 transition). This is indicated by the steeper mixing profile

Figure 6. Total folded spectrum of the J = 0 → 1 transition of mesospheric CO in absorption against the Moon taken on December 13, 14 and 15, 1980. Total bandwidth was 100 MHz, channel width was 200 KHz. τ_0 is the normal optical depth, ν_0 is the center line frequency of 115.271 GHz.

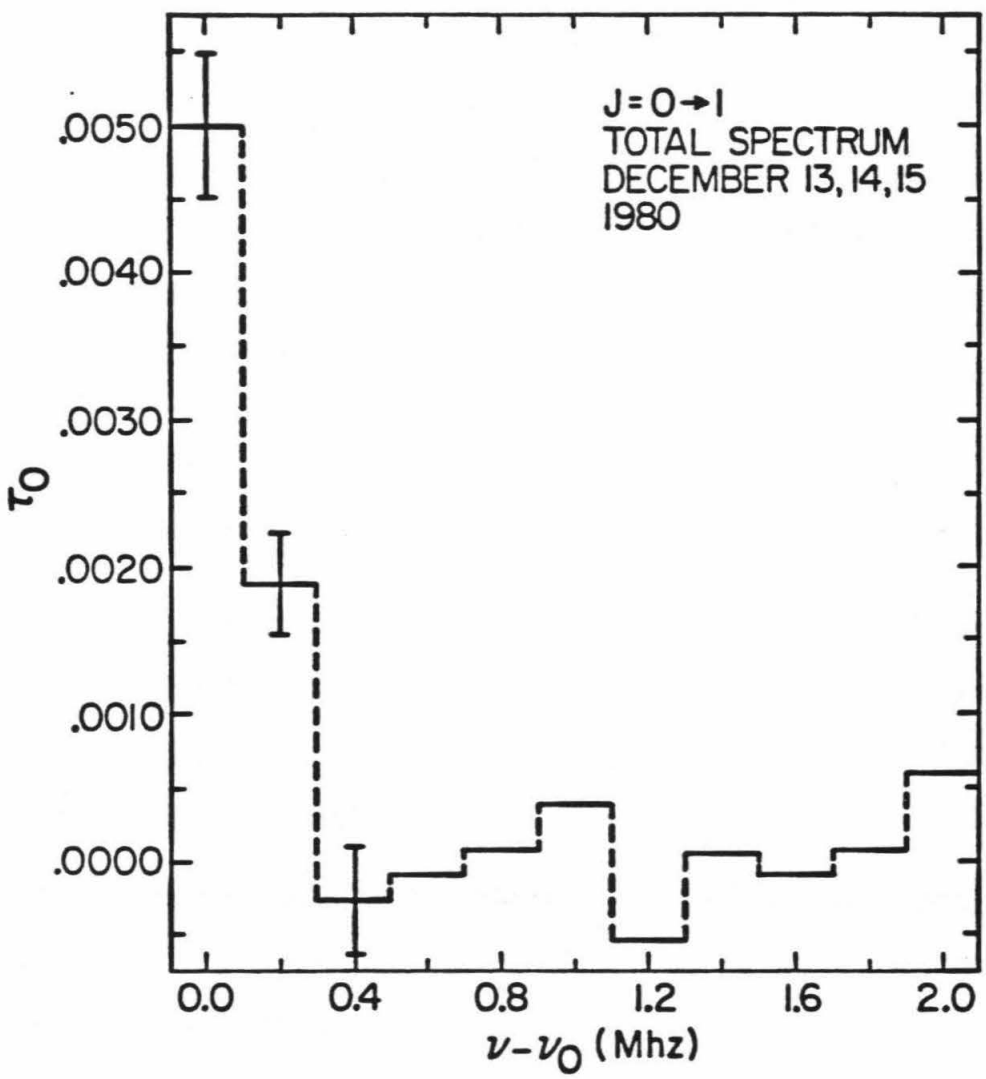
J=0→1
TOTAL SPECTRUM
DECEMBER 13, 14, 15
1980
.0050
.0040
.0030
.0020
.0010
.0000
τ_0
0.0
0.4
0.8
1.2
1.6
2.0
$\nu-\nu_0$ (Mhz)

found for the 1980 observations. We found that, when derived mixing ratio profiles for the two years are interchanged, the residuals are doubled for both data sets. Unfortunately, the non-uniqueness of the inversion does not allow a precise comparison of CO mixing profiles for December 1979 and 1980. The profiles of Figures 2 and 3 greatly exaggerate the differences, and illustrate the pitfalls of line inversion with limited signal-to-noise ratio. A several-fold increase in signal-to-noise ratio is required to convincingly distinguish the spectra of December 1979 and 1980. One can say with more confidence that, while the distribution of CO may have changed, similar column densities were found for the 1979 and 1980 observations (for $z \geq 65$km).

January 1982 Observations

Our 1982 absorption spectrum was taken on January 25 between 3 and 4:30 p.m. The 1982 emission spectrum was measured between 5 and 6 p.m. on the 25th and between 12:30 and 1:30 a.m. the following early morning of the 26th. During the limited time coverage of these spectra we did not find diurnal variations in line width or depth.

We use the spectral line area derived from the folded absorption spectrum (Figure 7) in order to estimate the total column density of CO above ~65 km because the calibration of the absorption spectrum in Figure 7 is more accurate than the calibration of the emission spectrum (unfolded in Figure 8).

$$\text{(Jan. 1982)} \quad \int_{\sim 65\text{km}}^{\infty} N_{CO}\, dz = 0.59 \pm 0.05 \times 10^{16}\ \text{cm}^{-2}$$

The above column density assumes slightly cooler mesospheric temperatures than those assumed for our December spectrum (200 K versus 200-210 K for the December spectra). This is in accordance with the general trend of

Figure 7. Total folded spectrum of the $J = 1 \rightarrow 2$ transition of mesospheric CO in absorption against the Moon taken on January 25, 1982. Total measured bandwidth was 25.6 MHz with 100 KHz resolution. τ_0 is the normal optical depth.

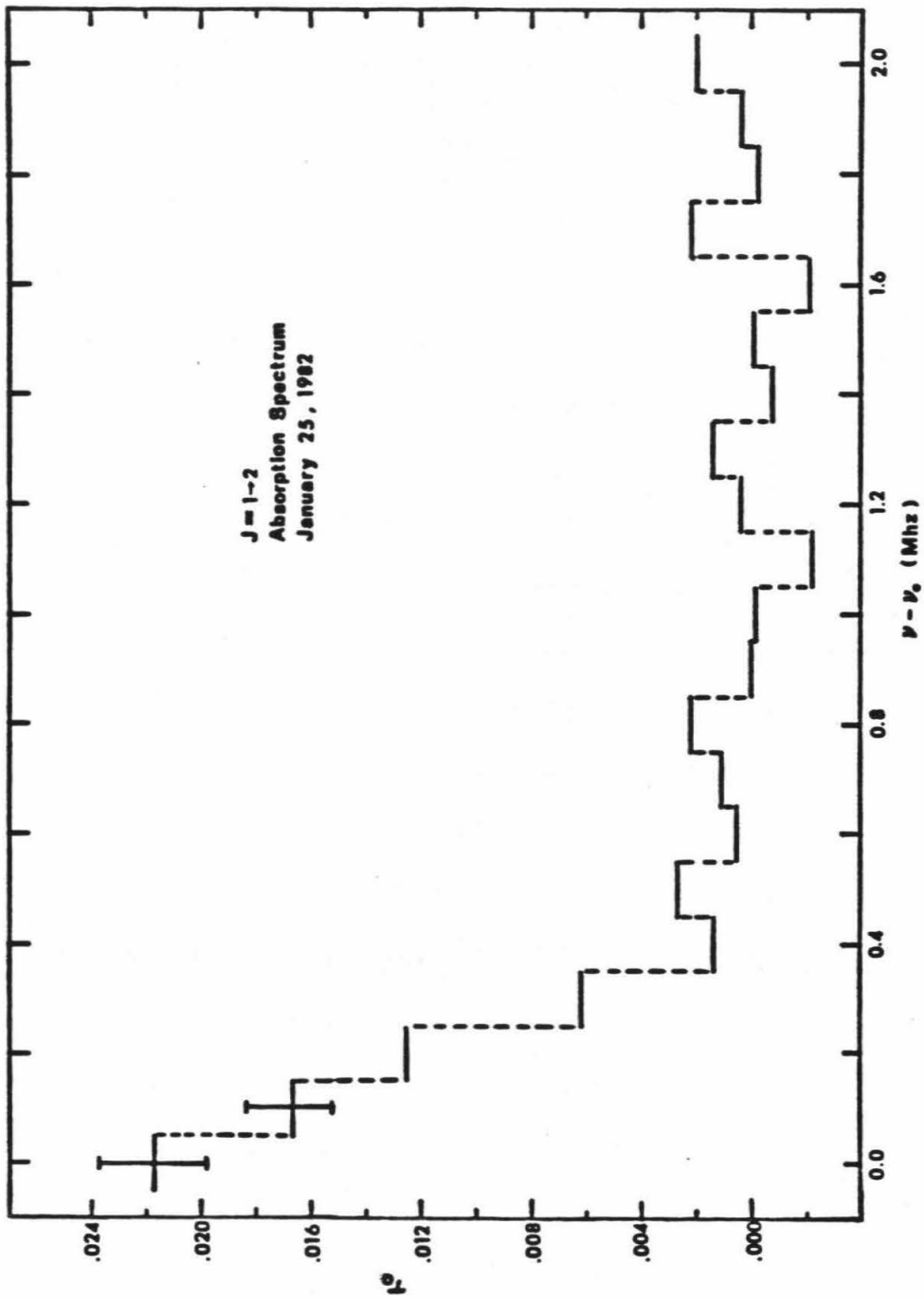
J = 1→2
Absorption Spectrum
January 25, 1982
t_A^*
.024
.020
.016
.012
.008
.004
.000
0.0
0.4
0.8
1.2
1.6
2.0
$\nu - \nu_0$ (Mhz)

decreasing mesospheric temperatures between winter and summer months (as given in the 1972 Cospar tables). Although the difference between the January and December column densities is not nearly sufficient evidence for seasonal variation of mesospheric CO, we will show through comparison with published spring and summer CO spectra that this observed difference is a likely consequence of seasonal variation.

We use our emission spectrum in order to invert for a CO mixing profile from our January 1982 observation. Although the emission spectrum (Figure 8) is not as accurately calibrated as the absorption measurement, it contains far better signal-to-noise ratios. Hence, the emission spectrum contains more information with regard to the altitude distribution of CO in the terrestrial mesosphere. Before proceeding with the inversion results we caution that absolute vaues of CO mixing ratios derived from the emission spectrum are uncertain to at least 20%. The spectral line area implied by the emission spectrum of Figure 8 is 20% greater than the spectral line area for the absorption spectrum of Figure 7. Nevertheless, the important point is that the relative altitude distribution of mesospheric CO is better constrained by the emission spectrum.

The unfolded emission spectrum is presented in Figure 8 along with several fitted synthetic spectra. These synthetic spectra correspond to CO mixing profiles found by inversions of the measured spectrum. As with the December observations we solve for discrete layers with constant CO mixing ratios and for linear and quadratic altitude dependences for the logarithm of the CO mixing ratio. Solutions for layered models are included in Table I. One of these solutions together with the solutions from the linear and quadratic parameterizations of $\ln(\xi_{CO})$ are presented in Figure 9. We also include the linear solution in Figure 3 for a comparison of mixing profiles among the 1979,

Figure 8. Total unfolded spectrum of the J = 1 → 2 transition of mesospheric CO in emission taken on January 25-26, 1982. Total measured bandwidth was 25.6 MHz with 100 KHz resolution. Zenith brightness temperature for the line emission is plotted against frequency from line center. Best fit synthetic spectra are plotted against the measured spectrum. The synthetic spectra are determined from least squares inversion solutions for linear and quadratic parameterizations of $\ln(\xi_{CO})$ as a function of altitude (see Figure 9).

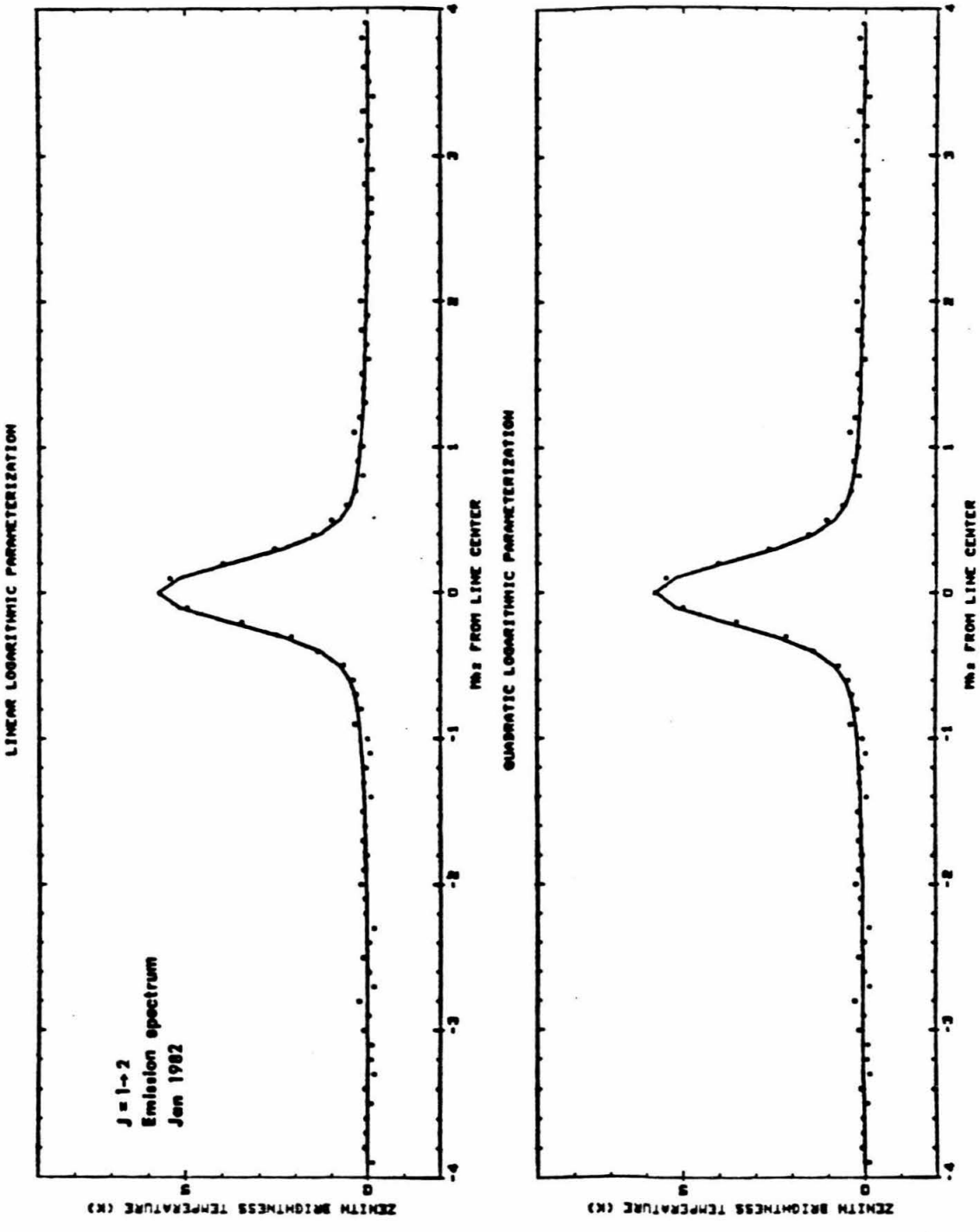
LINEAR LOGARITHMIC PARAMETERIZATION
J = 1→2
Emission spectrum
Jan 1982
ZENITH BRIGHTNESS TEMPERATURE (K)
MHz FROM LINE CENTER
QUADRATIC LOGARITHMIC PARAMETERIZATION
ZENITH BRIGHTNESS TEMPERATURE (K)
MHz FROM LINE CENTER

1980, and 1982 observations. Due primarily to the poor signal-to-noise ratios for the 1979, 1980 spectra, we cannot convincingly distinguish the altitude distribution of CO among the observations.

An important consequence of the high signal-to-noise ratios for the 1982 emission spectrum is that three parameters could be found from our inversions. We were, in fact, able to solve for four altitude layers in the discrete layer solutions. Thus we were not forced to specify either the CO mixing ratio for the lowest layer in our discrete layer models or the value of A $(= \ln[\xi(50\text{km})]$ for our quadratic parameterization of $\ln(\xi_{CO})$. In this sense the January emission spectrum allows us to constrain the mixing ratio of CO below 65 km better than do the 1979, 1980 December spectra.

However, even with the increased signal-to-noise ratios for our 1982 emission spectrum we still find that the CO mixing profile is not well defined. We note that the three inversion solutions of Figure 9 indicate considerably different CO mixing profiles even though the sum of the squared residuals after fitting are identical for all three solutions. The very low atmospheric pressures for the line forming region do not provide sufficient pressure broadening in order to distinguish the exact altitude mixing profile of CO. Below 50-60 km where pressure broadening becomes substantial there is simply not enough CO to produce measureable microwave absorption. Thus the mixing profiles of Figure 9 may be close to the optimum one can obtain from ground based observations.

Discussion

The primary interest of CO mesospheric observations is that of atmospheric change; whether daily, seasonal, or yearly. Such observations should

Figure 9. Three separate solutions for the mixing profile of CO in the terrestrial mesosphere as found by least squares inversion of the January 1982 emission spectrum (Figure 8). The vertical bars represent a solution with constant CO mixing ratios (ξ_{CO}) for four discrete altitude steps. The dashed and solid continuous profiles represent solutions for linear and quadratic parameterizations of $\ln(\xi_{CO})$ as a function of altitude.

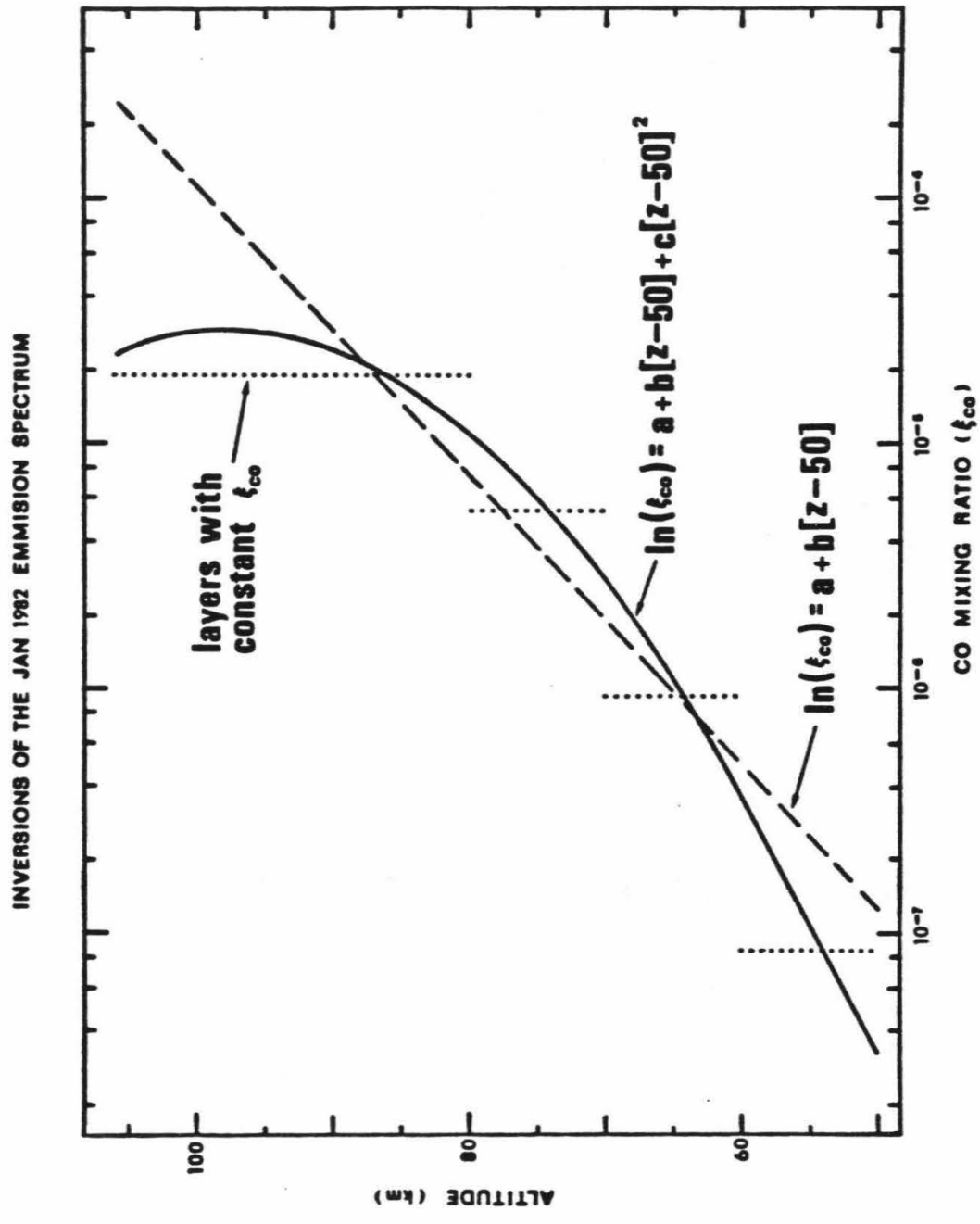
INVERSIONS OF THE JAN 1982 EMMISION SPECTRUM
layers with constant ξ_{co}
$\ln(\xi_{co}) = a + b[z-50] + c[z-50]^2$
$\ln(\xi_{co}) = a + b[z-50]$
ALTITUDE (km)
100
80
60
10^{-7}
10^{-6}
10^{-5}
10^{-4}
CO MIXING RATIO (ξ_{co})

provide constraints on the dynamics of the mesosphere just as ozone measurements prove diagnostic for the stratosphere (Cunnold *et al.*, 1975); O_2, O, and N_2 mesurements for the thermosphere (Kasting and Roble, 1981); and CO measurements for the mesosphere of Venus (Gulkis et al., 1977; Schloerb et al., 1980).

Variability of the Earth's mesospheric CO is illustrated in Figure 10. CO spectra (115 and 230 GHz) from five separate investigations are presented (this paper; Goldsmith et al., 1979; data of W.J. Wilson published in Allen, Yung, and Waters, 1981; Kunzi and Carlson, 1982; and a recent spectrum taken for the authors by Rick Howard at Kitt Peak Observatory). All of the spectra were measured between latitudes of 30 and 40° North. For the purpose of this comparison, 0-1 spectra have been translated into equivalent 1-2 spectra through the use of mixing ratios derived from the original data. Such a procedure is less dependent on the methods of inversion than would be direct comparison of CO mixing profiles. This technique also conserves spectrum area over frequency of the transition cubed, so that total line opacities from spectra of different transitions may be compared visually.

The 1981 spectrum presented in Figure 10 requires a short, separate description. This June, $J = 1 \rightarrow 2$ measurement was taken at our request by Rick Howard with the 36-foot Kitt Peak antenna on June 19, observing at an average elevation angle of 20° with a spectral resolution of 100 kHz. The observing system was identical to that of our own January, 1982 measurement with one important difference. The measurement is an absorption spectrum, but the continuum of the Moon (BL) was not recorded (a standard procedure at Kitt Peak) and, hence, emission style calibration was required. We wish to stress that calibration is the main uncertainty in the comparison of the spectra of Figure 10. Assumptions for calibration (such as ground spillover, antenna efficiency,

Figure 10. Comparison of published measurements of the CO mesospheric absorption spectrum. Both December spectra and the January, 1982 spectrum are from this paper. The March spectrum is the J = 1 → 2 data of Goldsmith *et al*. (1977) smoothed to a spectral resolution of 200 KHz. The May spectrum is from data taken by W.J. Wilson published in Allen, Yung, and Waters (1980). The June 1981, J = 1 → 2 spectrum was taken for the authors by Rick Howard at Kitt Peak, and is smoothed to a spectral resolution of 200 kHz. The February, 1979 spectrum is from Kunzi and Carlson (1982), and is also smoothed to a spectral resolution of 200 kHz. The December 1980 and May 1979 data sets are J = 0 → 1 spectra. CO mixing ratios derived from these spectra are used to synthesize equivalent J = 1 → 2 spectra of 200 KHz resolution. Rough error bars are drawn into indicate estimated signal-to-noise ratio for each data set.

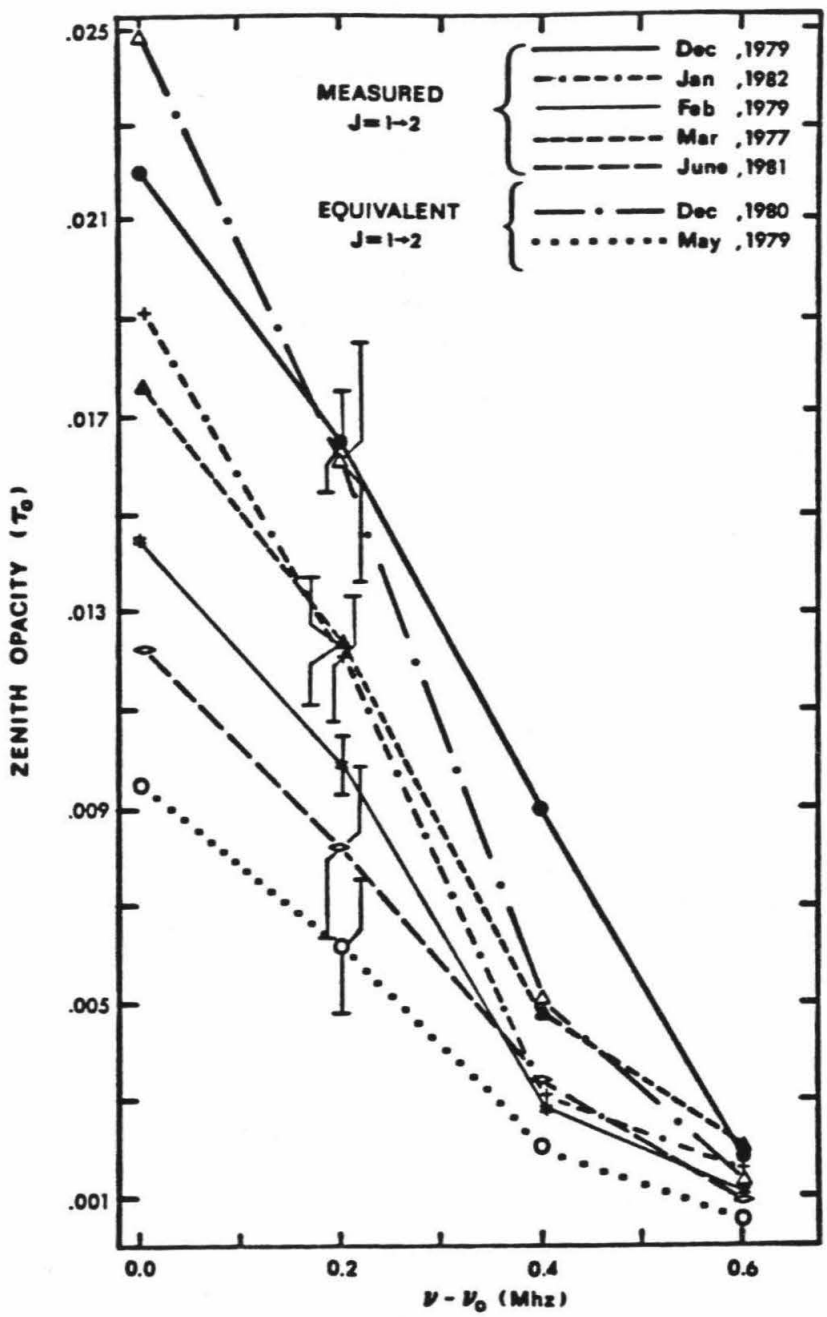
MEASURED
J=1→2
EQUIVALENT
J=1→2
Dec ,1979
Jan ,1982
Feb ,1979
Mar ,1977
June ,1981
Dec ,1980
May ,1979
ZENITH OPACITY (τ_0)
.025
.021
.017
.013
.009
.005
.001
0.0
0.2
0.4
0.6
$\nu - \nu_0$ (Mhz)

and effective mesospheric temperature), which may introduce uncertainties on the order of 25%, were required for all but the December and January spectra of Figure 10. We point out that our absorption and emission spectra of January 1982 produced agreement within roughly 20% for CO line opacities. This agreement suggests that the comparison of emission and absorpton spectra in Figure 10 is valid to within ~ 20% uncertainty.

The spectra were taken on December 1979-1980, January 1982, February 1978, March 1977, May 1979, and June 1981; and indicate large seasonal variation in the mesospheric CO. The two December spectra may show slight daily or yearly change but our measurements are not sufficient evidence for such a change. Note that the December-May/June variation is on the order of a factor of 2-3 in total CO column density above ~ 65 km as inferred from the total areas under each spectrum. Such a variation exceeds calibration uncertainties of the emission spectra.

A more quantitative presentation of seasonal CO variations is supplied by Table II, a comparison of CO column densities as derived from areas under each of the CO spectra. Also listed in Table II are the corresponding atmospheric temperatures assumed for the line forming region (from the 1972 Cospar tables). Note that summer months have lower temperatures than winter months in the 70-90 km region of the atmosphere, a fact which actually increases the seasonal variation of CO over that implied by the spectral line areas of Figure 10. Also note that we have included the discovery measurement of Waters et al. (1976). We have recalculated their column density using a more accurate value for the dipole moment of CO (0.112 Debye versus 0.1 Debye), and a lower atmospheric temperature (180° K versus 200° K) for the line forming region. This new value for column density is some 30% lower than their

TABLE II. Comparison of column densities of CO above ~65 km derived from previously published spectra and the spectra of this paper. Uncertainties for the values of column density may be as large as 25% for each of the tabulated observations except the December measurements, whose uncertainties are on the 10% level.

Author	Type Transition	Type Measurement	Date of Observation	Assumed Atmospheric Temperature for Column Density Calculation	Column Density (cm^{-2})
This	1-2	absorption against Moon	December (1979)	210-200 K	9.0×10^{15}
This	0-1	absorption against Moon	December (1980)	210-220 K	7.9×10^{15}
This	1-2	absorption against Moon	January (1982)	200 K	5.9×10^{15}
Kunzi and Carlson	1-2	emission	February (1979)	190 K	4.4×10^{15}*
	0-1	emission	March (1979)	190 K	4.5×10^{15}*
Goldsmith et al.	0-1	emission	March (1977)	190 K	4.2×10^{15}+
	1-2	emission	March (1977)	190 K	5.3×10^{15}+
Waters, Wilson and and Shimabukuro	0-1	absorption against Sun[	May (1975)	180 K	7.0×10^{15}]
Wilson (published in Allen et al., 1981)	0-1	emission	May (1979)	180 K	2.4×10^{15}
This (R. Howard)	1-2	absorption against Moon[	June (1981)	180 K	3.5×10^{15}

[Calibrated as an emission spectrum (background continuum not kept).

+Some 30% lower than originally published (see text).

*Some 50% lower than originally published (see text).

published value, but still quite high for a summer measurement in this comparison. We tend to discount their measurement partly because the spectrum was taken in absorption against the Sun, adding some 3000° K to the system temperature (which would surely complicate their emission-style calibration). More importantly, they have not been able to reproduce such a high measurement in any subsequent summer measurements (W.J. Wilson, personal communication). Also included in Table II are column densities we have calculated directly from the 0-1 and 1-2 spectra of Goldsmith *et al.* (1977) and Kunzi and Carlson (1982), rather than the single column densities these authors calculated from vertical integration of their derived CO mixing profiles. Column densities taken directly from the spectral line areas are much more reliable comparison parameters because CO mixing profiles (particularly below 65 km) are not well determined by the very narrow spectra.

The basic conclusion from Table II is that CO column density in the mesosphere varies seasonally by a factor between 3 and 4. The actual value for this variation depends as inverse temperature squared of the absorbing region. Hence, the seasonal variation of mesospheric temperatures must be known to determine accurate seasonal variation of mesospheric CO from spectral line areas. Without any seasonal temperature dependence, the inferred mesospheric CO variation is a factor between 2 and 3.

One expects some seasonal influence on CO abundance due to the seasonal dependence of insolation. However, such an effect is both smaller in magnitude and opposite in sign to the observed change. On the basis of insolation change alone, the winter line should be weaker than the summer line (Mark Allen, personal communication). As is the case for ozone, one is driven towards transport as a necessary explanation. We note two important seasonal

variations that are likely to influence mesospheric CO. Lindzen (1981) predicts that eddy diffusivity should peak near 50 km altitude in winter as compared to 70-80 km altitude during summer, an effect that can strongly influence distribution of CO in the mesosphere (M. Allen, personal communication, 1981). Also, vertical motions show a strong seasonal dependence at midlatitudes according to the dynamical models of Cunnold et al. (1975). Near 40° latitude, strong descending vertical motions characterize winter months whereas weak ascending vertical motions characterize summer motions. Analogous patterns of vertical motions in the Venus thermosphere and upper mesosphere lead to diurnal variations of mesospheric CO on Venus (e.g., Dickinson and Ridley, 1975).

We conclude from this work that our understanding of CO in the mesosphere can be improved with Earth-based microwave measurements, but data with high signal-to-noise ratios must be obtained. In order to avoid the ambiguities of calibration, self-calibrating absorption spectra are to be preferred. Furthermore, the limitations in line inversion techniques must be recognized.

Alcayde, D., P. Bauer, and J. Fontanari, Long-term variance of the thermospheric temperature and composition, *J. Geophys. Res.*, **78**, 629-637, 1974.

Allen, M. Y.L. Yung, and J.W. Waters, Vertical transport and photochemistry in the terrestrial mesosphere and lower thermosphere (50 - 120 km), *J. Geophys. Res.***86**, 3617-2627, 1981.

Cunnold, D., F.Alyea, N. Phillips, and R. Prinn, A three-dimensional dynamical-chemical model of atmospheric ozone, *J. Atmos. Sci.*, **32**, 170-194, 1975.

Dickinson, E.D., and E.C. Ridley, A numerical model for the dynamics and composition of the Venusian thermosphere, *J. Atmos. Sci.*, **32**, 1219-1231, 1975.

Draegert, D.A. and D. Williams, Collisional broadening of CO absorption lines by foreign gases, *J. Optical Soc. Am.* **58**, 1399-1403, 1968.

Dutsch, H., Photochemistry of atmospheric ozone, in *Advances in Geophysics, Vol. 15*, Academic Press, 219-322, 1971.

Goldsmith, P.F., M.M. Litvak, R.L. Plambeck, and D.R.W. Williams, Carbon monoxide mixing ratio in the mesosphere derived from ground-based microwave measurements, *J. Geophys. Res.*, **84**, 416-418, 1979.

Gulkis, S., R.K. Kakar,M.J. Klein, and E.T. Olsen, Venus: detection of variations in stratospheric carbon monoxide, *Proc. Symposium Planetary Atmos.*, **61**, 1977.

Hedin, A.E., J.E. Salah, J.V. Evans, C.A. Reber, G.P. Newton, N.W. Spencer, D.C. Kayser, D. Alcayde, P. Bauer, L. Cogger, and J.P. McClure, A global thermospheric model based on mass spectrometer and incoherent scatter data, MSIS 1, N_2, density and temperature, *J. Geophys. Res.* **82**, 2139-2147, 1977. Kasting, J.F., and R.G. Roble, A zonally averaged chemical-

dynamical model of the lower thermosphere, *J. Geophys. Res.* **86**, 9641-9653, 1981.

Kunzi, K.F., and E.R. Carlson, Atmospheric CO volume mixing ratio profiles determined from ground-based measurements of of the $J = 1 \rightarrow 0$ and $J = 2 \rightarrow 1$ emission lines, *J. Geophys. Res.* **87**, 7235-7241, 1982.

Lindzen, R.S., Turbulence and stress due to gravidy wave and tidal breakdown, *J. Geophys. Res.* **86**, 9707-9714, 1981.

Masson, C.R., A stable acousto-optical spectrometer for millimeter radio astronomy, submitted to *Astronomy and Astrophysics*, 1982.

Mauersberger, K., D.C. Kayser, W.E. Potter, and A.O. Nier, Seasonal variation of neutral thermospheric constituents in the northern hemisphere, *J. Geophys. Res.* **81**, 7-11, 1976.

Mayr, H.G., P. Bauer, H.C. Brinton, L.H. Brace, and W.E. Potter, Diurnal and seasonal variations in atomic and molecular oxygen inferred from Atmospheric Explorer-C, *Geophys. Res. Lett.* **3**, 77-80, 1976.

Newell, R., Transfer through the tropopause and within the stratosphere, *Quart. J. Royal Meteor. Soc.* **89**, 167-204, 1963.

Noxon, J.F., and A.E. Johanson, Changes in thermospheric molecular oxygen abundance inferred from twilight 6300 Å airglow, *Planet. Space Sci.* **20**, 2125-2151, 1972.

Offerman, D., Composition variation in the lower thermosphere, *J. Geophys. Res.* **79**, 4281-4293, 1974.

Penfield, H., M.M. Litvak, C.A. Gottlieb, and A.E. Lilley, Mesospheric ozone measured from ground-based millimeter observations, *J. Geophys. Res.*, **81**,

6115-6120, 1976.

Phillips, T.G. and K.B. Jefferts, A low temperature bolometer heterodyne receiver for millimeter wave astronomy, *Rev. Sci. Instrum.*, **44**, 1009-1014, 1973.

Phillips, T.G., D.P. Woody, T.J. Dolan, R.E. Miller, and R.A. Linke, Dayen-Martin [SIS tunnel junction] mixers for low noise heterodyne receivers, *IEEE Trans. on Magnetics*, **MAG-17**, 684-689, 1981.

Roble, R.G., and R.B. Norton, Thermospheric molecular oxygen from solar extreme ultraviolet occultation measurements, *J. Geophys. Res.* **77**, 3524-3533, 1972.

Rosenkranz, P.W., Shape of the 5 mm oxygen band in the atmosphere, *IEEE Trans. on Antennas and Propagation*, **AP-23**, 498-506, 1975.

Schloerb, F.P., S.E. Robinson, and W.M. Irvine, Observation of CO in the stratosphere of Venus via its $J = 0 \rightarrow 1$ rotational transition, *Icarus*, **42**, 121-128, 1980.

Scialom, G., Neutral composition in the lower thermosphere, *Radio Sci.* **9**, 253-262, 1974.

Shimabukuro, F.I., P.L. Smith, and W.J. Wilson, Estimation of the daytime and nighttime distribution of atmospheric ozone from ground-based millimeter wavelength observations, *J. Applied Met.*, **16**, 929-934, 1977.

Ulich, B.L., and R.W. Haas, Absolute calibration of millimeter-wavelength spectral lines, *Astrophys. J. Suppl. Series* **30**, 247-258, 1976.

Waldteufel, P., A study of seasonal changes in the lower thermosphere and their implications, *Planet. Space Sci.* **18**, 741-748, 1970.

Waters, J.W., Absorption and emission of atmospheric gases, in *Methods of Experimental Physics, Vol. 12 Astrophysics, Part B Radio Telescopes*, edited by M.L. Meeks, 142-176, Academic Press, Inc., N.Y., 1976.

Waters, J.W., W.J. Wilson, and F.I. Shimabukuro, Microwave measurement of mesospheric carbon monoxide, *Science*, **191**, 1174-1175, 1976.

Wofsy, S.C., J.C. McConnell, and M.B. McElroy, Atmospheric CH_4, CO and CO_2, *J. Geophys. Res.* **77**, 4477-4493, 1972.

Appendix I. The Absorption Measurement

For absorption measurements, we consider two cases: one in which the absorber is in the terrestrial atmosphere; and, two, in which the absorber is in a nonterrestrial atmosphere (Mars or Venus). For both cases the observing technique is position switching in which we define S_{off} as a spectral scan taken with the antenna beam pointing off or away from the continuum source, and S_{on} as a spectral scan taken while pointing at the continuum source. We use superscripts + and − to indicate upper and lower sidebands. Figure A illustrates the nature of sidebands, which are the result of mixing a local oscillator frequency, ν_{LO}, with the observing frequency, ν_{obs}, in order to work with an intermediate frequency, IF, that may be coherently amplified. Thus one detects

$$IF = \nu_{obs} - \nu_{LO}$$

the combined signal of two bandwidths (sidebands) that are symmetrically offset from the local oscillator frequency by $\pm IF$. For a given IF it is important to tune ν_{LO} so that the desired observing frequency is centered within one of the sidebands.

A. Terrestrial CO Absorbtion Spectra

We observed terrestrial CO in absorption against the continuum black body emission from the Moon. The calibration technique for these observations is developed for the general case of unequal gains and atmospheric opacities for the two sidebands.

A scan measured while pointing at the moon measures a signal from each sideband

FIGURE A: Local Oscillator, CO line, and intermediate frequencies.

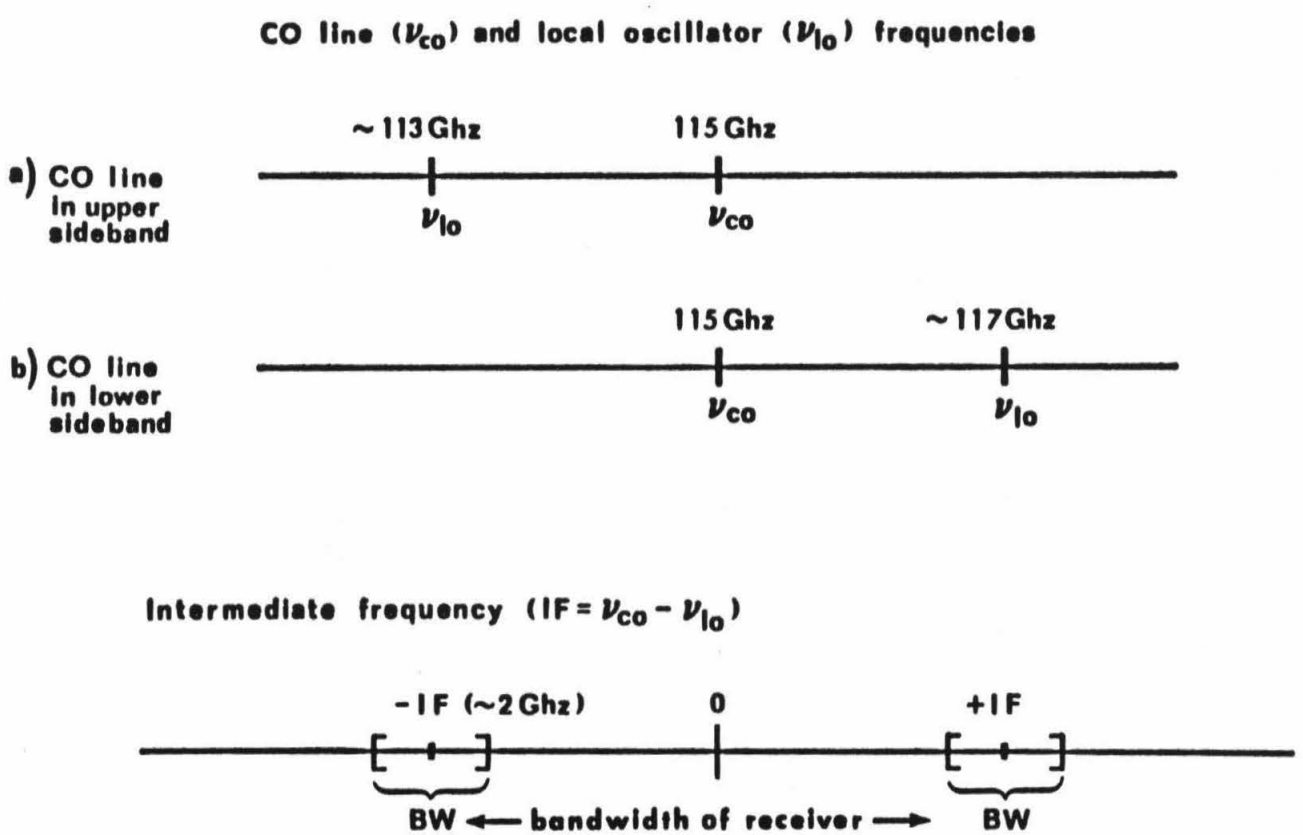
CO line (ν_{co}) and local oscillator (ν_{lo}) frequencies
~113Ghz
115Ghz
a) CO line in upper sideband
ν_{lo}
ν_{co}
115Ghz
~117Ghz
b) CO line in lower sideband
ν_{co}
ν_{lo}
Intermediate frequency (IF = $\nu_{co} - \nu_{lo}$)
-IF (~2Ghz)
0
+IF
BW ← bandwidth of receiver → BW

$$S_{on} = S_{on}^{+} + S_{on}^{-}$$

$$= G^{+}\left[T_M e^{-\tau(\nu)} e^{-\tau^{+}} + T_A\left(1 - e^{-\tau(\nu)} e^{-\tau^{+}}\right) + T_R\right]$$

$$+ G^{-}\left[T_M e^{-\tau^{-}} + T_A\left(1 - e^{-\tau^{-}}\right) + T_R\right] \qquad \text{(A1)}$$

where

G^{-}, G^{+} = lower, upper sideband gains

τ^{-}, τ^{+} = atmospheric (mainly tropospheric) opacity over the lower, upper sideband passes

$\tau(\nu)$ = spectral opacity due to CO in the mesosphere

T_A, T_M = atmospheric temperature of the troposphere and continuum temperature of the Moon

T_R = receiver temperature

Note that we place the CO line ($\tau(\nu)$) in the upper sideband. Similarly for scans measured while pointing off of the Moon, we have

$$S_{off} = S_{off}^{+} + S_{off}^{-}$$

$$= G^{+}\left[T_A\left(1 - e^{-\tau(\nu)} e^{-\tau^{+}}\right) + T_R\right] + G^{-}\left[T_A\left(1 - e^{-\tau^{-}}\right) + T_R\right]$$

The differencing of off and on spectra removes atmospheric emission and the receiver level

$$S_{on} - S_{off} = G^{+} T_m e^{-\tau(\nu)} e^{-\tau^{+}} + G^{-} T_m e^{-\tau^{-}}$$

Several convenient features of these difference spectra are the narrowness and very small opacity of the terrestrial CO line ($\tau(\nu) << 1$). We compute the average

level of the difference spectra for channels far from the line center where $\tau(\nu) \to 0$.

$$\left[S_{on} - S_{off}\right]_{\tau(\nu)\to 0} \equiv T_M\left[G^+e^{-\tau^+} + G^-e^{-\tau^-}\right] \tag{A2}$$

Dividing (1) by (2), we have

$$\frac{\left[S_{on} - S_{off}\right]}{\left[S_{on} - S_{off}\right]_{\tau(\nu)\to 0}} = \frac{\left[G^+e^{-\tau(\nu)}e^{-\tau^+} + G^-e^{-\tau^-}\right]}{\left[G^+e^{-\tau^+} + G^-e^{-\tau^-}\right]} \tag{A3}$$

We consider two cases, the simplest of which is $\tau^- = \tau^+$; $G^- = G^+$

$$(3) \to \frac{e^{-\tau(\nu)} + 1}{2} \xrightarrow{\tau(\nu) << 1} 1 - \frac{\tau(\nu)}{2}$$

Thus we arrive at a direct measure of the opacity of mesospheric CO without any calibration necessary. As a second case we consider $\tau^- \neq \tau^+$; $G^- = G^+$

$$1 - (3) \to \frac{\left[1 - e^{-\tau(\nu)}\right]}{\left[1 + e^{(\tau^+ - \tau^-)}\right]} \xrightarrow{\tau(\nu) << 1} \frac{\tau(\nu)}{\left[1 + e^{(\tau^+ - \tau^-)}\right]}$$

For our observations τ_o^+, the normal tropospheric opacity in the upper sideband, is always less than 0.3. Observing at an elevation angle of 30°.

$$\tau^+ \lesssim 0.3/\cos(60) = 0.6$$

Due to the 118 GHz O_2 opacity (see Figure B), $\tau^+ > \tau^-$ so that the maximum range of the calibration factor is 2-2.6.

CO Absorption Spectra of Venus and Mars

The calibration of CO spectra of Mars and Venus is similar to the procedure for terrestrial CO spectra. However, in this case the continuum absorption term in the on scan is not simply absorption. CO opacity in the Mars and

FIGURE B: Normal atmospheric opacity at microwave frequencies (from Waters, 1976). Vertical lines mark CO transitions at 115 and 230 gHz. Numerous short, vertical lines indicate ozone lines.

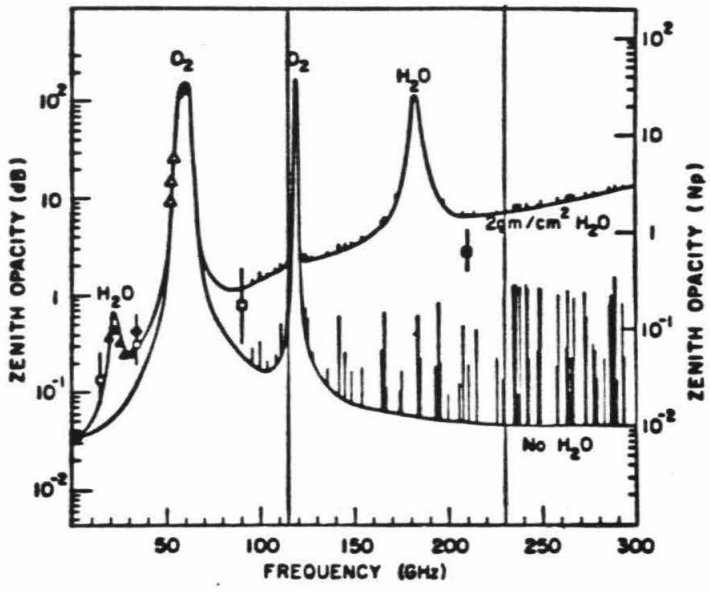
ZENITH OPACITY (dB)
ZENITH OPACITY (Np)
FREQUENCY (GHz)
O2
O2
H2O
H2O
2gm/cm2 H2O
No H2O
50
100
150
200
250
300

Venus atmospheres introduces emission and absorption both of which are contained in the final difference spectrum.

Thus for equal sideband gains we measure

$$\frac{S\left[\tau(\nu)\right]}{1 + e^{(\tau^+ - \tau^-)}}$$

where $S\left[\tau(\nu)\right]$ is no longer a direct measure of $\tau(\nu)$ but reflects the radiative transfer quantity

$$\frac{T_c}{T_e} e^{-\tau(\nu)} + \int_{z_i}^{\infty} \frac{T(z)}{T_e} e^{-\tau(\nu,z)} \, d\tau$$

in the observed planetary atmosphere T_c and $T(z)$ are the continuum and atmospheric temperatures of Venus or Mars. The quantity T_e indicates that these CO spectra are very broad so that dividing by the level in the wings of the spectra does not necessarily correspond to dividing by the continuum level.

The breadth of CO spectra for Mars and Venus introduces one further concern that should be mentioned regarding the baseline of CO microwave spectra. In general, the gain, G, of the system may show channel to channel variation. Gain variation across the spectrum is removed by dividing the difference spectrum (on-off), by the off spectrum channel by channel. The baseline of the spectrum is then quite flat (except for the desired CO absorption feature) if the system noise temperature ($\sim T_R$) is not a noticeable function of frequency across the bandwidth of the spectrum. In the case that T_R does show significant variation across the measured bandwidth, one may calibrate out the frequency response of T_R by measuring (on-off)/off spectra of a purely continuum source such as the Moon or a hot load. We note that such calibration is standard operating procedure at Kitt Peak.

Appendix II. The Absorption Coefficient of CO

The following development for the absorption coefficient of electric dipole transitions is taken from *Microwave Molecular Spectra* by Gordy and Cook (1970).

Consider the transition between rotational states m and n by absorption (emission) of radiation at frequency ν_m

$$\nu_m = \frac{\left(E_n - E_m\right)}{h}$$

The probability for this transition occurring per unit time is

$$\text{(absorption)} \qquad P_{m\to n} = \rho(\nu_m)\, B_{m\to n}$$

$$\text{(emission)} \qquad P_{n\to m} = \rho(\nu_m) B_{n\to m} + A_{n\to m}$$

where $B_{m\to n}$ and $B_{n\to m}$ are the Einstein coefficients of absorption and induced emission and $\rho(\nu_m)$ is the energy density of radiation at frequency, ν_m. $A_{n\to m}$ is the coefficient of spontaneous emission and is negligible at microwave frequencies. The coefficients of absorption and induced emission are identical

$$B_{mn} = B_{m\to n} = B_{n\to m} = \left(\frac{8\pi^3}{3h^2}\right)\left|\left(m\,|\mu|\,n\right)\right|^2$$

where h is Planck's constant and $\left(m\,|\mu|\,n\right)$ is the dipole moment matrix of the molecule.

The total number of transitions $m \to n$ occurring in a unit volume, V, is

$$R_{m\to n} = \rho(\nu_m) V N_m \frac{8\pi^3}{3h^2} \left| \langle m | \mu | n \rangle \right|^2$$

Similarly the total number of transitions $n \to m$ is

$$R_{n\to m} = \rho(\nu_m) V N_n \frac{8\pi^3}{3h^2} \left| \langle m | \mu | n \rangle \right|^2$$

N_n and N_m are the number densities of the states n and m. In the case of thermal equilibrium, the ratio of populations for the states n and m is defined by the Boltzmann distribution

$$\frac{N_n}{N_m} = e^{-h\nu_m/kT}$$

The net power absorbed in V is determined by the difference in absorption and emission

$$-\Delta P = h\nu_m \left[R_{m\to n} - R_{n\to m} \right]$$

$$= \frac{8\pi^3}{3h^2} \left| \langle m | \mu | n \rangle \right|^2 \rho(\nu_m) V N_m h\nu_m \left[1 - e^{-h\nu_m/kT} \right]$$

The absorption coefficient for the transition $m \to n$ is defined as the fractional power absorbed per unit length

$$\alpha \equiv -\Delta P / P \Delta X$$

We write the volume, V, as a cross sectional area, A, times the unit length, ΔX, and note that the total radiation power passing through A is

$$P = \rho(\nu_m)Ac$$

where c is the speed of light. Thus the absorption coefficient becomes

$$\alpha = \frac{8\pi^3}{3ch}\nu_m \left|\langle m|\mu|n\rangle\right|^2 N_m \left[1 - e^{-h\nu_m/kT}\right]$$

For microwave frequencies $h\nu << kT$ so that the exponential may be expanded

$$\alpha = \frac{8\pi^3}{3ch}\nu_m \left|\langle m|\mu|n\rangle\right|^2 Nm \left[\left(\frac{h\nu_m}{kT}\right) - \frac{1}{2}\left(\frac{h\nu_m}{kT}\right)^2 + \ldots\right]$$

$$\alpha = \frac{8\pi^3}{3ckT}\nu_m^2 \left|\langle m|\mu|n\rangle\right|^2 N_m \left[1 - \frac{1}{2}\left(\frac{h\nu_m}{kT}\right) + \ldots\right] \qquad \text{(A1)}$$

The number density of the absorbing molecules in the lower state, N_m, is

$$N_m = Nf F_m \qquad \text{(A2)}$$

where N is the total number density of the gas, f is the volume mixing ratio of the absorbing molecule, and F_m is the fraction of absorbing molecules in the lower state, m, relative to all other possible states of the molecule.

$$F_m = g_m e^{-E_m/kT}/Q$$

where g_m is the degeneracy of state m and Q is the partition function of the molecule

$$Q = \sum_i g_i e^{-E_i/kT}$$

i is taken over all states of the molecule. Q may be broken up into the various energy states of the molecule (electronic, vibrational, rotational, nuclear spin). For the case of CO at atmospheric temperature, the fraction of molecules in the

ground electronic and vibrational states is very nearly unity so that (see Gordy and Cook, pp. 55-58)

$$Q = Q_r \simeq kT/hB$$

and

$$F_m = \frac{hB}{kT}(2J + 1) \exp\left[-hBJ(J + 1)/kT\right]$$

where we have defined g_m and E_m for the rotational states of the linear molecule

$$g_m = (2J + 1)$$

$$E_m = hBJ(J + 1)$$

$$\nu_m = 2B(J + 1)$$

B = molecular rotation constant

For the specific case of the CO molecule we refer to the rotation constant and the dipole moment matrix from Waters (1976)

$$B = 57.9 \text{ GHz}$$

$$\left|\left(m \left|\mu\right| n\right)\right|^2 = \mu^2(J + 1)/(2J + 1)$$

$$\mu = 0.112 \text{ Debye (Kolbe et al., 1977)}$$

Thus the final form of our absorption coefficient for CO from equations (1)-(3) is

$$\alpha_{CO} = \frac{4\pi^3 \nu_m^3 \mu^2 N f_{CO}}{3c(kT)^2} e^{-E_m/kT}\left[1 - \frac{1}{2}\left[\frac{h\nu_m}{kT}\right] + \ldots\right] \qquad \text{(A4)}$$

The frequency dependence of the absorption coefficient is introduced by the normalized line shape function rather than the term, ν^3, which does not vary significantly over the limited bandwidth of our spectra. Our expression for the absorption coefficient of CO is

$$\alpha_{CO} = \frac{4\pi^3 \nu^3 N f_{CO}}{3c(kT)^2} e^{-E_m/kT}\left[1 - \frac{1}{2}\left[\frac{h\nu}{kT}\right]\right] S\left(P,T,\nu-\nu_o\right)$$

where $S(P,T,\nu-\nu_o)$ is the normalized Voigt line shape function, which is a function of atmospheric pressure and temperature.

Appendix III: Doppler Tracking

For CO microwave lines formed in the atmospheres of Venus and Mars, we must consider the variable Doppler shift due to the changing motions of these planets with respect to our antenna. The line of sight velocity between a planet and our antenna may be broken into two terms: the center of mass motion between the planet and the Earth, and the diurnal rotation of the Earth.

For the center of mass motion we fit a quadratic function to the planet-Earth distance as listed for three consecutive days in *The Astronomical Almanac*

d_1 = distance on first day (t = −24 hours)

d_2 = distance on second day (t = 0 hours)

d_3 = distance on third day (t = 24 hours)

$$d(t) = a + bt + ct^2$$

Substitution of d_1, d_2, and d_3 yields

$$a = d_2$$

$$b = \frac{d_3 - d_1}{48}$$

$$c = \frac{d_3 - 2d_2 + d_1}{1152}$$

In order to calculate the Doppler shift we need the apparent velocity between the planet and the Earth

$$\dot{d} = b + 2ct$$

$$= \frac{(d_3 - d_1)}{48} + \frac{(d_3 - 2d_2 + d_1)}{576} t$$

where t is measured in hours from the middle day and $\dot{d}$ is in units of d/hour. The Doppler shift is then

$$\Delta\nu_{cm} = -(\dot{d}/c)\nu_o$$

where c is the speed of light in the same units as $\dot{d}$.

For the rotational component, the Doppler shift is determined from the diurnal component of velocity, $\dot{R}$. $\dot{R}$ is equal to the dot product of the local rotational velocity with the unit directional vector to the planet.

$$\dot{R} = \vec{r} \cdot \hat{u}$$

$$\vec{r} = \left[\omega R\cos\varphi, 0, 0\right]$$

$$\hat{u} = \left[\cos\delta\sin HA, \cos\delta\cos HA, \sin\delta\right]$$

where δ and HA are declination and hour angle of the planet, respectively; then

$$\dot{R} = \omega R\cos\varphi\cos\delta\sin HA$$

and

$$\Delta\nu_R = -(\dot{R}/c)\nu_o$$

Doppler shifts due to the center of mass motion may be as large as ± 30 MHz over the entire phase cycles of Venus and Mars. The diurnal Doppler shift is less

than ± 200 kHz.

Appendix IV: Radiative Transfer for CO Spectra of Mars and Venus

Observing a given position on the disk of Mars or Venus at a given frequency, ν, the microwave brightness temperature will be:

$$T_B(\nu,\mu) = T_0 \exp\left[-\int_0^\infty k(\nu,z)\,dz/\mu\right] +$$

$$\int_0^\infty k(\nu,z)\,T(z)\exp\left[-\int_z^\infty k(\nu,z')\,dz'/\mu\right] dz/\mu \qquad \text{(A1)}$$

T_0 = lower boundary brightness temperature (i.e. continuum), generally a function of position on the observed disk of Mars (see Appendix II). In the case of Venus we used continuum brightness temperatures generated from the radio brightness model of Muhleman et al. (1979).

$k(\nu,z)$ = absorption coefficient of atmospheric CO

$T(z)$ = atmospheric temperature profile

μ = atmospheric path length, approximately the cosine of the angle from local zenith (a more accurate form including curvature is given in Appendix VI).

Note that for frequencies far from the line center of absorption,

$$k(\nu,z) \to 0 \quad \text{and} \quad T_B(\nu,\mu) \to T_0$$

The frequency dependence of $k(\nu,z)$ near the resonant frequency, ν_0, produces the CO spectrum. We perform the numerical integration of $T_B(\nu,\mu)$ over altitude, z, by discretely summing $k(\nu,z)\,dz/\mu$ over altitude intervals dz_n. (We used 2 km

intervals below 5 km altitude, 5 km above 5 km altitude, for Mars; 2 km intervals are used throughout for Venus, starting at an altitude of 65 km in the atmosphere.) Thus (A1) becomes:

$$T_B(\nu,\mu) = T_0 \prod_{n=1}^{u} e^{-\tau_n(\nu)/\mu} + \sum_{n=1}^{u} \left[T_n \tau_n(\nu)/\mu\right] \left[\prod_{i=n}^{u} e^{-\tau_n(\nu)/\mu}\right] \qquad \text{(A2)}$$

T_n = atmospheric temperature of layer n

u = uppermost altitude interval (80 km for Mars, 120 km for Venus)

$\tau_n(\nu)$ = opacity of layer n, $k_n(\nu)dz_n$

$k_n(\nu)$ = absorption coefficient of CO in layer n

For $k_n(\nu)$, we use the formulation of Waters (1976), corrected for a more accurate determination of the dipole moment of CO (0.112 Debye, Kolbe et al., 1977).

$$k_n(\nu) = I^3\left(9.21 \times 10^{-9}\right)\left(1 - \frac{5.53\, I}{T_n}\right)\frac{N_{CO}}{T_n^2} f_n(\nu) \text{ cm}^{-1}$$

$k_n^{(\nu)}$ = absorption coefficient for the CO transition

I = 1 for transition $J = 0 \rightarrow 1$

I = 2 for transition $J = 1 \rightarrow 2$

N_{CO} = number density of CO (cm^{-3})

T_n = temperature (K) of layer n

$f_n(\nu)$ = Voigt shape function (convolution of collisional and Doppler broadening)

$$f_n(\nu) = \int_{-\infty}^{\infty} \frac{1}{\pi} \frac{C_p P}{\left(\nu_i - \nu_o - y\right)^2 + C_p^2 P^2} \frac{e^{-\ln 2 (y/C_d)^2}}{\sqrt{\pi}\, C_d \sqrt{\ln 2}} dy$$

C_p = collisional broadening constant

(3300 $(300/T)^{0.75}$ hz/dyne/cm^2, (Varanasi, 1975))

C_d = Doppler broadening constant

$(3.581 \times 10^{-7}\ \nu_o \sqrt{T/m_{CO}})$

P = Pressure in dynes/cm^2

ν_o = Center line frequency (hz)

Two relations allow the pressure integration of $\tau_n(\nu)$ over the altitude interval dz_n. This integration is necessary for accuracy because of the high sensitivity of the shape function to pressure ($\Delta P/P$ over a 5 km layer in the Mars atmosphere is ~ 40%; $\Delta P/P$ over a 2 km layer in the Venus atmosphere is also ~ 40%).

$$N_{CO} = \xi_n \rho_n A_o / m \quad \text{(a)} \qquad dP_n = -\rho_n g_n dz_n \quad \text{(b)}$$

A_o = Avagadro's number (6.023×10^{23})

m = average molecular weight of the atmosphere (44)

ρ_n = atmospheric density

ξ_n = volume mixing ratio of CO in layer n

g_n = gravitational acceleration (372 gm/sec^2 for Mars; 863 cm/sec^2 for Venus)

Substitution of these relations into the expression $k_n(\nu)\xi_n dz_n$ for $\tau_n(\nu)$ leads to:

$$\tau_n(\nu) = C \int_{P_m}^{P_l} \int_{-\infty}^{\infty} \frac{\sqrt{\ln 2}\, C_p}{\pi^{3/2}\, C_d} \left[\frac{P}{\left(\nu - \nu_o - y\right)^2} + C_p^2 P^2 \right] e^{-\ln 2 (y/C_d)^2}\, dy\, dP$$

$$C = I^3 (9.21 \times 10^{-9}) \left(1 - \frac{I(5.53)}{T_n}\right) \frac{A_o \xi_n}{T_n^2 g_n \mu}$$

P_l = pressure at bottom of layer n

P_m = pressure at top of layer n

Integration yields

$$\tau_n(\nu) = \frac{C\sqrt{\ln 2}}{C_d \pi^{3/2} 2 C_p} \int_{-\infty}^{\infty} \ln\left[\frac{C_p^2 P_l^2 + (\nu - \nu_o - y)^2}{C_p^2 P_\mu + (\nu - \nu_o - y)^2}\right] e^{-\ln 2 (y/C_d)^2} \, dy \qquad \text{(A3)}$$

The integral in the expression for $\tau_n(\nu)$ is evaluated numerically.

The most basic features of $\tau_n(\nu)$ are the inverse temperature squared dependence and the pressure dependence through the Voigt line shape. Basically, the width of the absorption line increases linearly with the atmospheric pressure of the line forming region. A minimum width for the line is determined by the Doppler width.

For our spectral line synthesis program we used expressions (A2) and (A3) to generate 132 separate spectral corresponding to 132 separate positions on the visible hemisphere of Mars. These positions were chosen using a sub-Earth point centered latitude (60°, ± 15°, ± 30°, +42°, ± 50°, ± 65°, ± 80°) and longitude (0°, ± 15°, ± 30°, ± 50°, ± 65°, ± 80°) grid. Such a grid allowed adequate representation of surface temperatures and emissivity for the lower boundary brightness temperature. The individual spectra were averaged with weights determined by areas in the latitude-longitude coordinates, which produced disk averaged continuum temperatures of 1% numerical precision. We used 10 evenly spaced points from the center to the limb of Venus in order to adequately represent limb darkening for the lower atmosphere of that planet.

Appendix V: Absorption Coefficients for Terrestrial Mesospheric CO Spectra

The coefficients, P_{in}, given in the description of the line inversion technique are values of opacity at frequency, ν_i, in a height interval, n, per volume mixing ratio of CO. All units are cgs.

P_{in} = $k_{in} dz_n / \xi$

k_{in} = absorption coefficient for the CO transition J = 0 → 1 (I = 1)

J = 1 → 2 (I = 2)

$$k_{in}(\nu) = I^3 \left[9.21 \times 10^{-9}\right] \left[1 - \frac{5.53\, I}{T_n}\right] \frac{N_{CO}}{T_n^2} f_n(\nu_i) \text{ cm}^{-1}$$

N_{CO} = number density of CO (cm^{-3})

T = temperature (K)

$f_n(\nu_i)$ = Voigt shape function (convolution of collisional and Doppler broadening)

$$f_n(\nu_i) = \int_{-\infty}^{\infty} \frac{1}{\pi} \frac{C_p P}{(\nu_i - \nu_o - y)^2 + C_p^2 P^2} \frac{e^{-\ln 2 (y/\alpha)^2}}{\sqrt{\pi}\, C_d \sqrt{\ln 2}} dy$$

C_d = Doppler broadening constant $(3.581 \times 10^{-7}\, \nu_o \sqrt{T/m_{CO}})$

C_p = collisional broadening constant (2400 $(300/T)^{0.75}$ hz/dyne/cm^2, Draegert and Williams, 1968)

P = Pressure in dynes/cm^2

ν_o = Center line frequency (hz)

Two relations allow the pressure integration of P_{in} over the altitude interval dz_n. This integration is necessary for accuracy because of the high sensitivity of the shape function to pressure ($\Delta P/P$ over a 2 km layer in mesosphere is ~ 25%).

$$N_{CO} = \xi \rho_n A_o / \mu \qquad \text{(A1)}$$

$$dP_n = -\rho_n g_n dz_n \tag{A2}$$

μ = average molecular weight of the atmosphere (29)

ρ_n = atmospheric density

g_n = gravitational acceleration

Substitution of these relations into the expression for P_{in} leads to:

$$P_{in}(\nu) = C\int_{P_m}^{P_l}\int_{-\infty}^{\infty} \frac{\sqrt{\ln 2}\, C_p}{\pi^{3/2} C_d}\left[\frac{P}{\left(\nu-\nu_o-y\right)^2} + C_p^2 P^2\right] e^{-\ln 2(y/C_d)^2}\, dy\, dP$$

$$C = \frac{I^2(9.21\times 10^{-9})(1-I(5.53)/T)A_o}{T^2 g_n \mu}$$

P_l = pressure at bottom of layer n

P_u = pressure at top of layer n

Integration yields

$$P_{in} = \frac{C\sqrt{\ln 2}}{C_d \pi^{3/2} 2 C_p}\int_{-\infty}^{\infty} \ln\left[\frac{C_p^2 P_l^2 + (\nu_i-\nu_o-y)^2}{C_p^2 P_u + (\nu_i-\nu_o-y)^2}\right] e^{-\ln 2(y/C_d)^2}\, dy$$

The integral in the expression for P_{in} is evaluated numerically.

The most basic features of the coefficients, P_{in}, are the inverse temperature squared dependence and the pressure dependence through the Voigt line shape. Basically, the width of the absorption line increases linearly with the atmospheric pressure of the line forming region. A minimum width for the line is determined by the Doppler width.

Appendix VI. Path Length in an Atmospheric Layer

The path length of a ray passing at an inclined angle, ϑ, through a layer of width dz is $dz/\cos\vartheta$ (see Figure 10). If the layer is curved, such as concentric layers of an atmosphere, the exact expression for path length is dz/S where S is (e.g. Muhleman et al., 1979b)

$$[(\alpha^2\cos^2\vartheta + 2\alpha + 1)^{1/2} - \alpha\cos\vartheta]^{-1}$$

Note that $\alpha = r/dz$, where r is the distance of the layer from the center of the planet. Because $r >> dz$, the above expression is very accurately approximated by $dz/\cos\vartheta$. For ϑ as large as 85°, the expression $dz/\cos\vartheta$ overestimates the path length by ~ 1%.

Appendix VII: Millimeter Continuum Temperature of Mars

Assuming that an element of the Mars surface is a smooth, flat, semi-infinite, homogeneous surface, the millimeter-wave brightness temperature is given by:

$$T_B(\vartheta_0) = \left[1 - R(\vartheta_0)\right] \int_0^\infty T(x)\, e^{-k_\nu x/\cos\vartheta_i}\, \frac{k_\nu}{\cos\vartheta_i}\, dx \qquad \text{(A1)}$$

where R is the Fresnel coefficient for reflection of energy at an interface, ϑ_0 is the emission angle, $T(x)$ is the physical temperature at depth x beneath the surface, k_ν is the power absorption coefficient at frequency ν, and ϑ_i is the incidence angle for radiation beneath the surface (related to ϑ_0 by Snell's law). For subsurface physical properties independent of temperature and depth, the integral in (A1) can be solved analytically, such that:

$$T_B(\vartheta_0) = \left[1 - R(\vartheta_0)\right] \sum_{n=0}^{\infty} \frac{T_n \cos\left[n\omega t - \Phi_n - \psi_n(\vartheta_i)\right]}{\sqrt{1 + 2\delta_n(\vartheta_i) + 2\delta_n^2(\vartheta_i)}} \qquad \text{(A2)}$$

where the coefficients T_n and Φ_n are chosen so as to provide the Fourier expansion of the diurnal variation of surface temperature:

$$T_s = \sum_{n=0}^{\infty} T_n \cos(n\omega t - \Phi_n) \qquad \text{(A3)}$$

ψ_n and δ_n are given by:

$$\psi_n(\vartheta_i) = \tan^{-1}\left[\frac{\delta_n(\vartheta_i)}{\left[1 + \delta_n(\vartheta_i)\right]}\right] \qquad \text{(A4)}$$

$$\delta_n(\vartheta_i) = \left[\frac{\beta_n}{k_\nu}\right] \cos\vartheta_i \qquad \text{(A5)}$$

$1/\beta_n$ is the e-folding decay depth of the n^{th} temperature harmonic, given by

$$\beta_n = \left[\frac{n\omega}{2}\,\frac{\rho c}{k}\right]^{1/2} \tag{A6}$$

ω is the planetary rotation rate, and k, ρ, and c are the thermal conductivity, density, and specific heat of the surface, respectively (see Piddington and Minnet, 1949, or Muhleman, 1972).

The coefficients in (A3) are obtained using the thermal model of Kieffer et al. (1977, appendix I) and the albedo (A) and thermal inertia ($I = \sqrt{k\rho c}$) as mapped on Mars by Palluconi and Kieffer (1981). A and I were obtained by fitting this same model to the measured infrared brightness temperatures, such that using the inverse process leads directly back to the diurnal variation of surface temperature and also allows extrapolation to other seasons.

The values of β_n are obtained assuming that ρ and c in (A6) do not vary with inertia, such that $1/\beta_n \sim I$, and that $1/\beta_1$ has the nominal value of 4.5 cm (see Kieffer, 1976). The electrical skin depth, $1/\kappa_\nu$, is fixed at 1.0 cm for the 1.3 mm calculations and 2.0 cm for the 2.6 mm calculations. The strong dependence of the surface emission on the value of $1/\kappa_\nu$ has been shown by Cuzzi and Muhleman (1972); emission from deeper layers is also from cooler regions, while that from shallow layers is from warmer regions, resulting in up to a 40 K variation of the brightness temperature, depending on wavelength. Going from a 1.0 to a 2.0 cm electrical skin depth changes the whole-disk radio brightness temperature by ~ 10 K. The actual value for $1/\kappa_\nu$ for Mars is not known, nor are its possible variations with location or thermal inertia. On the Moon, $1/\kappa_\nu \approx 15\,\lambda$ (Muhleman, 1972); $1/\kappa_\nu$ may be as much as a factor of two different from this on Mars (Cuzzi and Muhleman, 1972). Surface roughness and scattering effects, caused by structure on the scale of the wavelength (here, 1-2 mm), will tend to cause the thermal emission to originate from nearer the surface, effectively

lowering $1/k_\nu$. The abundance of rocks seen at the Viking landing sites as well as inferred over the rest of the planet (Jakosky and Muhleman, 1981; Christensen, 1982) indicates that scattering may be an important effect; thus, we have arbitrarily chosen the relation $1/k_\nu = 7.7\ \lambda$.

In doing the integrals outlined above, the diurnal variation of mm-wave temperature is calculated for one location near the center of the visible disk for vertical viewing. The calculation includes the appropriate integral with depth (using terms up to $n = 10$ in (A2)). The amplitude of the variation of the difference between the radio and surface temperatures is extrapolated to other latitudes using a $\cos^{1/4}\vartheta_0$ law. The integral with depth does not depend strongly on the emission angle, ϑ_0, because ϑ_i does not vary much over the range of valid ϑ_0; therefore, all of the calculations were done for $\vartheta_i = 0$ for simplicity. The surface radio emissivity was calculated explicitly at each point on the disk using the Fresnel relationships for the appropriate ϑ_0. The emissivity used was the average of that for vertical and horizontal polarizations, and the dielectric constant was taken to be $\varepsilon = 2.5$. Spatial variations of ε almost certainly occur (see Jakosky and Muhleman, 1981), but there is insufficient information to allow these variations to be incorporated into the model (the global average ε cannot vary from 2.5 by more than ~ 0.5, however).

The whole-disk radio temperature of Mars will depend on the aspect of Mars for each observation. The geometry of Mars relative to the Earth and the Sun, as appropriate for each observation, was determined in order to calculate the separate radio brightness temperatures for each observation. This allowed the inclusion of variations in Martian surface temperatures due to observed local times of day, latitude and season.